E-ISSN: 2687 - 6167
Number 45
December 2020

JSR A

JOURNAL OF SCIENTIFIC REPORTS A

JOURNAL OF SCIENTIFIC REPORTS A - DECEMBER 2020 - NUMBER 45

Kutahya Dumlupinar University Scientific Reports A
Evliya Celebi Campus Tavsanli Road 10 KM. 43270 Kutahya
Phone : (0274) 443 19 42
E-mail : joursra@gmail.com
gsjsra.com

Dumlupinar University Press

gate of science

Kütahya Dumlupınar University
Institute of Graduate Studies

Journal of Scientific
Reports-A
E-ISSN: 2687-6167
Number 45, December 2020

Journal of Scientific Reports-A started its publication life in 2000 as name of Journal of Science and Technology of Dumlupınar University and is a national peer-reviewed journal published regularly twice a year in June and December. The language of the journal is English. Articles submitted to the journal are evaluated by at least two referees who are experts in the subject and selected by the editorial board. All articles submitted to the journal are evaluated by the double-blind method. Articles submitted to our journal for review should not be previously published, accepted for publication and in the process of being evaluated for publication in another journal. All responsibility for the articles published in the journal belongs to the author(s).

The journal aims to share scientific studies carried out in the fields of science and engineering at national and international level with scientists and the public. Original research articles, review articles and short notes in science and engineering disciplines are accepted for the journal. Original research articles are expected to contain theoretical and experimental results and should not be published in other journals. In the review articles, it is expected that scientific, technological and current developments on a specific subject are reflected by using an extensive bibliography and made a satisfying evaluation of these. Short notes should be brief writings prepared to announce the first findings of an original study.

Correspondence Address: Kütahya Dumlupınar Üniversitesi Evliya Çelebi Yerleşkesi Fen Bilimleri Enstitüsü 43270 KÜTAHYA
Phone: 0 274 443 19 42 **Fax:** 0 274 265 20 60
E-mail: joursra@gmail.com **Webpage:** gsjsra.com

JSR A
Journal of Scientific Reports

JSR A
Journal of Scientific Reports

JSR A
Journal of Scientific Reports

JOURNAL OF SCIENTIFIC REPORTS-A
E-ISSN: 2687-6167

CONTENTS

RESEARCH ARTICLES

The Effect of Dnase I, Rnase A, and Proteinase K on Facultative Thermophile Brevibacillus Ağrı D5050B Biofilms 1-11
Tuğba KILIÇ*, Arzu COLERI CIHAN

Investigation of the Action Mechanism of Ammonium Pyrrolidine Dithiocarbamate on Rat Trachea Smooth Muscle Contraction-Relaxation Response 12-27
Hayri DAYIOĞLU*, Ayhan YILMAZ, Merve AKTAŞ, Fatih ALAN, Sinan DARCAN

The Investigation of the Action Mechanism of Ammonium Pyrrolidine Dithiocarbamate on Rat Bladder Smooth Muscle Contraction-Relaxation Responses 28-49
Hayri DAYIOĞLU*, Ayhan YILMAZ, Aysun ERDOĞAN, Fatih ALAN, Sinan DARCAN

The Investigation of the Action Mechanism of Ammonium Pyrrolidine Dithiocarbamate on Rat Aorta Smooth Muscle Contraction-Relaxation Responses 50-69
Hayri DAYIOĞLU*, Ayhan YILMAZ, Zeynep KELEŞ, Fatih ALAN, Sinan DARCAN

Preliminary Study on Determination of Dna Damage of Cyprinus carpio by Single Cell Gel Electrophoresis in Işıklı Lake, Denizli 70-80
Hilal ÇAVUŞ*, Müge GİDİŞ

Solutions of Linear Fractional Differantial Equations of Order $n-1<nq<n$ 81-89
Sertaç ERMAN*

Bounds for the Norms of Toeplitz Matrices with k-Jacobsthal and k-Jacobsthal Lucas Numbers 90-100
Şükran UYGUN*, Hülya AYTAR

JSR A
Journal of Scientific Reports

Journal of Scientific Reports-A, Number 45, December 2020

RESEARCH ARTICLES

Diffusion Equation Including Local Fractional Derivative and Non-Homogenous Dirichlet Boundary Conditions 101-110
Süleyman ÇETİNKAYA*, Ali DEMİR

Gender Estimation with Convolutional Neural Networks Using Fingertip Images 111-125
Kerem SIRMA*, Pakize ERDOĞMUŞ

Characterization and Process Optimization of Ultrasound Extracted Polysaccharides from the 'Opuntia Ficus İndica' Cladodes 126-142
Tuncay YILMAZ

Experimental Analysis of the Air Defrost Process in an Industrial Cooling System 143-157
Süleyman ERTEN*, Meltem KOŞAN, Furkan İŞGEN, Mustafa AKTAŞ

Experimental Analysis of the Output Performance of the Abrasive Effect of Dust on Photovoltaic Cells 158-177
Hüseyin BENLİ*, Mert GÜRTÜRK, Neslihan KOÇDEMİR ERTÜRK

A New Mobile Application for Physical Measurement in a Cellular Network 178-200
Aygün VAROL*, Bilge KARTAL ÇETİN

Investigation of Soma Region Coals with Respect to Spontaneous Combustion Susceptibility 201-214
Hasan Hüseyin ILICA*, Özer ÖREN, Cem ŞENSÖĞÜT

Recovery of Coal Slime by Using the Knelson Concentrator 215-224
Ali UÇAR*, Oktay ŞAHBAZ, Nezahat EDİZ, Sevgi KARACA, İ. Göktay EDİZ

The Effect of PH and Current Density in the Removal of Aluminium Cobalt, Chromium and Zinc from Metal Processing Wastewater by Electrocoagulation Method 225-235
Nevzat BEYAZIT*, Banu TÜRK

JSR A
Journal of Scientific Reports

Journal of Scientific Reports-A, Number 45, December 2020

RESEARCH ARTICLES

Performance Comparison of UV, UV/H_2O_2, UV/Fe^{2+}, H_2O_2/Fe^{2+}, UV/H_2O_2/Fe^{2+} Processes in the Removal of Cod and Color from Textile Wastewater 236-252
Nevzat BEYAZIT*, Hande KARACA

REWIEV ARTICLES

Tissue Culture Techniques of Medicine and Aromatic Plants: History, Cultivation and Micropropagation 253-266
Betül AKIN*

The Role of Telomeric Activity and Telomerases in Aging with Neoplasic Changes 267-282
Esra BİLİCİ*

Kütahya Dumlupınar University
Institute of Graduate Studies

Journal of Scientific
Reports-A
E-ISSN: 2687-6167
Number 45, December 2020

RESEARCH ARTICLE

THE EFFECT OF DNASE I, RNASE A, AND PROTEINASE K ON FACULTATIVE THERMOPHILE *BREVIBACILLUS AGRI* D505B BIOFILMS

Tugba KILIC[1*], Arzu COLERI CIHAN[2]

[*1]Gazi University, Vocational School of Health Services, Medical Laboratory Techniques Program, 06830, Ankara,
tugbakilic@gazi.edu.tr, ORCID: 0000-0002-5474-0288
[2]Ankara University, Faculty of Science, Department of Biology, 06100, Ankara,
arzucoleri@gmail.com, ORCID: 0000-0002-7289-6251

Received Date:29.01.2020 *Accepted Date: 04.12.2020*

ABSTRACT

Thermophilic bacteria have been isolated from man-made thermal habitats and natural thermal habitats. *Brevibacillus agri* D505b was isolated from the geothermal region in Turkey. Thermophilic bacilli can form biofilm in areas such as dairy manufacturing plants, water systems, paper-machine, and can create serious problem due to their spore-forming. Therefore, determining the biofilm-forming properties of these bacteria is very significant for the areas. The aim of this study was to determine the effect of environmental conditions on planktonic growth and biofilm formation, the concentrations of protein, carbohydrate, and extracellular DNA (eDNA) from extracellular polymeric substances (EPSs), and the effects of DNase I, RNase A and proteinase K on eDNA in the biofilm matrix of the isolate. As a result, optimal values of the isolate for planktonic growth and biofilm formation were determined as pH 7.0, 1% NaCl, 50^{o}C, and pH 9.0, 0% NaCl, 45^{o}C, respectively. Genomic DNA (gDNA) and eDNA were isolated, then were treated with DNase I, RNase A and proteinase K. The gDNA was only all degraded by DNase I. However, eDNA was not affected by DNase I, RNase A and proteinase K. Moreover, eDNA was determined to be resistant to all the enzymes tested in this study. The eDNA might be protected by EPS components and/or extracellular membrane vesicles (EVs) structures. In addition, the molecular weights of the gDNA and eDNA were calculated larger than 20 kb. Thus, the presence of eDNA in the biofilm matrix of *B. agri* was confirmed with agarose gel imaging and spectrophotometric analysis.

Keywords: *Brevibacillus agri D505b, Biofilm formation, Extracellular DNA.*

1. INTRODUCTION

The Gram-positive spore-forming genus *Bacillus* occurs in a wide range of environments, from soil to food and dairy processing surfaces [1]. *Bacillus* spp. spores are often present in raw milk, playing a significant role in the bacterial impairment of milk and milk products. Several spore-forming species have been isolated on dairy farms so far [2]. Zhao et al. [3] identified thermophilic spore-forming bacteria such as *Brevibacillus* spp., *Anoxybacillus* spp., and *Geobacillus* spp. in the dairy industry. In another study, Lücking et al. [4] identified spore-forming bacteria in dairy products, including

Brevibacillus agri, *Bacillus pumilus*, and *Anoxybacillus flavithermus*. Moreover, *Brevibacillus* sp. was isolated from soil by Vivas et al. [5].

The contamination of industrial plants and products with spore-forming bacteria is a common problem [6]. Spore-forming bacteria have been shown to sporulate within single- and multiple-species biofilms and to release these immensely stress-resistant spores, thus increasing the risk of cross-contamination of food [7]. Paperboard and food-packaging paper primarily contain spore-forming bacteria belonging to the genera *Bacillus*, *Paenibacillus*, and *Brevibacillus* as contaminants [8]. In addition, Pereira and Sant'Ana [9] investigated spore-forming bacteria in raw materials such as sugar, cocoa, starch, and milk powder. These raw materials are contaminated by spore-forming bacteria and are significant for the quality of final products. Furthermore, spores of *Bacillus* species prevalently contaminate the food. Dried foods such as cereal and milk powders are frequently contaminated with spores and when water is present, these spores can germinate, leading to spoilage or food poisoning [10]. Moreover, aerobic spore-forming bacteria have serious impacts on food quality and safety, so the bacteria are a potential cause of disease [11]. *B. agri* has been associated with human infections [12]. Ogarkov et al. [13] showed that in the final late stages of chronic tuberculosis, samples obtained from patients contained strains of various species of *Bacillus* spp. and *Brevibacillus* spp. In addition, *B. agri* was isolated in association with an outbreak of waterborne illness. In a study, Logan et al. [14] identified *B. agri* from clinical, dairy, and industrial specimens (gelatin processing plant, antibiotic fermenter, sterilized milk), and 3 strains were associated with the outbreak of waterborne illness.

In our previous studies, we carried out the experiments including biofilm formation on six abiotic surfaces stainless steel, glass, polyvinyl chloride, polypropylene, polystyrene, and polycarbonate) used in industry and biofilm control with sanitation agents of *B. agri* D505b. We determined that the isolate was a strong biofilm producer [15] and [16]. The objective of this work was to determine the effect of environmental conditions on planktonic growth and biofilm formation, the concentrations of protein, carbohydrate, and eDNA from EPSs and the effects of DNase I, RNase A and proteinase K enzymes on *B. agri* D505b biofilms. eDNA is a major structural component of many bacteria. Enzymatic deterioration of eDNA can weaken the biofilm structure and release microbial cells from the surface. DNases could evidence a potent strategy for biofilm control [17].

2. MATERIAL AND METHODS

2.1. Culture Conditions of the Isolate

The endospore-forming, aerobic and facultative thermophilic *B. agri* D505b was isolated from sediment sample in the hot spring (Dikili, Izmir, Turkey). We used the isolate, which was previously isolated in our lab, to study its biofilm properties. The 16S rRNA gene of the isolate was registered with GenBank Accession Number FJ430048 [18]. The isolate was first cultured in Tryptic Soy Agar (TSA, Merck, Germany) at 55^{o}C for 18 h and was subsequently incubated in Tryptic Soy Broth (TSB, Merck, Germany) for 18 h at 55^{o}C in a shaking incubator (170 rpm). The culture was again incubated in TSB at 55^{o}C for 6 h under shaking. All biofilm assays were carried out with a culture that was 6 h old in the mid-exponential growth phase.

2.2. The Effects of Environmental Conditions on Planktonic Growth and Biofilm Formation

The effects of pH (4.0, 5.0, 6.0, 6.5, 7.0, 7.5, 8.0, 8.5, 9.0), salinity (0.0, 1.0, 1.5, 2.0, 2.5, 3.0, 3.5, 4.0%), and temperature (37, 40, 45, 50^{o}C) on planktonic growth and biofilm formation were determined in 96-well polystyrene microtiter plates (LP, Italy) spectrophotometrically (OD 595 nm) for 0, 6, 18, 24,

and 48 h in TSB. In addition, the crystal violet (CV) staining method was applied for optimal biofilm growth assay at the end of 48 h of incubation. For the pH adjust, NaOH and HCl solutions were used. In this study, we first-time determined optimal biofilm values, and the values were used in all experiments.

2.3. Quantification of Biofilm Formation with Crystal Violet in Microtiter Plates

This assay was carried out using the CV staining assay described by Woodward et al. [19] and Stepanović et al. [20] with a few changes. To the wells of 96-well polystyrene microtiter plates were added 90 µL of TSB without NaCl and 10 µL of bacterium culture. The plates were washed two times with physiological saline at the end of 48 h of incubation; thus, planktonic cells were removed. The remaining adhered cells were fixed with 95% methanol (Merck, Germany) and were incubated at 22^{o}C temperature for 15 min. Then the wells were stained with 1% crystal violet dye (Merck, Germany) at 22^{o}C for 30 min. Then, the plates were washed under running tap water to remove residues of stain and were air-dried. Afterward, the dye bound to the biofilm cells was dissolved with ethanol:acetone (Merck, Germany), and the amount of biofilm was measured at an optical density (OD) of 595 nm using a microplate reader (BioTek Elisa reader, µQuant, Biotek Inc., USA). The negative controls contained only TSB.

2.4. The Determination of Concentrations of Protein, Carbohydrate, and eDNA

The D505b isolate was grown at its optimal conditions on TSA plates for 18 h and 0.1 g of bacterium biomass was collected with sterile plastic loops. The biomass was entirely disintegrated by vortexing at maximum speed for 2 min in 2 mL of physiological saline, containing glass bead (diameter 3 mm). After vortexing, the suspension was centrifuged at 32.000 x *g* for 7 min. The pellet was used for gDNA isolation. The supernatant was primarily filtered through a 0.22 µm membrane filter (Sartorius, France) and used for protein, carbohydrate, and eDNA assays. Polysaccharide concentration was quantified by the phenol-sulfuric acid method [21]. Glucose was used as a standard for the determination of the calibration curve. The Lowry method was applied for the determination of the protein concentration. Bovine serum albumin (BSA) was used as a standard [22]. eDNA isolation was conducted partially by the method described by Wilson [23]. The filtered supernatant was treated with chloroform and isoamyl alcohol (volume 24:1) for eDNA isolation. Afterward, the solution was centrifuged and treated with phenol-chloroform-isoamyl alcohol (volume 25:24:1). The solution was again centrifuged. Isopropanol was added to the supernatant and was waited for 20 min at -20^{o}C. The solution was centrifuged and was added cold ethanol (70%) on precipitate. The solution was centrifuged, and the supernatant was poured. Tris-EDTA buffer was added on eDNA and was solved. The gDNA extraction was performed using a genomic DNA purification kit (Fermentas K0512, Thermo Fisher Scientific Inc., USA). Finally, gDNA and eDNA qualities were measured with the absorbance values at 260 nm/280 nm with a NanoDrop Spectrophotometer (Thermo Scientific NanoDrop Lite, USA). The DNA samples were subjected to 1.5% agarose gel electrophoresis at 120 V for 45 min. Then, the products were visualized with a Quantum ST4 Gel Documentation System (Vilber Lourmat, France). The molecular weights of DNA samples were determined via the Quantum-Capp software system (Vilber Lourmat).

2.5. The Treatment of gDNA and eDNA with DNase I, RNase A, and Proteinase K Enzymes

In this assay, gDNA and eDNA were first isolated according to section 2.4. Afterward, 10 µL of gDNA (295.5 ng/µL) or eDNA (604.6 ng/µL) samples were treated with DNase I (1.45, 1.7, 2.5, and 3.0 mg/mL) (Sigma-Aldrich, DN25, USA), RNase A (0.90 mg/mL) (Sigma-Aldrich, R6513, USA), and proteinase K (0.85 mg/mL) (Sigma-Aldrich, P2308, USA) enzymes at 37˚C for 1 h in 96-well polystyrene microtiter plates. Finally, agarose gel electrophoresis (1.5%) was applied at 120 V for 45 min. The products were visualized with the Vilber Lourmat Quantum ST4 Gel Documentation System.

The molecular weights of DNA samples were determined with the Quantum-Capp software system. As negative controls were used samples without enzyme treatment.

2.6. The Effect of DNase I on Mature Biofilm

This assay was conducted as defined previously by Grande et al. [24] with a few modifications. The purpose of the assay was to determine whether the eDNA was sensitive or resistant to DNase I. First, 95 µL of TSB and 5 µL of bacterium culture were added to a 96-well polystyrene microtiter plates and were incubated for 40 h (mature biofilm) at 45°C. The biofilms were then treated with 100 µL of DNase I (100 µg/mL) (Sigma-Aldrich, DN25) for 2, 4, 8, and 12 h at 37°C. The plate wells were washed with physiological saline. Subsequently, the CV staining assay was applied to the plates. The biofilm samples were treated with physiological saline for positive controls.

2.7. Statistical Data Analyses

All the experiments were conducted in three replicates on three independent days. All statistical analyses were performed using SPSS 17.0 statistical program (SPSS Inc., Chicago, IL, USA). The one-way analysis of variance (ANOVA) was applied to determine whether there are any statistically significant differences between the means of independent groups. Probability levels of $p < 0.05$ were considered statistically significant.

3. RESULTS

3.1. Optimization Assays

The optimal values of the isolate for planktonic growth were determined as pH 7.0 (OD_{595nm} 1.253 ± 0.003), 1% NaCl (OD_{595nm} 1.174 ± 0.04), and 50°C (OD_{595nm} 0.942 ± 0.17), whereas optimal values for biofilm formation were measured as pH 9.0 (OD_{595nm} 1.163 ± 0.3), 0% NaCl (OD_{595nm} 2.538 ± 0.2), and 45°C (OD_{595nm} 2.794 ± 0.3) in 96-well microtiter plates (Figs. 1, 2, and 3). All parameters were found different for the optimal planktonic growth and the biofilm formation of the isolate. The pH value for biofilm formation was much higher than that for optimal planktonic growth. In addition, the isolate preferred an alkaline and salt-free environment for optimal biofilm production. The biofilm formation decreased with the increased salt amount.

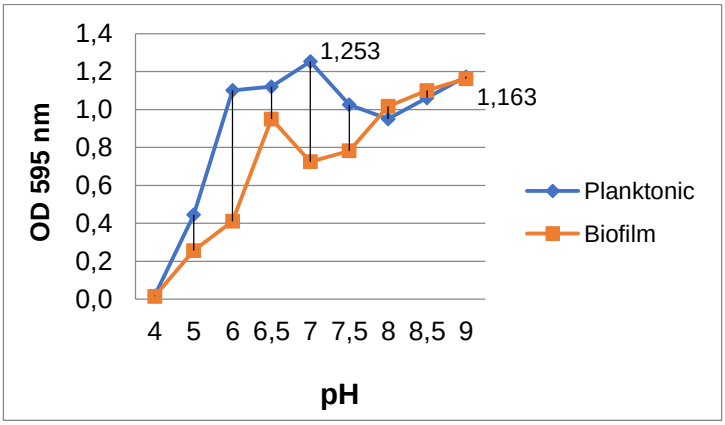

Figure 1. The effects of pH on the planktonic growth and biofilm formation of the isolate.

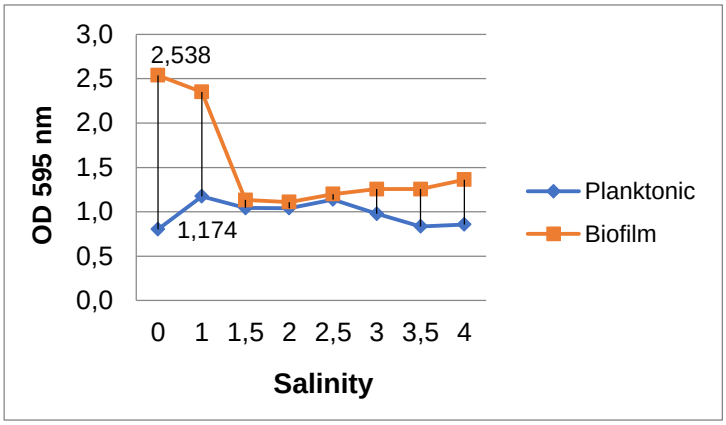

Figure 2. The effects of salinity (NaCl) on the planktonic growth and biofilm formation of the isolate.

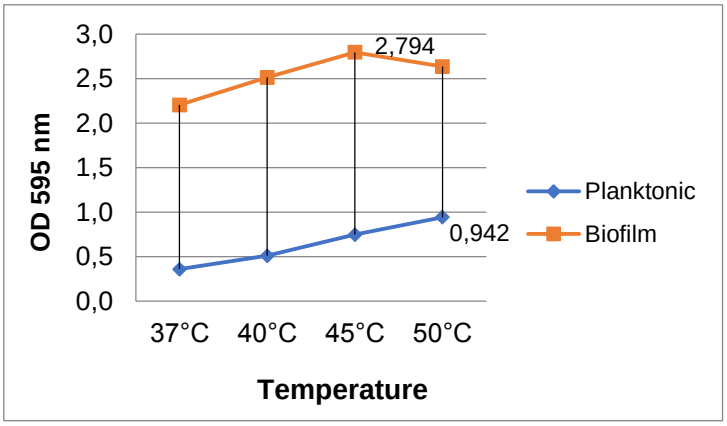

Figure 3. The effects of temperature on the planktonic growth and biofilm formation of the isolate.

3.2. Protein, Carbohydrate, and eDNA Analysis

The concentrations of total protein and carbohydrate were quantified as 600 µg/mL and 18.4 µg/mL, respectively. The amount of eDNA was measured as 604.6 ng/µL, whereas the gDNA was quantified as 295.5 ng/µL. Furthermore, the molecular weights of the gDNA and eDNA were calculated larger than 20 kb (Fig. 4). Thus, the presence of eDNA in the biofilm matrix of *B. agri* was confirmed for the first time with agarose gel imaging and spectrophotometric analysis.

3.3. The Treatment with DNase I, RNase A, and Proteinase K of gDNA and eDNA

The gDNA was only all degraded by DNase I. On the other hand, eDNA was not affected by any of the enzymes. To confirm the resistance, eDNA was treated with higher concentrations of DNase I (1.7, 2.5, and 3.0 mg/mL). But the results did not change (Fig. 4). Our results showed that the strong biofilm producer *B. agri* D505b was very resistant to DNase I, RNase A, and proteinase K.

JSR A
Journal of Scientific Reports

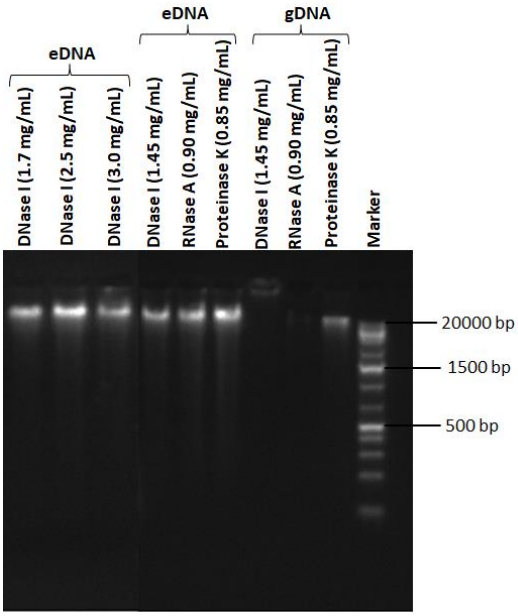

Figure 4. Agarose gel electrophoresis image of the eDNA and gDNA of D505b; different DNase I concentrations applied to eDNA (1.7, 2.5, and 3.0 mg/mL); DNase I (1.45 mg/mL), RNase A (0.90 mg/mL), and proteinase K (0.85 mg/mL) treatment of the eDNA and gDNA. Marker (Fermentas Gene Ruler 1 kb Plus DNA Ladder, 75-20000 bp).

3.4. The Effects of DNase I on Mature Biofilm

DNase I enzyme (100 µg/ mL) was applied to the mature biofilm (40 h) for 2, 4, 8, and 12 h in 96-well polystyrene microtiter plates. DNase I had no significant effect on the biofilm biomass of *B. agri* D505b. According to the results, the residual biofilm amounts measured after the DNase I treatment were as 16.56% for 2 h and 20.04% for 12 h.

4. DISCUSSION

The optimal values the isolate for planktonic growth were determined as pH 7.0, 1% NaCl, and 50^{o}C, whereas optimal biofilm formation was measured as pH 9.0, 0% NaCl, and 45^{o}C in 96-well polystyrene microtiter plates (Figs 1, 2, and 3). It was seen that all parameters were different for the planktonic growth and biofilm formation of the isolate. The pH value for biofilm formation was much higher than that for optimal growth. Furthermore, the isolate preferred an alkaline and salt-free environment for optimal biofilm production. The biofilm formation decreased as the salt amount increased. High salt concentration in the growth medium resulted in lower environmental water activity (a_w), which is destructive to cellular activities. Moreover, osmotic drift influences the response of the tested *Bacillus* species' biofilm growth on polystyrene [25].

Extracellular DNA (eDNA) of microbial origin is common in natural terrestrial and aquatic environments [26]. Catlin and Cunningham [27] obtained eDNA from *Staphylococcus, Pseudomonas* and *Alcaligenes faecalis*. The presence of eDNA was indicated for the facultative thermophile *Brevibacillus agri* for the first time in our study. Several studies demonstrated that the eDNA of biofilm

cells could be sensitive to the DNase I of eDNA. Nijland et al. [28] demonstrated that DNase I (above 15 ng/mL) caused the dispersal of biofilm of *Bacillus licheniformis.* We determined that the DNase I activity had limited effect at a concentration of 100 µg/mL within 12 h on the mature biofilm of the isolate (20.04%). On the other hand, our results showed that DNase I, RNase A and proteinase K enzymes had no effect on eDNA in the biofilm matrix of *B. agri* D505b (Fig. 4). Apparently, the eDNA of *B. agri* D505b could be protected from these enzymes. This could be explained by the rigid pellicle structure and strong biofilm structure of the isolate. We detected in our previous study that *B. agri* D505b was a strong biofilm producer (OD595 nm: 3.365) [16]. Moreover, the resistance to DNase I may possibly result from the conserved folded structure of eDNA after purification. The purified eDNA which has lost its carbohydrate and protein interactions might become rearranged after chemical treatments, and gain a more compact and condense structure with additional folding [29]. Similarly, DNase I had no effect on *Helicobacter pylori* eDNA. The eDNA might be protected by other EPS and/or EV-like structures [30]. The eDNA-containing EVs plays a part in biofilm production, bacterial colonization, and subsequent resistance to removal techniques [31]. EVs in biofilms interact with eDNA to strengthen structural integrity [32]. Rivera et al. [33] reported the isolation of EVs from Gram-positive, spore-forming *Bacillus anthracis.* The first hint of the presence of EVs in Firmicutes came from the studies on *Bacillus cereus* and *Bacillus subtilis* [32]. Soler et al. [34] observed that vesicles and eDNA were produced by hyperthermophilic archaea. In addition, DNA in vesicle preparation was found immensely resistant to DNase treatment. Their observations suggest that eDNA could be less or more strongly associated with the vesicles. Vesicles could be a significant factor determining the DNA stability and protecting it from degradation in natural environments. It is unclear how stable eDNA could exist in hydrothermal environments. However, their results demonstrated that eDNA could be preserved in high-temperature environments via its association with vesicles produced by hyperthermophilic archaea. Blesa and Berenguer [35] determined the long-term protection of thermophilic *Thermus thermophilus* eDNA from DNase associated with EVs generated by cell lysis. Vesicle-protected eDNA can withstand nuclease activity, which allows the movement of eDNA over long distances. EVs are frequently generated by bacteria during the growth phase or upon integration within a biofilm [36].

The characterization of the eDNA of bacterial biofilms revealed that it consists of fragments of high molecular weight (about 30 kb) [37]. We detected that the molecular weight of eDNA was larger than 20 kb with agarose gel electrophoresis (Fig. 4). On the other hand, Ali Mohammed et al. [38] reported that the size of the eDNA of *Fusobacterium nucleatum* and *Porphyromonas gingivalis* was detected to be about 100 bp. The size is generally larger than the one defined for other biofilms. Moreover, the size of eDNA has been reported to range from less than 100 bp to 10 kb [38]. In conclusion, this paper determined that changing environmental conditions could increase the biofilm formation abilities of the isolate. In addition, the presence of eDNA in the biofilm matrix of *B. agri* was confirmed with electrophoresis and spectrophotometric methods. It was seen in this study that DNase I, RNase A and proteinase K enzymes had no effect on the *B. agri* D505b biofilms. Therefore, our data suggest that the effect of different enzyme combinations and concentrations should be tested for the biofilm control of *B. agri* in future studies. The synergistic effect of enzymatic sanitation agents can be determined for biofilm removal. In addition, revealing the association between eDNA and EVs for *Brevibacillus agri* is significant. Any enzyme which can degrade eDNA holds a potential to be used along with antibiotics as a co-treatment agent.

ACKNOWLEDGMENT

This research was supported by the Scientific Research Project Office of Ankara University (project number 14B0430003).

REFERENCES

[1] Vilain, S. and Brözel, V. S., (2006), Multivariate approach to comparing whole-cell proteomes of *Bacillus cereus* indicates a biofilm-specific proteome, Journal of Proteome Research, 5(8), 1924-1930.

[2] Scheldeman, P., Pil, A., Herman, L., De Vos, P. and Heyndrickx, M., (2005), Incidence and diversity of potentially highly heat-resistant spores isolated at dairy farms, Applied and Environmental Microbiology, 71, 1480-1494.

[3] Zhao, Y., Caspers, M. P., Metselaar, K.I., De Boer, P., Roeselers, G., Moezelaar, R., Groot, M.N., Montijn, R.C., Abee, T. and Kort, R., (2013), Abiotic and microbiotic factors controlling biofilm formation by thermophilic sporeformers, Applied and Environmental Microbiology, 79, 5652-5660.

[4] Lücking, G., Stoeckel, M., Atamer, Z., Hinrichs, J. and Ehling-Schulz, M., (2013), Characterization of aerobic spore-forming bacteria associated with industrial dairy processing environments and product spoilage, International Journal of Food Microbiology, 166(2), 270-279.

[5] Vivas, A., Vörös, I., Biró, B., Campos, E., Barea, J. M. and Azcón, R., (2003), Symbiotic efficiency of autochthonous arbuscular mycorrhizal fungus (*G. mosseae*) and *Brevibacillus* sp. isolated from cadmium polluted soil under increasing cadmium level, Environmental Pollution, 126(2), 179-189.

[6] De Clerck, E. and De Vos, P., (2002), Study of the bacterial load in a gelatine production process focussed on *Bacillus* and related endosporeforming genera, Systematic and Applied Microbiology, 25(4), 611-617.

[7] Alvarez-Ordóñez, A., Coughlan, L. M., Briandet, R. and Cotter, P. D., (2019), Biofilms in food processing environments: Challenges and opportunities, Annual Review of Food Science and Technology, 10, 173-195.

[8] Sjöberg, A. M., Sillanpää, J., Sipiläinen-Malm, T., Weber, A. and Raaska, L., (2002), An implementation of the HACCP system in the production of food-packaging material, Journal of Industrial Microbiology and Biotechnology, 28(4), 213-218.

[9] Pereira, A. P. M. and Sant'Ana, A.S., (2018), Diversity and fate of spore forming bacteria in cocoa powder, milk powder, starch and sugar during processing: A review, Trends in Food Science and Technology, 76, 101-118.

[10] Logan, N. A., (2012), *Bacillus* and relatives in foodborne illness, Journal of Applied Microbiology, 112, 417-429.

[11] Gopal, N., Hill, C., Ross, P. R., Beresford, T. P., Fenelon, M. A. and Cotter, P. D., (2015), The prevalence and control of *Bacillus* and related spore-forming bacteria in the dairy industry, Frontiers in Microbiology, 6, 1418.

[12] Sanders, M. E., Morelli, L. and Tompkins, T. A., (2003), Sporeformers as human probiotics: *Bacillus*, *Sporolactobacillus*, and *Brevibacillus*, Comprehensive Reviews in Food Science and Food Safety, 2(3), 101-110.

[13] Ogarkov, O. B., Badleeva, V., Belkova, N. L., Adelshin, R. V., Tsyrenova, T. A., Khromova, P. A., Sinkov, V. V, Kostjunin, K. Y., Dashatsyrenova, S. B., Koshcheyev, M. E, Zarbuev, A. N. and Zhdanove, S. N., (2017), The phenomenon of the formation of biofilms by *Brevibacillus* spp. and *Bacillus* spp. in the presence of clinical strains of *Mycobacterium tuberculosis*, Molecular Genetics, Microbiology and Virology, 32(3), 148-154.

[14] Logan, N. A., Forsyth, G., Lebbe, L., Goris, J., Heyndrickx, M., Balcaen, A., Verhelst, A., Falsen, E., Ljungh, A., Hansson, H. B. and De Vos, P., (2002), Polyphasic identification of *Bacillus* and *Brevibacillus* strains from clinical, dairy and industrial specimens and proposal of *Brevibacillus invocatus* sp. nov., International Journal of Systematic and Evolutionary Microbiology, 52(3), 953-966.

[15] Kilic, T. and Cihan A. C., (2020), Biofilm formation and control of facultative thermophile *Brevibacillus agri* D505b, Communications Faculty of Sciences University of Ankara Series C Biology, 29(1), 119-130.

[16] Cihan, A. C., Karaca, B., Ozel, P. B. and Kilic, T., (2017), Determination of the biofilm production capacities and characteristics of members belonging to Bacillaceae family, World Journal of Microbiology and Biotechnology, 33, 118.

[17] Jakubovics, N. S., Shields, R. C., Rajarajan, N. and Burgess, J. G., (2013), Life after death: the critical role of extracellular DNA in microbial biofilms, Letters in Applied Microbiology, 57(6), 467-475.

[18] Cihan, A. C., Tekin, N., Ozcan, B. and Cokmus, C., (2012), The genetic diversity of genus *Bacillus* and the related genera revealed by 16S rRNA gene sequences and ardra analyses isolated from geothermal regions of turkey, Brazilian Journal of Microbiology, 43(1), 309-324.

[19] Woodward, M. J., Sojka, M., Sprigings, K. A. and Humphrey, T.J., (2000), The role of SEF14 and SEF17fimbriae in the adherence of *Salmonella enteric* serotype Enteritidis to inanimate surfaces, Journal of Medical Microbiology, 49(5), 481-487.

[20] Stepanović, S., Vuković, D., Dakić, I., Savić, B. and Švabić-Vlahović, M., (2000), A modified microtiter-plate test for quantification of staphylococcal biofilm formation, Journal of Microbiological Methods, 40(2), 175-179.

[21] Dubois, M., Gilles, K. A., Hamilton, J. K., Rebers, P. A. and Smith, F., (1951), A colorimetric method for the determination of sugar, Nature, 168(4265), 167.

[22] Lowry, O. H., Rosebrough, N. J., Farr, A. L. and Randall, R. J., (1951), Protein measurement with the Folin phenol reagent, Journal of Biological Chemistry, 193, 265-275.

[23] Wilson, K., (2001), Preparation of genomic DNA from bacteria, Current Protocols in Molecular Biology, 56, 2-4.

[24] Grande, R., Di Giulio, M., Bessa, L. J., Di Campli, E., Baffoni, M., Guarnieri, S. and Cellini, L., (2010), Extracellular DNA in *Helicobacter pylori* biofilm: a backstairs rumour, Journal of Applied Microbiology, 110(2), 490-498.

[25] Elhariry, H. M., (2008), Biofilm formation by endospore-forming bacilli on plastic surface under some food-related and environmental stress conditions, Global Journal of Biotechnology and Biochemistry, 3(2), 69-78.

[26] Ibáñez de Aldecoa, A. L., Zafra, O. and González-Pastor, J. E., (2017), Mechanisms and regulation of extracellular DNA release and its biological roles in microbial communities, Frontiers in Microbiology, 8, 1390.

[27] Catlin, B. W. and Cunningham, L. S., (1958), Studies of extracellular and intracellular bacterial deoxyribonucleic acids, Microbiology, 19, 522-539.

[28] Nijland, R., Hall, M. J. and Burgess, J. G., (2010), Dispersal of biofilms by secreted, matrix degrading, bacterial DNase, PloS One, 5, e15668.

[29] Kilic, T., Karaca, B., Ozel, B. P., Ozcan, B., Cokmus, C. and Coleri Cihan, A., (2017), Biofilm characteristics and evaluation of the sanitation procedures of thermophilic *Aeribacillus pallidus* E334 biofilms, Biofouling, 33(4), 352-367.

[30] Grande, R., Di Marcantonio, M. C., Robuffo, I., Pompilio, A., Celia, C., Di Marzio, L., Paolino, D., Codagnone, M., Muraro, R., Stoodley, P., Hall-Stoodley, L. and Mincione, G., (2015), *Helicobacter pylori* ATCC 43629/NCTC 11639 outer membrane vesicles (OMVs) from biofilm and planktonic phase associated with extracellular DNA (eDNA), Frontiers in Microbiology, 6, 1369.

[31] Brown, L., Wolf, J. M., Prados-Rosales, R. and Casadevall, A., (2015), Through the wall: extracellular vesicles in Gram-positive bacteria, mycobacteria and fungi, Nature Reviews Microbiology, 13(10),620-630.

[32] Gill, S., Catchpole, R. and Forterre, P., (2018), Extracellular membrane vesicles in the three domains of life and beyond, FEMS Microbiology Reviews, 43, 273-303.

[33] Rivera, J., Cordero, R. J., Nakouzi, A.S., Frases, S., Nicola, A. and Casadevall, A., (2010), *Bacillus anthracis* produces membrane-derived vesicles containing biologically active toxins, Proceedings of the National Academy of Sciences, 107(44), 19002-19007.

[34] Soler, N., Marguet, E., Verbavatz, J. M. and Forterre, P., (2008), Virus-like vesicles and extracellular DNA produced by hyperthermophilic archaea of the order Thermococcales, Research in Microbiology, 159(5), 390-399.

[35] Blesa, A. and Berenguer, J., (2015), Contribution of vesicle-protected extracellular DNA to horizontal gene transfer in *Thermus* spp., International Microbiology, 18, 177-187.

[36] Blesa, A., Averhoff, B. and Berenguer, J., (2018), Horizontal gene transfer in *Thermus* spp., Current Issues in Molecular Biology, 29, 23-36.

[37] Martins, M., Uppuluri, P., Thomas, D. P., Cleary, I.A., Henriques, M., Lopez-Ribot, J. L. and Oliveira, R., (2010), Presence of extracellular DNA in the *Candida albicans* biofilm matrix and its contribution to biofilms, Mycopathologia, 169, 323-331.

[38] Ali Mohammed, M. M., Nerland, A. H., Al-Haroni, M. and Bakken, V., (2013), Characterization of extracellular polymeric matrix, and treatment of *Fusobacterium nucleatum* and *Porphyromonas gingivalis* biofilms with DNase I and proteinase K, Journal of Oral Microbiology, 5 (1), 20015.

Kütahya Dumlupınar University
Institute of Graduate Studies

Journal of Scientific
Reports-A
E-ISSN: 2687-6167
Number 45, December 2020

RESEARCH ARTICLE

INVESTIGATION OF THE ACTION MECHANISM OF AMMONIUM PYRROLIDINE DITHIOCARBAMATE ON RAT TRACHEA SMOOTH MUSCLE CONTRACTION-RELAXATION RESPONSE

Hayri DAYIOĞLU[1], Ayhan YILMAZ[2], Merve AKTAŞ[3], Fatih ALAN[4] and Sinan DARCAN[5]

[1]Kütahya Dumlupınar University, Faculty of Science and Literature, Department of Biology, 43270, Kütahya, hayri.dayioglu@dpu.edu.tr, ORCID: 0000-0002-9270-8561
[2] Kütahya Dumlupınar University, Faculty of Science and Literature, Department of Biology, 43270, Kütahya, ayhan.yilmaz@dpu.edu.tr, ORCID: 0000-0003-0410-8687
[3]Yavuz Selim Mah., 1004. Sok., Bağcılar Merkez Evleri, No: 3/2, 34200, Bağcılar, İstanbul, merve611734@outlook.com, ORCID: 0000-0003-1953-1672
[4]General Directorate of Presidential Protection Services, Presidential Complex, 06530, Beştepe, Ankara, fatihalan06@hotmail.com,ORCID: 0000-0002-0561-6192
[5]Kütahya Health Science University, Evliya Çelebi Campus, Tavşanlı Yolu 10. Km, 43100, Kütahya, sinan.darcan@ksbu.edu.tr, ORCID: 0000-0002-2135-4807

Received Date: 20.04.2020 *Accepted Date: 15.09.2020*

ABSTRACT

Ammonium pyrrolidine dithiocarbamate (APDTC) is a suppressive thiol compound of Nuclear Factor kappa B (NF-κB) and works to prevent infections, regulate oxidation, prevent cell death, affects on viruses. Therefore, it is recommended to avoid harmful practices and to give importance to active substance research in medical ethics. In postoperative care, respiratory system relaxation treatments are important. There is insufficient research into how the functions of APDTC are regulated in human and animals. In our study, we aimed to evaluate the function of APDTC in rat trachea smooth muscle. 70 male Wistar albino rats were used. The rats were euthanized by giving anesthesia and after applying cervical dislocation the trachea was separated, connective tissues of trachea were separated and placed in Krebs solution. Potassium chloride (KCl), Acetylcholine (ACh), APDTC, Atropine, Phentolamine, Propranolol, Nifedipine and Tetraethylammonium (TEA) were added in to the solution. Eventually, APDTC produced a relaxation response in the tracheal smooth muscle induced by ACh, but this relaxation was not statistically significant. In our study, Half maximal effective concentration (EC50) dose was found to be ineffective. APDTC did not induce L-type Ca^{2+} channel and K^+ channel receptors to differentiate relaxation response by producing a cholinergic-adrenergic effect. We think that APDTC did not affect these channels. Further studies with the use of different doses are recommended.

Keywords: APDTC, trachea, adrenergic, cholinergic, Ca^{2+} channels, K^+ channels.

1. INTRODUCTION

Asthma is one of the most common and most often encountered diseases and generally affecting young people in developed and developing countries. Smoking, air pollution, gender, socioeconomic status, exposure to dust, smoke and gases due to occupational encountering are the factors that cause

asthma [1]. According to the Turkish Thoracic Society-Asthma and Treatment Guidelines, asthma is a disease characterized by shortness of breath, chest tightness, coughing and bronchial overactivity in the form of seizures with chronic airway inflammation and is a high cost disease [2]. It is included in the category of serious diseases that results in death if untreated [3]. Bronchodilator agents such as antagonists, methylxanthine and corticosteroid drugs are used during the treatment of asthma. Bronchodilator agents provide relaxation of bronchial smooth muscles [3]. The effect of TEA and K^+ on contractions with histamine and ACh in porcine isolated trachea were compared [4]. While neither TEA nor K^+ increased continuous depolarization with histamine (or induced by acetylcholine), released form of depolarizations were often observed in the presence of TEA. Verapamil and Ca^{+2} Krebs solution reduced histamine contractions and reduced or eliminated the effect of TEA and K^+ on histamine-induced contractions. These results suggest that different contraction mechanisms are masked by histamine and acetylcholine. It appears to be linked to mechanisms that are histamine-mediated, sensitive to TEA and high K^+ and possibly including increased Ca^{2+} translocation along the plasma membrane [4]. In vitro study in rabbit trachea smooth muscle determined that the relaxant effects of β-adrenergic receptor agonists as isoprenaline and salbutamol were caused by the activation of K^+ channels and the relaxant effects of phosphodiesterase inhibitors as theophylline and aminophylline by K^+ channels were less effective [5]. Smooth muscles are found in the structural architecture of organs such as uterus, blood vessels, intestines, trachea, bladder, stomach, penis and clitoral cavernosal sinuses. They receive neural innervation from the autononom nervous system. Hormonal and paracrine agents, autocrine and local chemical agents further control their contraction [6]. Smooth muscle is composed of cells with a diameter of 1-5 micrometers and only in 20-500 micrometers length [7]. Smooth muscles are composed of long fibers in some organs and short fibers in others [8]. The nucleus is large and at the middle in the smooth muscle. During the embryological development of smooth muscle, precursor cells are not fused and they develop separately in a single nucleus center [9]. Muscle fibers can be in longitudinal, circular and oblique forms [10]. They contain actin and myosin filaments as well as intermediate filaments such as desmin, vimentin and filamin. The adjacent smooth muscle cells are connected by gap junctions. The sarcoplasmic reticulum is the site where Ca is stored in the smooth muscle cell. The smooth muscle cell has both T and L channels [3]. Smooth muscles contain thrompomyosin but lacks troponin. The numbers of mitochondria are low, so glycolysis is used most of the time [11].

The trachea is the organ located after the larynx that transmits air to the bronchi [12]. Asthma is a chronic inflammatory disease of the airways, where mast cells, eosinophils and T lymphocytes and many other cells playing a role in the disease [13]. A neural modulator system composed of various neuropeptides released as cotransmitters from the autonomic nervous system is called NANC System. i-NANC system in human airways is the only neural expansion pathway that relaxes the airway smooth muscle because there is no functional sympathetic innervation. Adrenergic antagonists can not interfere with this system [14]. Excitatory Nonadrenergic-Noncholinergic System (e-NANC) in some species produces bronchoconstrictor effects that cannot be inhibited by atropine, but it can be inhibited by the breakdown of emotional neuropeptides through capsaicin and tachykinin antagonists. The response is produced via secretion of tachykines released from the sensory nerves of the airway [14].

Nitric oxide (NO) acts as an expander of the airways and is the neurotransmitter of the expanding nerves in the human airways. On the other hand, NO increase in plasma exudation may cause harmful effects on the respiratory tract by vasodilation and also cause inflammatory responses during asthma [15]. NO is a highly lipophilic molecule that can easily pass through the membranes. Nitric oxide sensor-I (NOS-I) is found in neural tissues and Nitric oxide sensor-III (NOS-III) is found in vascular

endothelium. Nitric oxide sensor-II (NOS-II) or Inhibitory Nitric oxide sensor (i-NOS) is found in the airway epithelium and various other cells and is not Ca-dependent. Once synthesized, NO rapidly migrates to target tissues and activates the guanylate cyclase enzyme in the cells and increases the "cyclic guanosine monophosphate" ratio, which provides smooth muscle contraction, by acting as a neurotransmitter of i-NANC neurons with the resulting effect within the smooth muscle cell. There are three neural mechanisms of the airways that cause bronchoconstriction as cholinergic (acetyl choline), α-adrenergic (norepinephrine) and e-NANC (neurokinin) systems. On the other hand, β adrenergic (epinephrine) and iNANC as vasoactive intestinal peptide (VIP) and NO are the mechanisms that cause bronchodilatation. The i-NANC neural system is actively present intermittently in the proximal airways, and this is the bronchodilator system found in human airways. NO in asthma is predominantly associated with lower respiratory tract and increased NOS-II activation. NO rates may be useful in differentiating asthma from other causes of chronic coughing [16]. Transient receptor potential (TRP) channel subtypes are TRP cononcial (TRPC) with seven different sub-channel groups, TRP vanilloid (TRPV) with six different sub-channels, TRP polycystein (TRPP) with three different sub-channels, TRP mucolipin (TRPML) with three different sub-channels, TRP ankyrin (TRPA) with one different sub-channel and TRP melastatin (TRPM) with eight different sub-channel groups. The majority of these ion channels are non-selective ion channels that are simultaneously permeable to Na^{+} and Ca^{+2}. In addition, there are twenty-eight types of TRP channels in mammals and they can be grouped in six sub-families [17, 18].

Atropine is a competitive antagonist of muscarinic (M) receptors of ACh in the parasympathetic system. Atropine receptors have five subtypes called M1, M2, M3, M4 and M5 and they show postsynaptic localization in various effector organs and ganglia, or located at the ends of cholinergic and adrenergic nerves [19]. The Ca^{2+} channels affect the passage of calcium ions into the cytoplasm through specific pores opened in response to depolarization of the cell membrane. The introduction of calcium into the cell produces a depolarizing effect, and the accumulation of calcium in cytoplasm increases the secretion of hormones and neurotransmitters and is a chemical activator for muscle contraction and various other calcium-sensitive interactions [20]. Nifedipine is a selective relaxant [21]. Adrenergic receptors are divided into two groups as alpha adrenergic receptors and beta adrenergic receptors. Alpha adrenergic receptors are divided into two groups as alpha 1 and alpha 2. Beta adrenergic receptors are divided into three groups as beta1, beta 2 and beta 3 receptors [22]. Phentolamine is a alpha-adrenergic blocker directing smooth muscle relaxation and it is a imidozine derivative with cholinometric, histaminic and sympathomic activity. Phentolamine and other alpha-adrenergic receptors show competitive effects and provide mild intrinsic activity [23]. Phentolamine has an equal affinity for alpha 1 and alpha 2 receptors. Phentolamine has agonistic activity on musacarinic, histamine H1 and H2 receptors. Phentolamine has a relaxing effect on vascular smooth muscles [24]. Propranolol inhibits all beta adrenergic effects, but does not block alpha adrenergic receptors [24]. Many potassium channels of different molecular structure help regulate potassium conductivity in smooth muscle cells [25]. The potassium channels are blocked by Tetraethyl ammonium, which is supplied externally. Sensitivity to tetraethyl ammonium is different in different types of potassium channels. Tetraethyl ammonium inhibits the return of voltage-dependent potassium channel inhibitor repolarization [26]. Research on how APDTC functions are regulated in humans and animals is insufficient. Therefore, the aim of this study was to investigate the mechanism of action of APDTC in the rat smooth muscle of the trachea by using some agonists and blocker chemical substances with a good designed experimental procedure.

JSR A
Journal of Scientific Reports

2. MATERIALS AND METHODS

70 male Saki Yenilli Wistar albino (200-250 g) male rats (6-7 months old) were obtained from The Experimental Animals Production Center. The study was approved by Dumlupınar University Animal Experiments Local Ethics Committee (HAYDEK) Desicion No. 2015.12.04. Wistar albino male rats allocated from 6-7 months old Saki Yenilli Experimental Animal Production Facility weighing 200-250 grams were grouped according to the chemicals used and placed in cages.

All the experimental groups and procedures are presented first as organ bath preperation and experimental procedures: Male Wistar albino rats were weighed sequentially, euthanized by cervical dislocation, and the neck was opened from larynx to bifurcation, and the trachea was isolated without any damage. The trachea was sampled and placed in a Petri dish with cold Krebs Henseleit physiological solution. Physiological solution of Krebs Henseleit was weighed and then the other chemicals such as $MgSO_4 \cdot 7H_2O$ (0.28 g), KH_2PO_4 (0.32 g), KCl (0.72 g), NaCl (13.8 g), Glucose (10 g), $NaHCO_3$ (4.2 g)), $CaCl_2 \cdot 2H_2O$ (0.56 g) were weighted and they were dissolved in other beakers with the help of some water. Then the $CaCl_2 \cdot 2H_2O$ solution was added slowly to the solution containing the other chemicals and was added up to 2 liters. After cleavage of the connective tissues around the trachea, the trachea was isolated in the shape of ring. Organ weight was determined by precision scale. For the trachea placed in the isolated organ bath, the temperature of the organ bath was stabilized at 37 °C. 95% O_2-5% CO_2 gas mixture was introduced into the isolated organ bath and the viability of the organ was maintained by providing oxygenation. The same conditions were applied to each group. One end of the trachea was placed in the organ bath and the other end to the transducer and 1 gram of tension was applied to it and the responses were recorded with the concentrator recorder device. APDTC was weighed as 0.016429 grams. It was dissolved with water, made up to 10 ml and a 10^{-2} M solution was obtained. 1 ml of this solution was taken and completed to 10 ml and 10^{-3} M stock solution was prepared, and then the stock solution was diluted to 1.5×10^{-6}. 0.031781 grams of phentolamine were weighed. It was dissolved with water, made up to 10 ml and a 10^{-2} M stock solution was prepared. The stock solution was then diluted to 10^{-3}. 0.02958 grams of propranolol was weighed. It was dissolved in some ethanol, made up to 10 ml and 10^{-2} M stock solution was prepared and this stock solution was diluted to 10^{-4}. 0.028938 grams of atropine was weighed. It was dissolved in some ethanol, made up to 10 ml and 10^{-2} M stock solution was prepared and this stock solution was diluted to 10^{-4}. 0.16571 grams of tetraethyl ammonium was weighed. It was dissolved in water, made up to 10 ml and 10^{-1} M solution was obtained. 0.034634 grams of nifedipine were weighed. It was dissolved in water, made up to 10 ml and 10^{-2} M stock solution was prepared and then the stock solution was diluted to 10^{-4}. 0.018166 grams of ACh was weighed. It was dissolved in water, 10^{-2} M stock solution was prepared after completed to 10 ml and stock solution was diluted to 10^{-4}. 0.4473 grams of KCl was weighed. It was dissolved in water, made up to 10 ml and a 6×10^{-1} M solution was obtained.

Experimental protocol for rat trachea smooth muscle contraction and relaxation response measurements are presented afterward as follow: 70 Wistar albino male rats were used. The rats were divided into seven groups of containing 10 animals each, respectively. Separate protocols were applied to the rats divided into groups. It was equilibrated using a crebs solution at every 15 minutes for 60 minutes. The viability of the trachea was controlled by means of KCl solution. It was precontracted using acetylcholine. The groups were as follow: Group 1 was used as the control group and 10 animals were used. Contraction and relaxation were examined. $1.5x10^{-6}$ M APDTC was used (10 animals). In Group 2, cholinergic receptors was inhibited by cholinergic receptor antagonist

JSR A
Journal of Scientific Reports

atropine (10^{-6} M). Trachea responses were observed (10 animals). In Group 3, 10^{-5} M alpha adrenoceptors were inhibited by alpha adrenoreceptor antagonist phentolamine and trachea response was examined (10 animals). The 10^{-6} M propranolol, the beta adreno-receptor antagonist, was given to the 4th group to prevent the effect of beta-adreno-receptors. Trachea responses were observed (10 animals). In Group 5, 10^{-6} M potassium channel blocker nifedipine blocked the potassium channel. Trachea responses were observed (10 animals). In the Group 6, L-type Calcium channels were blocked with 10^{-3} M TEA, an L-type calcium channel blocker (10 animals). In Group 7, the 10^{-5} M non-selective alpha adrenoceptor antagonist phentolamine, 10^{-6} M beta adrenoceptor antagonist propranolol and 10^{-6} M cholinergic receptor antagonist atropine were administered together for adrenergic receptor and cholinergic receptor blockage. The responses of the trachea were observed (10 animals).

In our experiment, after the preparation stage of our trachea smooth muscle strips, we performed an isolated organ bath application to maintain vitality after one gram stretching process. It was left in a Krebs solution for fifteen minutes. The smooth muscle strip was then allowed to equilibrate for forty-five minutes. Afterward, the vitality of tracheal smooth muscle strips were evaluated with 6×10^{-2} M KCl. After waiting five minutes, the trachea smooth muscle strip was cleaned in the organ bath system to get rid off the effect of KCl by repeating three times. By waiting for ten minutes, 10^{-6} M ACh was applied to the krebs solution to maintain anterior muscle tension. Waiting for ten minutes, 1.5×10^{-6} M APDTC to the control group, 10^{-6} M atropine to the second group, 10^{-5} M phentolamine to the third group, 10^{-6} M propranolol to the fourth group, 10^{-6} M nifedipine to the fifth group, 10^{-3} M TEA to the sixth group and 10^{-5} M phentolamine+10^{-6} M propranolol+10^{-6} M atropine to the seventh group were applied. Fifteen minutes later, 1.5×10^{-6} M pyrrolidine dithiocarbamate [3] was administered to the other groups except the control group. The obtained data were expressed as mean±standard error and evaluated by applying Kruskal Wallis and Mann-Whitney U tests and then $p<0.05$ values were considered statistically significant and effective and $p>0.05$ values were considered statistically not significant and uneffective.

3. RESULTS

In this applied organ bath system research, seven groups were included as follows: control, atropine, phentolamine, propranolol, nifedipine, TEA, and fentolamine+propranolol+atropine (mix) groups (Table 1 and Figure 1). We evaluated the effects of APDTC in the presence and absence of an antagonist or blocker on the trachea smooth muscle strip with the application of 10^{-4} M Acetylcholine. Every antagonist and blocker interaction with each other were tested in our designed experiment.

Table 1. Evaluation of differences between experimental groups of APDTC.

Groups	Control	Atropine	Phentolamine	Propranolol	Nifedipine	TEA	Mix
Control	-	0.762	0.650	0.940	0.762	0.597	0.070
Atropine	0.762	-	0.496	0.762	0.496	0.545	0.034
Phentolamine	0.650	0.496	-	0.450	0.821	0.762	0.199
Propranolol	0.940	0.762	0.450	-	0.473	0.597	0.023
Nifedipine	0.762	0.496	0.821	0.473	-	0.880	0.162
TEA	0.597	0.545	0.762	0.597	0.880	-	0.082
Mix	0.070	0.034	0.199	0.023	0.162	0.082	-

JSR A
Journal of Scientific Reports

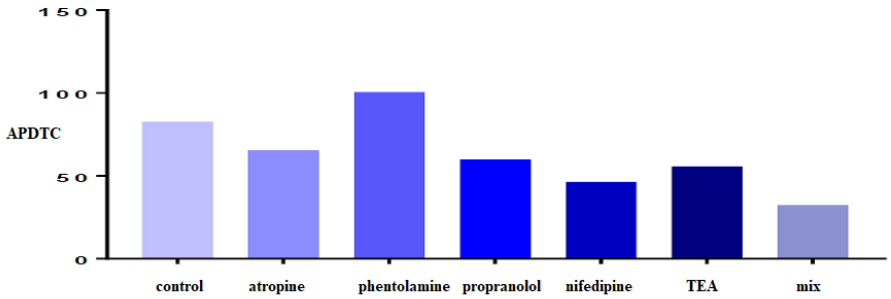

Figure 1. Evaluation of the effects of APDTC in the presence and absence of an antagonist or blocker on the trachea smooth muscle strip with the application of 10^{-4} M Acetylcholine.

There was a statistically significant difference on the tracheal smooth muscle strip between ACh applied precontraction responses and atropine-treated APDTC responses ($p<0.05$). The relaxation response of APDTC with atropine was observed on the contraction of the tracheal muscle with acetylcholine. However, no statistically significant difference was found between the control group and atropine group ($p>0.05$). It is revealed that APDTC relaxation responses on the contracted tracheal smooth muscle strip with ACh were not affected by atropine ($p>0.05$). There was a statistically significant difference between the atropine and propranolol group and the 10^{-6} M dose atropine applied group on the contractions treated with ACh mix group ($p<0.05$). No statistically significant difference was observed with atropine on contractions induced by ACh in the 10^{-6} M propranolol dose applied group ($p>0.05$) (Table 2 and Figure 2).

Table 2. Evaluation of the effect of APDTC on trachea smooth muscle by atropine treatment.

Atropine	**ACh**	**Antagonist**	**APDTC**
ACh	-	0.015	0.015
Antagonist	0.015	-	0.070
APDTC	0.015	0.070	-

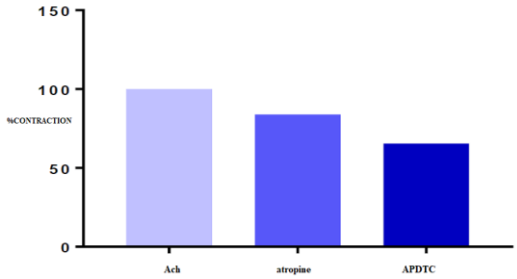

Figure 2. Evaluation of the effect of APDTC in the presence of atropine and atropine on the contraction of the tracheal smooth muscle strip treated with acetylcholine.

JSR A
Journal of Scientific Reports

There was a statistically significant difference between APDTC responses and ACh precontraction responses with phentolamine treatment in trachea smooth muscle ($p<0.05$). The contraction response of APDTC were formed in the tracheal smooth muscle strip contracted with ACh and then phentolamine treatment. However, no statistically significant difference was found between the control group and the group under phentolamine intervention. APDTC to the relaxation response to ACh contracted trachea smooth muscle strip with phentolamine application had no effect ($p>0.05$) (Table 3 and Figure 3).

Table 3. Evaluation of the comparison with the phentolamine only/phentolamine with APDTC administration.

Phentolamine	ACh	Antagonist	APDTC
ACh	-	0.015	0.015
Antagonist	0.015	-	0.406
APDTC	0.015	0.406	-

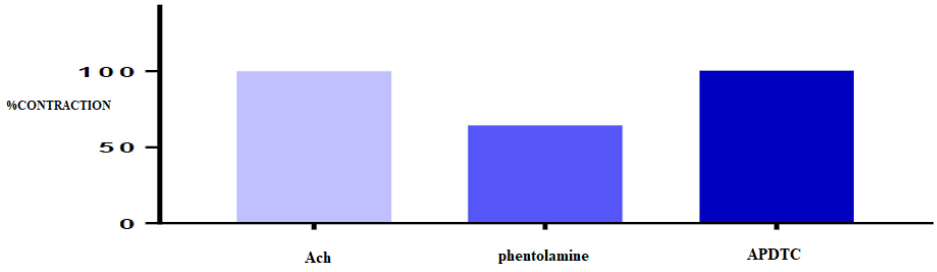

Figure 3. Evaluation of the effect of APDTC in the presence of phentolamine and phentolamine only on tracheal smooth muscle contracted with acetylcholine.

There was a statistically significant difference between APDTC and propranolol administration responses with precontractive responses on trachea smooth muscle treated with ACh ($p<0.05$). When propranolol was applied to the contraction formed on the tracheal smooth muscle strip with acetylcholine, the relaxation response with APDTC was observed. However, no statistically significant difference was found between the control group and the group under propranolol intervention. Propranolol did not affect the relaxation response of APDTC to Acetylcholine-contracted smooth muscle strip ($p>0.05$) (Table 4 and Figure 4).

Table 4. Evaluation of the comparison of Propranolol only/Propranolol administration with APDTC.

Propranolol	ACh	Antagonist	APDTC
ACh	-	0.001	0.004
Antagonist	0.001	-	0.705
APDTC	0.004	0.705	-

JSR A
Journal of Scientific Reports

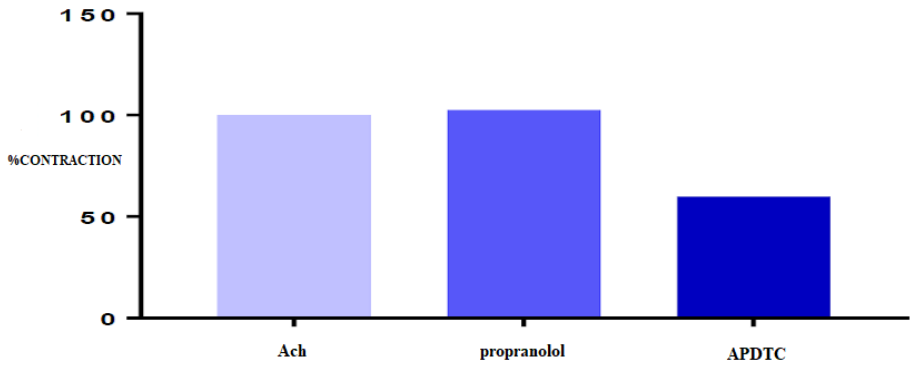

Figure 4. Evaluation of the effect of APDTC by applying propranolol only/propranolol on the contraction of tracheal smooth muscle strip where ACh is applied.

A statistically significant difference was found between the responses of APDTC by the application of nifedipine with the precontraction responses generated with ACh on the tracheal smooth muscle strip ($p<0.05$). Nifedipine applied to the contractions created in tracheal tissue with ACh has created a contraction response of APDTC. However, no statistically significant difference was found between the control group and the group under nifedipine intervention. Nifedipine did not affect the relaxation responses of acetylcholine-contracted tracheal smooth muscle strip of APDTC ($p>0.05$) (Table 5 and Figure 5).

Table 5. Evaluation of Nifedipine only/Nifedipine treated APDTC comparison.

Nifedipine	**ACh**	**Antagonist**	**APDTC**
ACh	-	0.001	0.001
Antagonist	0.001	-	0.940
APDTC	0.001	0.940	-

JSR A
Journal of Scientific Reports

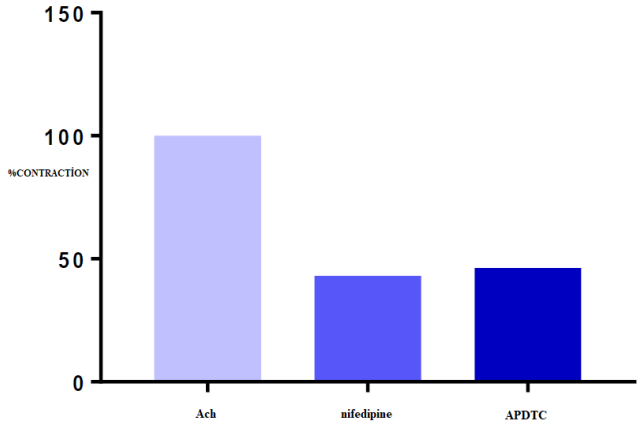

Figure 5. Evaluation of APDTC effect on tracheal smooth muscle strip with nifedipine treatment.

A statistically significant difference was found between precontraction responses with ACh treated tracheal smooth muscle strip and APDTC responses under TEA intervention ($p<0.05$). APDTC contraction response has occurred with the application of TEA on the contraction created in the trachea muscle strip with acetylcholine. However, there was no statistically significant difference between the control group and the group under TEA intervention. APDTC did not change the relaxation responses of the tracheal smooth muscle strip that was contracted with ACh by TEA administration ($p>0.05$) (Table 6 and Figure.6).

Table 6. Evaluation of APDTC in TEA only/with TEA application.

TEA	**ACh**	**Antagonist**	**APDTC**
ACh	-	0.001	0.015
Antagonist	0.001	-	0.151
APDTC	0.015	0.151	-

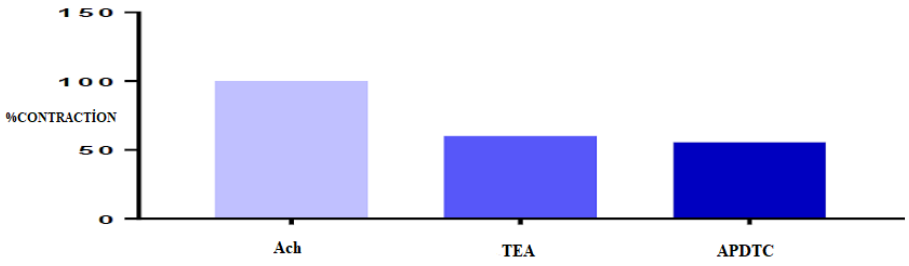

Figure 6. Assessment of the effect of APDTC with treatment of TEA only/TEA on trachea smooth muscle strip contracted with acetylcholine.

JSR A
Journal of Scientific Reports

A statistically significant difference was found between responses formed by contracting tracheal smooth muscle strip with ACh and responses to APDTC with administration of phentolamine+propranolol+atropine ($p<0.05$). APDTC relaxation response has occurred by applying phentolamine+propranolol+atropine on the trachea smooth muscle strip contraction treated with acetylcholine. However, the relaxation occurred statistically between the contraction response caused by phentolamine+propranolol+atropine and with the application of APDTC ($p<0.05$). APDTC did not change relaxation responses on the tracheal smooth muscle strip contracted with ACh with the phentolamine+propranolol+atropine ($p>0.05$) (Table 7 and Figure 7).

Table 7. Evaluation of comparison of APDTC when Mix only/Mix is applied.

Mix	**ACh**	**Antagonist**	**APDTC**
ACh	-	0.419	0.001
Antagonist	0.419	-	0.004
APDTC	0.001	0.004	-

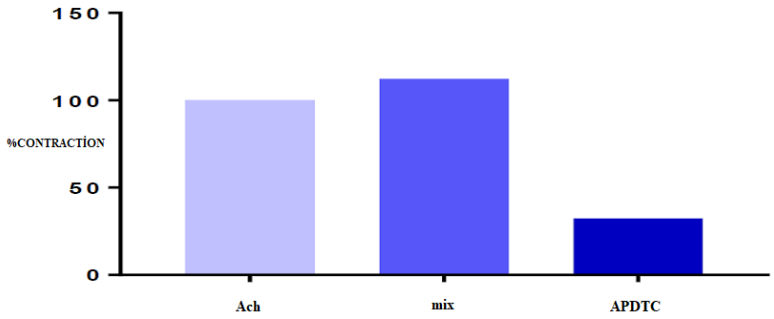

Figure 7. Assessment of the effect of APDTC by applying mix only and with mix on tracheal smooth muscle strip contraction with acetylcholine.

4. DISCUSSION AND CONCLUSION

In this study, the contraction was created by ACh treatment on the trachea smooth muscle strip and then KCl, acetylcholine, APDTC, atropine, phentolamine, propranolol, nifedipine and TEA interventions were made. The effecting function of APDTC on the tracheal smooth muscle strip was evaluated with organ bath application since the evidence-based APDTC mechanism for the relaxation of the trachea smooth muscle strip was not fully examined within previous studies. In this study, the effecting functions of APDTC in 7 designed different groups (control, atropine, phentolamine, propranolol, nifedipine, TEA and phentolamine+propranolol+atropine) were evaluated to find out whether some channels and receptors were used or not on the rat tracheal smooth muscle strip with ACh application. A study investigated the roles of NF-κB in lung injury initiated by single lung ventilation by treating rats with NF-κB-specific inhibitor PDTC, and then the NF-κB pathway was activated in the process after lung injury and the suppression of the NF-κB pathway prevented the development of lung damage from different routes [27]. It also affected the respiratory functions of APDTC [27]. A research reported that a decrease in smooth muscle contractions in colitis rat colon

stimulated with trinitrobenzene sulfonic acid (TNBS) can be attributed to the decreased activity of the L type Ca^{+2} channel. In this context, they concluded that L-type Ca^{+2} channel dysfunction can be mediated by NF-κB related pathways [28]. We discovered that $1.5x10^{-6}$ M APDTC produced a relaxation response in the tracheal smooth muscle.

There is a statistically significant difference between the precontraction responses with ACh and the responses of APDTC with atropine treatment in tracheal smooth muscle. The relaxation response to APDTC with the application of atropine on the contraction created with ACh in the tracheal smooth muscle strip. However, there was no statistically significant difference between the control group and the group that received atropine. APDTC replaced the relaxation responses in the tracheal smooth muscle strip contracted with ACh with a nonselective muscarinic receptor antagonist atropine [29]. Atropine can be considered as an ACh competing antagonist, mostly at the cholinergic nerve endings [29]. APDTC with the dose of $1.5x10^{-6}$ M was found that it uses muscarinic-cholinergic pathways in the tracheal smooth muscle strip. In our study, a statistically significant difference was found between the precontraction response formed with ACh in the trachea smooth muscle strip and the responses of APDTC when phentolamine was administered. The contraction response of APDTC was shown by the intervention of phentolamine on the contraction created in the trachea smooth muscle strip with acetylcholine. However, no statistically significant difference was found between the control group and the group in the presence of phentolamine. Phentolamine has changed the reflexation responses of tracheal smooth muscle strip contracted with ACh by APDTC. With the intervention of phentolamine, the relaxation response of APDTC has occurred.

If glibenclamide or phentolamine try to block the K^+ channels opened by cromakalim, such channels are not the same as those having trachealis plasmalemia with their strong rectifying behavior [30]. It has been concluded that each of the glibenclamide and phentolamine provides a selective contrast to the relaxant effect of cromakalim in the Guinea pig trachealis [30]. The effect of fentolamine is not related to the blockade of the α1 or α2 adrenoceptors. However, they stated that phentolamine provided APDTC to cause relief of relaxation. In this context, they stated that APDTC can use some of the α-adrenergic receptors [30]. In our study, a statistically significant difference was found between the precontraction responses with ACh in the trachea smooth muscle strip and the responses of APDTC in the intervention of propranolol. APDTC's relaxation response in the intervention of propranolol on the contraction created with ACh in the tracheal smooth muscle strip. However, no statistically significant difference was found between the control group and the propranolol group. Propranolol did not affect the relaxation responses of APDTC in the tracheal smooth muscle strip contracted with acetylcholine. The α–adrenergic blocker Propranolol is a non-selective beta adrenergic receptor blocker. It blocks competitively with both β1 and β2 receptors [24]. However, the blocking of β-adrenergic receptors with APDTC by propranolol did not increase the relaxation effect of APDTC. As a result, we can say that APDTC has its effect through these receptors. Propranolol did not affect relaxation response of APDTC's tracheal smooth muscle strip contracted with acetylcholine. There is a significant difference between the APDTC responses in the presence of nifedipine and pre-contraction responses created by ACh in the tracheal smooth muscle. APDTC showed a contraction response in the presence of nifedipine on contraction created in tracheal tissue with ACh. However, there is no significant difference between the control group and the nifedipine administered group. The nifedipine did not alter the APDTC tracheal smooth muscle relaxation responses contracted with ACh. It is understood from other studies that nifedipine directly inhibits smooth muscle contraction with the competitive inhibition of the transmembrane Ca^{+2} flow, thereby preventing the process in which pharmacological (or electrical) stimulation is converted into mechanical contraction. The failure of nifedipine to completely eliminate all restrictions in our experiments may result from the

secretion of histamine-induced Ca^{+2} stores used nifedipine or unaffected by calcium channel blocker, and nifedipine inhibits histamine-induced bronchoconstruction [31]. Nifedipine increased the APDTC effect even more, and blocking the channels could not change this effect. L-type calcium channels do not play a role in the mechanism of action of APDTC. There is a significant difference between the precontraction responses generated by ACh in the tracheal smooth muscle and the responses of APDTC in the presence of TEA. In the presence of TEA on contraction in tracheal tissue with ACh, APDTC showed a contraction response. However, there is no significant difference between the control group and the TEA administered group. TEA did not change APDTC's tracheal smooth muscle relaxation responses, which were contracted with ACh. It can be thought that $1.5x10^{-6}$ M dose of APDTC uses different routes other than potassium channels.

Cromakalim, an ATP-dependent K^+ channel opener, investigated for contraction mechanisms originating from Butylidenephthalide (Bdph), significantly increased basal tension due to Bdph [32]. Bdph also significantly antagonized cromakalim originated relaxation. Bdph, glibenclamide and TEA did not significantly affect the antagonistic effects against cromakalim originated relaxation. All calcium channel blockers did not affect neither basal tension nor Bdph's antagonistic effect against cromakalim [32]. In our study, it was determined that APDTC continues to relax. Blocking K^+ channels with TEA did not change the functional path of APDTC. To determine the effect of APDTC in the NANC system, 10^{-5} M phentolamine+10^{-6} M propranolol+10^{-5} M atropine (mix) were administered on the trachea smooth muscle strip. A statistically significant difference was found between ACh contraction responses in smooth muscle and the responses of APDTC in the presence of phentolamine+propranolol+atropine. APDTC created a relaxation effect in the presence of adrenergic-cholinergic receptor antagonists as mix in the tracheal smooth muscle strip contracted with acetylcholine.

In addition, the contraction effect caused by adenergic and cholinergic receptor antagonists as phentolamine+propranolol+atropine formed a statistical relaxation effect by the administration of Ammonium Pyrrolidine Dithiocarbamate. Phentolamine+propranolol+atropine did not affect the relaxation response of APDTC to tracheal smooth muscle strip contracted with acetylcholine. When our study evaluated the effects of APDTC with proven antioxidant and anti-inflammatory effects in the trachea smooth muscle strip, the relaxation response was formed by APDTC in the trachea smooth muscle strip induced by ACh but it was not found statistically significant. We are able to suggest that different doses of APDTC can be used. The EC50 dose was not effective. Adrenergic receptors, cholinergic receptors and substances that affect L-type calcium channels and potassium channels have not changed this response, and thefore we may think that APDTC does not use adrenergic receptors, cholinergic receptors, L-type calcium channels and potassium channels. On the other hand, as a result of this research, we can argue that the NANC system, which plays an important role in tracheal smooth muscle strip contraction-relaxation responses, may contribute to find out the functions of APDTC with different in vitro studies. Recently published articles were screened to see the direction of research on the subject and these are stated as pre-clinical safety evaluation of pyrrolidine dithiocarbamate [33], effects of ammonium pyrrolidine dithiocarbamate (PDTC) on osteopontin expression and autophagy in tubular cells in streptozotocin-induced diabetic nephropathy rat [34], bidirectional effects of pyrrolidine dithiocarbamate on severe acute pancreatitis in a rat model [35], effects of local anesthetics on Smooth muscle tissue in rat trachea: an in vitro study [36], niclosamide ethanolamine induces trachea relaxation and inhibits proliferation and migration of trachea smooth muscle cells [37], design, synthesis and biological evaluation of novel ring-opened cromakalim analogues with relaxant effects on vascular and respiratory smooth muscles and as stimulators of elastin synthesis [38], effect of hydroalcoholic extract of anethum graveolens L. seed on tracheal

smooth muscle contractions in male rats [39], effects of levobupivacaine on isolated rat tracheal smooth muscle [40] and bronchodilatory effect of hydrogen sulfide in rat [41]. The future research will help to solve the unknown pieces of puzzle in asthma biology.

REFERENCES

[1] Bölüm Yazarlığı: Kunter, E., (2007). Astım Epidemiyolojisi. In: Kartaloğlu Z, Kunter E (editörler). Astım. İstanbul: Mart Matbaacılık Sanatları, Bölüm Yazarlığı, ISBN: 975-8408-36-4.

[2] Derneği, T. T. (2010). Astım Tanı ve Tedavi Rehberi. Turkish Thoracic J,11, 6-60.

[3] Mercan. V., (2015). Sıçan Trakea'sı Düz Kası Kasılma-Gevşeme Yanıtları Üzerine Ammonium Pyrrolidine Dithiocarbamate, SG-Benz, Caffeic Acid Phenil Ester, Atorvastatin Kalsiyum'un etkileri. Yüksek lisans tezi, Dumlupınar üniversitesi fen bilimleri enstitüsü, Kütahya, s.1-29.

[4] Mitchell, H. W. (1987). Electromechanical effects of tetraethylammonium and K^+ on histamine-induced contraction in pig isolated tracheal smooth muscle. Lung,165(1), 129-142.

[5] Şahin, A.S., Atalık, K.E., Kılıç, M., Doğan, N. (1999).Tavşan Trachea Düz Kasında B-Adrenerjik Reseptör Agonistleri ve Fosfodiesteraz İnhibitörlerinin Gevşetici Etkilerinde K^+ -Kanallarının Rolü, Selçuk Üniversitesi Tıp Fakültesi Farmakoloji Anabilim Dalı Dergisi; 15: 173-177.

[6] Webb, R. C. (2003). Smooth muscle contraction and relaxation. Advances in physiology education, 27(4), 201-206.

[7] Guyton, A. C.and Hall, J. E. (2007). Tıbbi Fizyoloji. 11.Basım. Nobel Tıp Kitabevleri, 837, 1056-7.

[8] Akçay, M., (1971). Kas Fizyolojisi Ders Kitabı, Güven Matbaası, Ankara, s. 20-25.

[9] Terzioglu, M. and Çakar, L. (1989). Fizyoloji Ders Kitabı, Basım Atölyesi: İstanbul, s 106-111.

[10] Banli, O. and Unal, A. (1989). Fizyoloji Ders Notları. Metay Medikal Yayıncılık: Ankara, s. 38-45.

[11] Ganong, F. W.(1995). Tıbbi Fizyoloji, Barış Kitabevi, Çeviri Editörü: A. Doğan, İstanbul, s.85-121.

[12] Gökmen, F. G. (2003). Sistematik anatomi. İzmir, İzmir Güven Kitabevi, 67-197.

[13] Aydilek, R., Kartaloğlu,Z., Taşkapan, O., Işitmangil, G., Kunter, E., Küçükardalı Y. and Günen, H. (2007). Astım, Ankara; Ofset Hazırlık, s 1-191.

[14] Kartaloğlu, Z., Okutan, O., (2013). Solunum sistemi fonksiyonel Değerlendirilmesi. Deomed; İstanbul, s.1-7.

[15] Barnes, P. J. (1996). NO or no NO in asthma, Thorax, 51(2), 218-220.

[16] Özkan, M. Yüksekol İ. (2003). Nitrik oksit ve akciğerler. *Toraks dergisi*, *4*(1), 88-94.

[17] Saygin, M., ve Naziroğlu, M. (2010) TRPM2 Katyon Kanallarının Aktivasyonunda Rol Oynayan Moleküler Mekanizmalardaki Son Gelişmeler. Journal of Experimental and Clinical Medicine, 27(2), 42-45.

[18] Özgül, C. (2015). Protein Kinaz C Aktivatörü PMA'nın TRPV1 Kanalları Üzerindeki Etkileri. Hacettepe University Journal of the Faculty of Pharmacy, s 42-73.

[19] Mahrebel, A. A. (2018). Aç farelerde atropin ve yem ile oluşan konvülssiyonlara uzun süre haloperidol verilmesinin, olanzapinin ve antiepileptiklere amitriptilin eklenmesinin etkilerinin araştırılması, s.1-32.

[20] McCleskey, E. W., Fox, A. P., Feldman, D. ve Tsien, R. W. (1986). Different types of calcium channels, Journal of Experimental Biology, 124: 177-90.

[21] Katzung, B. G., Masters, S. B. and Trevor, A. J., (2012). Basic & Clinical Pharmacology, 12. Baskı, McGraw-Hill Higher Education, s. 87, 152.

[22] Guyton, A. C. and Hall, J. E. (2013). Tıbbi Fizyoloji (çev. Yeğen, B.), 12. Baskı, Nobel Tıp Kitabevleri, s. 91, 307, 308, 731, 773.

[23] DiPalma, J. R. (1986).Temel Tıp Farmakolojisi. Nobel Tıp Kitabevi, s.248-310.

[24] Bökesoy, T. A., Çakıcı, İ. and Melli, M. (2000). Farmakoloji Ders Kitabı, Ankara: Gazi Kitabevi Yayınları, s. 46, 165.

[25] Thorneloe, K.S. and Nelson, M. T. (2005). Ion channels in smooth muscle: regulators of intracellular calcium and contractility, Canadian Journal of Physiology and Pharmacology, 83: 215–242.

[26] Bisset, D. and Chung, S. H. (2008) .Efficacy of external tetraethylammonium block of the KcsA potassium channel: Molecular and Brownian dynamics studies, Biochimica et Biophysica Acta (BBA) -Biomembranes, 1778(10): 2273-82.

[27] Pan, W. Z., Du, J., Zhang, L. Y. and Ma, J. H., (2018). The roles of NF-kB in the developpment of lung injury after one-lung ventilation, European Review for Medical and Pharmacological Sciences, 22(21): 7414-7422.

[28] Kinoshita, K., Sato, K., Hori, M., Ozaki, H. and Karaki, H. (2003). Decrease in activity of smooth muscle L-type Ca^{2+} channels and its reversal by NF-κB inhibitors in Crohn's colitis model. American Journal of Physiology-Gastrointestinal and Liver Physiology, 285(3): G483-G493.

[29] Marshall, P. B. (1955). Antagonism of acetylcholine by (+) and (-) hyoscyamine. British Journal of Pharmacology,10(3), 354-355.

[30] Murray, M. A., Boyle, J. P. and Small, R. C. (1989). Cromakalim induced relaxation of guinea pig isolated trachealis: antagonism by glibenclamide and by phentolamine. British journal of pharmacology, 98(3), 865-874.

[31] Barnes, P. J. (1985). Clinical studies with calcium antagonists in asthma. British journal of clinical pharmacology, 20(S2), 289S-298S.

[32] Hsu, H. T., Yang, Y. L., Chen, W. C., Chen, C. M., and Ko, W. C. (2014). Butylidenephthalide blocks potassium channels and enhances basal tension in isolated guinea-pig trachea. BioMed research international, s.1-7.

[33] Chabicovsky, M., Prieschl-Grassauer, E., Seipelt, J., Muster, T., H. J. Szolar, O., Hebar, A. and Doblhoff-Dier, O. (2010). Pre-Clinical Safety Evaluation of Pyrrolidine Dithiocarbamate. Basic & Clinical Pharmacology & Toxicology, 107, 758–767. Doi: 10.1111/j.1742-7843.2010.00573.x

[34] Gao S, Jia JY, Yan TK, Yu YM, Shang WY, Wei L, Zheng ZF, Fang P, Chang BC, Lin S. (2016). Effects of ammonium pyrrolidine dithiocarbamate (PDTC) on osteopontin expression and autophagy in tubular cells in streptozotocin-induced diabetic nephropathy rat. Chinese Journal of Medical Science, 96(44): 3590-3595. DOI: 10.3760/cma.j.issn.0376-2491.2016.44.012

[35] Yang, H., Ma, S. C., Guo, Y., Cui, D. L., and Yao, J. F. (2019). Bidirectional Effects of Pyrrolidine Dithiocarbamate on Severe Acute Pancreatitis in a Rat Model. Dose-Response:An International Journal, s.1-7. DOI: 10.1177/1559325819825905

[36] Erdem, Ali Onur; Erel, Varlık K.; O., Özlem Girit; Erdoğan, Hasan; Özkısacık, Sezen; Yazıcı, Mesut. (2020). Effects of Local Anesthetics on Smooth Muscle Tissue in Rat Trachea: An In Vitro Study. Turk Toraks Dergisi / Turkish Thoracic Journal. Jul2020, Vol. 21 Issue 4, p223-227. 5p. DOI: 10.5152/TurkThoracJ.2019.19016.

[37] Wei, Yuan-Yuan; Xuan, Xiu-Chen; Zhang, Xi-Yue; Guo, Ting-Ting; Dong, De-Li. (2019). Niclosamide ethanolamine induces trachea relaxation and inhibits proliferation and migration of trachea smooth muscle cells. European Journal of Pharmacology. 853:229-235. DOI: 10.1016/j.ejphar.2019.03.047.

[38] Bouhedja, Mourad; Peres, Basile; Fhayli, Wassim; Ghandour, Zeinab; Boumendjel, Ahcène; Faury, Gilles; Khelili, Smail. (2018). Design, synthesis and biological evaluation of novel ring-opened cromakalim analogues with relaxant effects on vascular and respiratory smooth muscles and as stimulators of elastin synthesis. European Journal of Medicinal Chemistry. 144:774-796. DOI: 10.1016/j.ejmech.2017.12.071.

[39] Parastoo Jafarzade, Seyyed Mohammad Mohseni Mehran, Hassan Moladoust, Mohammad Reza Norasfard, Ahmad Ghorbani, Mahmood Abedinzade. (2018). Effect of Hydroalcoholic Extract of Anethum graveolens L. Seed on Tracheal Smooth Muscle Contractions in Male Rats. Journal of Mazandaran University of Medical Sciences (JMUMS). Vol. 28 Issue 160, p146-150.

[40] Chang, Hung-Chi; Chen, Shin-Yan; Huang, Yu-Feng; Liu, Feng-Lin; Cherng, Yih-Giun; Wang, Hsing-Won. (2015). Effects of levobupivacaine on isolated rat tracheal smooth muscle. Journal of Anesthesia. Vol. 29 Issue 5, p809-812. DOI: 10.1007/s00540-015-2026-8.

[41] Gharib-Naseri, Mohammad Kazem; Saberi, Shadan; Mard, Seyyed Ali; Latifi, Seyyed Mahmood. (2012). Bronchodilatory Effect of Hydrogen Sulfide in Rat. Iranian Journal of Basic Medical Sciences. Vol. 15 Issue 4, p907-915.

ATTACHMENTS

APPENDIX 1. Experimental Animals Local Ethics Committee Approval Certificate

T.C.
DUMLUPINAR ÜNİVERSİTESİ
HAYVAN DENEYLERİ YEREL ETİK KURULU
ARAŞTIRMA BAŞVURUSU ONAYI

BAŞVURU BİLGİLERİ	ARAŞTIRMANIN ADI	Sıçan trakea düz kası kasılma gevşeme cevapları üzerine Ammonium Pyrrolidine Dithiocarbamate'nın etki mekanizmasının araştırılması
	ARAŞTIRMA YÜRÜTÜCÜSÜ KURUMU	Doç.Dr.M.Kasım ÇAYCI DPÜ Fen-Edebiyat Fakültesi Genel Biyoloji ABD
	PROJE YÜRÜTÜCÜSÜ KURUMU	Doç.Dr.M.Kasım ÇAYCI DPÜ Fen-Edebiyat Fakültesi Genel Biyoloji ABD
	YARDIMCI ARAŞTIRICILAR	Doç.Dr.M.Kasım ÇAYCI Yls.Öğr.Zeynep KELEŞ Yls.Öğr.Merve AKTAŞ Yls.Öğr.Aysun ERDOĞAN Yls.Öğr.Merve ARAS
	ARAŞTIRMANIN TAHMİNİ SÜRESİ	12 Ay
	KULLANILACAK HAYVAN TÜRÜ VE SAYISI	Wistar Albino (E) – 70 Adet
	DESTEKLEYİCİ KURULUŞ	--

DEĞERLENDİRİLEN İLGİLİ BELGELER	Belge Adı	Tarihi
	ARAŞTIRMA BAŞVURU FORMU	16.12.2015

KARAR BİLGİLERİ	Karar No : 2015.12.06 Tarih : 23.12.2015
	Yukarıda başvuru bilgileri verilen araştırma projesi gerekçe, amaç ve yöntemler dikkate alınarak görüşüldü ve ilgili belgeler incelendi. Projenin etik açıdan uygun olduğuna, çalışmanın aşağıdaki hususlar dikkate alınarak yürütülmesine ve sorumlu araştırıcıya iletilmesine **OY BİRLİĞİ** ile karar verildi. 1) Projede herhangi bir değişiklik gerektiğinde kurulumuzdan onay alınması, 2) Projede çalışacağı bildirilen araştırıcılarda değişiklik olduğunda kurulumuzdan onay alınması, 3) Deney hayvanları üzerinde yapılacak girişimin başlangıç ve bitiş tarihinin bildirilmesi, 4) Çalışma süresinde tamamlanamaz ise ek süre talebinde bulunulması, 5) Çalışma tamamlandığında sonuç raporunun gönderilmesi

ETİK KURUL BİLGİLERİ

ÜYELER

Unvanı / Adı / Soyadı EK Üyeliği	Uzmanlık Dalı	Kurumu	İlişki (*)	İmza
Doç.Dr. Aynur GÜLCAN Başkan	Mikrobiyoloji ve Klinik Mikrobiyoloji Anabilim Dalı	Tıp Fakültesi	☐ E ■ H	
Yrd. Doç. Dr. Ahmet KOÇAK Üye	Histoloji ve Embriyoloji Anabilim Dalı	Tıp Fakültesi	☐ E ■ H	
Yrd. Doç. Dr. Sezer AKÇER Üye	Anatomi Anabilim Dalı	Tıp Fakültesi	☐ E ■ H	
Yrd. Doç. Dr. Ceylan AYADA Üye	Fizyoloji Anabilim Dalı	Tıp Fakültesi	☐ E ■ H	
Yrd.Doç. Dr. Hasan METİNEREN Üye	Ortopedi ve Travmatoloji Anabilim Dalı	Tıp Fakültesi	☐ E ■ H	
Doç.Dr. M.Kasım ÇAYCI Üye	Biyoloji Anabilim Dalı	Fen-Edebiyat Fakültesi	■ E ☐ H	
Doç.Dr. Muhammed OYLUMLU Üye	Kardiyoloji Anabilim Dalı	Tıp Fakültesi	☐ E ■ H	
Yrd. Doç. Dr. Zülfü BAYHAN Üye	Genel Cerrahi Anabilim Dalı	Tıp Fakültesi	☐ E ■ H	
Vet. HEKİM Aydın AKCILAR Üye	Veteriner HEKİM	Tıp Fakültesi DEHYUAM	☐ E ■ H	
Yrd.Doç.Dr.Ahmet Haris Selçuk ÖZEN Üye	Zooloji Anabilim Dalı	Fen-Edebiyat Fakültesi	☐ E ■ H	
Erkan ERKOL Üye			☐ E ■ H	

* Araştırma ile İlişkisi

Kütahya Dumlupınar University
Institute of Graduate Studies

Journal of Scientific
Reports-A
E-ISSN: 2687-6167
Number 45, December 2020

RESEARCH ARTICLE

THE INVESTIGATION OF THE ACTION MECHANISM OF AMMONIUM PYRROLIDINE DITHIOCARBAMATE ON RAT BLADDER SMOOTH MUSCLE CONTRACTION-RELAXATION RESPONSES

Hayri DAYIOĞLU[1], Ayhan YILMAZ[2], Aysun ERDOĞAN[3], Fatih ALAN[4] and Sinan DARCAN[5]

[1]Kütahya Dumlupınar University, Faculty of Science and Literature, Department of Biology, 43270, Kütahya, hayri.dayioglu@dpu.edu.tr, ORCID: 0000-0002-9270-8561
[2] Kütahya Dumlupınar University, Faculty of Science and Literature, Department of Biology, 43270, Kütahya, ayhan.yilmaz@dpu.edu.tr, ORCID: 0000-0003-0410-8687
[3]Kartaltepe Mah. Tıp Fakültesi Cad. No: 211, 06620 Mamak, Ankara, aysn_erdoğan@hotmail.com, ORCID: 0000-0002-4738-8132
[4]General Directorate of Presidential Protection Services, Presidential Complex, 06530, Beştepe, Ankara, fatihalan06@hotmail.com,ORCID: 0000-0002-0561-6192
[5]Kütahya Health Science University, Evliya Çelebi Campus, Tavşanlı Yolu 10. Km, 43100, Kütahya, sinan.darcan@ksbu.edu.tr, ORCID: 0000-0002-2135-4807

Received Date: 20.04.2020 *Accepted Date: 04.11.2020*

ABSTRACT

Ammonium pyrrolidine dithiocarbamate (PDTC), the specific inhibitor of NF-κB, is a thiol compound with anti-viral, anti-apoptotic, anti-inflammatory and antioxidant effects proven in many studies. There is not sufficient literature in what fashion that APDTC has produced these effects. We aimed to investigate the action mechanism of APDTC in rat bladder smooth muscle in our vitro study. In our study, 70 Wistar albino male rats were used. The rats were euthanized by cervical dislocation under the anesthesia and then abdomens were opened and bladders were isolated. After the removal of the connective tissues around the bladders, they were placed in the organ bath containing Krebs solution. KCl, ACh, APDTC, Atropine, Phentolamine, Propranolol, Nifedipine and TEA were applied to the bath with an appropriate protocol. The obtained data were evaluated with Kruskal Wallis and Mann-Whitney U tests. ACh induced bladder produced APDTC relaxation response in its own smooth muscle. Cholinergic receptor blocker Atropine, β-adrenergic receptor blocker Propranolol, L-type calcium channel blocker Nifedipine and atropine+phentolamine+propranolol mix have not changed the relaxation response that APDTC produced. In the presence of potassium channel blocker TEA, APDTC produced contraction response, but this was not a significantly important grade response. In the presence of α-adrenergic receptor blocker Phentolamine, APDTC produced significant contractile response. As a result, we think that APDTC shows its effect on rat bladder smooth muscle via α-adrenergic receptors and NANK system.

Keywords: adrenergic, APDTC, bladder, calcium channels, cholinergic, NANK system, potassium channels, TRP.

JSR A
Journal of Scientific Reports

1. INTRODUCTION

The bladder is a hollow, muscular organ that acts as a temporary reservoir for urine storage [1]. It is located inside the pelvic cavity, behind the symphysis pubis and under the peritoneum. In the male, it extends posteriorly to the rectum and in the woman, it contacts with the anterior walls of the uterus and vagina [2]. The main responsible system for bladder emptying is the parasympathetic system and acetylcholine is the main neurotransmitter in this duty [3]. Adenosine 5'-triphosphate (ATP) released in the bladder with acetyl choline (ACh) activates its specific $P2_x$ receptors. Pyrrolidine dithiocarbamate, a thiol compound derived from dithiocarbamates, has generally been described as an antioxidant [4]. KCl-treated bladder smooth muscle contractile responses were decreased, and the mechanism of action of CP (yarrow) extract and compounds was shown to be through voltage-sensitive L-type Ca^{2+} channels [5]. Silodosin has an inhibitory effect on ACh-induced contractions in the bladder, and also demonstrated that palonosetron inhibits ACh-induced in vitro bladder smooth muscle contractions [6]. Raflumilast in pig bladder neck increases endogenous H_2S production and EFS relaxation, and facilitates increased neuronal cAMP, NO and H_2S mediated bladder neck inhibitory nerve conduction following FDE4 (phosphodiesterase 4) inhibition [7]. While hexamethonium (non-specific nAChR antagonist), mesamylamine (α3β4 nAChR antagonist), dihydro-β-erythroidin (α4β2 nAChR antagonist) inhibit nicotine-mediated increase of EFS-induced contraction responses, α-bungarotoxin (α7 nAChR antagonist) partially inhibited this effect of nicotine [8]. These findings have demonstrated that EFS-induced neurogenic contractions in the rabbit urinary bladder smooth muscle lanes are mediated by purinergic and cholinergic transmissions and contribute to the therapeutic effect of nicotine on EFS-induced contractile responses of the a4β2, a3β4, and a7 subtypes of nAChRs. Stimulation of muscarinic receptors in the rat bladder induces the release of urothelial NO that inhibits detrusor contraction in the case of cystitis [9]. As a result of the present findings, it is pointed out that a muscarinic receptor other than M1 or M3 is the main mediator of this effect. Darblade et al. (2006) showed that the phasic contractions in the human detrusor are due to calcium input via L-type calcium channels, and that the BKCa and SKCa channels play an important role in regulating the phasic contractility of human detrusor smooth muscle [10].

Muscarinic receptor 5 subtypes (M1-M5) have been found in the bladder of different species, including human [11]. Although the M3 receptor is considered the most important subtype functionally fit for detrusor contraction, it is thought to have a dual effect between the activation of M3 and M2 receptors [12]. Atropine is the prototype of the antagonist that competes with acetylcholine to bind to the muscarinic-type receptor [13]. Atropine competes with ACh and other muscarinic agonists for a common binding site on the muscarinic receptor [14]. Atropine is a mixture of D and L hyosamine [15]. Atropine is highly selective for muscarinic receptors. Atropine does not distinguish between M1, M2 and M3 subgroups of muscarinic receptors [16]. Atropine relaxes the bladder detrusor smooth muscles, increases the tone of the trigone and sphincter smooth muscles, thus creating voiding difficulties [17]. Adrenergic receptors are divided into alpha adrenergic receptors and beta adrenergic receptors. Alpha adrenergic receptors are of two types: alpha1 and alpha2 receptors. Beta adrenergic receptors are divided and called as beta1, beta2 and beta3 receptors [18].

Phentolamine is the imidazoline-derived α-adrenergic receptor blocker [17]. Propranolol has equal affinity for β1 and β2 adrenergic receptors; thus, it is a non-selective β adrenergic receptor antagonist [14]. Nifedipine is a prototype of the dihydropyridine family calcium channel blockers [16] and is a uncharged hydrophobic substance [13]. Several K^+ channels with different molecular bases contribute to the regulatory base K^+ conductance in smooth muscle cells. These; voltage-gated K^+ channels (Kv),

JSR A
Journal of Scientific Reports

large conductivity Ca^{2+} activated K^+ channels (BKCa), small conductivity Ca^{2+} activated K^+ channels (SKCa), inward rectifier K^+ channels (Kir), two porous area K^+ channels (K2P), tension-dependent K^+ channels and ATP sensitive K^+ channels (KATP) [19]. Almost all potassium channels are blocked by externally supplied TEA (Tetraethyl Ammonium). However, sensitivity to TEA is different in different types of potassium channels [20]. Bladder contraction and relaxation are caused by adrenergic, cholinergic and non-adrenergic non-cholinergic (NANK) systems. NANK system and purinergic system are thought to be effective on bladder with neurotransmitters such as nitric oxide, transient receptor potential (TRP) channel, histamine, seratonin, VIP (vasoactive intestinal polypeptide), neuropeptide Y, substance P, calcitonin gene-associated peptide (CGRP), gamma amino butyric acid (GABA) and bradykinin [21]. Purinergic receptors in the cell membrane are divided into adenosine (P1) receptors and ATP receptors (P2X and P2Y receptors). The P1 and P2 receptors have various subtypes. Adenosine receptors and P2Y receptors mediate their responses through G proteins, while P2X receptors are a subfamily of ligand gated ion channels [14]. Nitric oxide (NO) is an unstable free radical gas that acts as a neurotransmitter and modulator in the central and peripheral nervous system [22]. Transient receptor potential (TRP) channels are class of ion channels characterized by variable activation mechanisms [23]. The TRP superfamily is one of the largest ion channel families and consists of several protein groups. In mammals, about 28 genes encode TRP ion channel subunits [24]. This class of ion channels known as TRPV (vaniloid), TRPC (canonical), TRPM (melastatin), TRPP (polysistin), TRPML (mucolipin) and TRPA (ankyrin) are six subtypes [25]. Pyrrolidine dithiocarbamate (PDTC) is a stable pyrrolidine derivative of dithiocarbamates [26]. Therefore, we aimed to investigate whether Ammonium Pyrrolidine Dithiocarbamate (APDTC), whose mechanism of action is not fully elucidated, blocks α-adrenergic and β-adrenergic receptors, cholinergic receptors, L-type calcium channels and potassium channels in bladder smooth muscle contraction and relaxation responses or these receptors and channels are effective in the mechanism.

2. MATERIALS AND METHODS

This study was carried out at Dumlupınar University Experimental Animal Breeding Application and Research Center and Dumlupınar University Faculty of Science and Arts Biology Department Physiology Laboratory. The study was approved by Kütahya Dumlupınar University Animal Experiments Local Ethics Committee (HADYEK) with the decision number of 2015.12.04. Animals used in the experiments obtained from Saki Yenilli Test Animals Production Center were 70 male Wistar albino rats weighing 300-350 gr and 6-7 months old. All the experimental groups and procedures are shown in Table 1, 2 and 3.

Table 1. Organ bath preparation for experimental procedures.

Steps	Procedure
1	Rats under standard conditions was kept in plastic cages with the ventilation (15 times/hour and 100% fresh air), at a humidity of 50±5%, at room temperature of 20±2°C for 12 hours night/12 hours daytime. ↓
2	Isolated organ bath was used to maintain the viability of smooth muscle strips prepared from rat bladder and to test their biological activity against active substances. ↓
3	Isolated organ bath consists of Data Acquisition analysis system (MP36, USA), Isometric transducers (Biopac, USA), Organ bath (Commat, Turkey), Water bath (WBC3044V3, May, Turkey), A double-chamber wells and O_2-CO_2 mixture tube. ↓

JSR A
Journal of Scientific Reports

4	Four wells each with a capacity of 10 ml were used in the experiments.
	↓
5	The wells are double chambers with distilled water circulation heated in the outer chambers of the water bath.
	↓
6	The inner chamber contains Krebs solution.
	↓
7	The strips prepared from the rat bladder are placed in the inner chamber and all experimental procedures are performed here.
	↓
8	Krebs solution in the chamber were gassed with a mixture of 95% O_2 and 5% CO_2 gas at the bottom of the chamber during the experiment.
	↓
9	The isometric transducer (Biopac, USA) transmits the responses of the bladder strips to the applied substance to the Data Acquisition analysis system (MP36, USA) by converting them into electrical signals.
	↓
10	These recordings were analyzed at the end of the experiment and the resulting contraction relaxation responses before and after administration of the active substance in the bladder smooth muscles were determined.
	↓
11	70 Wistar albino rats weighing 250-300 g and ages between 6-7 months were placed into cages in groups of 10.
	↓
12	There was no restriction in the maintenance and feeding conditions of the rats during the experiments.

Table 2. Test groups with used chemicals.

Group	**Addition**
1	Ammonium Pyrrolidine Dithiocarbamate group (control)
2	Cholinergic receptor antagonist (atropine)+Ammonium Pyrrolidine Dithiocarbamate
3	α adrenoreceptor antagonist (phentolamine)+Ammonium Pyrrolidine Dithiocarbamate
4	β adreneseptor antagonist (proprimanol)+Ammonium Pyrrolidine Dithiocarbamate
5	L-type Ca^{2+} channel blocker (nifedipine)+Ammonium Pyrrolidine Dithiocarbamate
6	K^+ channel blocker (tetraethylammonium)+Ammonium Pyrrolidine Dithiocarbamate
7	Both adrenergic and cholinegic receptor antagonist (phentolamine+propranol+atropine)+Ammonium Pyrrolidine Dithiocarbamate

JSR A
Journal of Scientific Reports

Table 3. Experimental protocol for rat bladder smooth muscle contraction and relaxation response measurements.

Steps	Experiment
1	Rats were euthanized by cervical dislocation method.
	↓
2	The abdomen was opened from the median line and the bladder was removed and taken to the petri dish containing Krebs Henseleit solution.
	↓
3	Connective tissues around the bladder were removed.
	↓
4	The bladder was then opened with a longitudinal incision from the neck to the top.
	↓
5	The bladder was sectioned 8 mm in length and 2 mm in width and bladder strips were prepared.
	↓
	The prepared strips were tied with ropes.
6	↓
	The bladder smooth muscle strips were inserted into the organ bath having a temperature of 37°C and a supplied gas mixture of 95% O_2 and 5% CO_2 with Krebs solution by attaching to the transducer with steel hooks at the upper and lower ends.
7	↓
	Bladder strips suspended in the isolated organ bath were stabilized for 45 minutes by washing with a Kreps solution every 15 minutes by applying 1 g of tension.
8	↓
	After the equilibration period, viability of the organs was tested with 6×10^{-2} M KCl.
9	↓
	After waiting 5 minutes, KCl was removed from the organ by washing 3 times in a row with Krebs solution.
	↓
10	After 10 minutes, 10^{-6} M Ach was given to the bath for pre-contraction.
	↓
11	After 10 min, the groups have received as follows: 2.5×10^{-5} M APDTC to the control group, 10^{-6} M atropine to the 2nd group, 10^{-5} M phentolamine to the 3rd group, 10^{-6} M propranolol to the 4th group, 10^{-6} M nifedipine to the 5th group, 10^{-3} M tetraethylammonium to the 6th group and 10^{-5} M phentolamine+10^{-6} M propranolol+10^{-6} M atropine to 7th group. Then, 2.5×10^{-5}M APDTC was applied to all groups except control group after 15 minutes.
12	↓
	The data obtained from the experiments were evaluated by Kruskal Wallis and Mann-Whitney U tests. $p < 0.05$ values was considered statistically significant.
13	

Bath recording lasted 1 hour 43 minutes. To compare, the phenylephrine and antagonist agent range was used, and then the antagonist PDTC range. The calculation was performed as follows. When phenylephrine is 100, % value was calculated by establishing the ratio of what would be the antagonist and what would be APDTC. Simultaneous experiments were carried out in four baths. SPSS program was used for statistical analysis. When statistical analysis was made in SPSS, both standard error and standard deviation were calculated and used in statistical processing. We drew the graphics according to our SPSS results in excel files. We also drew according to bladder

JSR A
Journal of Scientific Reports

phenylephrine values in the 100 file. We created p-p values according to this file. First we found the p-p values. Then we calculated how the drugs affected when the contraction was 100%. Then, we set the proportion to compare them with phenylephrine, such as what is the value of atropine when phenylephrine is 100. It also gave us statistical results if there were any significant results. The exact sig. or asymp. sig. from the mann-whitney test results made us decide whether the difference is meaningful or meaningless. The data obtained from the experiments were evaluated by applying mann-whitney u and kruskal wallis tests. $p<0.05$ values were considered statistically significant.

Figure 1. Rat bladder.

3. RESULTS

In our study, there are seven different groups as control, atropine, phentolamine, propranolol, nifedipine, tetraethyl ammonium and phentolamine+propranolol+atropine (Mix). Contraction-relaxation responses of 10^{-4} M ACh treated bladder smooth muscles against ammonium pyrrolidine dithiocarbamate in the presence and absence of antagonists or blockers were investigated in the groups (Table 4.).

Table 4. Comparison of APDTC between groups.

Groups	Control	Atropine	Phentolamine	Propranolol	Nifedipine	TEA	Mix
Control	-	0.096	0.008	0.049	0.000	0.940	0.000
Atropine	0.096	-	0.003	0.821	0.002	0.070	0.049
Phentolamine	0.008	0.003	-	0.000	0.000	0.010	0.000
Propranolol	0.049	0.821	0.000	-	0.005	0.041	0.082
Nifedipine	0.000	0.002	0.000	0.005	-	0.041	0.049
TEA	0.940	0.070	0.010	0.041	0.000	-	0.001
Mix	0.000	0.049	0.000	0.082	0.049	0.001	-

There was a statistically significant difference ($p <0.05$) on the ACh-induced contractions between the effect of atropine in the 10^{-6} M dose treated group and the groups of phentolamine, nifedipine and mix. It was found that there was a statistically significant difference ($p <0.05$) between the effect of phentolamine treated group with the 10^{-5} M dose and all other groups on the ACh-induced contractions. It was found that there was a statistically significant difference ($p<0.05$) between the effect of propranolol treated group with the 10^{-6} M dose and the control, phentolamine, nifedipine and

TEA groups on the ACh-induced contractions. It was found that there was a statistically significant difference ($p < 0.05$) between the effect of nifedipine treated group with the 10^{-6} M dose and all other groups on the ACh-induced contractions. There was a statistically significant difference ($p < 0.05$) on the ACh-induced contractions between the effect of TEA in the 10^{-3} M dose treated group and the groups of phentolamine, propranolol, nifedipine and mix. It was found that there was a statistically significant difference ($p < 0.05$) between the effect of Mix of known doses of the group administered simultaneously and the other groups except propranolol on the ACh-induced contractions (Figure 2.).

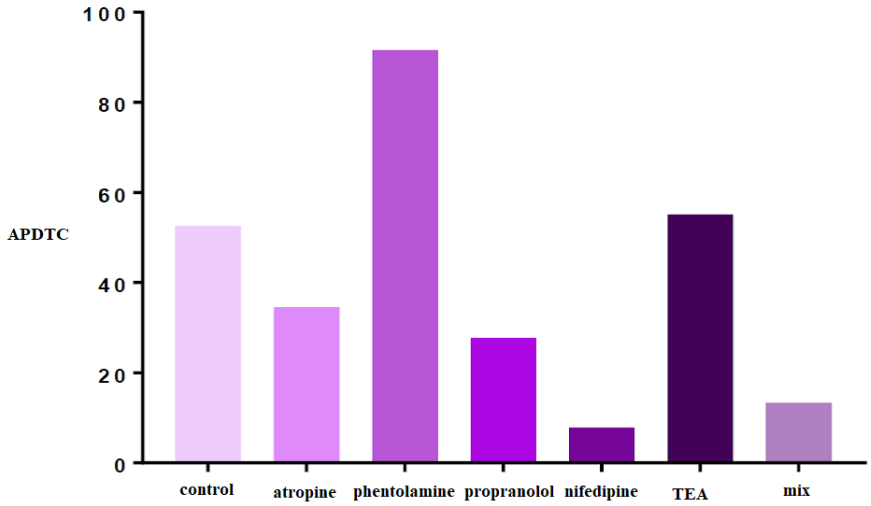

Figure 2. Effects of APDTC on bladder treated with 10^{-4} M Ach in the presence and absence of antagonist or blocker.

There was a statistically significant difference between ACh contracted bladder smooth muscle responses and treated APDTC in the presence of atropine. There was also a significant difference between antagonist atropine and APDTC ($p < 0.05$). The bladder smooth muscle was relaxed with atropine and continued to relax when APDTC was administered. However, there was no statistically significant difference ($p > 0.05$) between the ACh-contracted APDTC-treated control group and the APDTC-treated group in the presence of atropine. Bladder smooth muscle contraction responses were not changed after the atropine treatment (Table 5. and Figure 3).

Table 5. Comparison of APDTC in the presence of atropine and atropine.

Atropine	**ACh**	**Antagonist**	**APDTC**
ACh	-	0.015	0.000
Antagonist	0.015	-	0.010
APDTC	0.000	0.010	-

JSR A
Journal of Scientific Reports

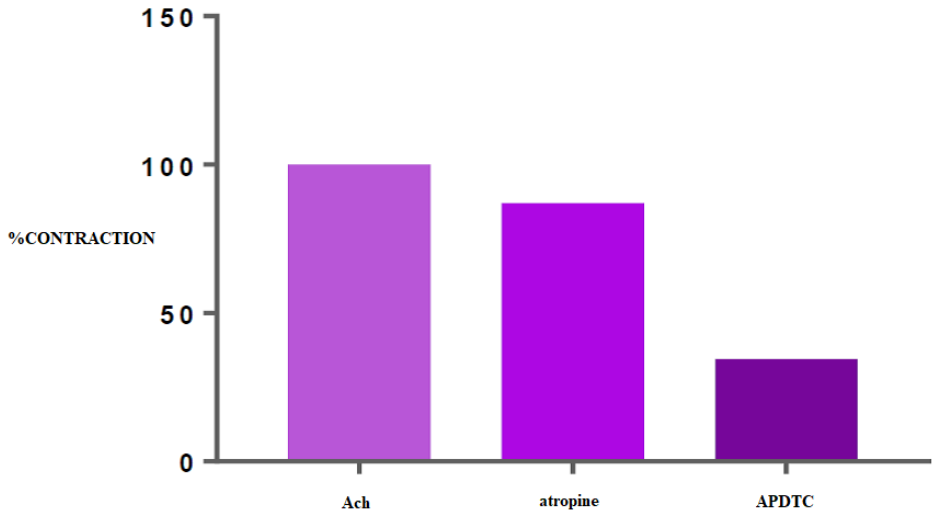

Figure 3. The effect of APDTC in the presence of atropine and atropine on bladder smooth muscle contraction treated with ACh.

There was a statistically significant difference ($p < 0.05$) between ACh-contracted bladder smooth muscle responses and APDTC in the presence of phentolamine. The bladder smooth muscle was relaxed with phentolamine and contracted when APDTC was administered in the presence of phentolamine. There was a statistically significant difference ($p<0.05$) between the ACh-contracted APDTC-treated control group and the APDTC-treated group in the presence of phentolamine. The antagonist phentolamine changed bladder smooth muscle contraction responses (Table 6 and Figure 4).

Table 6. Comparison of APDTC in the presence of phentolamine and phentolamine.

Phentolamine	**ACh**	**Antagonist**	**APDTC**
ACh	-	0.001	0.001
Antagonist	0.001	-	1.000
APDTC	0.001	1.000	-

JSR A
Journal of Scientific Reports

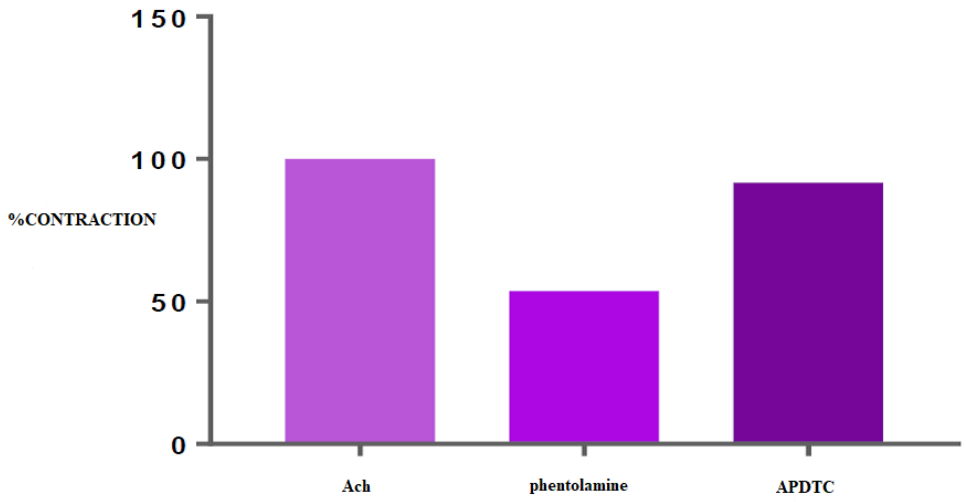

Figure 4. The effect of APDTC in the presence of phentolamine and phentolamine on bladder smooth muscle contraction treated with ACh.

There was a statistically significant difference ($p<0.05$) between ACh-contracted bladder smooth muscle responses and APDTC treatment in the presence of propranolol. The bladder smooth muscle is relaxed with propranolol and continued to relax when APDTC was administered in the presence of propranolol. There was a statistically significant difference ($p <0.05$) between ACh-contracted and APDTC treated control group and APDTC treated group in the presence of propranolol. β-adrenoceptor antagonist propranolol changed bladder smooth muscle responses (Table 7 and Figure 5).

Table 7. Comparison of APDTC in the presence of Propranolol and Propranolol.

Propranolol	**ACh**	**Antagonist**	**APDTC**
ACh	-	0.001	0.000
Antagonist	0.001	-	0.070
APDTC	0.000	0.070	-

JSR A
Journal of Scientific Reports

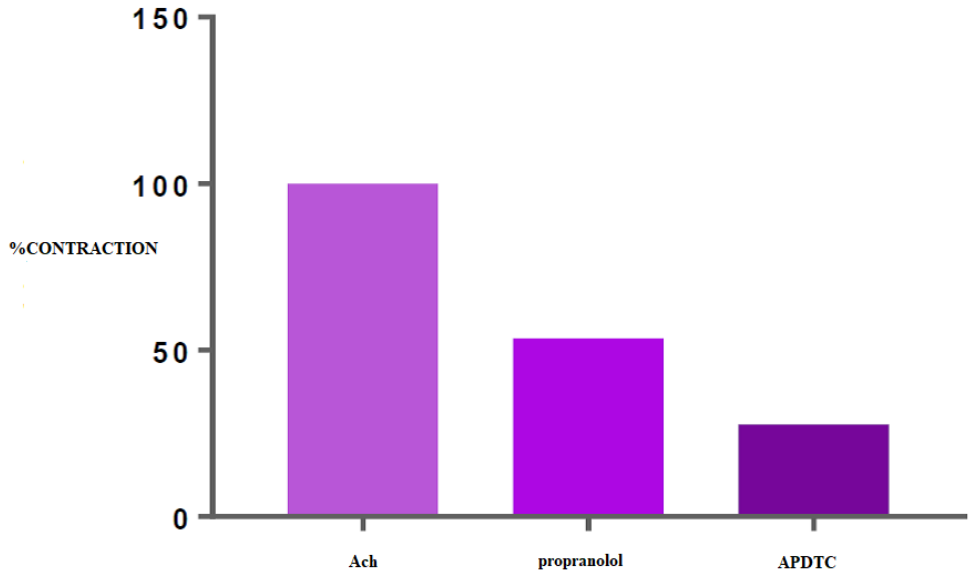

Figure 5. The effect of APDTC in the presence of propranolol and propranolol on bladder smooth muscle contraction treated with ACh.

There was a statistically significant difference between ACh-contracted bladder smooth muscle responses and administered APDTC in the presence of nifedipine. There was a statistically significant difference ($p<0.05$) between APDTC applied in the presence of nifedipine and calcium channel blocker nifedipine. The bladder smooth muscle is relaxed with nifedipine and continued to relax when APDTC was administered. There was a statistically significant difference ($p<0.05$) between ACh-contracted APDTC-treated control group and APDTC-treated in the presence of nifedipine group. Bladder smooth muscle responses were altered by nifedipine administration (Table 8 and Figure 6).

Table 8. Comparison of APDTC in the presence of nifedipine and nifedipine.

Nifedipine	**ACh**	**Antagonist**	**APDTC**
ACh	-	0.000	0.000
Antagonist	0.000	-	0.000
APDTC	0.000	0.000	-

JSR A
Journal of Scientific Reports

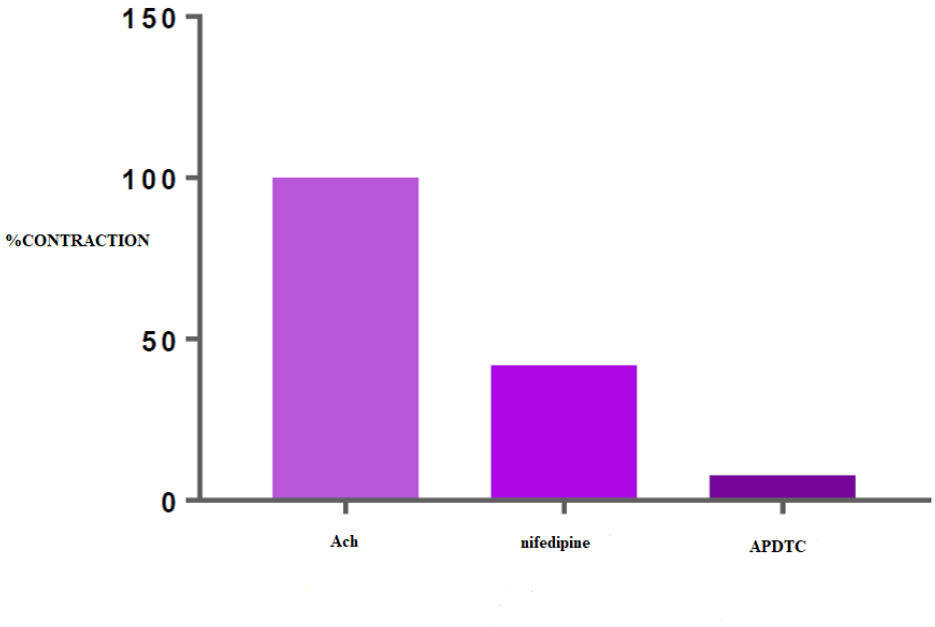

Figure 6. Effect of APDTC in the presence of nifedipine and nifedipine on ACh treated bladder smooth muscle contraction.

There was a statistically significant difference ($p<0.05$) between ACh-contracted bladder smooth muscle responses and APDTC applied in the presence of tetraethylammonium. The bladder smooth muscle was relaxed with tetraethyl ammonium and contracted when APDTC was administered in the presence of tetraethyl ammonium. There was no statistically significant difference ($p>0.05$) between ACh-contracted APDTC-treated control group and APDTC-treated group in the presence of tetraethylammonium. Potassium channel blocker tetraethylammonium did not alter bladder smooth muscle responses (Table 9 and Figure 7).

Table 9. Comparison of APDTC in the presence of TEA and TEA.

TEA	ACh	Antagonist	APDTC
ACh	-	0.000	0.001
Antagonist	0.000	-	0.290
APDTC	0.001	0.290	-

JSR A
Journal of Scientific Reports

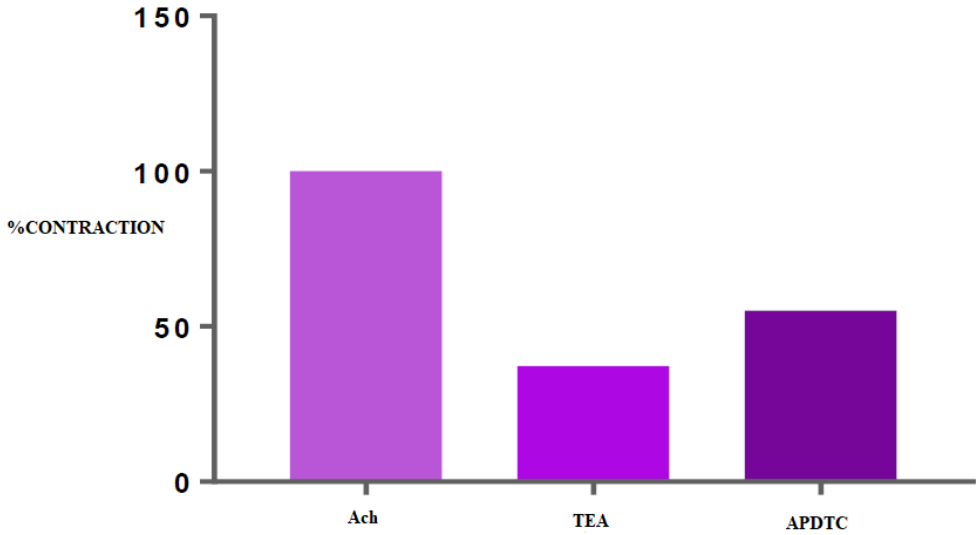

Figure 7. The effect of APDTC in the presence of tetraethyl ammonium and tetraethyl ammonium on bladder smooth muscle contraction treated with ACh.

There is a statistically significant difference between ACh-contracted bladder smooth muscle responses and APDTC applied in the presence of a mix. There was also a statistically significant difference ($p<0.05$) between the mix of phentolamine+propranolol+atropine and APDTC applied in the presence of mix. Bladder smooth muscle was relaxed with mix and continued to relax when APDTC was applied in the presence of the mix. There was a statistically significant difference ($p<0.05$) between ACh-contracted APDTC treated control group and APDTC treated group in the presence of the mix. Administration of phentolamine+propranolol+atropine changed bladder smooth muscle responses (Table 10 and Figure 8).

Table 10. Comparison of APDTC in the presence of Mix and Mix.

Mix	**ACh**	**Antagonist**	**APDTC**
ACh	-	0.001	0.000
Antagonist	0.001	-	0.000
APDTC	0.000	0.000	-

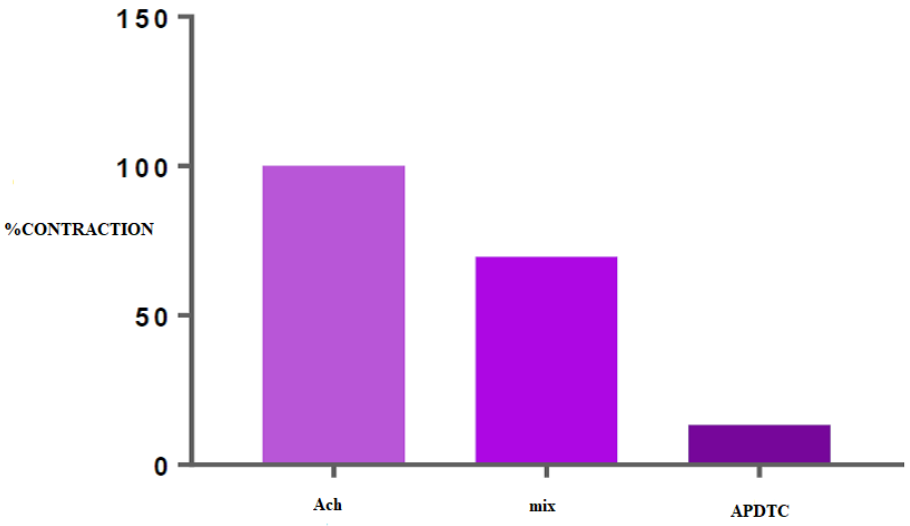

Figure 8. The effect of APDTC in the presence of phentolamine+propranolol+atropine (mix) and phentolamine+propranolol+atropine (mix) on bladder smooth muscle contraction treated with ACh.

4. DISCUSSION AND CONCLUSION

Nuclear factor kappa B (NF-κB), a common transcription factor, regulates various genes encoding inflammatory mediators. NF-κB signaling is a classic signaling pathway that plays a role in the inflammatory response as well as regulation of cell proliferation and apoptosis [27]. Pyrrolidine dithiocarbamate (PDTC) is an antioxidant and has been shown to be effective in the treatment of various human diseases [28], although it inhibits activation of NF-κB [29]. APDTC affected the contractile-relaxation responses in bladder smooth muscle and showed that APDTC produces dose-dependent increased relaxation responses in ACh-contracted bladder smooth muscle [30]. Therefore, it is necessary to explain the anti-viral, anti-apoptotic, anti-inflammatory and antioxidant effects of APDTC compound seperately in following examples of studies. According to a study, the anti-viral effects of PDTC were reported as follows: Previously, it was shown that PDTC inhibits proteolytic polyprotein processing and replication of human rhinovirus by transporting metal ions into cells. It is shown that PDTC also inhibits replication of two other picornaviruses: coxsackievirus B3 (CVB3), a closely related virus that belongs to the genus Enterovirus, and mengovirus, an encephalomyocarditis virus strain that belongs to the genus Cardiovirus, and that this inhibition is due to the dithiocarbamate moiety of the compound. Making use of subgenomic replicons, evidence is provided that PDTC inhibits replication of these two viruses by disturbing viral RNA synthesis. Furthermore, it is shown that PDTC transports zinc ions into cells and that these zinc ions play an important role in the antiviral activity mediated by PDTC. Finally, it is shown that PDTC interferes with proteolytic processing of the polyproteins of both CVB3 and mengovirus, but that the underlying mechanism between these two viruses differs. In CVB3-infected cells, PDTC interferes strongly with the proteolytic activity of 3CD(pro), as shown by the impaired production of the mature capsid proteins as well as the autocleavage of 3CD(pro) into 3C(pro) and 3D(pol). In mengovirus-infected cells, however, PDTC

had no effect on the proteolytic production of capsid proteins or the autocleavage of 3CD(pro). Instead, PDTC caused the accumulation of a high-molecular-mass precursor protein, due to an impairment in the primary 'break' that normally occurs at the 2A-2B junction. Thus, PDTC disturbs polyprotein processing and replication of two groups of picornaviruses, enteroviruses and cardioviruses, but the underlying mechanism is different [31]. According to an another study, the anti-apoptotic and anti-oxidant effects were reported as follows: Hypoxia induces vascular endothelial injuries; however, the mechanisms involved and effects of interventions remain unclear. Investigation was the inflammatory response and oxidative stress in co-cultured neutrophils and vascular endothelial cells, apoptotic changes in endothelial cells, and effects of the antioxidant, Tempol or the PDTC, upon endothelial cells under conditions of intermittent and/or continuous hypoxic exposure. Polymorphonuclear neutrophils co-cultured with human umbilical vein endothelial cells were subjected to the following conditions: intermittent normoxia (IN), intermittent hypoxia (IH), continuous hypoxia (CH), intermittent with continuous hypoxia (OS), OS+Tempol (OS+T), or OS+PDTC (OS+P) for 2, 5, or 8 h. Inflammatory factors, TNF-α and IL-6, the adhesion molecule, ICAM-1, CAT activity, and MDA concentrations in supernatants from the co-culture as well as pro-(Bak) and anti-(Bcl-xl) apoptotic gene expression levels in the endothelial cells were determined. Inflammatory factors, adhesion molecules, oxidative stress, and apoptosis genes in all groups showed significant, time-dependent increases as compared with the IN group. TNF-α, IL-6, ICAM-1, and MDA levels in the OS group were increased, while CAT was decreased as compared with that observed in the IH, CH, OS+T, and OS+P groups. Bcl-x1 expression and Bcl-x1/BAK ratios were decreased and BAX increased in the OS versus IH, CH, OS+T, or OS+P groups. Both pro- and anti-apoptotic proteins showed time-dependent increases, while the Bcl-x1/BAK ratio decreased over these times. Tempol and PDTC partially prevented these effects. Inflammation, oxidative stress, and apoptosis are all involved in vascular endothelial injury induced by OS. Anti-inflammatory and anti-oxidative interventions can partially improve effects of OS [32]. According also to an another study, the anti-inflammatory effects were reported as follows: PDTC is a thiol compound that elicits anti-inflammatory effects by inhibiting NF-κB signaling. Study report that regulator of calcineurin activity 1 (RCAN1) expression is induced by PDTC treatment and that increased RCAN1 expression is dependent on the generation of reactive oxygen species (ROS) and activation of p38 MAPK and JNK signaling. It is also reported that the ability of PDTC to induce RCAN1 is mediated by activator protein-1 (AP-1)-dependent gene transcription, and identified a functional AP-1 binding site in the RCAN1 promoter by producing mutations and conducting chromatin immunoprecipitation (ChIP) analyses. Moreover, we show that the PDTC-mediated inhibitory effect on NF-κB signaling is significantly perturbed by knocking out RCAN1. The data provide the first evidence that PDTC prevents in vivo expression of pro-inflammatory cytokines by inducing RCAN1 expression [33]. After all, since the mechanism of action of APDTC, which has been proven to relax bladder smooth muscle, has not been elucidated, we investigated the mechanism of action of APDTC in bladder smooth muscle *in vitro*.

In this study, seven different groups (control, atropine, phentolamine, propranolol, nifedipine, TEA and phentolamine+propranolol+atropine) were set to determine whether APDTC used some channels and receptors in rat bladder smooth muscle treated with ACh. 2.5×10^{-5} M APDTC produced a relaxation response in the bladder smooth muscle. According to the experimental results obtained from the atropine group, there was no significant difference in contraction responses between Ach treated rats with 2.5×10^{-5} M APDTC administration in the presence of 10^{-6} M atropine and 2.5×10^{-5} M APDTC administration to the control group. In the presence of 10^{-6} M atropine, APDTC relaxed the bladder smooth muscle. Similarly, 10^{-6} M atropine has been shown to inhibit the Ach caused

contraction of bladder rat bladder smooth muscle [34]. Admiministration of APDTC in the presence of atropine ensures that relaxation continues to increase significantly, indicating that 2.5×10^{-5} M doses of APDTC do not use muscarinic-cholinergic pathways in the bladder smooth muscle. Whether M3 cholinergic receptor signal transduction pathway is involved in regulation of the activation of NF-κB and the expression of chemokine MOB-1, MCP-l genes in pancreatic acinar cells were investigated. Rat pancreatic acinar cells were isolated, cultured and treated with carbachol, atropine and PDTC in vitro. The MOB-1 and MCP-1 mRNA expression was detected by using RT-PCR. The activation of NF-κB was monitored by using electrophoretic mobility shift assay. The results showed that as compared with control group, M3 cholinergic receptor agonist (10^{-3} mol/L, 10^{-4} mol/L carbachol) could induce a concentration-dependent and time-dependent increase in the expression of MOB-1, MCP-1 mRNA in pancreatic acinar cells. After treatment with 10^{-3} mol/L carbachol for 2 h, the expression of MOB-1, MCP-1 mRNA was strongest. The activity of NF-κB in pancreatic acinar cells was significantly increased ($p<0.01$) after treated with M3 cholinergic receptor agonist (10^{-3} mol/L carbachol) in vitro for 30 min. Either M3 cholinergic receptor antagonist (10^{-5} mol/L atropine) or NF-κB inhibitor (10^{-2} mol/L PDTC) could obviously inhibit the activation of NF-κB and the chemokine MOB-1, MCP-1 mRNA expression induced by carbachol ($p<0.05$). This inhibitory effect was significantly increased by atropine plus PDTC ($p<0.01$). The results of these studies indicated that M3 cholinergic receptor signal transduction pathway was likely involved in regulation of the expression of chemokine MOB-1 and MCP-l genes in pancreatic acinar cells in vitro through the activation of NF-κB [35].

According to the results of the phentolamine group, the administration of 2.5×10^{-5} M dose of APDTC in the presence of 10^{-5} M phentolamine in the bath caused a statistically significant difference compared to 2.5×10^{-5} M APDTC administrated to the control group. In the presence of 10^{-5} M doses of phentolamine, APDTC increased bladder smooth muscle contractions. Reversed relaxation effect of phentolamine by APDTC was not significant. APDTC acted as antagonist against phentolamine. Phentolamine, a potent adrenergic receptor antagonist, blocks the adrenergic receptors to which phenylephrine binds to cause urethral smooth muscle contraction. When these receptors are blocked, phentolamine cannot trigger the expected contraction response and the contraction cannot be expected in the urethral smooth muscles [36]. The increase in contractions is not important, and so APDTC continues its relaxation effect. However, phentolamine has caused a decrease in the relaxation caused by APDTC, and therefore APDTC may be partially using α-adrenergic receptors. Epinephrine increased gene- and protein-expression of interleukin-6 (IL-6) and interleukin-11 (IL-11), which are capable of stimulating the development of osteoclasts from their hematopoietic precursors, in human osteoblast (SaM-1) and human osteosarcoma (SaOS-2, HOS, and MG-63) cell lines. An increase in IL-6 and IL-11 synthesis in response to epinephrine appeared to be a common feature in osteoblastic cells, but the magnitude of expression was different in these cell lines. In HOS cells treated with epinephrine, increases of IL-6 and IL-11 synthesis were inhibited by timolol (a beta-blocker), H-89 (N-[2-((p-bromocinnamyl)amino)ethyl]-5-isoquinolinesulfonamide; an inhibitor of protein kinase A (PKA)) and SB203580 [4-(4-fluorophenyl)-2-(4-methylsulfinylphenyl)-5-(4-pyridyl)1H-imidazole; an inhibitor of p38 mitogen-activated protein kinase (MAPK)], but not by phentolamine (an alpha-blocker), calphostin C [an inhibitor of protein kinase C (PKC)], or PD98059 (2'-amino-3'-methoxyflavone; an inhibitor of classic MAPK), suggesting a common pathway mediated by beta-adrenergic receptors in the PKA and p38 systems involved in the signal transduction of IL-6 and IL-11. Furthermore, expression of both genes was inhibited by curcumin [an inhibitor of activating protein-1 (AP-1) activation], but not by PDTC. The pharmacological study suggested that co-induction of the two genes in response to epinephrine occurred via activation of AP-1. The findings

suggest that coinduction of IL-6 and IL-11 in response to epinephrine probably occurs via the PKA and p38 MAPK systems, leading to the transcriptional activation of AP-1 in human osteoblastic cells [37].

There was a statistically significant difference between 2.5×10^{-5} M APDTC in bladder smooth muscle in the presence of 10^{-6} M propranolol dose and 2.5×10^{-5} M APDTC applied to the control group. The dose of 10^{-6} M propranolol in the bladder smooth muscle treated with ACh produced relaxation. APDTC maintained its relaxation responses. APDTC and propranolol acted as agonists together, as relaxation continued to increase compared to control group results. Propranolol increases the amplitude of spinal reflex bladder contractions. It has been shown that α-1 and α-2 adrenergic receptors, possibly mediated by sympathetic efferent pathways in the hypogastric nerves or sympathetic chain, can suppress tonic contraction activation by affecting regions of the bladder smooth muscle [38]. Blocking of β-adrenergic receptors with propranolol increased the relaxation effect of APDTC. As a result, it cannot be said that APDTC exerts its effect through these receptors. Interaction of peroxisome proliferator-activated receptor γ coactivator-1α (PGC-1α) with other cellular signalling pathways plays an important role in training-induced mitochondrial adaptations. The study examined whether PDTC and propranolol would affect the PGC-1α-induced mitochondrial transcription factors, enzymes and proteins involved in energy metabolism and antioxidant defense in response to endurance training. Female Sprague-Dawley rats (aged 8 weeks) were randomly divided into two groups (n = 24), one subjected to 8 weeks of treadmill training and one remaining sedentary. Each group of rats was subdivided into three groups that were injected (i.p.) daily with PDTC (50 mg (kg body weight)$^{-1}$), propranolol (30 mg kg^{-1}) or saline as a control 1 h before the daily exercise session. Sedentary PDTC-treated rats showed 75% higher PGC-1α content ($p<0.01$) but lower mitochondrial transcription factor A and phosphorylated cAMP-responsive element binding protein (p-CREB) than control rats. Training increased PGC-1α by 57% ($p<0.01$), cytochrome c oxidase 4 by 30% ($p<0.05$) and p-CREB by 13% ($p<0.05$), whereas the mitochondrial mitofusin-2 level was decreased by 24% ($p<0.01$). Treatment with PDTC decreased PGC-1α and p-CREB content by 34 and 53% ($p<0.05$), respectively, in trained rats and abolished training effects on cytochrome c oxidase 4 and mitochondrial mitofusin-2. None of the training effects was abolished by propranolol treatment. Mitochondrial superoxide dismutase activity was decreased with PDTC, whereas training-induced glutathione peroxidase activity was unaltered by either drug. This indicates that nuclear factor-κB-inhibitory and antioxidant properties of PDTC can attenuate PGC-1α-mediated mitochondrial adaptation to endurance training, whereas the β-adrenergic pathway has little adverse effect [39].

There was a significant difference between 2.5×10^{-5} M APDTC in nifedipine 10^{-6} M dose group and the APDTC in ACh treated group. Nifedipine inhibited ACh contraction responses in the bladder, resulting in relaxation. L-type calcium channel blocker nifedipine was found to block 75-80% of contractile responses in isolated rat detrusor smooth muscle [40]. Nifedipine has been shown to reduce the number and amplitude of contractions on detrusor contractions and increase bladder capacity [41]. It is indicated that bladder Ca^{2+} in rats are collected from both intracellular and extracellular pools during both spontaneous and stimulated contractions. Nifedipine inhibits the tone and spontaneous activity of the isolated rat bladder [42]. The relaxation effect of nifedipine created continued with APDTC in statistically significant manner. Nifedipine increased the effect of APDTC even more, and blocking of the channels did not change this effect. We can say that blocking L-type calcium channels will increase the effect of APDTC. Ca^{2+}/calmodulin-dependent protein kinase II (CaMKII) and NF-κB play crucial roles in pathogenesis of doxorubicin (DOX)-induced cardiomyopathy. Their activities are regulated by intracellular Ca^{2+}. It is hypothesized that blockade of L-type Ca^{2+} channel (LTCC) could

attenuate DOX-induced cardiomyopathy by regulating CaMKII and NF-κB. DOX activated CaMKII and NF-κB through their phosphorylation and increased cleaved caspase 3 in cardiomyocytes. Pharmacological blockade or gene knockdown of LTCC by nifedipine or small interfering RNA, respectively, suppressed DOX-induced phosphorylation of CaMKII and NF-κB and apoptosis in cardiomyocytes, accompanied by decreasing intracellular Ca^{2+} concentration. Autocamtide 2-related inhibitory peptide (AIP), a selective CaMKII inhibitor, inhibited DOX-induced phosphorylation of NF-κB and cardiomyocyte apoptosis. Inhibition of NF-κB activity by APDTC suppressed DOX-induced cardiomyocyte apoptosis. DOX-treatment (18 mg/kg via intravenous 3 injections over 1 week) increased phosphorylation of CaMKII and NF-κB in mouse hearts. Nifedipine (10 mg/kg/day) significantly suppressed DOX-induced phosphorylation of CaMKII and NF-κB and cardiomyocyte injury and apoptosis in mouse hearts. Moreover, it attenuated DOX-induced left ventricular dysfunction and dilatation. Our findings suggest that blockade of LTCC attenuates DOX-induced cardiomyocyte apoptosis via suppressing intracellular Ca^{2+} elevation and activation of CaMKII-NF-κB pathway. LTCC blockers might be potential therapeutic agents against DOX-induced cardiomyopathy [43].

There was no statistically significant difference between the study results of 2.5×10^{-5} M APDTC administered organ bath containing 10^{-3} M TEA and study results of the control group. The bladder was relaxed by TEA. APDTC reversed the effect of TEA and caused contraction. It has been shown that TEA is able to block the potassium channels of the inducible membranes that prolapse repolarization and the penetration of calcium ions [44]. TEA blocks the calcium-activated potassium channel, causing membrane depolarization and increased muscle contractions [45]. Potassium channel blocker TEA showed an inhibitory effect on bladder contraction. Contractions created with APDTC are not important enough to alter the relaxation response. It was suggested that the 2.5×10^{-5} M dose of APDTC was using different pathways other than potassium channels. These result is a new finding and there is no study so far in the literature.

To determine the effect of the NANK system on the mechanism of action of APDTC, 10^{-5} M phentolamine+10^{-6} M propranolol+10^{-6} M atropine (mix group) was applied to the bladder smooth muscle. 2.5×10^{-5} M APDTC was applied to the organ bath containing the mix and there was a significant difference between the control group. Mix mixture in bladder smooth muscle produced a relaxation response. APDTC continued to increase relaxation by creating agonistic effect with the mix group. The mix group had more relaxant effects than phentolamine, propranolol and atropine administered in separate groups on ACh-induced contractions. Increasing effect of APDTC as a result of the significant difference between the APDTC relaxant effect in the control group and the mix group showed that it did not use adrenergic and cholinergic routes.

In this study, we investigated the mechanism of action of APDTC with proven antioxidant and anti-inflammatory effects in bladder smooth muscle, and showed that APDTC created relaxation response in rat bladder smooth muscle induced by ACh. This response was altered by the α-adrenergic receptor antagonist phentolamine, suggesting that APDTC may be effective through the α-adrenergic receptor. On the other hand, the results suggested that the NANK system, which plays an important role in bladder smooth muscle contraction-relaxation, will help to clarify the APDTC mechanism hopefully in further studies.

REFERENCES

[1] Martini, F. H., (2003), Fundamentals of Anatomy & Physiology, 6. Baskı, Yayımlayan Addison Wesley Longman, s. 1004.

[2] Hole, J.W., (1993), Human Anatomy and Physiology, 6. Baskı, William C. Brown Publisher, s. 770.

[3] Demirci, A., Canda, E.C., (2010), AGırı Aktif Mesanenin Patofizyolojisi, Türk Üroloji Seminerleri, 1: 23-6.

[4] Tahata, S., Yuan, B., Kikuchi, H., Tagaki, N., Hirano, T., Toyoda, H., (2014), Cytotoxic effects of pyrrolidine dithiocarbamate in small-cell lung cancer cells, alone and in combination with cisplatin, International Journal of Oncology, 45(4): 1749-1759.

[5] Şengül, E., (2014), *Achillea Millefolium* (Civan perçemi) Ekstraktlarının ve Bazı Biyolojik Aktif Bileşiklerinin In Vitro Ortamda Rat Mesanesi Düz Kasları Üzerine Etkilerinin Araştırılması, Doktora Tezi, Atatürk Üniversitesi, Erzurum, s. 2, 101.

[6] Ege, H., (2016), Silodosin ve Palonosetronun İzole Sıçan Mesane Kasılmaları Üzerindeki Etkileri, Yüksek Lisans Tezi, Necmettin Erbakan Üniversitesi, Konya, s. 2, 42, 43, 44.

[7] Agis-Torres, A., Recio, P., López-Oliva, M.E., Martínez, M.P., Barahona, M.V., Benedito, S., Bustamante, S., Jiménez-Cidre, M.A., García-Sacristán, A., Prieto, D., Fernandes, V.S., Hernández, M., (2018), Phosphodiesterase type 4 inhibition enhances nitric oxide- and hydrogen sulfide-mediated bladder neck inhibitory neurotransmission, Scientific Reports, 8: 4711.

[8] Ozturk Fincan G.S., Vural I.M., Yildirim S.S., Isli F., Dilekoz E., Ercan S., Sarioglu Y., (2016), Role of nicotinic acetylcholine receptor subtypes on nicotine's enhancing effect on electrical field stimulation elicited contractile responses in rabbit urine bladder, European Review for Medical and Pharmacological Sciences, 20(8): 1636-1641.

[9] Andersson, M., Aronsson, P., Doufish, D., Lampert, A., Tobin, G., (2012), Muscarinic receptor subtypes involved in urothelium-derived relaxatory effects in the inflamed rat urinary bladder, Autonomic Neuroscience: Basic and Clinical, 170(1-2): 5-11.

[10] Darblade, B., Behr-Roussel, D., Oger, S., Hieble, J.P., Lebret, T., Gorny, D., Benoit, G., Alexandre, L., Giuliano, F., (2006), Effects of potassium channel modulators on human detrusor smooth muscle myogenic phasic contractile activity: potential therapeutic targets for overactive bladder, Urology, 68(2): 442-8.

[11] Giglio, D., Tobin, G., (2009), Muscarinic receptor subtypes in the lower urinary tract, Pharmacology, 83(5): 259-69.

[12] Hegde, S.S., Eglen, R.M., (1999), Muscarinic receptor subtypes modulating smooth muscle contractility in the urinary bladder, Life Sciences, 64(6-7): 419-28.

[13] Lüllmann, H., Hein, L., Mohr, K., Bieger, D., (2005), Color Atlas of Pharmacology, 3. Baskı, Thieme Publishers New York, s. 6, 7, 54.

[14] Brunton, L., Chabner, B., Knollman, B., (2010), Goodman & Gilman's The Pharmacological Basis of Therapeutics, 12. Baskı, McGraw-Hill Higher Education, s. 214-320.

[15] Altinkurt, O., (1981), Farmakoloji I, Ankara Üniversitesi Basımevi, Ankara, s. 35, 105.

[16] Katzung, B.G., Masters, S.B., Trevor, A.J., (2012), Basic & Clinical Pharmacology, 12.Baskı, McGraw-Hill Higher Education, s. 87, 152.

[17] Kayaalp, S.O., (2002), Rasyonel Tedavi Yönünden Tıbbi Farmakoloji, 10.Baskı, Hacettepe-Taş, Ankara, s. 1093-1138.

[18] Guyton A.C. and Hall, J.E., (2013), Tıbbi Fizyoloji (çev. Yeğen, B.), 12. Baskı, Nobel Tıp Kitabevleri, s. 91, 307, 308, 731, 773.

[19] Thorneloe, K.S. and Nelson, M.T., (2005), Ion channels in smooth muscle: regulators of intracellular calcium and contractility, Canadian Journal of Physiology and Pharmacology, 83: 215–242.

[20] Bisset, D. and Chung, S.H., (2008), Efficacy of external tetraethylammonium block of the KcsA potassium channel: molecular and Brownian dynamics studies, Biochimica et Biophysica Acta (BBA) - Biomembranes, 1778(10): 2273-82.

[21] Gür, S., (1998), Mesane'nin Non-adrenerjik Non-kolinerjik Kontrolü, Ankara Eczacılık Fakültesi Dergisi, 27(1): 51-60.

[22] Vesela, R., Aronsson, P., Andersson, M., Wsol, V., Tobin, G., (2012), The potential of non-adrenergic, non-cholinergic targets in the treatment of interstitial cystitis/painful bladder syndrome, Journal of Physiology and Pharmacology, 63(3): 209-16.

[23] Daly, D.M., 1, Collins, V.M., Chapple, C.R., Grundy, D., (2011), The afferent system and its role in lower urinary tract dysfunction, Current Opinion in Urology, 21: 268–274.

[24] Gohar, O., (2005), The Transient Receptor Potential (TRP) Ion Channels, Modulator, 20: 20-23.

[25] Araki, I., Du, S., Kobayashi, H., Sawada, N., Mochizuki, T., Zakoji, H., Takeda, M., (2008), Roles of mechanosensitive ion channels in bladder sensory transduction and overactive bladder, International Journal of Urology, 15(8): 681-687.

[26] Si, X., McManus, BM., Zhang, J., Yuan, J., Cheung, C., Esfandiarei, M., Suarez, A., Morgan, A., Luo, H., (2005), Pyrrolidine dithiocarbamate reduces coxsackievirus B3 replication through inhibition of the ubiquitin-proteasome pathway, Journal of Virology, 79(13): 8014–8023.

[27] Xiang, N., Liu, J., Liao, Y., Huang, Y., Wu, Z., Bai, Z., Lin, X., Zhang, J., (2016), Abrogating ClC-3 Inhibits LPS-induced Inflammation via Blocking the TLR4/NF-κB Pathway, Scientific Reports, 6: 27583. 57

[28] Zhang, J., Jiang, W., Zuo, Z., (2014), Pyrrolidine dithiocarbamate attenuates surgery-induced neuroinflammation and cognitive dysfunction possibly via inhibition of nuclear factor kappaB, Neuroscience, 261: 1-10.

[29] Ivan, A.L., Campanini, M.Z., Martinez, R.M., Ferreira, V.S., Steffen, V.S., Vicentini, F.T., Vilela, F.M., Martins, F.S., Zarpelon, A.C., Cunha, T.M., Fonseca, M.J., Baracat, A.A., Georgetti, S.R., Verri, W.A.Jr., Casagrande, R., (2014), Pyrrolidine dithiocarbamate inhibits UVB-induced skin inflammation and oxidative stress in hairless mice and exhibits antioxidant activity in vitro, Journal of Photochemistry and Photobiology B: Biology, 138: 124-33.

[30] İnan, O. A., (2015), Sıçan Mesane'si Düz Kası Kasılma-GevŞeme Yanıtları Üzerine Ammonium Pyrrolidine Dithiocarbamate, SG-Benz, Caffeic Acid Phenil Ester, Atorvastatin Kalsiyum' un Etkileri, Yüksek Lisans Tezi, Dumlupınar Üniveristesi Fen Bilimleri Enstitüsü, Kütahya, s. 39.

[31] K Lanke, BM Krenn, W J G Melchers, J Seipelt and FJM van Kuppeveld, (2007), PDTC inhibits picornavirus polyprotein processing and RNA replication by transporting zinc ions into cells, J Gen Virol. 88 (Pt 4): 1206-1217. doi: 10.1099 / vir.0.82634-0. PMID: 17374764 DOI: 10.1099 / vir.0.82634-0.

[32] Yanjie D., Qing Z., Laifang W., (2019), Pro-apoptotic and anti-inflammatory effects of araloside A on human rheumatoid arthritis fibroblast-like synoviocytes, Chem Biol Interact., 306:131-137. doi: 10.1016 / j.cbi.2019.04.025. PMID: 31004595 DOI: 10.1016 / j.cbi.2019.04.025.

[33] Eun H. L., Seon K. S., Su R. S., (2017), Pyrrolidine dithiocarbamate (PDTC) inhibits inflammatory signaling via expression of regulator of calcineurin activity 1 (RCAN1): Anti-inflammatory mechanism of PDTC through RCAN1 induction, Biochem Pharmacol.; 143:107-117. doi: 10.1016 / j.bcp.2017.07.011. PMID: 28712932 DOI: 10.1016 / j.bcp.2017.07.011 .

[34] Han, J.S., Kim, S.J., Nam, Y., Lee, H.Y., Kim, G.M., Kim, D.M., Sohn, U.D., (2019), The Inhibitory Mechanism on Acetylcholine-Induced Contraction of Bladder Smooth Muscle in the Streptozotocin-Induced Diabetic Rat, Biomolecules & Therapeutics, 27 (1): 101-106.

[35] Hai Z., Daoda C., Jinghui Z., Yuan T., (2004), Involvement of M3 cholinergic receptor signal transduction pathway in regulation of the expression of chemokine MOB-1, MCP-1 genes in pancreatic acinar cells, J Huazhong Univ Sci Technolog Med Sci.; 24 (2): 140-3, 157. doi: 10.1007 / BF02885413. PMID: 15315164 DOI: 10.1007 / BF02885413.

[36] Rembetski, B.E., Cobine, C.A., Drumm, B.T., (2018), Laboratory practical to study the differential innervation pathways of urinary tract smooth muscle, American Physiological Society, 1;42(2): 295-304.

[37] A Kondo, M Mogi, Y Koshihara, A Togari., (2001), Signal transduction system for interleukin-6 and interleukin-11 synthesis stimulated by epinephrine in human osteoblasts and human osteogenic sarcoma cells, Biochem Pharmacol.; 61(3):319-26. doi: 10.1016/s0006-2952(00)00544-x. PMID: 11172736 DOI: 10.1016/s0006-2952(00)00544-x.

[38] Rogers, M.J., Xiao, Z., Shen, B., Wang, J., Schwen, Z., Roppolo, J.R., de Groat, W.C., Tai, C., (2015), Propranolol, but not naloxone, enhances spinal reflex bladder activity and reduces pudendal inhibition in cats, American Physiological Society, 1;308(1): R42-9.

[39] Hong F., Chounghun K., Jonathan R. D., Ryan K., Iwalola A., Yong Z., Li L. J., (2013), Training-induced mitochondrial adaptation: role of peroxisome proliferator-activated receptor γ coactivator-1α, nuclear factor-κB and β-blockade, Exp Physiol.; 98 (3): 784-95. doi: 10.1113 / expphysiol.2012.069286. PMID: 23104933 DOI: 10.1113 / expphysiol.2012.069286.

[40] Zar, M.A., Iravani, M.M., Luheshi, G.N., (1990), Effect of nifedipine on the contractile responses of the isolated rat bladder, The Journal of Urology, 143(4): 835-9.

[41] Rud, T,. Andersson, K.E., Ulmsten, U., (1979), Effects of Nifedipine in Women with Unstable Bladders, Urologia Internationalis, 34: 421–429.

[42] Maggi, C.A., Manzini, S., Parlani, M., Conte, B., Giuliani, S., Meli, A., (1988), The effect of nifedipine on spontaneous, drug-induced and reflexly-activated contractions of the rat urinary bladder: evidence for the participation of an intracellular calcium store to micturition contraction, General Pharmacology: The Vascular System, 19(1): 73-81.

[43] Soichiro I., Shouji M., Kosuke O., Masataka I., Akihito I., Tomonori T., Nobuyuki E., Taishi Y., Masashi S., Hiroko D., Sachio M., Tomomi I., Hiroyuki T., (2019), Blockade of L-type Ca 2+ channel attenuates doxorubicin-induced cardiomyopathy via suppression of CaMKII-NF-κB pathway, Sci Rep.; 9(1):9850. doi: 10.1038 / s41598-019-46367-6. PMID: 31285514 PMCID: PMC6614470 DOI: 10.1038 / s41598-019-46367-6.

[44] Carpenter, F.G., (1978), Potentiation of nevre-induced bladder responses by tetraethylammonium in reletion to junctionaland extrajunctional muscarinic receptors, British journal of pharmacology, 64(3): 331-9.

[45] Oh, S.J., Ahn, S.C., (2003), Inhibitory effects of potassium channel blockers on carbachol induced contraction in rat detrusor muscle, Journal of Korean Medical Science, 18(5): 701-6.

JSR A
Journal of Scientific Reports

ATTACHMENTS

APPENDIX 1. Experimental Animals Local Ethics Committee Approval Certificate

T.C.
DUMLUPINAR ÜNİVERSİTESİ
HAYVAN DENEYLERİ YEREL ETİK KURULU
ARAŞTIRMA BAŞVURUSU ONAYI

BAŞVURU BİLGİLERİ	ARAŞTIRMANIN ADI	**Sıçan mesane düz kası kasılma gevşeme cevapları üzerine Ammonium Pyrrolidine Dithiocarbamete'nın etki mekanizmasının araştırılması**
	ARAŞTIRMA YÜRÜTÜCÜSÜ KURUMU	Doç.Dr.M.Kasım ÇAYCI DPÜ Fen-Edebiyat Fakültesi Genel Biyoloji ABD
	PROJE YÜRÜTÜCÜSÜ KURUMU	Doç.Dr.M.Kasım ÇAYCI DPÜ Fen-Edebiyat Fakültesi Genel Biyoloji ABD
	YARDIMCI ARAŞTIRICILAR	Doç.Dr.M.Kasım ÇAYCI Yls. Öğr.Zeynep KELEŞ Yls.Öğr.Aysun ERDOĞAN Yls.Öğr.Merve AKTAŞ Yls.Öğr.Merve ARAS
	ARAŞTIRMANIN TAHMİNİ SÜRESİ	12 Ay
	KULLANILACAK HAYVAN TÜRÜ VE SAYISI	Wistar Albino (E) – 70 Adet
	DESTEKLEYİCİ KURULUŞ	--

DEĞERLENDİRİLEN İLGİLİ BELGELER	Belge Adı	Tarihi
	ARAŞTIRMA BAŞVURU FORMU	**16.12.2015**

KARAR BİLGİLERİ	Karar No : 2015/02 Da Tarih: 30.12.2015 Yukarıda başvuru bilgileri verilen araştırma projesi gerekçe, amaç ve yöntemler dikkate alınarak görüşüldü ve ilgili belgeler incelendi. Projenin etik açıdan uygun olduğuna, çalışmanın aşağıdaki hususlar dikkate alınarak yürütülmesine ve sorumlu araştırıcıya iletilmesine **OY BİRLİĞİ** ile karar verildi. 1) Projede herhangi bir değişiklik gerektiğinde kurulumuzdan onay alınması, 2) Projede çalışacağı bildirilen araştırıcılarda değişiklik olduğunda kurulumuzdan onay alınması, 3) Deney hayvanları üzerinde yapılacak girişimin başlangıç ve bitiş tarihinin bildirilmesi, 4) Çalışma süresinde tamamlanamaz ise ek süre talebinde bulunulması, 5) Çalışma tamamlandığında sonuç raporunun gönderilmesi

ETİK KURUL BİLGİLERİ

ÜYELER

Unvanı / Adı / Soyadı EK Üyeliği	Uzmanlık Dalı	Kurumu	İlişki (*)	İmza
Doç.Dr. Aynur GÜLCAN Başkan	Mikrobiyoloji ve Klinik Mikrobiyoloji Anabilim Dalı	Tıp Fakültesi	☐ E ■ H	
Yrd. Doç. Dr. Ahmet KOÇAK Üye	Histoloji ve Embriyoloji Anabilim Dalı	Tıp Fakültesi	☐ E ■ H	
Yrd. Doç. Dr. Sezer AKÇER Üye	Anatomi Anabilim Dalı	Tıp Fakültesi	☐ E ■ H	
Yrd. Doç. Dr. Ceylan AYADA Üye	Fizyoloji Anabilim Dalı	Tıp Fakültesi	☐ E ■ H	
Yrd.Doç. Dr. Hasan METİNEREN Üye	Ortopedi ve Travmatoloji Anabilim Dalı	Tıp Fakültesi	☐ E ■ H	
Doç.Dr. M.Kasım ÇAYCI Üye	Biyoloji Anabilim Dalı	Fen-Edebiyat Fakültesi	■ E ☐ H	
Doç.Dr. Muhammed OYLUMLU Üye	Kardiyoloji Anabilim Dalı	Tıp Fakültesi	☐ E ■ H	
Yrd. Doç. Dr. Zülfü BAYHAN Üye	Genel Cerrahi Anabilim Dalı	Tıp Fakültesi	☐ E ■ H	
Vet. HEKİM Aydın AKCILAR Üye	Veteriner HEKİM	Tıp Fakültesi DEHYUAM	☐ E ■ H	
Yrd.Doç.Dr.Ahmet Haris Selçuk ÖZEN Üye	Zooloji Anabilim Dalı	Fen-Edebiyat Fakültesi	☐ E ■ H	
Erkan ERKOL Üye			☐ E ■ H	

* Araştırma ile İlişkisi

Kütahya Dumlupınar University
Institute of Graduate Studies

Journal of Scientific
Reports-A
E-ISSN: 2687-6167
Number 45, December 2020

RESEARCH ARTICLE

THE INVESTIGATION OF THE ACTION MECHANISM OF AMMONIUM PYRROLIDINE DITHIOCARBAMATE ON RAT AORTA SMOOTH MUSCLE CONTRACTION-RELAXATION RESPONSES

Hayri DAYIOĞLU[1], Ayhan YILMAZ[2], Zeynep KELEŞ[3], Fatih ALAN[4] and Sinan DARCAN[5]

[1]Kütahya Dumlupınar University, Faculty of Science and Literature, Department of Biology, 43270, Kütahya, hayri.dayioglu@dpu.edu.tr, ORCID: 0000-0002-9270-8561
[2] Kütahya Dumlupınar University, Faculty of Science and Literature, Department of Biology, 43270, Kütahya, ayhan.yilmaz@dpu.edu.tr, ORCID: 0000-0003-0410-8687
[3]Fevzi Çakmak Mah., Muhsin Yazıcıoğlu Cad. No:10, 34899, Pendik, İstanbul, zeynep.keles@outlook.com, ORCID: 0000-0003-3440-0785
[4]General Directorate of Presidential Protection Services, Presidential Complex, 06530, Beştepe, Ankara, fatihalan06@hotmail.com,ORCID: 0000-0002-0561-6192
[5]Kütahya Health Science University, Evliya Çelebi Campus, Tavşanlı Yolu 10. Km, 43100, Kütahya, sinan.darcan@ksbu.edu.tr, ORCID: 0000-0002-2135-4807

Received Date: 20.04.2020 *Accepted Date:09.10.2020*

ABSTRACT

Ammonium Pyrrolidine Dithiocarbamate (APDTC) is an inhibitor of nuclear factor kappa b (NF-κB). Beside of these function, its antitumoral, antioxidant, anticarcinogenic and antiviral properties and also apoptosis inhibiting effect in smooth muscle cells were determined. Our experiments aimed to investigate the mechanism of action of APDTC on rat aortic smooth muscle. Some adrenergic and cholinergic receptors, l-type Ca^{2+} channels and K^{+} channels were blocked in 7 different groups, and therefore the action mechanism of APDTC whether is used or not on which channels and receptors and the extent to which they are effective were aimed to be determined. The contraction-relaxation responses after the administration of APDTC, atropine, phentolamine, propranolol, nifedipine, tetraethylammonium (TEA) and mix (atropine+phentolamine+propranolol) on living state controlled with potassium chloride (KCl) and blocked nitric oxide (NO) synthesis with l-n^{g}-nitro arginine methyl ester (L-NAME) in the pre-contraction-induced aortic preparations with phenylephrine were investigated. The obtained data were evaluated by kruskal wallis and mann-whitney u tests. APDTC created the relaxation response in the aortic smooth muscle. Cholinergic receptor blocker atropine, α-adrenergic receptor blocker fentolamine, β-adrenergic receptor blocker propranolol, l-type calcium channel blocker nifedipine and potassium channel blocker TEA did not alter the relaxation response of APDTC. In the mix group consisting of atropine+phentolamine+propranolol, APDTC created a significant contraction response. It has been determined that APDTC can be effective on these systems via different mechanisms.

Keywords: APDTC, aorta, non- adrenergic non- cholinergic (NANC) system, L-NAME, phenylephrine, adrenergic, cholinergic, calcium channels, potassium channels.

JSR A
Journal of Scientific Reports

1. INTRODUCTION

The aorta is the most functional vessel that transmits blood to all parts of the body. The thickness of the aorta is approximately 2.5 cm. The blood cycle in the body lasts 60 seconds. The pressure in the aorta, brachial and other large arteries in a young adult human increases to a peak of approximately 120 mm Hg (systolic pressure) during each heart cycle and decreases to a minimum (diastolic pressure) of about 70 mm Hg [1].

APDTC is a NF-κB inhibitor. APDTC has antioxidant effects. It inhibits apoptosis in vascular endothelial cells, lymphocytes and neurons. It inhibits apoptosis in leukemia cells (HL-60) [2]. A significant increase in TAK was detected in rats treated with APDTC (0.70±0.01 μmol/mg protein). APDTC has been found to increase anti-oxidant enzyme activity in cholestasis dependent hepatic injury model. This result with APDTC is actually not surprising [3]. After showing that aldesterone was effective in 1992, it was revealed that there were aldesterone receptors in the corpus cavernosum. After investigating the penile tissues obtained from mature men, it was revealed that aldesterone did not have a direct relaxant effect, but increased the effect of neurarenaline [4] . APDTC inhibits DON-induced mitochondrial dysfunction and apaptosis via the NF-κB/iNOS pathway [5]. In models with inflammatory disease, the therapeutic effect of antioxidants as potential NF-κB inhibitors has been determined [6]. In the collagen-induced joint inflammation model, the anti-oxidant effect of APDTC in brain, stomach, lung, myocardia, organ injuries, renal ischemia/reperfusion was investigated. APDTC protects against NF-κB through pathological effects induced by some different stimuli, including lipopolysaccharide and cytokines [7]. AMTB and APDTC administered intrathecally affect TRPM8 and NF-κB in the spinal dorsal horn, even the brain [8]. It revealed the fact that inactivation of autophagy using APDTC reduces damage to the intestinal mucosal barrier. The effects of autophagy inactivation were largely dependent on the dosage of APDTC. Overactive autophagy may be weakened in accordance with physiology when using low or medium dose of APDTC. Using high-dose APDTC can completely inhibit autophagy and lead to decreased survival of instestinal mucosal cells. In this study, 10 mg/kg APDTC was shown to inhibit autophagy and perform best in maintaining inestinal mucosal integrity. The bi-directional efficacy of APDTC also requires the therapeutic window of APDTC, or other autophagy inhibitors, to be carefully investigated in humans [9]. The effects of Klotho were determined to be comparable to NF-κB inhibition, with the inhibition of NF-κB nuclear translocation and inhibition of APDTC administration, which is reported to inhibit DNA binding activity. Accumulating evidence suggests that the anti-aging protein Klotho plays an important role in inhibiting NF-κB and preventing nuclear translocation [10]. After injecting the APDTC, the pH of the gastric juice did not change significantly, but the promotional effect of NaHS on gastric acid secretion can be inhibited by APDTC. The pH value of the gastric juice changed values from 5.41±0.32 before injection, to 5.34±0.36 ($p > 0.05$) after injection. There is no significant difference after enterocele is injected with APDTC+NaHS. These results show that NaHS is involved in the control of gastric acid secretion by activating the NF-kB pathway [11].

Muscle fibers are structures that convert chemical energy into mechanical energy by spending ATP energy [12]. According to their microscopy, they are classified as striped and smooth muscles. The reason is due to the different physical properties of contractile proteins [13]. Muscle tissues can be stimulated, contracted, stretched and relaxed [14]. Smooth muscle cells are found on the walls of various organs and pipes of the body along with blood vessels, stomach, intestine, bladder, respiratory tract, penis, uterus and clitoral carenosal sinuses. Smooth muscle usually consists of smaller fibers, 1.5 μm in diameter and 20-500 μm in length [15]. The concentration of myosin in smooth muscle is only

one third of myosin in striated muscle, while the actin concentration can be twice as high. Despite these differences, the maximal tension per sectional unit developed from smooth muscles and the maximal tension developed in skeletal muscle are similar [16]. Smooth muscle activities are different. In some organs, smooth muscle cells are active by constantly maintaining a tonus level [12]. Smooth muscle cells cause tonic and phasic contractions in response to load or length changes. Smooth muscle cells, completely separate from the stimulant, use the cross-bridge between actin and myosin strands to produce strength, and Ca^{2+} ions trigger contraction [17]. Similar to skeleton and heart muscles, Ca^{2+} plays a significant role in initiating smooth muscle contraction. However, the source of Ca^{2+} increase in unitary smooth muscle may be very different [18]. In order to relax contracted smooth muscle, myosin needs to be dephosphorylated because dephosphorylated myosin can not bind to actin. Myosin light chain phosphotase enzyme, which is constantly active in the smooth muscle during rest and contraction periods, mediates dephosphorilation. When cytosolic calcium rises, the myosin phosphorylation rate of activated kinase exceeds the phosphotase dephosphorylation rate, and therefore the amount of phosphorylated myosin in the cell increases and the tension increases. When the cytosolic calcium concentration decreases, the dephosphorylation rate exceeds the phosphorylation rate, and the amount of phosphorylated myosin is low and relaxation occurs [16]. However, dephosphorylation of myosin light chain kinase does not lead to smooth muscle relaxation. There are several mechanisms. One is the latch bridge mechanism, that is, the myosin cross bridges continue to hold on to actin for a while after the cytoplasmic calcium concentration has decreased. This little energy produces continuous contraction and is especially important in vascular smooth muscles [18]. In addition to the cellular mechanisms that increase smooth muscle contraction, there are also cellular mechanisms that cause relaxation. This feature is important in the smooth muscles surrounding the blood vessels in order to increase blood circulation. It has long been known that endothelial cells, which line the inside of blood cells, secrete a substance NO that relaxes smooth muscle. NO produced in endothelial cells can spread into smooth muscle to act. Once becoming intramuscular, NO directly activates the soluable guanylate cyclase to produce another second messenger molecule, cyclic guanosine monophosphate (cGMP). This molecule activates ion channels, Ca homeostasis, phosphatases, or cGMP-specific protein kinases that may affect them all, leading to smooth muscle relaxation [18].

Atropine or l-hyocyanimine is an alkaloid obtained from the leaves of *Atropa bellodona* and *Datura stramonium* plants of solanacea family and effective in the peripheral system [19]. Atropine is a non-selective muscarinic receptor antagonist. The binding strength of muscarinic receptor antagonists to the receptor may overlap among various subtypes [20]. It reduces parasympathetic tone to keep sympathetic activity high. Atropine has the ability to change the cardiac rhythm [19]. Atropine and bomatropine and similar drugs such as scopolamine inhibit the effect of acetylcholine on the muscarinic types of cholinergic effector organs [21]. Imidazoline-derived phentolamine is a non-selective α-adrenergic receptor antagonist. Phentolamine effects are nonselective. Phentolamine have equal binding points on alpha-1 and alpha-2 receptors [22]. Nifedipine is a predominant calcium antagonist with vascular effects. Nifedipine inhibits voltage-dependent L-type Ca^{2+} channels in cardiac-related smooth muscle cell membranes. Nifedipine is a short-acting Ca^{2+} antagonist [19]. TEA has K^+ channel blocker effect. It is the first substance showing ganglion blocker effect [23]. Taurine is blocked by TEA. However, 4-AP facilitates K^+ flow by a mechanism which is not affected by glibenclamide, iberiotoxin or barium chloride ($BaCl_2$). TEA has the effect of blocking the potassium channel, which may be contrary to the effect of taurine. The vasorelaxan effect of taurine in rat isolated arteries is reduced by TEA [24]. Most K^+ channels are blocked by externally supplied TEA. However, sensitivity to TEA is different in various K^+ channel types [25]. The system that is not

related to neither the cholinergic nor adrenergic part of the autonomic nervous system is called the NANC system.

Both neuronal NO and endothelial NO have vasodilation effects. NO is thought to be the major neuromediatory of NANC in most parts of the body. NO is synthesized from an amino acid (l-arginine) at the nerve endings by NO synthetase [19]. In addition to adrenergic and cholinergic conduction in the autonomic nervous system, it provides conduction in dopaminergic, peptidergic and purinergic nerves [23]. NANC fibers were defined in 3 groups. The neurotransmitter of the purinergic fibers is ATP and cause vasoconstriction. The neurotransmitter of nitrosidergic fibers is NO. It causes vasodilatation. The neurotransmitter of the peptidergic nerves is vasoactive intestinal peptide (VIP) or peptide related to the calcitonin gene (CGRP) [26]. Phenylephrine is a synthetic alpha antagonist that is partially selective to alpha-1 receptors. It increases systolic and diastolic blood pressures by causing vasoconstriction [23].

Isolated tissue and isolated organ preparations have been in use for over one hundred years, providing researchers with convenient biological models that exist without the systemic influences of the intact animal [27]. Isolated preparations can permit molecular biologists to quantitate the physiological impact of the expression of these altered genetic sequences at the tissue and organ level [28]. Some isolated organ baths are ADInstruments, DMT, Orchid Scientific, Ugo Basile and Campden Instruments Ltd. [29].

Our experiments aimed to investigate the mechanism of action of APDTC on rat aortic smooth muscle. The mechanism of action of APDTC is not fully elucidated and, therefore, it is possible to inhibit the effects of α-adrenergic and β-adrenergic receptors, cholinergic receptors, l-type Ca^{2+} channels and K^{+} channels in aortic smooth muscle contraction and dilatation responses with the aim of investigating whether these factors are effective or not in the mechanism of action of APDTC. Some adrenergic and cholinergic receptors, l-type Ca^{2+} channels and K^{+} channels were blocked in 7 different groups, and therefore the action mechanism of APDTC whether is used or not on which channels and receptors and the extent to which they are effective were aimed to be determined. The contraction-relaxation responses after the administration of APDTC, atropine, phentolamine, propranolol, nifedipine, TEA and mix (atropine+phentolamine+propranolol) on living state controlled with potassium chloride (KCl) and blocked nitric oxide (NO) synthesis with L-NAME in the pre-contraction-induced aortic preparations with phenylephrine were investigated.

2. MATERIALS AND METHODS

2.1. Laboratory Animal Supply

This study was carried out at Kütahya Dumlupınar University (KDPÜ) Experimental Animals Breeding Application and Research Center in the Faculty of Science and Art, Biology Department, Physiology Laboratory. The study was approved by KDPÜ Animal Experiments Local Ethics Committee (HAYDEK) with the decree of 2015.12.05. In the experiments, 70 male wistar albino rats, produced in Saki Yenilli Experimental Animals Production Center, were used. The rats were fed ad libitum in well ventilated rooms, at the normal day and night cycles, with standard industrial feed and tap water. The studies were carried out immediately after obtaining the permission of the Animal Ethics Committee. 70 male rats weighing 300-350 g with ages of 6 and 7 months held by Experimental Animal Breeding Application and Research Center Laboratory were placed in cages as

following groups presented in 2b and 2c sections with all the experimental groups and procedures were explained.

2.2. Designing Test Groups

Test groups with used chemicals were as follows: 1st group is APDTC group (control), 2nd group is alpha adrenoreceptor antagonist (phentolamine)+APDTC, 3rd group is beta adrenoceptor antagonist (propranolol)+APDTC, 4th group is cholinergic receptor antagonist (atropine)+APDTC, 5th group is l-type calcium channel blocker (nifedipine)+APDTC, 6th group is potassium channel blocker (TEA)+APDTC and finally 7th group is both adrenergic and cholinegic receptor antagonist (phentolamine+propranolol+atropine)+APDTC. 10 animals were used per group.

2.3. Experimental Protocol

Experimental protocol for rat aorta smooth muscle contraction and relaxation response measurements is in detail as follows: After the animals were killed by cervical dislocation method, the thoracic aorta was removed by cutting from the neck to the abdomen (Figure 2.1). The reason that we use the cervical dislocation method is to avoid hormonal changes. Then, it was left into krebs-henseleit solution and was seperated from the surrounding connective tissue and then 3 mm circular sections were obtained. The weight of each organ was determined by precision scales. Isolated organs were placed in an organ bath. The temperature of the isolated organ bath was brought to 37°C and the a gas mixture of 95% O_2-% CO_2 was applied to the bath to oxygenate tissues. Tissue preparations under 1 g strain in the isolated organ bath were equilibrated by washing them with a krebs-henseleit solution for 45 minutes in every 15 minutes. The viability of the organs was tested with 6×10^{-2} M KCl. The organ was washed three times with krebs-henseleit solution by fill-and-empty technique to remove KCl from the bath. After 5 minutes, 10^{-2} M L-NAME was given to stop the NO effects. 10^{-4} M phenylephrine was added to the bath for precontraction. After 10 minutes, the antagonist or blocking agent was added to the designated groups in the bath. As the 1st group was the control group, only APDTC was administered, 10^{-5} M phentolamine in the 2nd group, 10^{-6} M propranolol in the 3rd group, 10^{-6} M atropine in the 4th group, 10^{-6} M nifedipine in the 5th group, 10^{-3} M TEA in the 6th group and finally 7th group with phentolamine+propranolol+atropine were used. 5.5×10^{-5} M APDTC was added 15 minutes after the antagonist administered to the other groups except the first group. We waited 10 minutes and the relaxation responses of the organ to the given chemicals were recorded in the data acquisition analysis system via the isometric transducer. All solutions during the experiment were prepared with distilled water. We used the isolated organ bath from Commat, Turkey with data acquisition analysis system from MP36, USA and isometric transducers from Biopac, USA.

2.4. Statistical Analysis

Bath recording lasted 1 hour 43 minutes. To compare, the phenylephrine and antagonist agent range was used, and then the antagonist PDTC range. The calculation was performed as follows. When phenylephrine is 100, % value was calculated by establishing the ratio of what would be the antagonist and what would be APDTC. Simultaneous experiments were carried out in four baths. SPSS program was used for statistical analysis. When statistical analysis was made in SPSS, both standard error and standard deviation were calculated and used in statistical processing. We drew the graphics according to our SPSS results in excel files. We also drew according to aortic phenylephrine values in the 100 file. We created p-p values according to this file. First we found the p-p values. Then we calculated how the drugs affected when the contraction was 100%. Then, we set the proportion to compare them with phenylephrine, such as what is the value of atropine when phenylephrine is 100. It also gave us statistical results if there were any significant results. The exact sig. or asymp. sig. from

JSR A
Journal of Scientific Reports

the mann-whitney test results made us decide whether the difference is meaningful or meaningless. The data obtained from the experiments were evaluated by applying mann-whitney u and kruskal wallis tests. $p<0.05$ values were considered statistically significant.

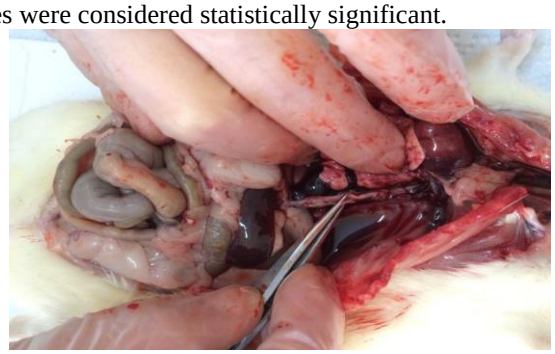

Figure 1. Rat Aorta.

3. RESULTS

In our study, 7 different groups were studied as 1st group as the control group, 2nd group as atropine group, 3rd group as phentolamine group, 4th group as propranolol group, 5th group as nifedipine group, 6th group as TEA group and 7th group as mix group (phentolamine+propranolol+atropine).
In our study, contraction-dilatation responses of the tissue to APDTC were investigated by applying various antagonists or channel blockers to pre-contracted aortic tissue with phenylephrine. There was a significant difference between nifedipine administered group and phentolamine group, propranolol group and mix groups ($p<0.05$). There was a significant difference between phentolamine+propranolol+atropine-treated mix group and control group, atropine group and nifedipine group ($p<0.05$) (Table 1 and Figure 2). APDTC on y axis in Figure 2 shows contraction percentage of smooth muscle of aorta by adding APDTC on pre-contracted aorta with phenylephrine in the presence and absence of antagonists or blockers in all 7 groups. Figure 2 is the comparison of all groups in one graph.

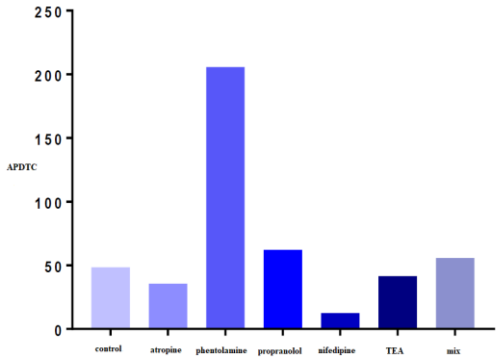

Figure 2. Effects of APDTC on pre-contracted aorta with phenylephrine in the presence and absence of antagonists or blockers.

JSR A
Journal of Scientific Reports

Table 1. Comparison of APDTC among groups. There was a significant difference between nifedipine administered group and phentolamine group, propranolol group and mix groups ($p < 0.05$). There was a significant difference between phentolamine+propranolol+atropine-treated mix group and control group, atropine group and nifedipine group ($p < 0.05$). Values that are smaller than 0.05 are in bold.

Groups	Control	Atropine	Phentolamine	Propranolol	Nifedipine	TEA	Mix
Control	-	0.450	0.070	0.174	0.450	0.450	**0.041**
Atropine	0.450	-	0.131	0.326	0.070	0.940	**0.023**
Phentolamine	0.070	0.131	-	0.734	**0.008**	0.199	0.880
Propranolol	0.174	0.326	0.734	-	**0.023**	0.364	0.940
Nifedipine	0.450	0.070	**0.008**	**0.023**	-	0.131	**0.000**
TEA	0.450	0.940	0.199	0.364	0.131	-	0.112
Mix	**0.041**	**0.023**	0.880	0.940	**0.000**	0.112	-

There was a significant difference between precontraction responses induced by phenylephrine in the aortic smooth muscle and APDTC responses in the presence of atropine ($p < 0.05$). APDTC showed a contraction response in the presence of atropine on the contraction induced by phenylephrine in aortic tissue. However, there was no significant difference between the control and atropine group. Phenylephrine-contracted aortic smooth muscle relaxation responses of APDTC did not affect atropine, a nonselective muscarinic receptor antagonist ($p > 0.05$) (Table 2 and Figure 3).

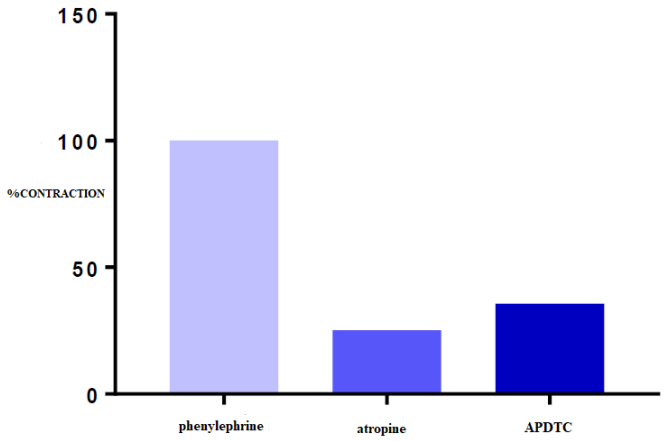

Figure 3. The effect of APDTC in the presence of atropine and atropine substance on aortic contraction.

JSR A
Journal of Scientific Reports

Table 2. Comparison of APDTC in the presence of atropine and by atropine. There was a significant difference between precontraction responses induced by phenylephrine in the aortic smooth muscle and APDTC responses in the presence of atropine ($p < 0.05$). Values that are smaller than 0.05 are in bold.

Atropine	Phenylephrine	Antagonist	APDTC
Phenylephrine	-	**0.001**	**0.001**
Antagonist	**0.001**	-	0.257
APDTC	**0.001**	0.257	-

There was a significant difference between the contraction responses of phenylephrine and phentolamine in aortic smooth muscle ($p<0.05$). APDTC showed contraction response in the presence of phenylephrine. There was no significant difference between the control group and phentolamine group. Phenylephrine-contracted aortic smooth muscle relaxation responses of APDTC were not affected by ($p>0.05$) (Table 3 and Figure 4).

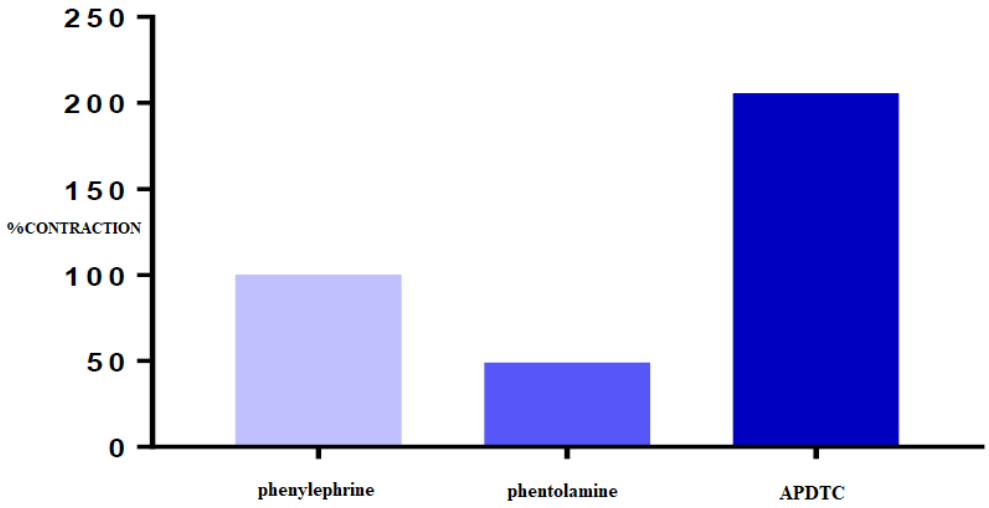

Figure 4. The effect of APDTC on aortic contraction in the presecence of phenilephrine and phentolamine.

Table 3. Comparison of APDTC in the presence of phentolamine and phenylephrine. There was a significant difference between the contraction responses of phenylephrine and phentolamine in aortic smooth muscle ($p<0.05$). Values that are smaller than 0.05 are in bold.

Phentolamine	Phenylephrine	Antagonist	APDTC
Phenylephrine	-	**0.000**	0.419
Antagonist	**0.000**	-	0.762
APDTC	0.419	0.762	-

JSR A
Journal of Scientific Reports

There was no significant difference between precontraction responses in the aortic smooth muscle with phenylephrine and APDTC responses in the presence of propranolol (p> 0.05). APDTC showed a relaxing effect in the presence of propranolol on contraction of aortic tissue with phenylephrine. At the same time, the contraction effect of propranolol turned into a relaxing effect with the administration of APDTC. There was no significant difference between the control group and the propranolol administered group (p> 0.05) (Table 4 and Figure 5).

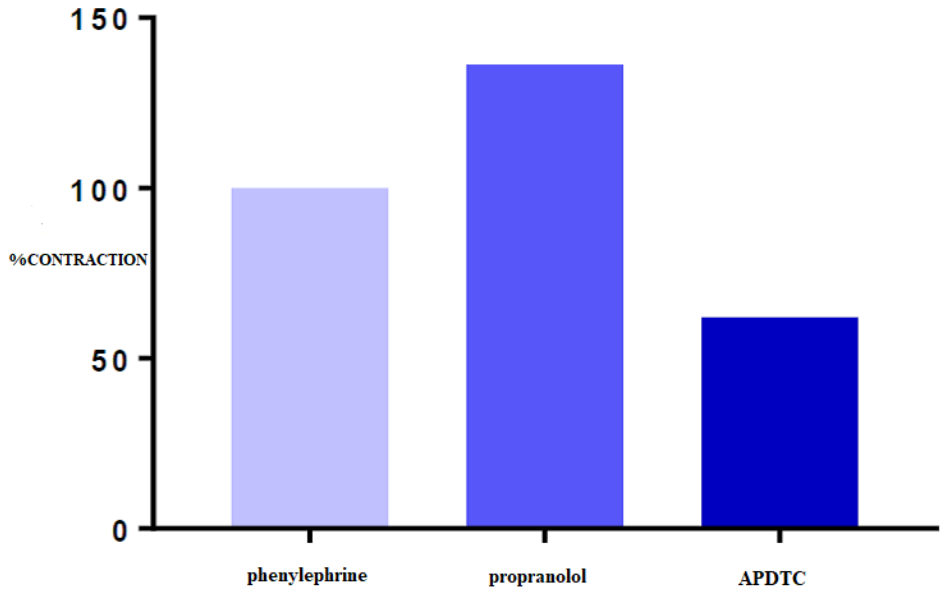

Figure 5. Effect of APDTC on aortic contraction with and presence of propranolol.

Table 4. Comparison of APDTC with and in the presence of propranolol.

Propranolol	**Phenylephrine**	**Antagonist**	**APDTC**
Phenylephrine	-	0.419	0.106
Antagonist	0.419	-	0.307
APDTC	0.106	0.307	-

There is a significant difference in aortic smooth muscle contractile responses between APDTC responses in the presence of nifedipine and phenylephrine (p <0.05). There was no significant difference between the control group and nifedipine administered group (p> 0.05). APDTC showed a relaxing effect on contraction of aortic tissue with phenylephrine in the presence of nifedipine. In addition, the relaxant effect of nifedipine continued increasing gradually with the administration of APDTC (p <0.05) (Table 5 and Figure 6).

JSR A
Journal of Scientific Reports

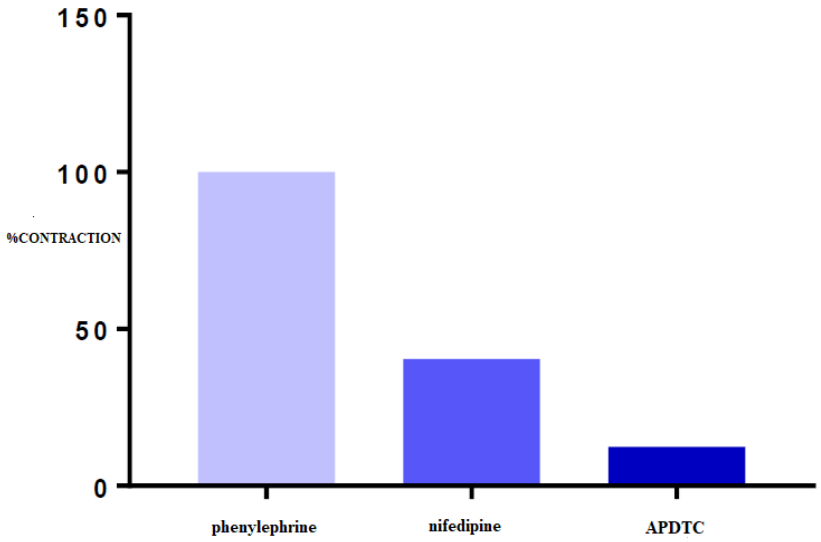

Figure 6. The effect of APDTC on aortic contraction with and in the presence of nifedipine.

Table 5. Comparison of APDTC with and in the presence of nifedipine. There is a significant difference in aortic smooth muscle contractile responses between APDTC responses in the presence of nifedipine and phenylephrine ($p < 0.05$). The relaxant effect of nifedipine continued to increase gradually with the administration of APDTC ($p < 0.05$). Values that are smaller than 0.05 are in bold.

Nifedipine	**Phenylephrine**	**Antagonist**	**APDTC**
Phenylephrine	-	**0.001**	**0.000**
Antagonist	**0.001**	-	**0.016**
APDTC	**0.000**	**0.016**	-

There was a statistically significant difference between contraction responses with phenylephrine and potassium channel blocker TEA in aortic smooth muscle ($p < 0.05$). TEA, a potassium channel blocker in the aortic tissue, produced a relaxation response. However, there was no significant difference between the control group and the TEA administered group ($p > 0.05$) (Table 6 and Figure 7).

JSR A
Journal of Scientific Reports

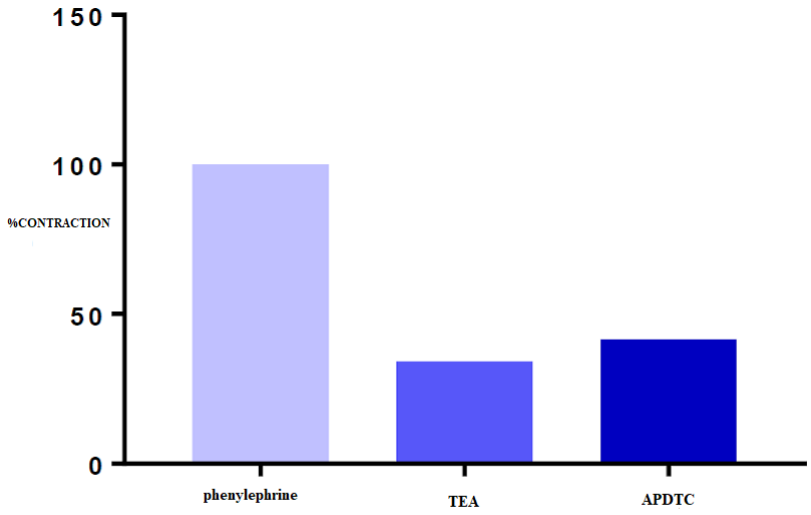

Figure 7. The effect of APDTC on aortic contraction with and in the presence of TEA substance.

Table 6. Comparison of APDTC in the presence of TEA and TEA. There was a statistically significant difference between contraction responses with phenylephrine and potassium channel blocker TEA in aortic smooth muscle ($p < 0.05$). Values that are smaller than 0.05 are in bold.

TEA	**Phenylephrine**	**Antagonist**	**APDTC**
Phenylephrine	-	**0.001**	**0.001**
Antagonist	**0.001**	-	0.791
APDTC	**0.001**	0.791	-

There is a significant difference in contractile responses of aortic smooth muscle induced between APDTC responses in the presence of phentolamine+propranolol+atropine and phenylephrine ($p < 0.05$). APDTC showed a relaxation effect on contraction of phenylephrine-induced aortic tissue in the presence of adrenergic and cholinergic receptor antagonists as phentolamine+propranolol+ atropine. In addition, the contraction effect of fentolamine+propranolol+atropine, which are adrenergic and cholinergic receptor antagonists, turned into a statistically relaxing effect with the application of APDTC ($p<0.05$). There was a significant difference between the control group and the mix group. Phentolamine+propranolol+atropine changed APDTC's phenylephrine-contracted aortic smooth muscle relaxation responses ($p<0.05$) (Table 7 and Figure 8).

JSR A
Journal of Scientific Reports

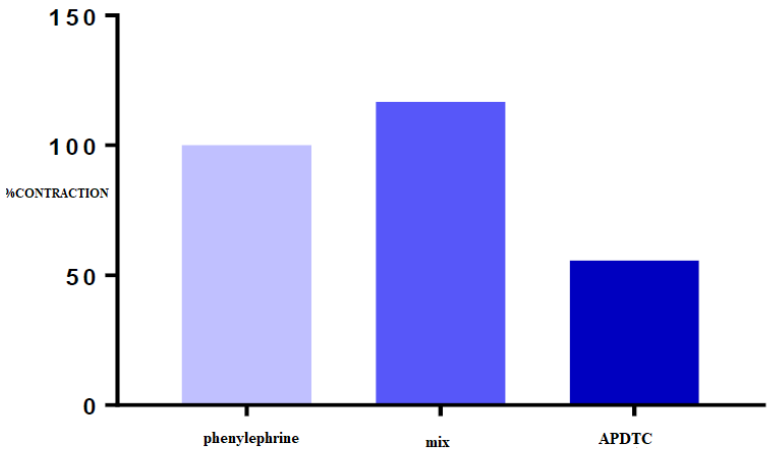

Figure 8. The effect of APDTC in aortic contraction with and in the presence of phentolamine+ propranolol+atropine.

Table 7. Comparison of APDTC with and in the presence of mix. There is a significant difference in contractile responses of aortic smooth muscle induced between APDTC responses in the presence of phentolamine+propranolol+atropine and phenylephrine ($p<0.05$). The contraction effect of fentolamine+propranolol+atropine turned into a statistically relaxing effect with the application of APDTC ($p<0.05$). There was a significant difference between the control group and the mix group. Phentolamine+propranolol+atropine changed APDTC's phenylephrine-contracted aortic smooth muscle relaxation responses ($p<0.05$). Values that are smaller than 0.05 are in bold.

Mix	**Phenylephrine**	**Antagonist**	**APDTC**
Phenylephrine	-	0.419	**0.001**
Antagonist	0.419	-	**0.001**
APDTC	**0.001**	**0.001**	-

4. DISCUSSION AND CONCLUSION

APDTC, a specific inhibitor of low molecular weight NF-κB exibiting antioxidant ability to eliminate free toxic radicals, interferes with the production of pro-inflammatory cytokines [30]. All substances capable of inducing NF-κB can be blocked by antioxidants. It reduces the ability to bind to DNA, interferes with the activation signal pathway for NF-κB, and stabilizes or increases the IκBa synthesis mechanism to inhibit NF-κB activity [31]. Investigating the contraction-relaxation responses of APDTC, a dose-dependent relaxation response against precontraction of KCl after contraction was obtained [32]. We have investigated the mechanism of action of APDTC in vitro in aortic smooth muscle as a result of the fact that the mechanism of action of APDTC, which is determined to relax the aortic smooth muscle, has not been revealed yet.

JSR A
Journal of Scientific Reports

In order to determine the mechanism of action of APDTC, our experiments were carried out in seven groups (control, atropine, phentolamine, propranolol, nifedipine, TEA, and fentolamine+propranolol +atropine) to determine which receptors and channels were used in the aortic smooth muscle contracted by phenylephrine whose NO synthesis was stopped by L-NAME. We used L-NAME to prevent the relaxation effect of NO and for the pre-contraction to run smoothly. 5.5×10^{-5} M APDTC produced a relaxation response in the aortic smooth muscle. In a study, the cellular mechanism of nitric oxide (NO)-induced relaxation in corporeal smooth muscle (CSM) of the guinea-pig was investigated. Changes in the intracellular concentration of calcium ions ($[Ca^{2+}]_i$), membrane potential and isometric tension were measured. CSM cells exhibited spontaneous depolarizations and transient increases in $[Ca^{2+}]_i$ (Ca^{2+} transients) which were accompanied by contractions. This spontaneous activity was abolished by nifedipine (10 **μ**M). NO released by 3-morpholino-sydnonimine (SIN-1, 10 **μ**M) hyperpolarized the membrane and prevented the generation of spontaneous depolarizations. SIN-1 also abolished Ca^{2+} transients and associated contractions. These effects of SIN-1 were blocked by 1*H*-[1,2,4]oxadiazole[4,3-a]quinoxalin-1-one (ODQ, 10 **μ**M), an inhibitor of guanylate cyclase. Noradrenaline (NA, 1 **μ**M) increased $[Ca^{2+}]_i$ to levels similar to those produced by high potassium-containing solution (high K^+ solution, $[K^+]_o$ = 40 mM), however, NA-induced contractions were three times greater in amplitude than those induced by high K^+ solution. In NA precontracted preparations, SIN-1 inhibited 80% of the contraction and decreased $[Ca^{2+}]_i$ by 20%. In contrast, nifedipine reduced $[Ca^{2+}]_i$ by 80%, while the level of contraction was decreased by only 20%. SIN-1-induced reduction in $[Ca^{2+}]_i$ but not the tension effect, was abolished by pretreatment with cyclopiazonic acid (CPA, 10 μM). In high K^+ precontracted preparations, SIN-1 inhibited 80% of the contraction and reduced $[Ca^{2+}]_i$ by 20%. Nifedipine, however, largely abolished increases in both $[Ca^{2+}]_i$ and tension under these circumstances. These results suggest that decreasing the sensitivity of contractile proteins to Ca^{2+} is probably the key mechanism of NO-induced relaxation in CSM of the guinea-pig [33].

In the atropine group, there was no statistically significant difference in phenylephrine-contracted aortic smooth muscle contraction responses between the administration of 5.5×10^{-5} M APDTC in the presence of atropine and the administration of 5.5×10^{-5} M APDTC to the control group. In the presence of 10^{-6} M atropine, APDTC caused contraction of the aortic smooth muscle. Previous studies have shown that atropine causes relaxation in rat aortic smooth muscle [34]. Atropine has a double effect on rat aortic contraction [34]. It causes a contraction effect at lower concentrations (10 nM-1 μM) and relaxation effect at higher concentrations (1-100 μM) on smooth muscle [34, 35]. Atropine administration reversed the relaxation response of APDTC, but was not statistically significant. This indicates that the APDTC dose of 5.5×10^{-5} M does not use muscarinic-cholinergic pathways in the aortic smooth muscle. A comparative study explain some details as follow: 1. In the rabbit isolated aorta, atropine ($3 \times 10^{(-6)}$ M-$10^{(-4)}$ M) inhibited contractile response to noradrenaline without affecting contraction to KCl. 2. In the presence of contraction to noradrenaline, atropine ($3 \times 10^{(-7)}$ M-$10^{(-4)}$ M) caused concentration-dependent relaxation. Pretreatment with theophylline ($10^{(-3)}$ M) potentiated the relaxant action of atropine. Relaxation to atropine was not affected by the specific guanosine 3':5'-cyclic monophosphate phosphodiesterase inhibitor, M & B 22,948 ($10^{(-4)}$ M), tetraethylammonium (10 mM), indomethacin ($10^{(-5)}$ M), propranolol ($10^{(-7)}$ M), nifedipine ($10^{(-6)}$ M) or removal of the endothelium. 3. Relaxation to either atropine or prazosin was not affected by preincubation with prazosin and atropine, respectively. 4. In $Ca^{(2+)}$-free medium containing EGTA and nifedipine, atropine ($10^{(-7)}$ M-$10^{(-4)}$ M) inhibited the residual noradrenaline response more than the subsequent $Ca^{(2+)}$-induced contraction. Pretreatment with either theophylline ($10^{(-3)}$ M), forskolin ($3 \times 10^{(-7)}$ M) or a low concentration of prazosin ($3 \times 10^{(-9)}$ M) also inhibited the residual contraction to noradrenaline and Ca^{2+}. The effect of combined treatment of atropine and any of these agents was much greater than

JSR A
Journal of Scientific Reports

with each individual agent. 5. Atropine ($10^{(-6)}$ M-$10^{(-4)}$ M) also inhibited increases in the level of inositol monophosphates (IP) in response to noradrenaline. Theophylline ($10^{(-3)}$ M) and a low concentration of prazosin (3 x $10^{(-9)}$ M) also inhibited IP formation. Combined with atropine, the effect was much greater than with each of these agents individually. 6. Atropine did not affect adenosine 3':5'-cyclic monophosphate (cyclic AMP) levels in the aorta and also failed to displace specific [3H]-prazosin binding.7. These results suggest the possibility that smooth muscle relaxation to atropine may be due to the inhibition of phosphoinositide metabolism. The relaxation is not apparently due to an action of atropine on ax-adrenoceptors, or a change in the level of cyclic AMP [36].

In the phentolamine group results, administration of 5.5×10^{-5} M dose of APDTC in the presence of phentolamine in the bath did not cause a statistically significant difference compared to 5.5×10^{-5} M APDTC applied to the control group. There was a statistically insignificant increase in APDTC aortic smooth muscle contractions in the presence of a 10^{-5} M dose of phentolamine. Electrical field stimulation (EFS)-induced contractions were found to be significantly reduced in the presence of phentolamine [37]. APDTC reversed the relaxant effect of phentolamine, but APDTC maintains its relaxation response. For this reason, we thought that APDTC did not use α-adrenergic receptors. A comparative study explain some details as follow: Endothelium is the main source of catecholamine release in the electrical-field stimulation (EFS)–induced aortic contractions of the non- venomous snake *Panterophis guttatus*. However, adrenergic vasomotor control in venomous snakes such as *Crotalus durissus terrificus* and *Bothrops jararaca* has not yet been investigated. *Crotalus* and *Bothrops* aortic rings were mounted in an organ bath system. EFS-induced aortae contractions were performed in the presence and absence of guanethidine (30 μM), phentolamine (10 μM) or tetrodotoxin (1 μM). Frequency-induced contractions were also performed in aortae with endothelium removed. Immunohistochemical localization of both tyrosine hydroxylase (TH) and S-100 protein in snake aortic rings and brains, as well as in human tissue (paraganglioma tumour) were carried out. EFS (4 to 16 Hz) induced frequency-dependent aortic contractions in both *Crotalus* and *Bothrops*. The EFS-induced contractions were significantly reduced in the presence of either guanethidine or phentolamine in both snakes ($p<0.05$), whereas tetrodotoxin had no effect in either. Removal of the endothelium abolished the EFS-induced contractions in both snakes aortae ($p<0.05$). Immunohistochemistry revealed TH localization in endothelium of both snake aortae and human vessels. Nerve fibers were not observed in either snake aortae. In contrast, both TH and S100 proteins were observed in snake brains and human tissue. Vascular endothelium is the main source of catecholamine release in EFS-induced contractions in *Crotalus* and *Bothrops* aortae. Human endothelial cells also expressed TH, indicating that endothelium- derived catecholamines possibly occur in mammalian vessels [38].

There was no statistically significant difference between 5.5×10^{-5} M APDTC in the presence of a propranolol dose of 10^{-6} M and 5.5×10^{-5} M APDTC administered to the control group in aortic smooth muscle. In phenylephrine-contracted aortic smooth muscle, 10^{-6} M propranolol produced contraction. Adrenaline-induced relaxation in rat thoracic aorta has been shown to be suppressed by propranolol [39]. However, APDTC continued its relaxation responses. Blocking β-adrenergic receptors did not alter the relaxation effect of APDTC and thus we cannot conclude that it acts through these receptors. A comparative study explain some details as follow: AD-induced relaxation was completely suppressed by propranolol (10^{-7} M) or by ICI-118,551 (10^{-8} M) plus atenolol (10^{-6} M), and was also very strongly inhibited by ICI-118,551 (10^{-8} M) alone. AD (10^{-5} M) increased tissue cAMP levels by approximately 1.9-fold compared with that in non-stimulated aortic tissue, but did not significantly

JSR A
Journal of Scientific Reports

increase cAMP levels in the presence of ICI-118,551 (10^{-8} M) or SQ 22,536 (10^{-4} M). AD-induced relaxation was strongly suppressed by SQ 22,536 (10^{-4} M). NA-induced relaxation was almost completely suppressed by atenolol (10^{-6} M) plus ICI-118,551 (10^{-8} M) although it was hardly affected by ICI-118,551 (10^{-8} M) alone. NA (10^{-5} M) increased tissue cAMP levels by approximately 2.2-fold compared with that in non-stimulated aortic tissue, but did not significantly increase cAMP levels in the presence of atenolol (10^{-6} M) or SQ 22,536 (10^{-4} M). NA-induced relaxation was strongly suppressed by SQ 22,536 (10^{-4} M). In rat thoracic aorta, AD- and NA-induced relaxations, which are both strongly dependent on increased tissue cAMP levels, are mainly mediated through β_2- and β_1-adrenoceptors respectively [40].

In the nifedipine treated group, there was no significant difference between the 5.5×10^{-5} M APDTC control group and the phenylephrine-contracted APDTC administered group. Nifedipine inhibited phenylephrine contraction responses in the aorta and caused relaxation. In aortic preparations, it inhibits KCI-induced contractions in a concentration-dependent manner [41]. It has been found that leptin-induced vasoconstriction in the thoracic aorta with endothelium is completely destroyed in the presence of an l-type calcium blocker nifedipine [42]. The relaxation response caused by nifedipine was continued with APDTC in statistically significant manner. Nifedipine increased the relaxation effect of APDTC even more, and blocking the channel did not change this effect. L-type calcium channels do not play a role in the mechanism of action of APDTC. A comparative study explain some details as follow: Circulating leptin concentrations were increased in SHR. Serum metabolic parameters, including glucose, insulin, total cholesterol and triglyceride levels, were also elevated in SHR. Leptin did not modify the angiotensin II-induced vasoconstriction in SHR either in intact or endothelium-denuded aortic rings. In addition, leptin was not able either to diminish the angiotensin II-induced the peak rise of [Ca^{2+}]i or to accelerate the recovery rate to basal calcium levels in VSMCs from SHR. However, OB-Ra and OB-Rb mRNA and protein expression were increased in SHR VSMCs. The lack of effect of leptin on angiotensin II-induced contraction in the aorta of SHR is due to an impaired handling of [Ca2+]i in VSMCs. Hyperleptinemia and overexpression of OB-R in VSMCs could be compensatory mechanisms against VSMC leptin resistance in genetically hypertensive rats [43].

No statistically significant difference was found between the control group and the group of 5.5×10^{-5} M APDTC administered organ bath containing 10^{-3} M TEA. The aorta showed relaxation response with TEA. The administration of APDTC to the relaxed aorta with TEA caused contraction. In rat isolated aortic rings contracted with phenylephrine, the vasorelaxation with taurine is blocked by TEA [24]. The relaxant activity of T. fagifolia aqueous fraction (Tf-AQF) has been shown to decrease in the presence of TEA (a non-selective inhibitor of K^+ channels) and the pharmacological potential is weakened [44]. Contractions with APDTC are not important enough to alter the relaxation response and therefore suggesting that APDTC does not use potassium channels. A comparative study explain some details as follow: The acute toxicity, the antioxidant activity, and the pharmacological activity on the gastrointestinal tract of rodents of the ethanolic extract (TFEE) from the bark of Terminalia fagifolia Mart. & Zucc. (Combretaceae) and of its aqueous (TFAqF), hydroalcoholic (TFHAF), and hexanic (TFHEXF) partition fractions have been evaluated. TFEE presented low acute toxicity, antioxidant, and antiulcerogenic activity against ethanol-induced ulcers, which was partially blocked by pretreatment with L-NAME and indomethacin. It reduced the total acidity and raised the pH of gastric secretion. Additionally, TFEE delayed gastric emptying and slightly inhibited the small intestinal transit and also presented a weakly antidiarrheal activity. The antiulcerogenic and antioxidant activity were also detected in TFAqF and TFHAF but not in TFHEXF. The antisecretory

and gastroprotective activity of TFEE partially involve the nitric oxide and prostaglandin participation. Nevertheless, TFEE, TFAqF, and TFHAF drastically reduced the mucus layer adhered to the gastric wall of rats treated with ethanol or indomethacin. Complementary studies are required in order to clarify the paradox of the presence of a gastroprotector activity in this plant that, at the same time, reduces the mucus layer adhered to the gastric Wall [45].
In the mix group, we tried to determine whether the NANC system plays a role on the mechanism of action of APDTC. 5.5×10^{-5} M APDTC was applied to the organ bath containing the mix and a significant difference between the control group was founded. Mix group in aortic smooth muscle produced contraction response. APDTC inhibited the contraction by producing an antagonistic effect with the mix group and produced a relaxation response. Significant decrease in relaxation in the mix group compared to the APDTC relaxant effect in the control group showed that the mechanism of action of APDTC could be either adrenergic or cholinergic.

In our investigative mechanism of action of APDTC study, with proven anti-oxidant, anti-viral and anti-inflammatory effects in aortic smooth muscle, we determined that APDTC showed relaxation response in rat aortic smooth muscle contracted with phenylephrine. This response was altered by the mix group, suggesting that APDTC may be effective through adrenergic and cholinergic receptors. We also think that the NANC system, which plays an important role in aortic smooth muscle contraction-relaxation, or different pathways, will help to elucidate the mechanism of APDTC by further studies.

REFERENCES

[1] Barrett, K.E., Barman, S.M., Boitano,S., Brooks, H., (2010), Ganong's Review of Medical Physiology, 23. Baskı, New York: McGraw-Hill Higher Education, s.110, 111 , 112, 544, 563, 564.

[2] https://www.sigmaaldrich.com

[3] Parlak, N., (2009), Pirolizidin Alkaloidinin Neden Olduğu Hepatotoksisitede Nükleer Faktör Kappa B İnhibitörü Pirolidin Ditiyokarbamat'ın Koruyucu Etkinliğinin Değerlendirilmesi, Uzmanlık Tezi, Abant İzzet Baysal Üniversitesi Tıp Fakültesi, Fizyoloji Anabilim Dalı, Bolu.

[4] Parlaktaş, S.B., Fırat, F., Erdemir, F., (2010), Erektil Disfonksiyonunun Medikal Tedavisindeki Yeni Gelişmeler, Türk Üroloji Seminerleri, s. 1, 92-98.

[5] Wan, D., Wu, Q., Qu, W., Liu, G., Wang, X., (2018), Pyrrolidine Dithiocarbamate (PDTC) Inhibits DON-Induced Mitochondrial Dysfunction and Apoptosis via the NF-κB/iNOS Pathway, Oxidative Medicine and Cellular Longevity, 1324173:8.

[6] Kovacich, J.C., Boyle, E.M.Jr., Morgan, E.N., Canty, T.G.Jr., Farr, A.L., Caps, M.Y., Frank, N., Pohlman, T.H., Verrier, E.D., (1999), Inhibition Of The Transcriptional Activator Protein Nuclear Factor Kappa B Prevents Hemodynamic Instability Associated With The Wholebody İnflammatory Response Syndrome. J. Thorac, Cardiovasc, Surg., 118, s.154–162.

[7] Hagar, H.H., Medany, A.E., Eter, E.E., Arafa, M., (2007), Ameliorative Effect Of Pyrrolidinedithiocarbamate On Acetic Acid–Induced Colitis In Rats, European Journal Of Pharmacology, 554, s.69–77.

[8] Cao, S., Li. Q., Hou. J., Li, Z., Cao, X., Liu, X., Qin, B., (2019), Intrathecal TRPM8 blocking attenuates cold hyperalgesia via PKC and NF-κB signaling in the dorsal root ganglion of rats with neuropathic pain, Journal of Pain Research, 18;12:1287-1296.

[9] Yang, H., Ma. S., , Guo. Y., Cui. D., Yao. J.,(2019), Bidirectional Effects of Pyrrolidine Dithiocarbamate on Severe Acute Pancreatitis in a Rat Model, Dose Response, 31;17(1):1559325819825905.

[10] Zhang, B., Xu, J., Quan, Z., Qian, M., Liu, W., Zheng, W., Yin, F., Du, J., Zhi, Y., Song, N., (2018), Klotho Protein Protects Human Keratinocytes from UVB-Induced Damage Possibly by Reducing Expression and Nuclear Translocation of NF-κB, Medical Sciense Monitor, 24: 8583–8591.

[11] Sun, H, Z., Gong, X, Y., Wu, L., Wang, X, X., Nie , Y, N., Shang, R., Wang, H., Li. Y, C., Sun ,QF., Gao, PF., Bi .JX., (2018), Journal of Physıology and Pharmacology, 69, 3, 419-422.

[12] Berne, R.M., Levy, M.N., Koeppen, B.M., Stanton, B.A., (2008), Fizyoloji (Çeviri. Türk Fizyolojik Bilimler Derneği), Beşinci baskı, Güneş Kitabevi, İstanbul, s. 223-358.

[13] Ackermann, U., (2006), Fizyoloji, (çev. Alican, İ.), İstanbul Medikal Yayıncılık, s,36, 199, 191.

[14] Akçay , M., (1971), Kas Fizyolojisi ders Kitabı, Güven matbaası, Ankara, s. 1-10.

[15] Guyton, A.C., Hall, J. E., (2007), Tıbbi Fizyoloji, (çev. Yeğen B. Çavuşoğlu, H), Onbirinci baskı, Nobel Tıp Kitabevi, İstanbul, s. 72, 92, 94.

[16] Widmaier, E, P. , Raff, H. , Strong, K.T., (2004), Vander's Human Psikology: the Mescanisms of Body Function, 10. Baskı, San Fransisco: Mc Graw- Hill Higher Education, s. 304.

[17] Webb, R, C., (2003), Smooth Muscle contraction and Relaxion, American physiological society, 27 (1-4):201-6.

[18] Barrett, K.E., Barman, S.M., Boitano,S., Brooks, H., (2010), Ganong's Review of Medical Physiology, 23.Baskı, New York: McGraw-Hill Higher Education, s.110,111,112, 544, 563, 564.

[19] Dökmeci, Ġ., (2000), Kısaltılmış Bilgiler ve Sınav Hazırlık Soruları, Nobel Tıp Kitabevleri, s.81, 75, 96, 248.

[20] Altınkurt, O., (1981), Farmakoloji I, Ankara üniversitesi Basımevi, Ankara, s. 35, 105.

[21] Guyton A. C., Hall, J.E., (1996) Tıbbi Fizyoloji (çev. ÇavuĢoğlu, H.), 9. Baskı, Nobel Tıp Kitabevleri, İstanbul, s. 780, 781.

[22] Bökesoy, T. A., Çakıvı, İ., Melli, M., (2000), Farmakoloji Ders Kitabı, Ankara: Gazi Kitabevi Yayınları, s. 46, 165, 166.

[23] Süzer, Ö., (2005), Premium Süzer Farmakoloji, 3. Baskı Klinisyen Kitabevleri, S.78, 65, 72.

[24] Niu, L.G., Zhang, M. S., Liu, Y., Xue, W. X., Liu, D. B., Zhang, J., Liang, Y. Q., (2008), Vasorelaxant effect of taurine is diminished by tetraethylammonium in rat isolated arteries, European Journal of Pharmacology, 580: 169–174.

[25] Bisset, D., Chung, S.H., (2008), Efficacy of external tetraethylammonium block of the KcsA potassium channel: Molecular and Brownian dynamics studies, Biochimica et Biophysica Acta (BBA) - Biomembranes, 1778(10): 2273-82.

[26] Ackermann, U., (2006), Fizyoloji, İstanbul Medikal Yayıncılık, s.36, 199, 191.

[27] Chien, K.R., (1996), Genes and physiology: molecular physiology in genetically engineered animals, J. Clin. Investigation 97:901-909.

[28] Blinks, J.R., (1965), Convenient apparatus for recording contractions of isolated muscle. J. Appl. Physiol. 20:755-7.

[29] https://www.adinstruments.com

[30] Yin, J., Wu, M., Duan, J., Liu, G., Cui, Z., Zheng, J., Chen, S., Ren, W., Deng, J., Tan, X., Al-Dhabi, N. A., Duraipandiyan, V., Liao, P., Li, T., Yulong, Y., (2015), Pyrrolidine Dithiocarbamate Inhibits NF-KappaB Activation and Upregulates the Expression of Gpx1, Gpx4, Occludin, and ZO-1 in DSS-Induced Colitis, Applied Biochemistry and Biotechnology, 177(8): 1716-1728.

[31] Kan, S., Zhou, H., Jin, C., Yang, H., (2015), Effects of PDTC on NF-κB expression and apoptosis in rats with severe acute pancreatitis-associated lung injury, International journal of clinical & experimental medicine, 8(3): 3258–3270.

[32] Akca, S. D., (2015), L-NAME Uygulanmış Sıçan Aortunda Atorvastatin Ca, Kafeik Asit Fenil Ester, Ammonium Pyrrolidine Dithiocarbamate ve SG-Benz' in Kasılma-Gevşeme Üzerine Etkisi, Yüksek Lisans Tezi, Dumlupınar Üniveristesi Fen Bilimleri Enstitüsü, Kütahya, s. 45.

[33] Hikaru Hashitani, Hiroyasu Fukuta, Emma J Dickens, and Hikaru Suzuki, (2002), Cellular mechanisms of nitric oxide-induced relaxation of corporeal smooth muscle in the guinea-pig, J. Physiol. ; 538(Pt 2): 573–581. doi: 10.1113/jphysiol.2001.013049, PMCID: PMC2290081, PMID: 11790820.

[34] Kwan, C. Y., Zhang, W. B., Kwan, T. K., Sakai, Y., (2003), In vitro relaxation of vascular smooth muscle by atropine: involvement of K^+ channels and endothelium, Naunyn-Schmiedeberg's Arch Pharmacol, 368: 1-9.

[35] Choi, Y. D., Chung, W. S., Choi, H. K., (1999), The action mechanism of relaxation effect of atropine on the isolated rabbit corpus cavernosum, The Journal of Urology, 161(6): 1976-79.

[36] N Satake 1, S Kiyoto, S Shibata, V Gandhi, D J Jones, M Morikawa, (1992), Possible mechanisms of inhibition with atropine against noradrenaline-induced contraction in the rabbit aorta,
[37] Br J Pharmacol;107(2):553-8. doi: 10.1111/j.1476-5381.1992.tb12782.x. PMID: 1330185 PMCID: PMC1907863.

[38] Campos, R., Justo, A.F.O., Mónica, F.Z., Cogo, J.C., Moreno, R.A., de Souza, V.B., Schenka, A.A., De Nucci, G., (2018), Electrical field-induced contractions on Crotalus durissus terrificus and Bothrops jararaca aortae are caused by endothelium-derived catecholamine, Plos one, 10;13(9):e0203573.

[39] [38] Campos R, Justo AFO, Mónica FZ, Cogo JC, Moreno RA, de Souza VB, et al., (2018), Electrical field-induced contractions on *Crotalus durissus terrificus* and *Bothrops jararaca* aortae are caused by endothelium-derived catecholamine. PLoS ONE 13(9): e0203573.

[40] Shiina, S., Kanemura, A., Suzuki, C., Yamaki, F., Obara, K., Chino, D., Tanaka, Y., (2018), β-Adrenoceptor subtypes and cAMP role in adrenaline- and noradrenaline-induced relaxation in the rat thoracic aorta, Journal of smooth muscle research, 54: 1–12.

[41] Shunsuke Shiina, Ayaka Kanemura, Chihiro Suzuki, Fumiko Yamaki, Keisuke Obara, Daisuke Chino, and Yoshio Tanaka, (2018), β-Adrenoceptor subtypes and cAMP role in adrenaline- and noradrenaline-induced relaxation in the rat thoracic aorta, J Smooth Muscle Res.; 54: 1–12. doi: 10.1540/jsmr.54.1. PMCID: PMC5863045. PMID: 29540622.

[42] Takahara, A., Nozaki, S., Ishiguro, A., Okamura, K., Cao, X., Aimoto, M., Nagasawa, Y., (2018), Selectivity of Ca^{2+} channel blockers for dilator actions on the isolated lower esophageal sphincter and aorta from rats, Journal of pharmacological sciences, 137(1): 98-100.

[43] Gomart, S., Gaudreau-Ménard, C., Jespers, P., Dilek, O. G., Hupkens, E., Hanthazi, A., Naeije, R., Melot, C., Labranche, N., Dewachter, L., Mc Entee, K., (2017), Leptin-Induced Endothelium-Independent Vasoconstriction in Thoracic Aorta and Pulmonary Artery of Spontaneously Hypertensive Rats: Role of Calcium Channels and Stores, Plos one, 12(1): e0169205.

[44] Rodríguez A, Frühbeck G, Gómez-Ambrosi J, Catalán V, Sáinz N, Díez J, Zalba G, Fortuño A., (2006), The inhibitory effect of leptin on angiotensin II-induced vasoconstriction is blunted in spontaneously hypertensive rats, Journal of Hypertension, 24(8):1589-1597. DOI: 10.1097/01.hjh.0000239295.17636.6e PMID: 16877962.

[45] de Carvalho, E. F., Nunes, A. F., Silva, N. C. B., da Silva Gomes, J. P., de Sousa, R. P., Silva, V. G., Nunes, P. H. M., Santos, R. F., Chaves, M. H., Oliveira, A. P., Oliveira, R. C. M., (2019), *Terminalia fagifolia* Mart. & Zucc. elicits vasorelaxation of rat thoracic aorta through nitric oxide and K^+ channels dependent mechanism, Biology open, 27; 8(2).

[46] Paulo Humberto M Nunes, Maria do Carmo C Martins, Rita de Cássia M Oliveira, Mariana H Chaves, Elcilene A Sousa, José Roberto S A Leite, Leiz Maria Véras, Fernanda Regina C

JSR A
Journal of Scientific Reports

Almeida, (2014), Gastric antiulcerogenic and hypokinetic activities of Terminalia fagifolia Mart. & Zucc. (Combretaceae), Biomed Res Int.;2014:261745. doi: 10.1155/2014/261745. PMID: 24900960. PMCID: PMC4036414.

ATTACHMENTS

APPENDIX 1. Experimental Animals Local Ethics Committee Approval Certificate

T.C.
DUMLUPINAR ÜNİVERSİTESİ
HAYVAN DENEYLERİ YEREL ETİK KURULU
ARAŞTIRMA BAŞVURUSU ONAYI

BAŞVURU BİLGİLERİ	ARAŞTIRMANIN ADI	**Sıçan aorta düz kası kasılma gevşeme cevapları üzerine Ammonium Pyrrolidine Dithiocarbamate'nın etki mekanizmasının araştırılması**
	ARAŞTIRMA YÜRÜTÜCÜSÜ KURUMU	Doç.Dr.M.Kasım ÇAYCI DPÜ Fen-Edebiyat Fakültesi Genel Biyoloji ABD
	PROJE YÜRÜTÜCÜSÜ KURUMU	Doç.Dr.M.Kasım ÇAYCI DPÜ Fen-Edebiyat Fakültesi Genel Biyoloji ABD
	YARDIMCI ARAŞTIRICILAR	Doç.Dr.M.Kasım ÇAYCI Yls.Öğr.Merve ARAS Yls. Öğr.Zeynep KELEŞ Yls.Öğr.Merve AKTAŞ Yls.Öğr.Aysun ERDOĞAN
	ARAŞTIRMANIN TAHMİNİ SÜRESİ	12 Ay
	KULLANILACAK HAYVAN TÜRÜ VE SAYISI	Wistar Albino (E) – 70 Adet
	DESTEKLEYİCİ KURULUŞ	--

	Belge Adı	Tarihi
DEĞERLENDİRİLEN İLGİLİ BELGELER	ARAŞTIRMA BAŞVURU FORMU	**16.12.2015**

KARAR BİLGİLERİ

Yukarıda başvuru bilgileri verilen araştırma projesi gerekçe, amaç ve yöntemler dikkate alınarak görüşüldü ve ilgili belgeler incelendi. Projenin etik açıdan uygun olduğuna, çalışmanın aşağıdaki hususlar dikkate alınarak yürütülmesine ve sorumlu araştırıcıya iletilmesine **OY BİRLİĞİ** ile karar verildi.

1) Projede herhangi bir değişiklik gerektiğinde kurulumuzdan onay alınması,
2) Projede çalışacağı bildirilen araştırıcılarda değişiklik olduğunda kurulumuzdan onay alınması,
3) Deney hayvanları üzerinde yapılacak girişimin başlangıç ve bitiş tarihinin bildirilmesi,
4) Çalışma süresinde tamamlanamaz ise ek süre talebinde bulunulması,
5) Çalışma tamamlandığında sonuç raporunun gönderilmesi

ÜYELER

Unvanı / Adı / Soyadı EK Üyeliği	Uzmanlık Dalı	Kurumu	İlişki (*)	İmza
Doç.Dr. Aynur GÜLCAN Başkan	Mikrobiyoloji ve Klinik Mikrobiyoloji Anabilim Dalı	Tıp Fakültesi	☐ E ■ H	
Yrd. Doç. Dr. Ahmet KOÇAK Üye	Histoloji ve Embriyoloji Anabilim Dalı	Tıp Fakültesi	☐ E ■ H	
Yrd. Doç. Dr. Sezer AKÇER Üye	Anatomi Anabilim Dalı	Tıp Fakültesi	☐ E ■ H	
Yrd. Doç. Dr. Ceylan AYADA Üye	Fizyoloji Anabilim Dalı	Tıp Fakültesi	☐ E ■ H	
Yrd.Doç. Dr. Hasan METİNEREN Üye	Ortopedi ve Travmatoloji Anabilim Dalı	Tıp Fakültesi	☐ E ■ H	
Doç.Dr. M.Kasım ÇAYCI Üye	Biyoloji Anabilim Dalı	Fen-Edebiyat Fakültesi	■ E ☐ H	
Doç.Dr. Muhammed OYLUMLU Üye	Kardiyoloji Anabilim Dalı	Tıp Fakültesi	☐ E ■ H	
Yrd. Doç. Dr. Zülfü BAYHAN Üye	Genel Cerrahi Anabilim Dalı	Tıp Fakültesi	☐ E ■ H	
Vet. HEKİM Aydın AKCILAR Üye	Veteriner HEKİM	Tıp Fakültesi DEHYUAM	☐ E ■ H	
Yrd.Doç.Dr.Ahmet Haris Selçuk ÖZEN Üye	Zooloji Anabilim Dalı	Fen-Edebiyat Fakültesi	☐ E ■ H	
Erkan ERKOL Üye			☐ E ■ H	

* Araştırma ile İlişkisi

Kütahya Dumlupınar University
Institute of Graduate Studies

Journal of Scientific
Reports-A
E-ISSN: 2687-6167
Number 45, December 2020

RESEARCH ARTICLE

PRELIMINARY STUDY ON DETERMINATION OF DNA DAMAGE OF *Cyprinus carpio* BY SINGLE CELL GEL ELECTROPHORESIS IN IŞIKLI LAKE, DENIZLI

Hilal ÇAVUŞ[1,*], Müge GİDİŞ[2]

[1] Kutahya Dumlupınar University, Science Instute, Biochemistry, Kutahya, hilal.cavus@ogr.dpu.edu.tr, ORCID: 0000-0001-6024-4005
[2] Kutahya Dumlupınar University, Science and Art Faculty, Biochemistry Department, Kutahya,, muge.gidis@dpu.edu.tr, ORCID: 0000-0002-5623-1698

Received Date: 08.07.2020 *Accepted Date: 30.10.2020*

ABSTRACT

In this study, DNA damage was examined in blood samples taken from *Cyprinus carpio* between October 2019 and December 2019. The aim of this study is to determine single strand breaks in DNA by single cell gel electrophoresis (comet analysis). Different concentrations of Methyl methanesulfonate (MMS) was applied *in vitro* conditions and pollution of lake was evaluated on a cell basis. DNA damage was found to be less than the concentrations of MMS applied in October 2019. In December 2019, DNA damage was found to be less than on the basis of cells compared to different concentrations of MMS. Average Arbitrary Units (AAU) was calculated. Accordingly, the samples taken in October 2019 AAU values were obtained 1,4044±0,2725, after MMS application the results were between 2,38±1,1637 and 2,824444±0,6556. And in December 2019, AAU values in blood samples were found to be between 298278±0,2213, and MMS values between 2,35±0,8381 and 2,884167±0,657. Comet head and tail lengths were calculated from the comet images obtained from the comet parameters. Comet tail lengths were determined as 15.784 ± 6.97 µm in October 2019 and 10.899 ± 4.75 µm in December 2019. The data obtained from results, there is not much DNA damage of *C. carpio* in Işıklı Lake. As a result *Cyprinus carpio* is an efficient organism to evaluate genotoxicity of environmental pollution and the pollution in Işıklı Lake is not at critical level.

Keywords*: DNA damage, Single cell gel electrophoresis, Işıklı Lake, Cyprinus carpio.*

1. INTRODUCTION

The environment is continuously loaded with exogenous and endogenous substances released by anthropogenic activities and, this effect directly or indirectly the genetic material of living organisms. Environmental pollution by the deposition of contaminants during a long time causes an increase in the aquatic habitat. The pollutants can cause damage on the aquatic organisms' genetic material, and this can pass onto the next generation. [1]. Endogenous and exogenous changes that affect the molecular integrity of living things are called "DNA damage" [2]. When the DNA cannot be repaired, genomic instability occurs, which is important for the future of the organism [3].

Aquatic organisms accumulate pollutants directly from contaminated water and indirectly by feeding on contaminated organisms. Fish populations are decreasing due to increase in industrialization which causes destruction of habitats with adding mutagenic and genotoxic chemicals to wetland ecosystems. [4,5]. In addition, it produces effective chemical products such as pesticide, heavy metals, food additives, industrial residues, radiation, relative oxygen species (ROS) in the organism. These products interact with macromolecules such as DNA, lipid and protein in the cells of the organism, leading to DNA damage, mutagenicity, carcinogenicity and aging [5,6].

Detection of DNA damage is provided by biological monitoring tests. The comet assay is a suitable technique to measure various types of DNA damage. This test used in genotoxicology, detects single strand breaks in DNA by single cell gel electrophoresis, which is a fast, reliable method [7]. This method was applied for the first time by Ostling and Johansenn (1984), and Singh et al. (1988) and named as single cell electrophoresis (Comet analysis) [8,9]. DNA damage is quantified by the proportion of DNA which migrates out of the nuclei toward the anode when individual cells or isolated nuclei, embedded in a thin agarose laye are subjected to electrophoresis that results on a comet-like shape of nuclei. This enables quantification of DNA in comet tails after staining with ethidium bromide. The longer the comet's tail observed means the more single strand breaks in DNA which points the genetic material of the organism is damaged for various reasons. Undamaged DNA appears as a tailed ring.

Işıklı Lake is located in the upper basin of the Büyük Menderes River, south of Akdağ, with a maximum surface area of approximately 64.00 km^2 within the borders of Denizli province, in Çivril district [10,11,12]. The lake is fed by Akçay Stream, Kufi Stream, Işıklı Founts, two large tributaries in the upper basin of Büyük Menderes and groundwater at the bottom. There are reed islands in the middle of the lake [10,12,13]. The lake water is used for agricultural irrigation. Işıklı Lake is a natural lake with the floods where the water level rises. In order to protect the agricultural areas and settlements, the State Hydraulic Works (DSI) made a dam and turned into a dam lake [10,12,14].

In this study, we described the application of the comet assay to nuclei of *Cyprinus carpio*. The purpose of the study was to evaluate the induction of DNA damage in this fish species. For that purpose Methyl methanesulfonate (MMS), a genotoxic chemical causing DNA breaks was used.

2. MATERIAL AND METHODS

2.1. Material

Carp fish *(Cyprinus carpio)* blood samples were taken from two different stations (38°15'33.8"N 29°55'10.0"E and 38°15'06.8"N 29°53'26.8"E) from the local fishermen and stored in the laboratory.

2.2. Chemicals

Dulbecco's Phosphate-Buffered Saline (DPBS) (PanBiotech), Tris (BioShop, CAS 77-86-1), Triton X-100 (BioShop, CAS 9002-93-1), N-Laurylsarcosine-sodium salt (Sigma-Aldrich Co, CAS 137-16-6), Methyl methanesulfonate (MMS) (Sigma Aldrich, CAS 56-27-3), Ethidium Bromide (BioShop, CAS 239-45-8), Normal melting agarose (NMA) (Amresco,), Low melting agarose (LMA) (Sigma-Aldrich, CAS 9012-36-6).

2.3. Method

2.3.1. In vitro positive control application in cells

Methyl methanesulfonate (MMS) concentration of 60uM, 70uM and 80uM were used to trigger DNA damage, respectively. DNA was exposed to MMS for 15 minutes at 0^{o}C and washed with DPBS.

2.3.2. Single cell gel electrophoresis (Comet assay)

The Comet assay protocol was performed with minor modifications from the literature [15]. Blood samples taken from the species were washed with DPBS and mixed with 0.5% low melting point agarose. After taking 10ul of this mixture, the slide covered with 1% normal melting point agarose was spread and the agarose was frost by covering the coverslip (10 min, 4^{o}C). The coverslips on the slides were removed and placed in cold lysis solution (2,5M NaCl, 100mM EDTA, 10mM Tris, (%10 DMSO, %1 Triton X-100, %1 N-Laurylsarcosine-sodium salt pH 10) for 1 hour at 4^{o}C. Slides were placed in a gel-electrophoresis filled with electrophoresis buffer (10M NaOH, 5M EDTA, pH 13) for 20 minutes. Electrophoresis was performed in the same buffer and run for 20 minutes at 25V, 300mA. After electrophoresis, slides were neutralized with the solution (pH 7.5) for 5 minutes. Each slide was stained with Ethidium bromide (20ul/ml) for 20 minutes and examined under a fluorescent microscope (Nikon ECLIPSE 50i) in a suitable barrier filter light. The CometScore2.0.0.38 program was used to distinguish the cells visually and ranges them from 0 to 4 to assess the extent of the contamination. In addition, head and tail lengths were calculated from the comet parameters of 20 selected comet.

2.3.3. Statistical analysis

SPSS V25.0 package program was used for statistical analysis of the data. The normality of the data was evaluated with the Shapiro-Wilk test. After the groups that did not show normal distribution in the comet categories, Kruskal-Wallis test was used for the comparison ($p>0.05$). The average of cell numbers obtained from each sample, their standard deviations were calculated and Arbitrary Units (AU) evaluation was made at $p> 0.05$ significance level. The measurements of the tail and head parts of the comets were made with the Image J program. The Shapiro-Wilk test was applied to determine the distribution of the data. Normally distributed data were evaluated with Student-T test with $p> 0.05$ significance level.

3. RESULTS

In this study, single cell gel electrophoresis (comet analysis) was applied to blood samples taken from *Cyprinus carpio* in October 2019 and December 2019. The results of comet damage levels from the samples taken in October 2019 was found to be 0 degrees and meaning the genetic damage was not very high. Methyl methanesulfonate (MMS) was applied to cells at 60uM, 70uM and 80uM concentrations (Fig. 1). Previous studies have shown that MMS causes DNA-strand breaks. In this study we also observed that higher MMS concentrations show higher DNA damage. A decrease was observed between samples that received 4th degree damage and the control groups.

JSR A
Journal of Scientific Reports

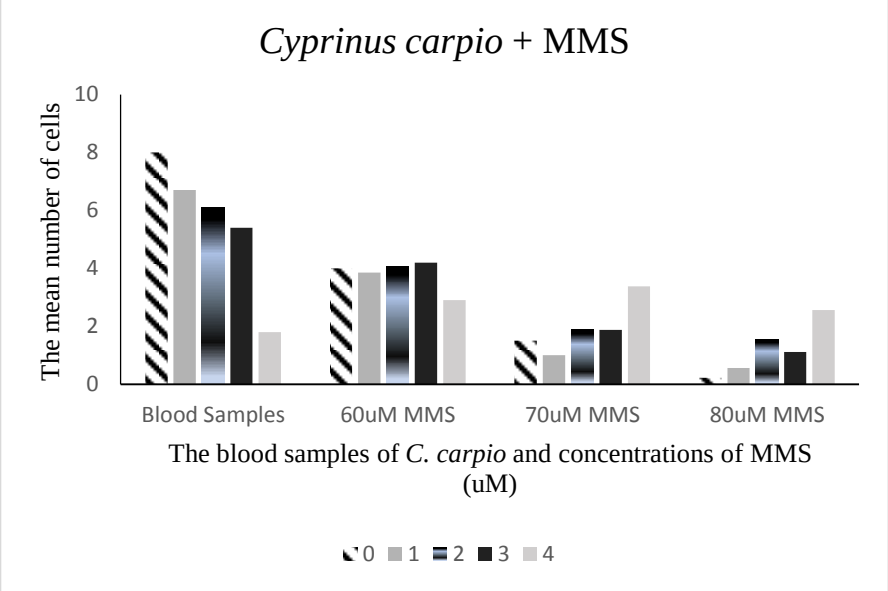

Figure 1. Comparisons between the DNA damage levels of samples (October 2019)

The comet categories of the samples (December 2019) and the comet categories of MMS-induced samples are given in Figure 2. A decrease is observed when blood concentrations of 0 degree are compared with 60uM, 70uM and 80uM concentrations of MMS. Compared to cells containing damaged DNA of grade 4, an increase was observed between blood samples and MMS concentrations applied at 60uM, 70uM and 80uM and this increase caused less damage to the 60uM MMS concentration (Figure 2).

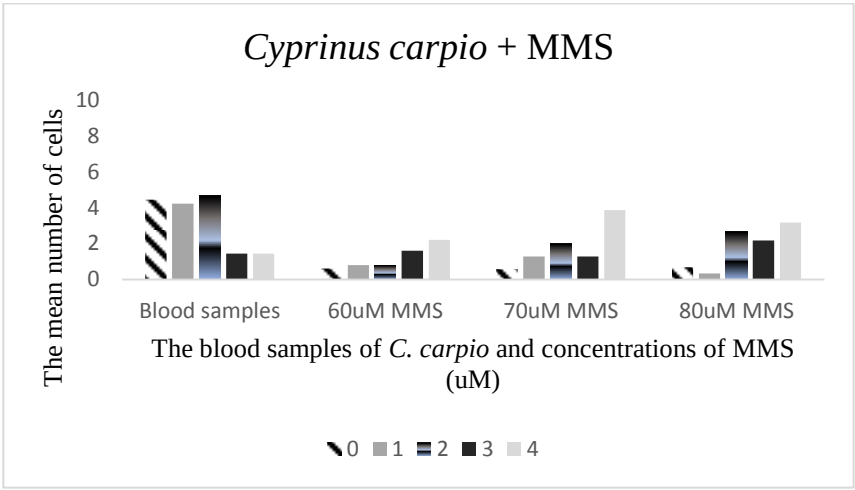

Figure 2. Comparisons between the DNA damage levels of samples (December 2019).

JSR A
Journal of Scientific Reports

Arbitrary units were calculated by classifying and counting the cells. To calculate Arbitrary units: 0xA + 1xB + 2xC + 3xD + 4xE / N where 0, 1, 2, 3 and 4 comet categories, A, B, C, D and E are the number of cells counted in these categories and N represents the total number of cells [16]. The average arbitrary unit data of the blood samples and the samples exposed to MMS are given in Table 1. There is an increase in average Arbitrary units (AAU) values in blood samples compared to positive controls. The results support that the fish species from the lake has less DNA damage than the MMS induced samples. Cells were classified according to comet tail length. Class A has no tail and spotted, class B has a small tail head (nucleus) diameter, class C has a tail longer than class B head diameter, class D has a tail longer than class C head diameter, class E has the longest comet tail (apoptotic cells) (Figure 3).

Table 1. Average arbitrary units (AAU) values (±standard deviation). (Data were evaluated at p>0,05 significant difference).

October 2019 Samples	**Average Arbitrary Units (AAU)**	**December 2019 Samples**	**Average Arbitrary Units (AAU)**
Without MMS	1,4044±0,2725	Without MMS	1,298278±0,2213
60uM MMS	2,38±1,1637	60uM MMS	2,35±0,8381
70uM MMS	2,341563±0,7777	70uM MMS	2,937857±0,696
80uM MMS	2,824444±0,6556	80uM MMS	2,884167±0,657

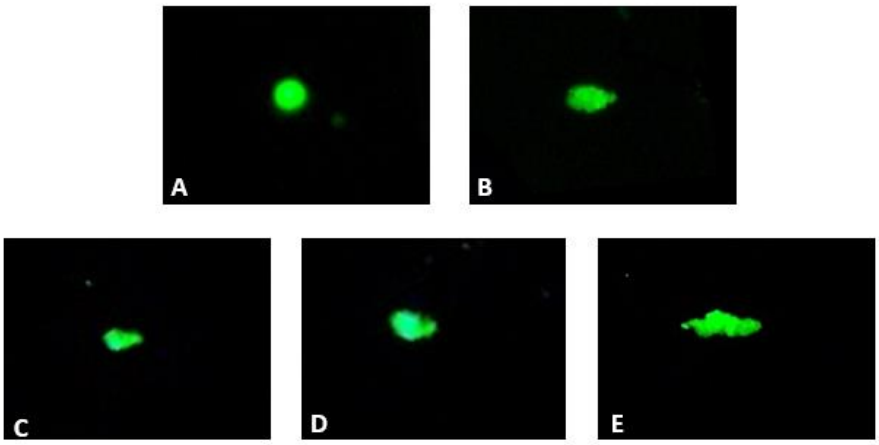

Figure 3. Comets categories of Comet assay, A, undamaged DNA, B, C, D damaged DNA, E very damaged DNA.

The percentages of the observed cells separared by comet categories (Table 2). According to the results, comets of 0 degree in the blood samples without MMS were observed more than other samples in December 2019. It is observed that in the MMS induced samples, 43% of the 4th degree comets were in the range of 70uM MMS in December 2019 and 80uM MMS in October 2019. The results prove the

JSR A
Journal of Scientific Reports

DNA damage of 70uM MMS. When the fish samples taken from the lake are compared with the ones treated with MMS, it is seen that the lake is not damaged more than MMS induced samples.

Table 2. Comet categories and their percentages of *Cyprinus carpio* from Işıklı Lake-Turkey.

Comet Categories						
					Seasons	
0	**1**	**2**	**3**	**4**		
26%	30%	23%	13%	7%	October 2019	**Without MMS**
36,13%	18%	25%	13%	8%	December 2019	
27%	21%	12%	18%	22%	October 2019	**60uM MMS**
10%	13%	13%	27%	37%	December 2019	
16%	10%	19%	19%	35%	October 2019	**70uM MMS**
6%	14%	22%	14%	43%	December 2019	
4%	9%	26%	19%	43%	October 2019	**80uM MMS**
7%	4%	30%	24%	35%	December 2019	

Table 3. Results of the tail length and head length of comets (±standard deviation). (Data were evaluated at p>0,05 significant difference).

		The tail lenght of comets (µm)		**The head lenght of comets (µm)**	
	N	**October 2019 Samples**	**December 2019 Samples**	**October 2019 Samples**	**December 2019 Samples**
Without MMS	20	15,784±6,97	10,899±4,75	7,484±2,60	5,138±1,81
60uM MMS	10	36,131±15,27	27,115±10,56	12,078±5,92	16,461±3,48
70uM MMS	10	30,781±9,22	22,088±6,72	19,249±6,55	21,282±8,22
80uM MMS	10	37,277±20,20	41,201±18,58	21,027±8,99	22,932±7,77

In this study, no significant difference was found between 10.899 ± 4.75 µm and 15.784 ± 6.97 µm in the comet tail length analyzes (p> 0.05). The comet queue lengths of the MMS applied samples are approximately 2 times longer than the lake samples. Comparing comet tail lengths between October and

December, the comet tail length in October 2019 is approximately 1.5 times longer. When comet head lengths were examined, the values were evaluated as 7.484 ± 2.60 µm and 5.138 ± 1.81 µm ($p > 0.05$). Comet head lengths are longer in the samples with MMS than MMS (-) samples (Table 3). The comet head length in the samples in October 2019 occurred more than the December 2019 samples, and the difference between them was approximately 0.5 times. without MMS (Table 3). This length is approximately 0.5 times longer in MMS induced samples. The comet head length in the samples in October 2019 occurred more than December 2019 samples, and the difference between them was approximately 0.5 times. The highest tail length was found at 80uM MMS concentration in December 2019 and comet head length at 80uM MMS concentration in December 2019.

4. DISCUSSION AND CONCLUSION

In this study, degree of DNA damage of *C. carpio* from Işıklı Lake, *in vitro* conditions were evaluated by single cell gel electrophoresis (comet assay). The mutagenic effect of whole blood cells exposed to Methyl methanesulfonate (MMS) was examined as a positive control. The pollution status of the lake was evaluated by comparing the blood samples of the fish taken from the lake and at the different concentrations of MMS. Considering the Comet percentages, the results showed that DNA damage occurred in December 2019 was the highest. When samples were induced to MMS, the most DNA damage was in December 2019 samples compared to October 2019 samples (Table 2). According to MMS concentration of DNA damage, in October 2019 samples was less than in December 2019 samples. When the average arbitrary units values were examined, for October 2019 samples it is 1.4044 ± 0.2725 and 1.298278 ± 0.2213 for December 2019 samples were determined (samples without MMS) (Table 2). After the MMS induction, values incresed to 2.38 ± 1.1637 for October 2019 samples and 2.35 ± 0.8381 for December 2019 samples. For the samples that were induced to MMS, we can say that the DNA damage has increased gradually as there is an increase in OAU values. The highest increase occurred as 70uM MMS from the December 2019 samples. The tail and head lengths of the comets were calculated from the comet parameters. According to these calculations, DNA damage increases as the tail and head length of the comets increase.

Methyl methanesulfonate (MMS) is an alkylating agent that causes DNA damage [17]. In this study, an increase was observed in cells damaged by the 4th degree. Kammann et al. (1999), applied comet analysis of leucocyte samples of *C. carpio* from the North Sea using various concentrations and various terms of H_2O_2 as a positive control in their study. They emphasized that organic sediment has a genotoxic potential and the comet technique is a powerful technique detecting DNA breaks [18]. Rank and Jensen (2003) applied comet assay on the gill cells and hemocytes of *Mytilus edulis* with exposed to MMS *in vitro* and *in vivo* conditions. As a result, the cells exposed to MMS did not show toxicological effects even at high concentrations [19]. Lemos et al., (2005) performed a comet analysis on *Tilapia rendalli*, and the number of scores in the MMS applied cells was higher than the score number of the control groups. Kammann et al., (1999) found the lowest result from arbitrary unit points as 4, which is 2 times higher than the Işıklı Lake. Besides this, Lemos et al. (2005) DNA damage results were 13 times more than the Işıklı Lake, and 16 times more DNA damage was found in the MMS induced samples.

Çok et al. (2011) detected DNA damage on *C. carpio* from Lake Mogan using with Comet assay method. And they found the length of the comet tail as 31.10 ± 10.39 µm. According to results of their study we can say that there is more DNA damage in fish samples in Lake Mogan than the samples from our study. [21]. Kontaş and Bostancı (2020), conducted heavy metal analyzes and genotoxic

investigations on *Capoeta banarescui* taken from Melet River and the tail lengths of comets in autumn season were determined as 20.47 ± 1.30 µm. Compared to Işık Lake, it has approximately 1.5 times longer tail length, and this indicates that Melet River suffers more DNA damage than Işık Lake [22]. On the other hand, Arslan et al., (2016) found that comet tail lengths were approximately similar to Lake Işıklı in a study conducted with comet assay on *Oncorhynchus mykiss* in Pınarbaşı district of Kayseri [23].

Single cell gel electrophoresis has a very fast, sensitive and common protocol [24]. This method, also known as comet analysis, is often used in ecotoxicology to detect the genotoxic effect of some chemical or physical agents on the model organism [3,25,26]. The mutagenic effect of Methyl methanesulfonate (MMS) used in the research is evident in the results and has played a role in the DNA damage as a direct alkylating agent.

The comet assay is now widely used to measure DNA damage and it is becoming a primary tool for pollutant biomonitoring in the aquatic environment and some authors suggest that the comet assay is more sensitive than the other genotoxicity tests [27,28,29]. In conclusion, the pollution in Işıklı Lake was not worrying and *Cyprinus carpio* is an efficient organism to evaluate genotoxicity of environmental pollution, they are sensitivity to pollutants, especially in comet assay. However, these studies are the preliminary studies about the pollution of Işıklı Lake and further work is needed, including analyzing the DNA damage in fish tissues, ecotoxicological studies of water and sediment samples.

ACKNOWLEDGEMENTS

This research was supported by a grant from Scientific Research Projects (BAP) Kütahya Dumlupınar University (Project No 2019-08).

REFERENCES

[1] Vanzella, T. P., Martinez, C. B. R., & Cólus, I. M. S. (2007). Genotoxic and mutagenic effects of diesel oil water soluble fraction on a neotropical fish species. Mutation Research/Genetic Toxicology and Environmental Mutagenesis, 631(1), 36–43.

[2] Kulaksız, G., & Sancar, A. (2007). Nükleotid Eksizyon Onarımı ve Kanser. Türk Biyokimya Dergisi.; 32: 10.

[3] Dikilitaş, M., & Koçyiğit, A. (2010). Canlılarda "Tek Hücre Jel Elektroforez" Yöntemi ile DNA Hasar Analizi (Teknik Not): Comet Analiz Yöntemi. Harran Tarım ve Gıda Bilimleri Dergisi, 14(2), 77–89.

[4] Arkoosh, M. R., Casillas, E., Clemons, E., Kagley, A. N., Olson, R., Reno, P., & Stein, J. E. (1998). Effect of Pollution on Fish Diseases: Potential Impacts on Salmonid Populations. Journal of Aquatic Animal Health, 10(2), 182–190.

[5] Frenzilli, G., Nigro, M., & Lyons, B. (2009). The Comet assay for the evaluation of genotoxic impact in aquatic environments. Mutation Research/Reviews in Mutation Research, 681(1), 80–92.

[6] Yoku, B., & Çakir, D. Ü. (2002). İn vivo Oksidatif DNA Hasarı Biyomarkerı; 8-Hydroxy-2'-deoxyguanosine. Türkiye Klinikleri Journal of Medical Sciences 22(5):535-43.

[7] Buschini, A., Martino, A., Gustavino, B., Monfrinotti, M., Poli, P., Rossi, C., Santoro, M., Dörr, A. J. M., & Rizzoni, M. (2004). Comet assay and micronucleus test in circulating erythrocytes of *Cyprinus carpio* specimens exposed in situ to lake waters treated with disinfectants for potabilization. Mutation Research/Genetic Toxicology and Environmental Mutagenesis, 557(2), 119–129.

[8] Ostling, O., & Johanson, K. J. (1984). Microelectrophoretic study of radiation-induced DNA damages in individual mammalian cells. Biochemical and Biophysical Research Communications, 123(1), 291–298.

[9] Singh, N. P., McCoy, M. T., Tice, R. R., & Schneider, E. L. (1988). A simple technique for quantitation of low levels of DNA damage in individual cells. Experimental Cell Research, 175(1), 184–191.

[10] Balik, İ., Özkök, R., Çubuk, H., & Uysal, R. (2004). Investigation of some biological characteristics of the silver crucian carp, *Carassius gibelio* (Bloch 1782) population in Lake Eğirdir. Turkish Journal of Zoology, 28(1), 19–28.

[11] Apaydın Yağcı, M., Yağcı, A., & Dölcü, B. (2016). Relationships between the physicochemical parameters and zooplankton in Eğirdir Lake (Turkey). Iranian Journal of Fisheries Sciences, 15(1), 118–132.

[12] Ustaoğlu, M. R., Balık, S., & Özbek, M. (2015). Işıklı Gölü (Çivril-Denizli)'nün Mollusca Faunası. Su Ürünleri Dergisi, 18(1).

[13] Tekin-Özan, S. (2012). Relationship of Heavy Metals in Water, Sediment and Tissues with Total Length, Weight and Seasons of *Cyprinus carpio* L., 1758 From. 15.

[14] Aygen, C. & Balık, S. (2015). Işıklı Gölü ve Kaynaklarının (Çivril-Denizli) Crustacea Faunası. *Su Ürünleri Dergisi* **22**, 371–375

[15] McKelvey-Martin, V. J., Green M. H. L., Schmezer P., Pool-Zobel B. L., De Meo M. P., Collins A. (1993). The single cell gel electrophoresis assay (comet assay): A European review. Mutation Research/Fundamental and Molecular Mechanisms of Mutagenesis **288**, 47–63.

[16] Azqueta, A., Shaposhnikov, S., & Collins, A. R. (2009). DNA oxidation: Investigating its key role in environmental mutagenesis with the comet assay. Mutation Research/Genetic Toxicology and Environmental Mutagenesis, 674(1), 101–108.

[17] Cuce, G., Cetinkaya, S., Isitez, N., Kuccukturk, S., Sozen, M. E., Kalkan, S., Cigerci, I. H., & Demirel, H. H. (2016). Effects of curcumin on methyl methanesulfonate damage to mouse kidney. Biotechnic & Histochemistry, 91(2), 122–127.

[18] Kammann, U., Riggers, J. C., Theobald, N., & Steinhart, H. (2000). Genotoxic potential of marine sediments from the North Sea. Mutation Research/Genetic Toxicology and Environmental Mutagenesis, 467(2), 161–168.

[19] Rank, J., & Jensen, K. (2003). Comet assay on gill cells and hemocytes from the blue mussel Mytilus edulis. Ecotoxicology and Environmental Safety, 54(3), 323–329.

[20] Lemos, N. G., Dias, A. L., Silva-Souza, A. T., & Mantovani, M. S. (2005). Evaluation of environmental waters using the comet assay in Tilapia rendalli. Environmental Toxicology and Pharmacology, 19(2), 197–201. 4-11.

[21] Çok, İ., Ulutas, O. K., Okusluk, Ö., Durmaz, E. & Demir, N. (2011). Evaluation of DNA Damage in Common Carp (*Cyprinus carpio* L.) by Comet Assay for Determination of Possible Pollution in Lake Mogan (Ankara). The Scientific World JOURNAL **11**, 1455–1461.

[22] Kontaş, S. & Bostanci, D. (2020). The Study on Determination of Genotoxic Damage in Fish: *Capoeta banarescui*. Journal of Limnology and Freshwater Fisheries Research 144–152.

[23] Arslan, K., Duman, F., Kanbur, M. & Akyüz, B. (2016). Kayseri İli, Pınarbaşı İlçesinde Doğal Olarak Yakalanan ve Yetiştiriciliği Yapılan Gökkuşağı Alabalıklarının (*Oncorhynchus mykiss*) Genotoksisite Yönünden İncelenmesi, Erciyes Üniversitesi Veteriner Fakultesi Dergisi, (13)2, 131-138.

[24] Collins, A. R., Dobson, V. L., Dušinská, M., Kennedy, G., & Štětina, R. (1997). The comet assay: What can it really tell us? Mutation Research/Fundamental and Molecular Mechanisms of Mutagenesis, 375(2), 183–193.

[25] Cotelle, S., & Férard, J. F. (1999). Comet assay in genetic ecotoxicology: A review. Environmental and Molecular Mutagenesis, 34(4), 246–255.

[26] Ulutas, O. K., Okusluk, O., Demir, N., Durmaz, E., & Cok, I. (2008). Determination of possible pollution in Lake Mogan (Ankara) by Comet assay using common carp (*meth carpio* L.). Toxicology Letters, Supplement (180), S204–S205.

[27] Akcha, F. Arzul G, Rousseau S, Bardouil M. (2008). Comet assay in phytoplankton as biomarker of genotoxic effects of environmental pollution. Mar Environ Res 6:59–61.

[28] Klobuear, GLV., Pavlica M., Erben R, Pape D. (2003). Application of the micronucleus and comet assays to mussel *Dreissena polymorpha* haemocytes for genotoxicity monitoring of freshwater environments. Aquat Toxicol 64:15–23.

[29] Mitchelmore C.L., Chipman J.K. (1998). DNA strand breakage in aquatic organisms and the potential value of the comet assay in environmental monitoring Mutat. Res., 399 pp. 135-147.

Kütahya Dumlupınar University
Institute of Graduate Studies

Journal of Scientific
Reports-A
E-ISSN: 2687-6167
Number 45, December 2020

RESEARCH ARTICLE

SOLUTIONS OF LINEAR FRACTIONAL DIFFERENTIAL EQUATIONS OF ORDER $n-1<nq<n$

Sertaç ERMAN[1,*]

[1] Sakarya University of Applied Science, Faculty of Technology, Departement of Engineering Basic Science, Sakarya, sertacerman@subu.edu.tr, ORCID: 0000-0002-3156-5173

Received Date:03.04.2020 *Accepted Date:13.07.2020*

ABSTRACT

In this study, the linear Caputo fractional differential equation of order $n-1<nq<n$ is investigated. First, the solution of the equation of order $0<q<1$, with variable coefficients, is obtained by using the solution of differential equation of integer order which is the least integer greater than fractional order. Moreover, the solution of linear fractional differential equations of order $n-1<nq<n$ is considered. The solutions of the equation are presented in terms of Mittag-Leffler function with three parameters. The main goal of this study is to present a closed-series form of the solutions. To demonstrate the accuracy and the effectiveness of the proposed approach, some numerical solutions are given.

Keywords: *Fractional Differential Equation, Mittag-Leffler function, Three parameters*

1. INTRODUCTION

The fractional derivative is very appropriate in modelling of physical pneumonias which involves past memory. Since fractional differential equations hold memory and are non-local in nature, it is known that mathematical models with fractional derivatives are more convenient and economical (See [1-8] and the references there in for more details). Due to this fact, they have been drawing increasing importance from scientist in past three decades (See [9-15] for some applications).

In this study, the Caputo fractional derivative is used. Since properties of Caputo fractional derivative are closed to properties of integer derivative, enormous studies on Caputo fractional differential equation and their applications can be found in the literature.

The linear Caputo fractional differential equation of order $0<q<1$, with variable coefficients, is considered and its solution is obtained as a series form. Next, the solution of linear sequential Caputo fractional differential equations of order $n-1<nq<n$ is examined. The solutions of the equation are presented in terms of Mittag-Leffler function with three parameters.

2. PRELIMINARY DEFINITIONS

Definition 1. The derivative operator D^q of order $q>0$ is defined as follows

JSR A
Journal of Scientific Reports

$$D^q u(t) = \frac{1}{\Gamma(n-q)} \int_{t_0}^{t} (t-s)^{n-q-1} u^{(n)}(s) ds \quad for \quad n-1 < q < n, \tag{1}$$

where n is the smallest integer that exceeds q, $t \in [t_0, t_0 + T]$ and $u^{(n)}(t) = \frac{d^n u(t)}{dt}$.

The expression (1) is definition of Caputo (left-sided) fractional derivative of $u(t)$ for $n-1 < q < n$ [7].
Moreover, it is clear that Caputo fractional derivative of order $0 < q < 1$ is defined as follows:

$$D^q u(t) = \frac{1}{\Gamma(1-q)} \int_{t_0}^{t} (t-s)^{-q} u'(s) ds. \tag{2}$$

Definition 2. The Mittag-Leffler function is defined by the series expansion as shown below

$$E_q(z) = \sum_{k=0}^{\infty} \frac{z^k}{\Gamma(qk+1)}, \tag{3}$$

where $q > 0$ [8].

In [7], some properties of Mittag-Leffler function and Caputo derivative are given as follows:

(i) $D^{nq} u(t) = D^{(n-1)q}(D^q) u(t)$ for $n-1 < nq < n$.
(ii) If $q = 1$, $E_{1,1}(t) = e^t$, then it can be said that Mittag-Leffler function is generalization of usual exponential function.
(iii) $D^q(E_q(t^q)) = E_q(t^q)$.
(iv) $D^{nq}(E_q(rt^q)) = r^n E_q(rt^q)$ where $0 < q < 1$, r is a constant and $n \in \mathbb{N}$.

Definition 3. The Mittag-Leffler function with two parameters is defined by the series expansion as shown below

$$E_{\alpha,\beta}(z) = \sum_{k=0}^{\infty} \frac{z^k}{\Gamma(\alpha k+\beta)}, \tag{4}$$

where $\alpha, \beta > 0$ [8].

Definition 4. The Mittag-Leffler function with three parameters is defined by the series expansion as shown below

$$E_{\alpha,\beta}^{\gamma}(z) = \sum_{k=0}^{\infty} \frac{(\gamma)_k z^k}{\mathrm{k}!\,\Gamma(\alpha k+\beta)}, \tag{5}$$

where $\alpha, \beta, \gamma > 0$ and $(\gamma)_k = \gamma(\gamma+1)\cdots(\gamma+k-1)$ [8].

JSR A
Journal of Scientific Reports

3. METHODOLOGY

In this study, fractional power series expansion method is used for linear Caputo fractional differential equation. The method is presented in [16] to obtain approximate solutions of fractional partial differential equations. The numerical results show that the method is significant method for fractional differential equation because of its simplicity and accuracy.

The main idea of the method is based on solving the differential equation of integer order which is the least integer greater than fractional order. Then, this solution is transformed the solution of fractional differential equation by using following series expansion:

$$u(t) \cong T\big(v(t)\big) = \sum_{k=0}^{m-1} \frac{v^{(k)}(0)t^k}{k!} + \sum_{k=1}^{\infty} \sum_{i=0}^{m-1} \frac{v^{(mk+i)}(0)t^{kq+i}}{\Gamma(kq+1+i)}, \tag{6}$$

where $u(t)$ and $v(t)$ are solutions of fractional and ordinary differential equations respectively, m is the least integer greater than fractional order q. For $0 < q < 1$, transformation (6) is expressed as follows:

$$u(t) \cong T\big(v(t)\big) = \sum_{k=0}^{\infty} \frac{v^{(k)}(0)t^{kq}}{\Gamma(kq+1)}. \tag{7}$$

4. SOLUTION OF THE LINEAR FRACTIONAL DIFFERENTIAL EQUATION

4.1. Fractional Differential Equation of Order $0 < q < 1$

Let us consider the following linear differential equation with initial condition:

$$\begin{aligned} D^q u(t) &= p(t,q)u(t) + f(t,q), \quad t\epsilon[0,T], \quad T > 0 \\ u(0) &= u_0, \end{aligned} \tag{8}$$

where $p(t,q)$ and $f(t,q)$ are continuous on $t\epsilon[0,T]$ for $0 < q \leq 1$ and $p(t,1)$, $f(t,1) \in C^{\infty}([0,T],\mathbb{R})$.

In order to obtain the solution $u(t)$ of the problem (8) by using fractional power series expansion method, we need to have the solution of following ordinary differential equation

$$\begin{aligned} v'(t) &= \tilde{p}(t)v(t) + \tilde{f}(t), \quad t\epsilon[0,T], \quad T > 0 \\ v(0) &= u_0, \end{aligned} \tag{9}$$

where $\tilde{p}(t) = p(t,1)$ and $\tilde{f}(t) = f(t,1)$.

The solution of problem (9) is well known and as follows:

$$v(t) = u_0 e^{\int \tilde{p}(t)dt} + e^{\int \tilde{p}(t)dt} \int_0^t \tilde{f}(\tau) e^{\int \tilde{p}(\tau)d\tau} d\tau. \tag{10}$$

JSR A
Journal of Scientific Reports

By plugging the following derivatives of the solution $v(t)$ at $t = 0$

$$v(0) = u_0$$
$$v^{(n)}(0) = \sum_{k=0}^{n-1} \binom{n-1}{k} \tilde{p}^{(k)}(0) v^{(n-1-k)}(0) + \tilde{f}^{(n-1)}(0) \tag{11}$$

into transformation (7), the solution $u(t)$ of the problem (8) is obtained as follows:

$$u(t) \cong u_0 + \sum_{n=1}^{\infty} \sum_{k=0}^{n-1} \left(\binom{n-1}{k} \tilde{p}^{(k)}(0) v^{(n-1-k)}(0) + \tilde{f}^{(n-1)}(0) \right) \frac{t^{nq}}{\Gamma(nq+1)} . \tag{12}$$

If $p(t,q) = \lambda$ is a constant in problem (8), the solution of problem (9) is obtained as follows:

$$v(t) = u_0 e^{\lambda t} + e^{\lambda t} \int_0^t \tilde{f}(\tau) e^{\lambda \tau} d\tau . \tag{13}$$

Moreover, derivatives of $v(t)$ are formed as follows:

$$v^{(n)}(0) = \lambda^n u_0 + \sum_{k=1}^{n} \lambda^{n-k} \tilde{f}^{(k-1)}(0). \tag{14}$$

Thus, by using transformation (7), the solution $u(t)$ of the problem (8) for $p(t,q) = \lambda$ (constant) is obtained in the following form:

$$u(t) \cong u_0 E_q(\lambda t^q) + \sum_{n=1}^{\infty} \sum_{k=1}^{n} \left(\lambda^{n-k} \tilde{f}^{(n-1)}(0) \right) \frac{t^{nq}}{\Gamma(nq+1)} . \tag{15}$$

Additionally, for $p(t,q) = \lambda$, the problem (8) is investigated in [5,6] and its solution is presented in the following explicit form

$$u(t) = u_0 E_q(\lambda t^q) + \int_0^t (t-s)^{q-1} E_{q,q}(\lambda (t-s)^q) f(s,q) ds . \tag{16}$$

Hence, because of existence and uniqueness of the solution, the solution (15) equals to the solution (16) and this equality implies the following proposition.

Proposition 1. Let $f(t,q)$ be continuous on $t \epsilon [0,T]$ for $0 < q \leq 1$ and $\lambda \in \mathbb{R}$. The following equality is satisfied

$$\int_0^t (t-s)^{q-1} E_{q,q}(\lambda (t-s)^q) f(s,q) ds \cong \sum_{n=1}^{\infty} \sum_{k=1}^{n} \frac{\left(\lambda^{n-k} \tilde{f}^{(n-1)}(0) \right) t^{nq}}{\Gamma(nq+1)} , \tag{17}$$

JSR A
Journal of Scientific Reports

where $\tilde{f}(t) = f(t,1) \in C^{\infty}([0,T],\mathbb{R})$.

In order to show efficiency of the method, Proposition 1 is used. In Figure 1 and Figure 2, numerical simulations of the difference of both side of the equality (17) are given for some values of q and functions $f(t,q) = \frac{t^q}{\Gamma(q+1)}$ and $(t,q) = \frac{t^{2q}}{\Gamma(2q+1)}$.

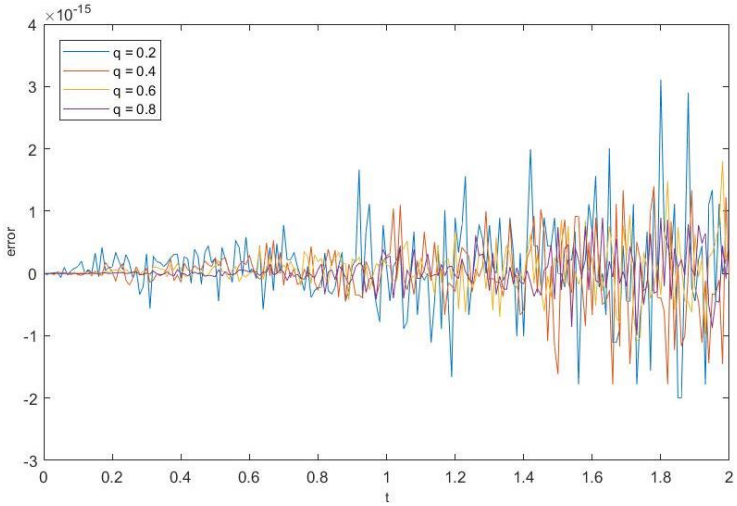

Figure 1: When $q = 0.2, 0.4, 0.6, 08$, the graph of difference of both side of the equality (17) for function $f(t,q) = \frac{t^q}{\Gamma(q+1)}$ and for 10 iteration

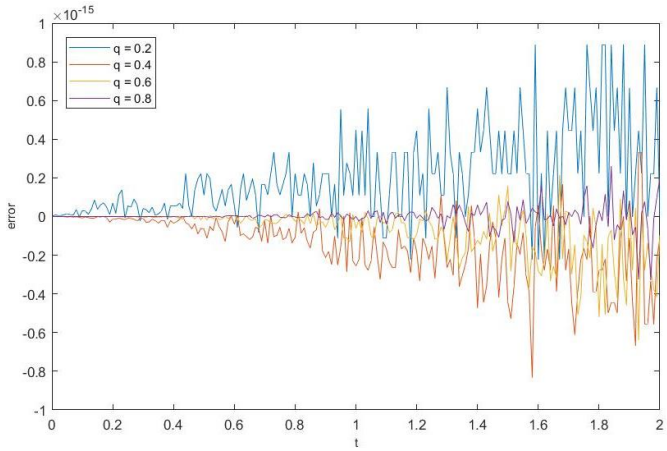

Figure 2: When $q = 0.2, 0.4, 0.6, 08$, the graph of difference of both side of the equality (17) for function $f(t,q) = \frac{t^{2q}}{\Gamma(2q+1)}$ and for 10 iteration

JSR A
Journal of Scientific Reports

4.2. Fractional Differential Equation of Order $m-1<mq<m$

The following linear sequential fractional differential equation with initial conditions is investigated in this section.

$$\begin{aligned} &D^{mq}u(t)+b_{m-1}D^{(m-1)q}u(t)+\cdots+b_1D^{q}u(t)+b_0u(t)=0, \quad t\epsilon[0,T], \quad T>0 \\ &\qquad u(0)=u_0, \quad D^{iq}u(0)=u_{i,0}, \quad i=1,2,\cdots,m-1 \end{aligned}, \tag{18}$$

where $(m-1)<mq<m$ for $m\in\mathbb{N}$ and $b_i\in\mathbb{R}$, $i=1,2,\cdots,m-1$.

It is well known that the solutions of equation (18) are given in the form of $u=E_q(rt^q)$ where r is the solution of the corresponding characteristic equation of the following form:

$$P(r)=r^m+b_{m-1}r^{m-1}+\cdots+b_1r+b_0=0\,. \tag{19}$$

If equation (19) has k distinct roots r_i for $i=1,2,\cdots,k$ and $k\leq m$, a solution of the equation (18) is obtained as follows:

$$u(t)=\sum_{i=1}^{k}c_iE_q(r_it^q)\,. \tag{20}$$

Moreover, if equation (19) has k coincident roots r_0 for $k\leq m$, the solutions $U_i(t)$ of the equation (18) can be constructed by the following recursive relation which is obtained from equation (16).

$$\begin{aligned} U_0(t)&=E_{q,1}(r_0t^q) \\ U_i(t)&=u_0E_{q,1}(r_0t^q)+U_{i-1}(0)\int_0^t(t-s)^{q-1}E_{q,q}(\lambda(t-s)^q)U_{i-1}(s)ds\,, \end{aligned} \tag{21}$$

where $i=1,2,\cdots,k-1$. Hence, the solution of the equation (18) is formed as follows:

$$u(t)=\sum_{i=1}^{k}c_iU_i(t)\,. \tag{22}$$

In the following subsection, the closed forms of the solutions $U_i(t)$ related with the coincident roots of characteristic equation are presented by using fractional power series method.

4.2.1. The closed forms of the solutions related with the m coincident roots

If the characteristic equation (19) has m coincident roots r_0, sequential differential equation (18) reduced to

$$(D^q-r_0)(D^q-r_0)^{m-1}u=0\,. \tag{23}$$

Letting $(D^q-r_0)^{m-1}u(t)=U_0(t)$, the following fractional differential equation is obtained

$$(D^q-r_0)U_0(t)=0$$

JSR A
Journal of Scientific Reports

and by using the solution (15) with $f(t) = 0$, the solution is obtained as follows:

$$U_0(t) = E_q(r_0 t^q)\,. \tag{24}$$

Moreover, letting $(D^q - r_0)^{m-2}u(t) = U_1(t)$, the following fractional differential equation is obtained

$$\begin{gathered}(D^q - r_0)U_1(t) = U_0(t)\\ \Rightarrow D^q U_1(t) - r_0 U_1(t) = E_q(r_0 t^q)\end{gathered} \tag{25}$$

Now, we solve the equation (25) by using fractional power series method. Let us consider the following ordinary differential equation which is obtained from equation (25) by equaling q to 1

$$V'_1(t) - r_0 V_1(t) = e^{r_0 t}. \tag{26}$$

The solution of equation (26) is $V_1(t) = te^{r_0 t}$. Then, applying transformation (7) to $V_1(t) = te^{r_0 t}$, it is obtained that

$$U_1(t) = \frac{t^q}{q} E_{q,q}(r_0 t^q)\,, \tag{27}$$

which is exact solution of (25). Similarly, letting $(D^q - r_0)^{m-3}u(t) = U_2(t)$, the following fractional differential equation is obtained

$$\begin{gathered}(D^q - r_0)U_2(t) = U_1(t)\\ \Rightarrow D^q U_2(t) - r_0 U_2(t) = \frac{t^q}{q} E_{q,q}(r_0 t^q)\,.\end{gathered} \tag{28}$$

Also, the solution of the equation (28) is obtained in the form of Mittag-Leffler function with three parameters as follows:

$$U_2(t) = \frac{t^{2q}}{2q} E^2_{q,2q}(r_0 t^q) \tag{29}$$

which is exact solution of (28). After applying m times these calculations recursively, the following solutions are obtained

$$\begin{aligned}U_1(t) &= \frac{t^q}{q} E^1_{q,q}(r_0 t^q)\\ U_2(t) &= \frac{t^{2q}}{2q} E^2_{q,2q}(r_0 t^q)\\ U_3(t) &= \frac{t^{3q}}{3q} E^3_{q,3q}(r_0 t^q)\,.\\ &\vdots\end{aligned}$$

Moreover, these solutions can be written as follows:

JSR A
Journal of Scientific Reports

$$U_n(t) = \frac{t^{nq}}{nq} E_{q,nq}^{n}(r_0 t^q), \quad n = 1,2,\cdots,m-1\,. \tag{30}$$

Consequently, if characteristic equation (19) has m coincident roots r_0, there exists m linearly independent solutions as follows:

$$\begin{aligned} U_0(t) &= E_q(r_0 t^q), \\ U_n(t) &= \frac{t^{nq}}{nq} E_{q,nq}^{n}(r_0 t^q), \quad n = 1,2,\cdots,m-1\,. \end{aligned} \tag{31}$$

5. CONCLUSION

The approximate solution of linear Caputo fractional equation of order $0 < q < 1$ with variable coefficients is constructed as a series form. In this construction, the solution of differential equation of integer order which is the least integer greater than fractional order and its derivatives are used. Numerical results show that the approximation is significantly efficient when components of $f(t,q)$ are formed as $\frac{t^{nq}}{\Gamma(nq+1)}$ and $p(t,q)$ is constant in equation (8). Moreover, this result yields to obtain the solution of linear sequential fractional differential equation of higher order with constant coefficient. Specifically, when characteristic equation has coincident root, the solutions are presented in terms of Mittag-Leffler function with three parameters.

REFERENCES

[1] Debnath, L., (2003), Recent applications of fractional calculus to science and engineering, International Journal of Mathematics and Mathematical Sciences, 54, 3413–3442.

[2] Ross, B., (1975), A Brief History and Exposition of the Fundamental Theory of Fractional Calculus. Fractional calculus and its Applications, Lecture notes in Mathematics, Springer: Berlin, Germany, 457, 1–36.

[3] Oldham, K.B., Spanier, J., (1974), The Fractional Calculus: Theory and Applications of Differentiation and Integration to Arbitrary Order, Academic Press: Newyork.

[4] Podlubny, I., (1998), Fractional Differential Equations, Volume 198: An Introduction to Fractional Derivatives, Fractional Differential Equations, to Methods of their solutions, Mathematics in Science and Engineering, Academic Press: San Diego.

[5] Podlubny, I., (2002), Geometric and physical interpretation of fractional integration and fractional differentiation, Fractional Calculus and Applied Analysis 5, 4, 367–386.

[6] Kilbas, A.A., Srivastava, H.M., Trujillo, J.J., (2006), Theory and Applications of Fractional Differential Equations, North-Holland Mathematics Studies, Elsevier: Amsterdam, The Netherlands.

[7] Deithelm, K., (2004), The Analysis of Fractional Differential Equations, Volume 2004 of Lecture Notes in Mathematics, Springer: Berlin, Germany.

[8] Gorenflo, R., Kilbas, A.A., Mainardi, F., Rogosin S.V., (2014), Mittag-Leffler Functions, Related Topics and Applications, Springer: Berlin, Germany.

[9] Pooseh, S., Rodrigues, H.S., Torres, D.F.M., (2011), Fractional Derivatives in Dengue Epidemics, AIP Conf. Proc., 1389, 739–742.

[10] Debnath, L., (2003), Recents Applications of Fractional Calculus to Science and Engineering, Int. J. Math. Appl. Sci, 54, 3413–3442.

[11] Singh, J., Kumar, D., Kılıçman, A., (2014), Numerical Solutions of Nonlinear Fractional Partial Differential Equations Arising in Spatial Diffusion of Biological Populations, Abstr. Appl. Anal., 2014, 535793.

[12] Koeller, R.C., (1984), Applications of Fractional Calculus to the Theory of Viscoelasticity, J. Appl. Mech., 51, 299–307.

[13] Saha, R.S., Bera, R.K., (2000), The random walk's guide to anomalous diffusion: a fractional dynamics approach, Phys. Rep. 339, 2000, 1-77

[14] Waggas, G.A., (2010), Application of Fractional Calculus Operators for a New Class of Univalent Functions with Negative Coefficients Defined by Hohlov Operator, Math. Slovaca, 1, 75–82.

[15] Aliev, F.A., Aliev, N.A., Safarova, N.A., Gasimova K.G.,, Velieva N.I., (2018), Solution of Linear Fractional-Derivative Ordinary Differential Equations with Constant Matrix Coefficients, Applied and Computational Mathematics, 17, 3, 317-322

[16] Demir, A., Erman, S., Özgür, B., and Korkmaz, E., (2013), Analysis of fractional partial differential equations by Taylor series expansion, Boundary Value Problems, 68

Kütahya Dumlupınar University
Institute of Graduate Studies

Journal of Scientific
Reports-A
E-ISSN: 2687-6167
Number 45, December 2020

RESEARCH ARTICLE

BOUNDS FOR THE NORMS OF TOEPLITZ MATRICES WITH k-JACOBSTHAL AND k-JACOBSTHAL LUCAS NUMBERS

Şükran UYGUN[1*], Hülya AYTAR[2]

[1]Gaziantep University, Science and Arts Faculty, Departments of Mathematics, Gaziantep, suygun@gantep.edu.tr, ORCID: 0000-0002-7878-2175
[2] Gaziantep University, Science and Arts Faculty, Departments of Mathematics, Gaziantep, aytarhulya93@gmail.com, ORCID: 0000-0002-1430-1782

Received Date: 12.04.2020 *Accepted Date:04.09.2020*

ABSTRACT

This work is concerned with the spectral, Euclid norms of Toeplitz matrices with generalized *k*-Jacobsthal and *k*- Jacobsthal Lucas entries. *k*- Jacobsthal and *k*- Jacobsthal Lucas sequences are two generalizations of two very popular special integer sequences called Jacobsthal and Jacobsthal Lucas sequences. Upper and lower bounds for the spectral norms of these matrices, that is, the matrices of the forms $A = T\left(j_{k,0}, j_{k,1}, \ldots, j_{k,n-1}\right)$ and $B = T\left(c_{k,0}, c_{k,1}, \ldots, c_{k,n-1}\right)$ are obtained. The upper bounds for the Euclidean and spectral norms of Kronecker and Hadamard product matrices of Toeplitz matrices with *k*-Jacobsthal and the *k*- Jacobsthal Lucas numbers are computed.

Keywords: *Hadamard product, k -Jacobsthal numbers, k -Jacobsthal Lucas numbers, Kronecker product, Norm, Toeplitz matrix*

1. INTRODUCTION

Special matrices is a widely studied subject in matrix analysis. Especially special matrices whose entries are well-known number sequences have become a very interesting research subject in recent years and many authors have obtained some good results in this area. Sequences are the building blocks of special matrices such as circulant, Toeplitz, Hankel, geometric matrices. There have been many papers about the norms of special matrices. Recently, there has been much interest in investigation of some special matrices. Because of this, various number sequences are used as entries, and the properties of the resulting matrices are investigated. Research on these special matrices normally would revolve around the investigation of their determinants, eigenvalues, norms, inverses and bounds of norms.

In [6], the authors have studied bounds of the spectral norms of circulant matrices with Fibonacci numbers. In [7], Akbulak and Bozkurt studied the norms of Toeplitz matrices involving Fibonacci and Lucas numbers. Shen [8] investigated the upper and lower bounds for the spectral norms of Toeplitz matrices involving *k*-Fibonacci and *k*-Lucas numbers. In [9], Daşdemir demonsrated the norms of Toeplitz matrices with the Pell, Pell-Lucas and modified Pell numbers. Kocer [10] has given some properties of the modified Pell, Jacobsthal and Jacobsthal-Lucas numbers, then she has defined the

JSR A
Journal of Scientific Reports

circulant, negacyclic and semicirculant matrices with these numbers and she has investigated the norms, eigenvalues and determinants of these matrices. Raza and Ali [11] studied on the norms of some special matrices with generalized Fibonacci sequence. Uygun, constructed bounds for the norms of circulant matrices with the *k* -Jacobsthal and *k* -Jacobsthal Lucas numbers [13].

Considering the above articles, on the one hand, we obtain new lower and upper bounds estimates for the spectral norms of Toeplitz matrices with *k*-Jacobsthal and *k*-Jacobsthal Lucas numbers. Furthermore, Euclidean norms, and maximum row and maximum column norms of Toeplitz matrices with *k*-Jacobsthal and *k*-Jacobsthal Lucas numbers are computed**.** Then bounds for Euclidean and sprectral norms of Kronecker and Hadamard product of the matrices are calculated.

Now, we give some fundamental information related to our study. For n∈Z, the classic Jacobsthal and Jacobsthal Lucas sequences are defined respectively by the second order homogeneous linear recurrence relations

$$\boldsymbol{j_{n+2} = j_{n+1} + 2j_n}\,, \quad \boldsymbol{j_0 = 0}\,, \quad \boldsymbol{j_1 = 1},$$

$$\boldsymbol{c_{n+2} = c_{n+1} + 2c_n}\,, \quad \boldsymbol{c_0 = 2}\,, \quad \boldsymbol{c_1 = 1}.$$

Many generalizations of the well-known Jacobsthal sequence have been introduced and studied. For example, the generalized *k* -Jacobsthal and *k* -Jacobsthal Lucas numbers have been studied [12]. For $\boldsymbol{n \geq 2}$, $\boldsymbol{n} \in \mathbb{N}$, the *k*-Jacobsthal $\{\boldsymbol{j_{k,n}}\}_{\boldsymbol{n}\in\mathbb{N}}$, and the *k*-Jacobsthal Lucas $\{\boldsymbol{c_{k,n}}\}_{\boldsymbol{n}\in\mathbb{N}}$ sequences are defined recurrently by

$$\boldsymbol{j_{k,n} = k\, j_{k,n-1} + 2\, j_{k,n-2}}\,, \qquad \boldsymbol{j_{k,0} = 0}\,,\ \boldsymbol{j_{k,1} = 1}\,, \tag{1}$$

$$c_{k,n} = k\, c_{k,n-1} + 2\, c_{k,n-2,} \qquad c_{k,0} = 2\,,\ c_{k,1} = \boldsymbol{k}. \tag{2}$$

respectively in [12]. The first *k*-Jacobsthal numbers are 0, 1, k, $\boldsymbol{k^2 + 2}$, $\boldsymbol{k^3 + 4k}$, $\boldsymbol{k^4 + 6k^2 + 4}$ …The first *k*- Jacobsthal Lucas numbers are 2 , k , $\boldsymbol{k^2 + 4}$, $\boldsymbol{k^3 + 6k}$, $\boldsymbol{k^4 + 8k^2 + 8}$…

Recurrences (1) ve (2) involve the characteristic equation $x^2 - kx - 2 = 0$ with roots $\alpha = \frac{k+\sqrt{k^2+8}}{2}$, $\beta = \frac{k-\sqrt{k^2+8}}{2}$. Binet's formulas of the *k*-Jacobsthal and *k*- Jacobsthal Lucas are defined respectively by

$$j_{k,n} = \frac{\alpha^n - \beta^n}{\alpha - \beta}\,, \qquad c_{k,n} = \alpha^n + \beta^n. \tag{3}$$

Extension to negative values of *n* can be made, *k*-Jacobsthal and *k*-Jacobsthal Lucas sequence with negative indices are demonstrated by

$$j_{k,-i} = \frac{(-1)^{i+1} j_{k,i}}{2^i}, \qquad c_{k,-i} = \frac{(-1)^i c_{k,i}}{2^i}.$$

An $n \times n$ matrix $T = \{t_{ij}\} \in M_n(C)$ is called a Toeplitz matrix if it is of the form $t_{ij} = t_{i-j}$ for each $i\,; j = 1, \dots, n$.

JSR A
Journal of Scientific Reports

$$T_n = \begin{bmatrix} t_0 & t_{-1} & t_{-2} & \cdots & t_{1-n} \\ t_1 & t_0 & t_{-1} & \cdots & t_{2-n} \\ t_2 & t_1 & t_0 & \cdots & t_{3-n} \\ \vdots & \vdots & \vdots & \ddots & \vdots \\ t_{n-1} & t_{n-2} & t_{n-3} & \cdots & t_0 \end{bmatrix} \quad (4)$$

Toeplitz matrix is determined by its first row (or column).

For any $A = [a_{ij}] \epsilon M_{\{m,n\}}(C)$, the largest absolute column sum (1-norm) and the largest absolute row sum(∞-norm) norms are

$\|A\|_1 = \max_j \sum_{i=1}^{n} |a_{ij}|$,

$\|A\|_\infty = \max_i \sum_{j=1}^{n} |a_{ij}|$.

For any $A = [a_{ij}] \epsilon M_{\{m,n\}}(C)$, the Frobenious (or Euclidean) norm of matrix *A* is

$$\|A\|_E = \left(\sum_{i=1}^{n} \sum_{j=1}^{m} |a_{ij}|^2 \right)^{1/2}, \quad (5)$$

and the spectral norm of matrix *A* is

$$\|A\|_2 = \sqrt{\boxed{\frac{max}{1 \le i \le n}} \lambda_i (A^H A)} \ , \quad (6)$$

where $\lambda_i (A^H A)$ is an eigenvalue of $A^H A$, and A^H is the conjugate transpose of matrix *A*.

The maximum column length norm c_1 *(A)* and the maximum row length norm r_1 *(A)* of a matrix of order $n \times n$ are defined as

$c_1(A) = \max_j \sqrt{\sum_{i=1}^{n} |a_{ij}|^2}$,

$r_1(A) = \max_i \sqrt{\sum_{j=1}^{m} |a_{ij}|^2}$.

For any $A, B \epsilon M_{\{m,n\}}(C)$, the Hadamard product of *A*, *B* is entrywise product and defined by [3,4]

$A \circ B = (a_{ij} b_{ij})$

and have the following properties

$$\|A \circ B\|_2 \le r_1(A) c_1(B), \quad \|A \circ B\| \le \|A\| \, \|B\|. \quad (7)$$

Let $A \epsilon M_{\{m,n\}}(C)$, and $B \epsilon M_{\{p,q\}}(C)$ be given, then the Kronecker product of *A*, *B* is defined by [4,6,8]

JSR A
Journal of Scientific Reports

$$\|A \otimes B\| = \begin{bmatrix} a_{11}B & \cdots & a_{1n}B \\ \vdots & \ddots & \vdots \\ a_{m1}B & \cdots & a_{mn}B \end{bmatrix}$$

and have the following properties

$$\|A \otimes B\|_2 = \|A\|_2 \ \|B\|_2, \quad \|A \otimes B\|_E = \|A\|_E \ \|B\|_E. \tag{8}$$

Let $A \in M_{\{m,n\}}(C)$ be given, then the inequality is hold [1,2]

$$\frac{1}{\sqrt{n}} \|A\|_E \leq \|A\|_2 \leq \|A\|_E. \tag{9}$$

2. SOME SUM FORMULAS FOR k-JACOBSTHAL AND k-JACOBSTHAL LUCAS NUMBERS

Let $k \neq -1, 1$. The summation formulas for the *k*-Jacobsthal and *k*-Jacobsthal Lucas sequences are

$$\sum_{i=0}^{n-1} j_{k,i} = \frac{j_{k,n+2} j_{k,n-1} - 1}{k+1}, \tag{10}$$

$$\sum_{i=0}^{n-1} c_{k,i} = \frac{c_{k,n+2}\, c_{k,n-1} + k - 2}{k+1}. \tag{11}$$

The summation of the squares of *k*-Jacobsthal sequence and *k*-Jacobsthal Lucas sequence are

$$\sum_{i=1}^{n} j_{k,i}^2 = \frac{1}{k^2+8}\left[\frac{4c_{k,2n} - c_{k,2n+2} - c_{k,2} + 2}{5 - c_{k,2}} + 2\,(-1)^{n+1} j_{n+1}\right], \tag{12}$$

$$\sum_{i=1}^{n} c_{k,i}^2 = \frac{4c_{k,2n} - c_{k,2n+2} - c_{k,2} + 2}{5 - c_{k,2}} - 2\,(-1)^{n+1} j_{n+1}\ . \tag{13}$$

The summation of the squares of *k*-Jacobsthal and *k*-Jacobsthal Lucas sequence with negative indices are demonstrated

$$\sum_{i=1}^{n} \left(j_{k,-i}\right)^2 = \sum_{i=1}^{n} \left(\frac{j_{k,i}}{2^i}\right)^2 = \frac{1}{k^2+8}\left[\frac{1}{1-k^2}\left(\frac{c_{k,2n} - c_{k,2n+2}}{2^{2n}} - k^2 + 4\right) - \frac{j_{n+1}}{2^{n-1}}\right], \tag{14}$$

$$\sum_{i=1}^{n} \left(c_{k,-i}\right)^2 = \sum_{i=1}^{n} \left(\frac{c_{k,i}}{2^i}\right)^2 = \frac{1}{1-k^2}\left(\frac{c_{k,2n} - c_{k,2n+2}}{2^{2n}} + 4 - k^2\right) + \frac{j_{n+1}}{2^{n-1}} - 4. \tag{15}$$

Some summation formulas for *k*-Jacobsthal sequence and *k*-Jacobsthal Lucas sequence are as follows

$$\sum_{i=1}^{n-1} c_{k,2i} = \frac{4c_{k,2n-2} - c_{k,2n} + k^2 - 4}{1-k^2}, \tag{16}$$

$$\sum_{i=1}^{n-1} \frac{c_{k,2i}}{4^i} = \frac{c_{k,2n-2} - c_{k,2n}}{4^{n-1}(1-k^2)} + \frac{k^2+2}{1-k^2}, \tag{17}$$

$$\sum_{i=1}^{n-1} \frac{c_{k,2i+2}}{4^i} = \frac{c_{k,2n} - c_{k,2n+2}}{4^{n-1}(1-k^2)} + 4\frac{k^2+2}{1-k^2}, \tag{18}$$

JSR A
Journal of Scientific Reports

$$\sum_{i=1}^{n-1} c_{k,2i+2} = \frac{4c_{k,2n}-c_{k,2n+2}+k^2-4}{1-k^2} - (k^2+4), \tag{19}$$

$$\sum_{i=1}^{n-1}(-1)^{i+1} j_{i+1} = \frac{4(-1)^n j_{n-1}-n+1}{3}, \tag{20}$$

$$\sum_{i=1}^{n-1} \frac{j_{i+1}}{2^{i-1}} = -\frac{j_{n-1}}{3.2^{n-2}} + \frac{4n-4}{3}\ . \tag{21}$$

3. LOWER AND UPPER BOUNDS OF TOEPLITZ MATRICES INVOLVING k-JACOBSTHAL NUMBERS

Theorem 1: Let $A = T\left(j_{k,0}, j_{k,1}, \dots, j_{k,n-1}\right)$ be a Toeplitz matrix with *k*-Jacobsthal numbers, then the largest absolute column sum (1-norm) and the largest absolute row sum (∞-norm) of *A* are

$$\|A\|_1 = \|A\|_\infty = \frac{(k+2)\, j_{k,n} + 2j_{k,n-1} - 1}{k+1}.$$

Proof. Clearly, the explicit form of this matrix as follows:

$$A = \begin{bmatrix} j_{k,0} & j_{k,-1} & j_{k,-2} & \cdots & j_{k,1-n} \\ j_{k,1} & j_{k,0} & j_{k,-1} & \cdots & j_{k,2-n} \\ j_{k,2} & j_{k,1} & j_{k,0} & \cdots & j_{k,3-n} \\ \vdots & \vdots & \vdots & \ddots & \vdots \\ j_{k,n-1} & j_{k,n-2} & j_{k,n-3} & \cdots & j_{k,0} \end{bmatrix} \tag{22}$$

By the definitions of 1-norm and ∞-norm, and (10), it is easily seen

$$\|A\|_1 = \max_j \sum_{i=1}^{n} |a_{ij}| = \sum_{i=1}^{n} |a_{i1}| = \sum_{i=0}^{n-1} j_{k,i} = \frac{j_{k,n} + 2j_{k,n-1} - 1}{k+1},$$

$$\|A\|_\infty = \max_i \sum_{j=1}^{n} |a_{ij}| = \sum_{j=1}^{n} |a_{nj}| = \sum_{i=0}^{n-1} j_{k,i} = \frac{j_{k,n}+2j_{k,n-1}-1}{k+1}. \qquad \blacksquare$$

Theorem 2: Let $A = T\left(j_{k,0}, j_{k,1}, \dots, j_{k,n-1}\right)$ be a Toeplitz matrix, then the Frobenious (or Euclidean) norm of matrix *A* is

$$\|A\|_E = \sqrt{\begin{array}{l} \frac{1}{(k^2+8)(1-k^2)^2}\left[c_{k,2n+2} + \frac{c_{k,2n+2}}{2^{2n-2}} - 8c_{k,2n} - \frac{2c_{k,2n}}{2^{2n-2}} + 16c_{k,2n-2} + \frac{c_{k,2n-2}}{2^{2n-2}} - 18\right] \\ + \frac{(n-1)(2k^2-2)-4-k^2}{(k^2+8)(k^2-1)} + \frac{1}{3(k^2+8)}\left[8(-1)^n j_{n-1} - \frac{4\, j_n}{2^n} - 6n + 8\right]. \end{array}} \tag{23}$$

Proof. Let *A* be an $n \times n$ matrix . Then by (5), (12), (14)

JSR A
Journal of Scientific Reports

$$\|A\|_E{}^2 = \sum_{i=1}^{n}\sum_{j=1}^{n} a_{ij}^2 = n{j_{k,0}}^2 + \sum_{m=1}^{n-1}(n-m){j_{k,m}}^2 + \sum_{m=1}^{n-1}(n-m){j_{k,-m}}^2$$
$$= \sum_{m=1}^{n-1}\sum_{i=1}^{m}{j_{k,i}}^2 + \sum_{m=1}^{n-1}\sum_{i=1}^{m}\left(\frac{j_{k,i}}{2^i}\right)^2$$
$$= \frac{1}{(k^2+8)}\sum_{m=1}^{n-1}\left[\frac{4c_{k,2m}-c_{k,2m+2}-k^2-2}{1-k^2} + 2\,(-1)^{m+1}j_{m+1}\right]$$
$$+ \frac{1}{(k^2+8)}\sum_{m=1}^{n-1}\frac{1}{1-k^2}\left(\frac{c_{k,2m}-c_{k,2m+2}}{2^{2m}} - k^2 + 4\right) - \frac{j_{m+1}}{2^{m-1}}$$

And then by using the sum formulas (16), (19), (21), the following result is obtained:

$$= \frac{1}{(k^2+8)}\left[\frac{16c_{k,2n-2}-4c_{k,2n}+4k^2-16}{(1-k^2)^2} + \frac{c_{k,2n+2}-4c_{k,2n}-k^2+4}{(1-k^2)^2} - \frac{(k^2+4)}{k^2-1}\right.$$
$$\left. + \frac{(k^2+2)(n-1)}{k^2-1} + \frac{8(-1)^n j_{n-1}-2n+2}{3}\right]$$
$$+ \frac{1}{(k^2+8)}\left\{\frac{1}{(1-k^2)^2}\left[\frac{-c_{k,2n}+c_{k,2n-2}}{2^{2n-2}} + 2 + k^2 + \frac{-c_{k,2n}+c_{k,2n+2}}{2^{2n-2}} - 8 - 4k^2\right]\right.$$
$$\left. + (n-1)\left[\frac{k^2-4}{k^2-1}\right] + \frac{j_{n-1}}{3.2^{n-2}} - \frac{4n-4}{3}\right\}$$
$$= \frac{1}{(k^2+8)(1-k^2)^2}\left[c_{k,2n+2} + \frac{c_{k,2n+2}}{2^{2n-2}} - 8c_{k,2n} - \frac{2c_{k,2n}}{2^{2n-2}} + 16c_{k,2n-2} + \frac{c_{k,2n-2}}{2^{2n-2}} - 10\right]$$
$$+ \frac{(n-1)(2k^2-2)-4-k^2}{(k^2+8)(k^2-1)} + \frac{1}{3(k^2+8)}\left[8(-1)^n j_{n-1} + \frac{j_{n-1}}{2^{n-2}} - 6n + 6\right].$$ ■

Theorem 3: Let $A = T\left(j_{k,0}, j_{k,1}, \dots, j_{k,n-1}\right)$ be Toeplitz matrix, then the lower and upper bounds for the spectral norm of A are obtained as

$$\sqrt{\begin{matrix}\frac{1}{n(k^2+8)(1-k^2)^2}\left[c_{k,2n+2} + \frac{c_{k,2n+2}}{2^{2n-2}} - 8c_{k,2n} - \frac{2c_{k,2n}}{2^{2n-2}} + 16c_{k,2n-2} + \frac{c_{k,2n-2}}{2^{2n-2}} - 10\right] \\ + \frac{(n-1)(2k^2-2)-4-k^2}{n(k^2+8)(k^2-1)} + \frac{1}{3n(k^2+8)}\left[8(-1)^n j_{n-1} + \frac{j_{n-1}}{2^{n-2}} - 6n + 6\right]\end{matrix}} \le \|A\|_2 \qquad (24)$$

$$\|A\|_2 \le \sqrt{\begin{matrix}\left[\frac{1}{k^2+8}\left(\frac{4c_{k,2n-4}-c_{k,2n-2}-k^2-2}{1-k^2} + 2(-1)^{n-1}j_{n-1}\right) + 1\right] \\ \left[\frac{1}{k^2+8}\left(\frac{4c_{k,2n-2}-c_{k,2n}-k^2-2}{1-k^2} + 2(-1)^n j_n\right)\right]\end{matrix}} \qquad (25)$$

Proof. By (23) and using the property (9), the left hand side of the inequality is completed.
On the other hand, let $A = B \circ C$ whereas

$$B = b_{ij} = \begin{cases} b_{ij} = 1 & j = 1 \\ b_{ij} = j_{k,i-j} & j \neq 1 \end{cases} \text{ and } \quad C = c_{ij} = \begin{cases} c_{ij} = j_{k,i-j} & j = 1 \\ c_{ij} = 1 & j \neq 1 \end{cases}$$

JSR A
Journal of Scientific Reports

$$B=\begin{bmatrix}1 & j_{k,-1} & j_{k,-2} & \cdots & j_{k,1-n}\\ 1 & j_{k,0} & j_{k,-1} & \cdots & j_{k,2-n}\\ 1 & j_{k,1} & j_{k,0} & \cdots & j_{k,3-n}\\ \vdots & \vdots & \vdots & \ddots & \vdots\\ 1 & j_{k,n-2} & j_{k,n-3} & \cdots & j_{k,0}\end{bmatrix} \quad \text{and} \quad C=\begin{bmatrix}j_{k,0} & 1 & 1 & \cdots & 1\\ j_{k,1} & 1 & 1 & \cdots & 1\\ j_{k,2} & 1 & 1 & \cdots & 1\\ \vdots & \vdots & \vdots & \ddots & \vdots\\ j_{k,n-1} & 1 & 1 & \cdots & 1\end{bmatrix}$$

$$r_1(B)=\max_{1\le i\le n}\sqrt{\sum_{j=1}^{n}|b_{ij}|^2}=\sqrt{\sum_{j=1}^{n}|b_{nj}|^2}=\sqrt{\sum_{i=0}^{n-2}{j_{k,i}}^2+1}$$
$$=\sqrt{\frac{1}{k^2+8}\left(\frac{4c_{k,2n-4}-c_{k,2n-2}-k^2-2}{1-k^2}+2(-1)^{n-1}j_{n-1}\right)+1}$$

$$c_1(C)=\max_{1\le i\le n}\sqrt{\sum_{i=1}^{n}|c_{ij}|^2}=\sqrt{\sum_{i=1}^{n}|c_{j1}|^2}=\sqrt{\sum_{i=0}^{n-1}{j_{k,i}}^2}$$
$$=\sqrt{\frac{1}{k^2+8}\left(\frac{4c_{k,2n-2}-c_{k,2n}-k^2-2}{1-k^2}+2(-1)^{n}j_{n}\right)}\ .$$

By using the property (7), the right hand side of the inequality is completed:

$$r_1(B)c_1(C)=\sqrt{\begin{matrix}\left[\frac{1}{k^2+8}\left(\frac{4c_{k,2n-4}-c_{k,2n-2}-k^2-2}{1-k^2}+2(-1)^{n-1}j_{n-1}\right)+1\right]\\ \left[\frac{1}{k^2+8}\left(\frac{4c_{k,2n-2}-c_{k,2n}-k^2-2}{1-k^2}+2(-1)^{n}j_{n}\right)\right]\end{matrix}}$$ ■

4. LOWER AND UPPER BOUNDS OF TOEPLITZ MATRICES INVOLVING k-JACOBSTHAL LUCAS NUMBERS

Theorem 4: Let the elements of the Toeplitz matrix be *k*-Jacobsthal Lucas numbers $A=T\left(c_{k,0}\,,c_{k,1}\,,\ldots,c_{k,n-1}\right)$, then 1-norm and ∞-norm of *A* are

$$\|A\|_1=\|A\|_\infty=\frac{(k+2)\,j_{k,n}+2j_{k,n-1}-1}{k+1}.$$

Proof. Clearly, the explicit form of this matrix as follows:

$$A=\begin{bmatrix}c_{k,0} & c_{k,-1} & c_{k,-2} & \cdots & c_{k,1-n}\\ c_{k,1} & c_{k,0} & c_{k,-1} & \cdots & c_{k,2-n}\\ c_{k,2} & c_{k,1} & c_{k,0} & \cdots & c_{k,3-n}\\ \vdots & \vdots & \vdots & \ddots & \vdots\\ c_{k,n-1} & c_{k,n-2} & c_{k,n-3} & \cdots & c_{k,0}\end{bmatrix}. \qquad (26)$$

By the definitions of 1-norm and ∞-norm, and (11), it is easily seen

JSR A
Journal of Scientific Reports

$$\|A\|_1 = \max_j \sum_{i=1}^{n} |a_{ij}| = \sum_{i=1}^{n} |a_{i1}| = \sum_{i=0}^{n-1} c_{k,i} = \frac{c_{k,n+2}\, c_{k,n-1}+k-2}{k+1},$$

$$\|A\|_\infty = \max_i \sum_{j=1}^{n} |a_{ij}| = \sum_{j=1}^{n} |a_{nj}| = \sum_{i=0}^{n-1} c_{k,i} = \frac{c_{k,n} + 2\, c_{k,n-1} + k - 2}{k+1}.$$

In the following theorem, we give the Euclidean (Frobenius) norm of the matrix involving *k*-Jacobsthal Lucas numbers.

Theorem 5: Let $A = T\,(c_{k,0}\,, c_{k,1}\,, \dots, c_{k,n-1}\,)$ be Toeplitz matrix with *k*-Jacobsthal Lucas numbers, then the Frobenious (or Euclidean) norm of matrix *A* is

$$\|A\|_E = \sqrt{\frac{16c_{k,2n-2}-8c_{k,2n}+c_{k,2n+2}-k^2-20}{(1-k^2)^2} + \frac{c_{k,2n-2}-2c_{k,2n}+c_{k,2n+2}}{2^{2n-2}(1-k^2)^2} + \frac{(k^2+4)+(n-1)(6k^2-6)}{1-k^2} + \frac{-8(-1)^n j_{n-1}+6n-8}{3} + \frac{j_n}{3.2^{n-2}}}. \tag{27}$$

Proof. Let *A* be an *n*×*n* matrix as in (26). Then by the definition of Frobenius norm and by (5), (13), (15), we can obtain the following equations for matrix A

$$\begin{aligned}
\|A\|_E{}^2 &= \sum_{i=1}^{n}\sum_{j=1}^{n} a_{ij}^2 = n{c_{k,0}}^2 + \sum_{i=1}^{n-1}(n-i){c_{k,i}}^2 + \sum_{i=1}^{n-1}(n-i){c_{k,-i}}^2 \\
&= 4n + \sum_{m=1}^{n-1}\sum_{i=1}^{m} {c_{k,i}}^2 + \sum_{m=1}^{n-1}\sum_{i=1}^{m}\left(\frac{c_{k,i}}{2^i}\right)^2 \\
&= \sum_{m=1}^{n-1} \frac{4c_{k,2m} - c_{k,2m+2} - k^2 - 4}{1-k^2} - 2(-1)^{m+1} j_{m+1} + \sum_{m=1}^{n-1} \frac{c_{k,2m} - c_{k,2m+2}}{2^{2m}(1-k^2)} + \frac{3k^2}{1-k^2} + \frac{j_{m+1}}{2^{m-1}} \\
&= \frac{16c_{k,2n-2} - 8c_{k,2n} + c_{k,2n+2} - (k^2-4)^2}{(1-k^2)^2} + \frac{c_{k,2n-2} - 2c_{k,2n} + c_{k,2n+2}}{2^{2n-2}(1-k^2)^2} \\
&\quad + \frac{(-4k^2-8) + (n-1)(2k^2-4)}{1-k^2} + \frac{-8(-1)^n j_{n-1} + 6n - 6}{3} - \frac{j_{n-1}}{3.2^{n-2}}.
\end{aligned}$$

■

Theorem 6: Let $A = T\,(c_{k,0}\,, c_{k,1}\,, \dots, c_{k,n-1})$ be Toeplitz matrix, then the lower and upper bounds for the spectral norm of *A* are obtained as

$$\sqrt{\frac{16c_{k,2n-2}-8c_{k,2n}+c_{k,2n+2}-(k^2-4)^2}{n(1-k^2)^2} + \frac{c_{k,2n-2}-2c_{k,2n}+c_{k,2n+2}}{2^{2n-2}n(1-k^2)^2} + \frac{(-4k^2-8)+(n-1)(2k^2-4)}{(1-k^2)n} + \frac{-8(-1)^n j_{n-1}+6n-6}{3n} - \frac{j_{n-1}}{3n.2^{n-2}}} \le \|A\|_2 \tag{28}$$

$$\|A\|_2 \le \sqrt{\frac{4\, c_{k,2n-4}-c_{k,2n-2}-k^2-2}{1-k^2} - 2(-1)^{n-1} j_{n-1} + 5 \quad \frac{4\, c_{k,2n-2}-c_{k,2n}-k^2-2}{1-k^2} - 2(-1)^n j_n + 4} \tag{29}$$

JSR A
Journal of Scientific Reports

Proof. By (27), and using the property (9), the left hand side of the inequality is completed. On the other hand, let $A = B \circ C$ whereas

$$B = b_{ij} = \begin{cases} b_{ij} = 1 & j = 1 \\ b_{ij} = c_{k,i-j} & j \neq 1 \end{cases} \quad \text{and} \quad C = c_{ij} = \begin{cases} c_{ij} = c_{k,i-j} & j = 1 \\ c_{ij} = 1 & j \neq 1 \end{cases}$$

$$B = \begin{bmatrix} 1 & c_{k,-1} & c_{k,-2} & \cdots & c_{k,1-n} \\ 1 & c_{k,0} & c_{k,-1} & \cdots & c_{k,2-n} \\ 1 & c_{k,1} & c_{k,0} & \cdots & c_{k,3-n} \\ \vdots & \vdots & \vdots & \ddots & \vdots \\ 1 & c_{k,n-2} & c_{k,n-3} & \cdots & c_{k,0} \end{bmatrix} \quad \text{and} \quad C = \begin{bmatrix} c_{k,0} & 1 & 1 & \cdots & 1 \\ c_{k,1} & 1 & 1 & \cdots & 1 \\ c_{k,2} & 1 & 1 & \cdots & 1 \\ \vdots & \vdots & \vdots & \ddots & \vdots \\ c_{k,n-1} & 1 & 1 & \cdots & 1 \end{bmatrix}.$$

Then, by using the sum formula (13) and the definition of the maximum column length norm and the maximum row length norm, the following equalities are hold:

$$r_1(B) = \max_{1\leq i\leq n} \sqrt{\sum_{j=1}^{n} |b_{ij}|^2} = \sqrt{\sum_{j=1}^{n} |b_{nj}|^2} = \sqrt{\sum_{i=0}^{n-2} {c_{k,i}}^2 + 1}$$
$$= \sqrt{\frac{4\, c_{k,2n-4} - c_{k,2n-2} - k^2 - 2}{1-k^2} - 2(-1)^{n-1} j_{n-1} + 5},$$

$$c_1(C) = \max_{1\leq i\leq n} \sqrt{\sum_{i=1}^{n} |c_{ij}|^2} = \sqrt{\sum_{i=1}^{n} |c_{j1}|^2} = \sqrt{\sum_{i=0}^{n-1} {c_{k,i}}^2}$$
$$= \sqrt{\frac{4\, c_{k,2n-2} - c_{k,2n} - k^2 - 2}{1-k^2} - 2(-1)^{n} j_{n} + 4}.$$

If we use the equations given in (7), the right hand side of the inequality is completed. ■

Corollary 7: Let $A = T\,(j_{k,0}\,, j_{k,1}\,, \ldots, j_{k,n-1}\,)$ and $B = T\,(c_{k,0}\,, c_{k,1}\,, \ldots, c_{k,n-1})$ be Toeplitz matrix with *k*-Jacobsthal and the *k*-Jacobsthal Lucas numbers, then the Euclidean norm of Kronecker product of these matrices is given as:

$$\|A \otimes B\|_E = \sqrt{\frac{1}{(k^2+8)(1-k^2)^2}\left[c_{k,2n+2} + \frac{c_{k,2n+2}}{2^{2n-2}} - 8c_{k,2n} - \frac{2c_{k,2n}}{2^{2n-2}} + 16c_{k,2n-2} + \frac{c_{k,2n-2}}{2^{2n-2}} - 18\right]} + \frac{(n-1)(2k^2-2)-4-k^2}{(k^2+8)(k^2-1)} + \frac{1}{3(k^2+8)}\left[8(-1)^n j_{n-1} - \frac{4\, j_n}{2^n} - 6n + 8\right]$$
$$\cdot \sqrt{\frac{16c_{k,2n-2} - 8c_{k,2n} + c_{k,2n+2} - k^2 - 20}{(1-k^2)^2} + \frac{c_{k,2n-2} - 2c_{k,2n} + c_{k,2n+2}}{2^{2n-2}(1-k^2)^2}} \sqrt{\frac{(k^2+4)+(n-1)(6k^2-6)}{1-k^2} + \frac{-8(-1)^n j_{n-1} + 6n - 8}{3} + \frac{j_n}{3.2^{n-2}}}$$

Proof. The proof is seen easily by $\|A \otimes B\|_E = \|A\|_E \, \|B\|_E$ and (23), (27).

JSR A
Journal of Scientific Reports

Corollary 8: Let $A = T\,(j_{k,0}\,, j_{k,1}\,, \dots, j_{k,n-1}\,)$ and $B = T\,(c_{k,0}\,, c_{k,1}\,, \dots, c_{k,n-1})$ be Toeplitz matrix with *k*-Jacobsthal and the *k*-Jacobsthal Lucas numbers, then the upper bound for the spectral norm of Kronecker product of these matrices is given as:

$$\|A \otimes B\|_2 \leq \sqrt{\left[\frac{1}{k^2+8}\left(\frac{4c_{k,2n-4}-c_{k,2n-2}-k^2-2}{1-k^2}+2(-1)^{n-1}j_{n-1}\right)+1\right]\left[\frac{1}{k^2+8}\left(\frac{4c_{k,2n-2}-c_{k,2n}-k^2-2}{1-k^2}+2(-1)^{n}j_{n}\right)\right]} \cdot \sqrt{\frac{4\,c_{k,2n-4}-c_{k,2n-2}-k^2-2}{1-k^2}-2(-1)^{n-1}\,j_{n-1}+5 \quad \frac{4\,c_{k,2n-2}-c_{k,2n}-k^2-2}{1-k^2}-2(-1)^{n}\,j_{n}+4}$$

Proof. The proof is seen easily by $\|A \otimes B\,\|_2 = \|A\|_2\,\|B\|_2$ and (25), (29). ■

Corollary 9 : Let $A = T\,(j_{k,0}\,, j_{k,1}\,, \dots, j_{k,n-1}\,)$ and $B = T\,(c_{k,0}\,, c_{k,1}\,, \dots, c_{k,n-1})$ be Toeplitz matrix with *k*-Jacobsthal and the *k* -Jacobsthal Lucas numbers, then the upper bound for the spectral norm of Hadamard product of the matrices is

$$\|A \circ B\,\|_2 \leq \sqrt{\left[\frac{1}{k^2+8}\left(\frac{4c_{k,2n-4}-c_{k,2n-2}-k^2-2}{1-k^2}+2(-1)^{n-1}j_{n-1}\right)+1\right]\left[\frac{1}{k^2+8}\left(\frac{4c_{k,2n-2}-c_{k,2n}-k^2-2}{1-k^2}+2(-1)^{n}j_{n}\right)\right]} \cdot \sqrt{\left(\frac{4\,c_{k,2n-4}-c_{k,2n-2}-k^2-2}{1-k^2}-2(-1)^{n-1}\,j_{n-1}+5\right) \quad \left(\frac{4\,c_{k,2n-2}-c_{k,2n}-k^2-2}{1-k^2}-2(-1)^{n}\,j_{n}+4\right)}$$

Proof. The proof is seen easily by $\|A \circ B\,\|_2 \leq \|A\|_2\,\|B\|_2$ and (25), (29). ■

Corollary 10 : Let $A = T\,(j_{k,0}\,, j_{k,1}\,, \dots, j_{k,n-1}\,)$ and $B = T\,(c_{k,0}\,, c_{k,1}\,, \dots, c_{k,n-1})$ be Toeplitz matrix with *k*-Jacobsthal and the *k* -Jacobsthal Lucas numbers, then the upper bound for the Euclid norm of Hadamard product of the matrices is

$$\|A \circ B\,\|_E \leq \sqrt{\frac{1}{(k^2+8)(1-k^2)^2}\left[c_{k,2n+2}+\frac{c_{k,2n+2}}{2^{2n-2}}-8c_{k,2n}-\frac{2c_{k,2n}}{2^{2n-2}}+16c_{k,2n-2}+\frac{c_{k,2n-2}}{2^{2n-2}}-18\right] + \frac{(n-1)(2k^2-2)-4-k^2}{(k^2+8)(k^2-1)}+\frac{1}{3(k^2+8)}\left[8(-1)^n j_{n-1}-\frac{4\,j_n}{2^n}-6n+8\right]} \cdot \sqrt{\frac{16c_{k,2n-2}-8c_{k,2n}+c_{k,2n+2}-k^2-20}{(1-k^2)^2}+\frac{c_{k,2n-2}-2c_{k,2n}+c_{k,2n+2}}{2^{2n-2}(1-k^2)^2} + \frac{(k^2+4)+(n-1)(6k^2-6)}{1-k^2}+\frac{8(-1)^{n+1}j_{n-1}+6n-8}{3}+\frac{j_n}{3.2^{n-2}}}$$

Proof. By $\|A \circ B\,\|_E \leq \|A\|_E\,\|B\|_E$ and (23), (27), the result is found. ■

JSR A
Journal of Scientific Reports

REFERENCES

[1] Mathias, R., (1990), The spectral norm of nonnegative matrix, Linear Algebra and its Applications, 131, 269-284.

[2] Zielke, G., (1988), Some remarks on matrix norms, condition numbers and error estimates for linear equations, Linear Algebra and its Applications, 110, 29-41.

[3] Reams, R., (1999), Hadamard inverses square roots and products of almost semi-definite matrices, Linear Algebra and its Applications, 288, 35-43.

[4] Horn, R. A., Johnson, C. R., (1991), Topics in matrix analysis, Cambridge University Press, Cambridge.

[5] Visick, G., (2000), A quantitative version of the observation that the Hadamard product is a principal submatrix of the Kronecker product, Linear Algebra Appl., 304, 45-68.

[6] Solak, S., (2005), On the norms of circulant matrices with the Fibonacci and Lucas numbers, Appl. Math. Comput., 160, 125-132.

[7] Akbulak, M., Bozkurt, D., (2008), On the norms of Toeplitz matrices involving Fibonacci and Lucas numbers, Hacettepe Journal of Mathematics and Statistics, 37(2), 89-95.

[8] Shen, S., (2012), On the Norms of Toeplitz Matrices Involving k-Fibonacci and k-Lucas Numbers, Int. J. Contemp. Math. Sciences, 7(8), 363-368.

[9] Daşdemir, A., (2016), On the norms of Toeplitz Matrices with the Pell, Pell-Lucas and Modified Pell numbers, Journal of Engineering Technology and Applied Sciences, 1(2), 51-57.

[10] Kocer, E. G., (2007), Circulant, Negacyclic and Semicirculant matrices with the modified Pell, Jacobsthal and Jacobsthal- Lucas numbers, Hacettepe Journal of Mathematics and Statistics, 36(2), 133-142.

[11] Raza, Z., Ali, M.A., (2015), On the Norms of Some Special Matrices with Generalized Fibonacci Sequence, J. Appl. Math. & Informatics, 33(5–6), 593–605.

[12] Uygun, S., Eldoğan, H., (2016), The *k* -Jacobsthal and *k* -Jacobsthal Lucas sequences, General Mathematics Notes, 36(1), 34-47.

[13] Uygun, ,S. , (2016), Some Bounds for the Norms of Circulant Matrices with the *k* -Jacobsthal and *k* -Jacobsthal Lucas Numbers, Journal of Mathematics Research, 8(6), 133-138.

Kütahya Dumlupınar University
Institute of Graduate Studies

Journal of Scientific
Reports-A
E-ISSN: 2687-6167
Number 45, December 2020

RESEARCH ARTICLE

DIFFUSION EQUATION INCLUDING LOCAL FRACTIONAL DERIVATIVE AND NON-HOMOGENOUS DIRICHLET BOUNDARY CONDITIONS

Süleyman ÇETİNKAYA[1], Ali DEMİR[2]

[1] Kocaeli University, Faculty of Arts and Sciences, Department of Mathematics, 41380, Kocaeli, suleyman.cetinkaya@kocaeli.edu.tr, ORCID: 0000-0002-8214-5099
[2] Kocaeli University, Faculty of Arts and Sciences, Department of Mathematics, 41380, Kocaeli, ademir@kocaeli.edu.tr, ORCID: 0000-0003-3425-1812

Received Date: 30.10.2020 *Accepted Date: 07.12.2020*

ABSTRACT

In this research, we discuss the construction of analytic solution of non-homogenous initial boundary value problem including PDEs of fractional order. Since non-homogenous initial boundary value problem involves local fractional derivative, it has classical initial and boundary conditions. By means of separation of variables method and the inner product defined on $L^2[0,l]$, the solution is constructed in the form of a Fourier series with respect to the eigenfunctions of a corresponding Sturm-Liouville eigenvalue problem including local fractional derivative used in this study. Illustrative example presents the applicability and influence of separation of variables method on fractional mathematical problems.

Keywords: *Local fractional derivative, Time-fractional diffusion equation, Initial-boundary-value problems, Spectral method, Non-homogenous Dirichlet boundary conditions*

1. INTRODUCTION

Since mathematical models including fractional derivatives play a vital role fractional derivatives draw a growing attention of many researchers in various branches of sciences. Therefore there are many different fractional derivatives such as Caputo, Riemann-Liouville, Atangana-Baleanu. However these fractional derivatives don't satisfy most important properties of ordinary derivative which leads to many diffuculties to analyze or obtain the solution of fractional mathematical models. As a result many scientists focus on defining new fractional derivatives to cover the setbacks of the defined ones. Moreover the success of mathematical modelling of systems or processes depends on the fractional derivative, it involves, since the correct choice of the fractional derivative allows us to model the real data of systems or processes accurately.

In order to the define new fractional derivatives, various methods exists and these ones are classfied based on their features and formation such as nonlocal fractional derivatives and local fractional derivatives. From a physical aspect, the intrinsic nature of the physical system can be reflected to the

JSR A
Journal of Scientific Reports

mathematical model of the system by using fractional derivatives. Therefore the solution of the fractional mathematical model is in excellent agreement with the predictions and experimental measurement of it. The systems whose behaviour is non-local can be modelled better by fractional mathematical models and the degree of its non-locality can be arranged by the order of fractional derivative. In order to analyze the diffusion in a non-homogenous medium that has memory effects it is better to analyze the solution of the fractional mathematical model for this diffusion. As a result in order to model a process, the correct choices of fractional derivative and its order must be determined.

Rheology is known as the scientific study of material diffusion. In rheology, mathematical models of diffusion process are employed to analyze the behaviour of materials which allow us to classify and compare them. In this study, we focus on fractional diffusion problem including time fractional derivative. The novelty of this research is that the materials can be classified as liquid, gas and temperature based on the order of time fractional derivative. For instance, fractional diffusion model of materials which behaves slower, the order of time fractional derivative is between zero and one and the order of time fractional derivative for materials which behaves faster is greater than one. Moreover based on the complexity of the material, suitable fractional derivative need to be chosen to facilitate the correct analysis of the material. In this study, we classify non-complex materials therefore local fractional derivative is used. Mathematical model of diffusion problems including local fractional derivatives gives better results than ones including integer order derivatives [1]. There are many published work on the diffusion of various matters in science especially in fluid mechanics and gas dynamics [2-7].

2. MAIN RESULTS

The proportional derivative is a newly defined fractional derivative which is generally defined as

$$ {}^{P}D_{\alpha}f(t) = \mathrm{K}_1(\alpha,\mathrm{t})\,\mathrm{f(t)} + \mathrm{K}_0(\alpha,\mathrm{t})\mathrm{f}'(\mathrm{t}), \tag{1}$$

where the functions K_0 and K_1 satisfy certain properties in terms of limit [8] and f is a differentiable function. Notice that this derivative can be regarded as an extension of conformable derivative and is used in control theory.

In this study we focus on obtaining the solution of following fractional diffusion equation including various proportional derivative operator by making use of the separation of variables method:

$$ {}^{P}D_t^{\alpha}u(x,t) = \gamma^2 u_{xx}(x,t), \tag{2}$$
$$ u(0,t) = u_0, u(l,t) = u_1, \tag{3}$$
$$ u(x,0) = f(x) \tag{4}$$

where $0 < \alpha < 1, \gamma \in \mathbb{R}, 0 \leq x \leq l,\ 0 \leq t \leq T,\ u_0$ and u_1 are constants. Here we use the following forms of the proportional derivatives:

$$ {}^{P}D_{\alpha}f(t) = K_1(\alpha)\,f(t) + K_0(\alpha)f'(t). \tag{5}$$

Especially we consider the following ones:

$$ {}^{P}_{1}D_{\alpha}f(t) = (1-\alpha)\,f(t) + \alpha f'(t) \tag{6}$$

JSR A
Journal of Scientific Reports

and

$${}_2^P D_\alpha f(t) = (1-\alpha^2)\, f(t) + \alpha^2 f'(t). \tag{7}$$

Let us consider the following problem including the proportional derivative in (6)

$${}^P D_t^\alpha u(x,t) = \gamma^2 u_{xx}(x,t), \tag{8}$$
$$u(0,t) = u_0, u(l,t) = u_1, \tag{9}$$
$$u(x,0) = f(x), \tag{10}$$

where $0 < \alpha < 1, \gamma \in \mathbb{R}, 0 \leq x \leq l,\ 0 \leq t \leq T,\ u_0$ and u_1 are constants.

Before investigating the solution of the problem (8)-(10), let us define the function $v(x,t)$ which homogenizes boundary conditions (9) as follows:

$$v(x,t) = u(x,t) + \frac{x}{l}(u_0 - u_1) - u_0. \tag{11}$$

Via (11), the problem (8)-(10) turns into the following problem (12)-(14).

$${}^P D_t^\alpha v(x,t) = \gamma^2 v_{xx}(x,t), \tag{12}$$
$$v(0,t) = 0, v(l,t) = 0 \tag{13}$$
$$v(x,0) = f(x) + \frac{x}{l}(u_0 - u_1) - u_0, \tag{14}$$

where $0 < \alpha < 1, \gamma \in \mathbb{R}, 0 \leq x \leq l,\ 0 \leq t \leq T,\ u_0$ and u_1 are constants.

By means of separation of variables method, The generalized solution of above problem is constructed in analytical form. Thus a solution of problem (12)-(14) have the following form:

$$v(x,t;\alpha) = X(x)T(t;\alpha) \tag{15}$$

where $0 \leq x \leq l,\ 0 \leq t \leq T$.

Plugging (15)into (12) and arranging it, we have

$$\frac{{}^P D_t^\alpha (T(t;\alpha))}{T(t;\alpha)} = \gamma^2 \frac{X''(x)}{X(x)} = -\lambda^2. \tag{16}$$

Equation (16) produce a fractional differential equation with respect to time and an ordinary differential equation with respect to space. The first ordinary differential equation is obtained by taking the equation on the right hand side of Eq. (16). Hence with boundary conditions (13), we have the following problem:

$$X''(x) + \lambda^2 X(x) = 0, \tag{17}$$
$$X(0) = X(l) = 0. \tag{18}$$

The solution of eigenvalue problem (17)-(18) is accomplished by making use of the exponential function of the following form:

JSR A
Journal of Scientific Reports

$$X(x) = e^{rx}. \tag{19}$$

Hence the characteristic equation is computed in the following form:

$$r^2 + \lambda^2 = 0. \tag{20}$$

Case 1: If $\lambda = 0$, then the characteristic equation have coincident solutions $r_{1,2} = 0$, leading to the general solution of the eigenvalue problem (17)-(18) have the following form:

$$X(x) = k_1 x + k_2.$$

The first boundary condition yields

$$X(0) = k_2 = 0 \Rightarrow k_2 = 0. \tag{21}$$

which leads to the following solution

$$X(x) = k_1 x. \tag{22}$$

Similarly second boundary condition leads to

$$X(l) = k_1 l = 0 \Rightarrow k_1 = 0. \tag{23}$$

which implies that

$$X(x) = 0. \tag{24}$$

As a result, the characteristic equation (20) can not have the solution $\lambda = 0$.

Case 2. If $\lambda > 0$, the Eq. (20) have two distinct real roots r_1, r_2 yielding the general solution of the problem (17)-(18) in the following form:

$$X(x) = c_1 e^{r_1 x} + c_2 e^{r_2 x}. \tag{25}$$

By making use of the first boundary condition, we have

$$X(0) = c_1 + c_2 = 0. \qquad c_1 = -c_2. \tag{26}$$

From second boundary condition

$$X(l) = (-c_2)e^{r_1 l} + c_2 e^{r_2 l} = c_2(-e^{r_1 l} + e^{r_2 l}) = 0$$

Which indicates that $c_2 = 0$. Hence $c_1 = 0$ which implies that $X(x) = 0$ which implies that there is not any solution for $\lambda > 0$.

Case 3: If $\lambda < 0$, then the characteristic equation have the solutions

JSR A
Journal of Scientific Reports

$$r_{1,2} = \mp i\lambda \tag{27}$$

which leads to the general solution of the eigenvalue problem (17)-(18) have the following form:

$$X(x) = c_1 \cos(\lambda x) + c_2 \sin(\lambda x). \tag{28}$$

By making use of the first boundary condition we have

$$X(0) = c_1 = 0 \Rightarrow c_1 = 0. \tag{29}$$

Hence the solution becomes

$$X(x) = c_2 \sin(\lambda x). \tag{30}$$

Similarly last boundary condition leads to

$$X(l) = c_2 \sin(\lambda l) = 0 \tag{31}$$

which implies that

$$\sin(\lambda l) = 0. \tag{32}$$

Let $w_n = \lambda_n l$. The solutions of (32) can be denoted by means of $w_n = n\pi$, $n = 0,1,2,3, \ldots$ which are eigenvalues of the problem (17)-(18), as follows:

$$\lambda_n = \frac{w_n^2}{l^2},\ 0 < w_1 < w_2 < w_3 < \cdots,\ n = 0,1,2,3, \ldots \tag{33}$$

As a result the solution is obtained as follows:

$$X_n(x) = c_n \sin\left(w_n \left(\frac{x}{l}\right)\right) = \sin\left(w_n \left(\frac{x}{l}\right)\right),\ n = 0,1,2,3, \ldots \tag{34}$$

The second equation in (16) for eigenvalue λ_n yields the ordinary differential equation below:

$$\frac{{}^{P}D_t^{\alpha}(T(t;\alpha))}{T(t;\alpha)} = -\gamma^2\lambda^2, \tag{35}$$

$$\frac{K_1(\alpha)\,T_n(t;\alpha) + K_0(\alpha)T_n{}'(t;\alpha)}{T_n(t;\alpha)} = -\gamma^2\lambda_n^2,$$

$$K_0(\alpha)T_n{}'(t;\alpha) + \left(\gamma^2\lambda_n^2 + K_1(\alpha)\right)T_n(t;\alpha) = 0$$

which yields the following solution

$$T_n(t;\alpha) = exp\left(-\frac{\gamma^2\lambda_n^2 + K_1(\alpha)}{K_0(\alpha)}t\right),\ n = 0,1,2,3, \ldots \tag{36}$$

The solution for every eigenvalue λ_n is constructed as

JSR A
Journal of Scientific Reports

$$v_n(x,t;\alpha) = X_n(x)T_n(t;\alpha) = exp\left(-\frac{\gamma^2\lambda_n^2+K_1(\alpha)}{K_0(\alpha)}t\right)\sin\left(w_n\left(\frac{x}{l}\right)\right),\ n = 1,2,3,\ldots \tag{37}$$

which leads to the following general solution

$$v(x,t;\alpha) = \sum_{n=1}^{\infty} d_n \sin\left(w_n\left(\frac{x}{l}\right)\right) exp\left(-\frac{\gamma^2\lambda_n^2+K_1(\alpha)}{K_0(\alpha)}t\right). \tag{38}$$

Note that it satisfies boundary condition and fractional differential equation.

The coefficients of general solution are established by taking the following initial condition into account:

$$v(x,0) = f(x) + \frac{x}{l}(u_0 - u_1) - u_0 = \sum_{n=1}^{\infty} d_n \sin\left(w_n\left(\frac{x}{l}\right)\right). \tag{39}$$

The coefficients d_n for $n = 0,1,2,3,\ldots$ determined by the help of inner product defined on $L^2[0,l]$:

$$d_n = \frac{2}{l}\left[\int_0^l \sin\left(\frac{n\pi x}{l}\right) f(x)dx + (u_0 - u_1)\int_0^l \sin\left(\frac{n\pi x}{l}\right)\frac{x}{l}dx - u_0\int_0^l \sin\left(\frac{n\pi x}{l}\right)dx\right]. \tag{40}$$

Substituting (40) in (38) leads to the solution of the problem (12)-(14). By making use of (11) and this solution we obtain the general solution of the problem (8)-(10).

$$u(x,t) = u_0 + \frac{x}{l}(u_1 - u_0) + \sum_{n=1}^{\infty} d_n \sin\left(w_n\left(\frac{x}{l}\right)\right) exp\left(-\frac{\gamma^2\lambda_n^2+K_1(\alpha)}{K_0(\alpha)}t\right). \tag{41}$$

If γ^2 is replaced by the fractional diffusion coefficient $c^2\tau_\alpha^{1-\alpha}$ where c^2 is ordinary diffusion coefficient and τ_α is a time constant the solution takes the following form:

$$u(x,t;\alpha) = u_0 + \frac{x}{l}(u_1 - u_0) + \sum_{n=1}^{\infty} d_n \sin\left(w_n\left(\frac{x}{l}\right)\right) exp\left(-\frac{c^2\tau_\alpha^{1-\alpha}\lambda_n^2+K_1(\alpha)}{K_0(\alpha)}t\right). \tag{42}$$

3. ILLUSTRATIVE EXAMPLE

In this section, we first consider the following non-homogenous initial boundary value problem:

$$\begin{aligned} &u_t(x,t) = u_{xx}(x,t),\\ &u(0,t) = 1\ ,\ u(2,t) = 1,\\ &u(x,0) = -\sin(\pi x) + 1 \end{aligned} \tag{43}$$

which has the solution in the following form:

$$u(x,t) = -\sin(\pi x)\, e^{-\pi^2 t} + 1 \tag{44}$$

where $0 \le x \le 2$, $0 \le t \le T$.

Example 1. Now let the following problem called fractional heat-like problem be taken into consideration:

JSR A
Journal of Scientific Reports

$$P_t^{\alpha}(x,t)=u_{xx}(x,t), \quad (45)$$
$$u(0,t)=1,\ u(2,t)=1, \quad (46)$$
$$u(x,0)=-\sin(\pi x)+1 \quad (47)$$

where $0<\alpha<1,\ 0\le x\le 2, 0\le t\le T$.

To make the boundary condition (46) homogenous, we apply the transformation

$$v(x,t)=u(x,t)-1 \quad (48)$$

to the above problem which leads to the following fractional heat-like problem

$$P_t^{\alpha}(x,t)=v_{xx}(x,t), \quad (49)$$
$$v(0,t)=0\ ,\ v(2,t)=0, \quad (50)$$
$$v(x,0)=-\sin(\pi x) \quad (51)$$

where $0<\alpha<1,\ 0\le x\le 2, 0\le t\le T$. It is clear from Eq. (38) that the solution of above problem can be obtained in the following form:

$$v(x,t;\alpha)=\sum_{n=1}^{\infty} d_n \sin\left(\frac{n\pi x}{2}\right) exp\left(-\frac{n^2\pi^2+4-4\alpha}{4\alpha}t\right). \quad (52)$$

Plugging $t=0$ in to the general solution (52) and making equal to the initial condition (51) we have

$$-\sin(\pi x)=\sum_{n=1}^{\infty} d_n \sin\left(\frac{n\pi x}{2}\right). \quad (53)$$

The coefficients d_n for $n=0,1,2,3,\ldots$ are determined by the help of the inner product as follows:

$$d_n=\int_0^2 -\sin\left(\frac{n\pi x}{2}\right)\sin(\pi x)\,dx.$$

$d_n=0$ for $n\neq 2$. For $n=2$, d_2 is obtained as follows:

$$\Longrightarrow d_2=-\int_0^2 \sin^2(\pi x)\,dx=-\frac{1}{2}\left(x+\frac{\sin(2\pi x)}{4\pi}\right)\Big|_{x=0}^{x=2}=-1. \quad (54)$$

Substituting (54) in (52) leads to the solution of the problem (49)-(51).

$$v(x,t;\alpha)=-\sin(\pi x)\,exp\left(-\frac{\pi^2+1-\alpha}{\alpha}t\right). \quad (55)$$

By making use of (48) and the solution (55), we obtain the general solution of the problem (45)-(47) as follows:

$$u(x,t;\alpha)=-\sin(\pi x)\exp\left(-\frac{\pi^2+1-\alpha}{\alpha}t\right)+1. \quad (56)$$

It is important to note that plugging $\alpha=1$ in to the solution (56) gives the solution (44) which confirm the accuracy of the method we apply.

JSR A
Journal of Scientific Reports

Example 2. Now let the following problem called fractional heat-like problem be taken into consideration:

$$P t^{\alpha}(x,t)=u_{xx}(x,t), \quad (57)$$
$$u(0,t)=1, u(2,t)=1, \quad (58)$$
$$u(x,0)=-\sin(\pi x)+1 \quad (59)$$

where $0<\alpha<1,\ 0\le x\le 2, 0\le t\le T$. To make the boundary condition (58) homogenous, we apply the transformation

$$v(x,t)=u(x,t)-1 \quad (60)$$

to the above problem which leads to the following fractional heat-like problem

$$2P t^{\alpha}(x,t)=v_{xx}(x,t), \quad (61)$$
$$v(0,t)=0\ , v(2,t)=0, \quad (62)$$
$$v(x,0)=-\sin(\pi x) \quad (63)$$

where $0<\alpha<1,\ 0\le x\le 2, 0\le t\le T$. It is clear from Eq. (38) that the solution of above problem can be obtained in the following form:

$$v(x,t;\alpha)=\sum_{n=1}^{\infty} d_n \sin\left(\frac{n\pi x}{2}\right) exp\left(-\frac{n^2\pi^2+4-4\alpha^2}{4\alpha^2}t\right). \quad (64)$$

As in Example 1, after similar computations the solution can be constructed as follows:

$$u(x,t;\alpha)=-\sin(\pi x)\exp\left(-\frac{\pi^2+1-\alpha^2}{\alpha^2}t\right)+1. \quad (65)$$

It is important to note that plugging $\alpha=1$ in to the solution (65) gives the solution (44) which confirm the accuracy of the method we apply. The graphics of solutions, obtained by MATLAB 2016b, for Ex.1, Ex. 2 and Problem (43) in 2D and 3D are given in Fig.1 and Fig.2 respectively.

JSR A
Journal of Scientific Reports

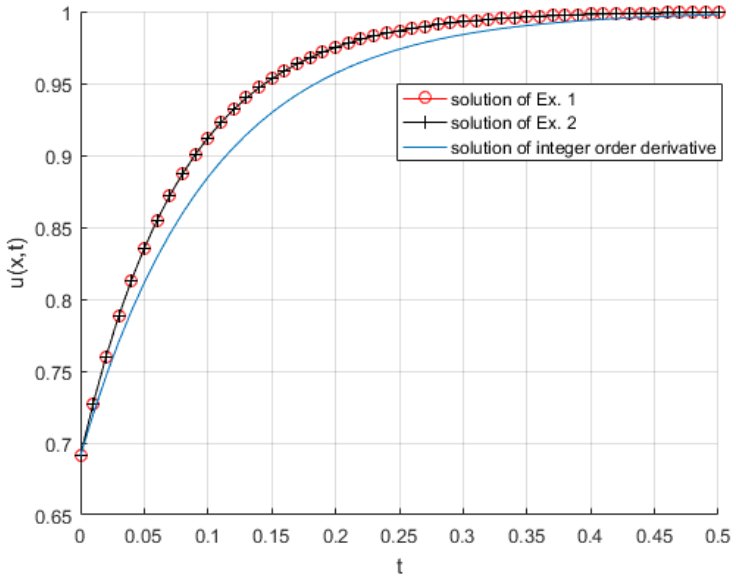

Figure 1. The graphics of solutions for Ex. 1 and Ex. 2. in 2D at x=0.1 for $\alpha = 0.8$.

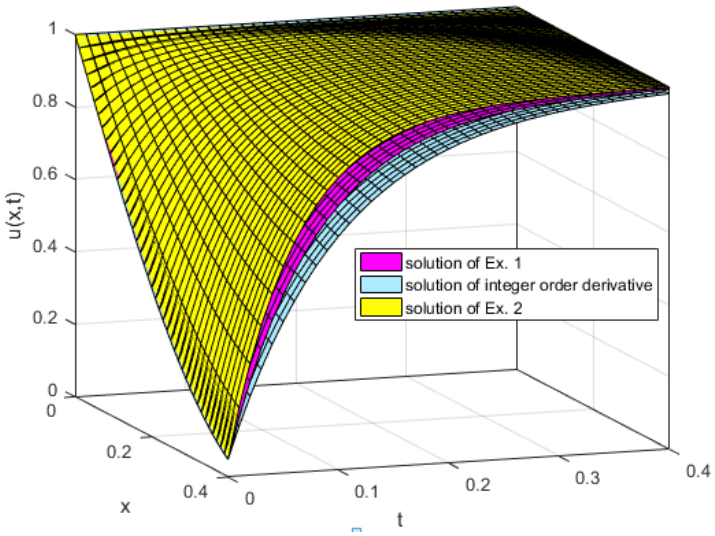

Figure 2. The graphics of solutions for Ex. 1 and Ex. 2 in 3D for $\alpha = 0.8$.

4. CONCLUSION

In this study, the analytic solution of time fractional diffusion problem including local fractional derivatives in one dimension is constructed analytically in Fourier series form. Taking the separation of variables into account, the solution is formed in the form of a Fourier series with respect to the

eigenfunctions of a corresponding Sturm-Liouville eigenvalue problem including fractional derivative in a proportional sense.

Based on the analytic solution, we reach the conclusion that diffusion processes decays exponential with time until initial condition is reached. As α tends to 0, the rate of decaying increases. This implies that in the mathematical model for diffusion of the matter which has small diffusion rate the value of α must be close to 0. This model can account for various diffusion processes of various methods.

REFERENCES

[1] Hao, Y.J., Srivastava, H. M., Jafari, H., Yang, X.J., (2013), Helmholtz and di usion equations associated with local fractional derivative operators involving the Cantorian and Cantor-type cylindrical coordinates, Advances in Mathematical Physics, 2013, Article ID 754248, 1-5.

[2] Bisquert, J., (2005), Interpretation of a fractional diffusion equation with non-conserved probability density in terms of experimental systems with trapping or recombination, Physical Review E, 72(1), 011109.

[3] Sene, N., (2019), Solutions of Fractional Diffusion Equations and Cattaneo-Hristov Diffusion Model, International Journal of Analysis and Applications, 17(2), 191-207.

[4] Aguilar, J.F.G. and Hernández, M.M., (2014), Space-Time Fractional Diffusion-Advection Equation with Caputo Derivative, Abstract and Applied Analysis, 2014, Article ID 283019.

[5] Naber, M., (2004), Distributed order fractional sub-diffusion, Fractals, 12(1), 23-32.

[6] Nadal, E., Abisset-Chavanne, E., Cueto, E. and Chinesta, F., (2018), On the physical interpretation of fractional diffusion, Comptes Rendus Mecanique, 346, 581-589.

[7] Zhang, W. and Yi, M., (2016), Sturm-Liouville problem and numerical method of fractional diffusion equation on fractals, Advances in Difference Equations, 2016:217.

[8] Baleanu, D., Fernandez, A. and Akgül, A., (2020), On a Fractional Operator Combining Proportional and Classical Differintegrals, Mathematics, 8(360).

Kütahya Dumlupınar University
Institute of Graduate Studies

Journal of Scientific
Reports-A
E-ISSN: 2687-6167
Number 45, December 2020

RESEARCH ARTICLE

GENDER ESTIMATION WITH CONVOLUTIONAL NEURAL NETWORKS USING FINGERTIP IMAGES

Kerem SIRMA[1], Pakize ERDOĞMUŞ[2]

[1]Düzce University, Computer Engineering, Düzce, kerem.sirma@hotmail.com, ORCID:0000-0003-2902-1617
[2]Düzce University, Computer Engineering,, Düzce, pakizeerdogmus@duzce.edu.tr, ORCID:0000-0003-2172-5767

Received Date: 29.05.2020 *Accepted Date: 10.08.2020*

ABSTRACT

Bringing several innovations to our daily life, the importance of artificial intelligence technology has been increasing day by day and has created new fields for researchers. Gender classification is also an important research topic in the field of artificial intelligence. Studies on gender prediction from face, body, and even fingerprint images have been done. Also, today, biometric recognition systems have reached levels that can determine people's fingerprints, face, iris, palm prints, signature, DNA, and retina. In this study, various models were trained and tested on gender classification from fingertip images. In the, a ready dataset was not used and finger images were collected from more than 200 people. Rotation, cutting, and background reduction are applied to the collected images and made ready for the training. 4 different network models were set in the fieldwork. Data augmentation and transfer learning were used in these models. Working in a limited area, the model we created has achieved high-performance results, for all that the quality and angles of each image are different. The model proposed in this study has a performance rate of 86.39%.

Keywords: *Gender Prediction, Deep Learning. Fingertip*

1. INTRODUCTION

Increasing the scope areas of deep learning applications, which are the sub-branch of machine learning, are a natural result of the rise in big data formation. Speech recognition, object recognition, emotion analysis, and image classification are some of the areas of deep learning. Researchers are trying to create human-like computer models by developing artificial learning techniques, which are a vast area of research [1, 2].

In this study, the answer to the question of whether sex discrimination can be made from fingertip images, which has not been done before and is a difficult task, was sought. CNN structures provide very good results in estimating gender, especially from facial images. Methods were developed and tests were carried out on how successful they could be in solving this problem.

One of the main challenges here is that many obstacles and noises can lead to wrong conclusions. Shooting finger images in the right light conditions and with a quality camera will ensure accurate extraction of features and increased predictive accuracy at the same rate. However, since more than

200 people used different finger images, and all were taken from mobile phones with different angles and different quality cameras, the study will result in high-performance reductions. To avoid these problems, the loss was minimized by applying rotation, cropping, and background reduction. Apart from these processes, no filtering, blurring processes have been applied to produce results that are close to natural life and reality.

While collecting the data, the participants were explained the purpose of the study and the personal data would be protected. It is clearly stated that the data will be uploaded to environments such as Kaggle for the benefit of the researchers and the identity information will not be shared for the protection of personal data. The data was sent to the author only by mail and in a compressed form. It was not uploaded to any server except the Kaggle environment and no information was shared with third parties. For gender classification, 2110 finger images were studied.

Apart from the basic model created in the study, methods such as transfer learning, data enhancement, and combined forms of these methods are used. The results are compared with each other. To achieve the best results, hyperparameters such as learning rate, optimization method, mini-batch size, and maximum epoch number were changed and tests were repeated.

In the literature, generally, Adience data set containing facial images have been used for gender classification studies [3, 4]. Due to its ease of use, high predictive power, and graphics card-supported parallel operation, Convolutional Neural Networks (CNN) are among the methods that remain up-to-date in pattern classification [5, 6, 7]. Besides, CNN architecture was first used in a large training set of ImageNet. One of the most common problems that researchers who prefer CNN for Problem-solving are the preparation of a problem-specific data set. With the high number of layers of CNN, a training set containing adequate patterns for the problem needs to be established by the researchers. The ImageNet dataset, for example, is the result of one million images being tagged with one of 1000 classes. A CNN trained using this set, prepared as a result of large studies, can make high-accuracy predictions.

In the absence of sufficient data, the problem arises how to use CNN with high-performance rates. “Transfer learning” or “knowledge transfer” approach is used to solve this problem. Information transfer is the realization of information transfer from a trained ANN (Artificial Neural Network) network with ImageNet or a data set that has proven educational success. Transfer learning with AlexNet was attempted in this study. This method has become an important research topic with the development of deep learning methods. Transfer learning is similar to the human learning model, as in classical ANN models. People also use the solution of problems they have experienced before to solve a problem they have not encountered before while learning [8, 9].

2. LITERATURE REVIEW

There is no study in the literature that uses artificial intelligence and fingertip images together. For this reason, there is no data set as in the study. However, there are studies that stand out with the similarity of purpose and method.

Similar to the study, Illouz et al. [10] designed a CNN that can predict gender from handwriting. English and Hebrew handwriting was used by 405 participants and a total of 810. They achieved a minimum accuracy of 71.05% and a maximum accuracy of 78.95%. Baek et al. [11] aimed to make a

gender prediction by using the whole-body image, unlike many facial images and gender estimation studies. Since factors such as shade, clothing, and accessories will affect performance, they use infrared cameras and focus only on body shape. Liu et al. [12] intended to estimate gender from human gait and used SVM instead of SoftMax. They increased the accuracy rate of 87.10% with VGG16 to 89.62% using SVM. Akbulut et al. [13] have performed gender recognition from facial images with deep learning. As a method of deep learning, Local Receptive Fields – Extreme Learning Machine (lRF-ELM) and Convolutional Neural Networks (CNN) were used. The experiments were carried out in a facial dataset created for age and gender recognition. Viedma et al. [14] are a CNN design that estimates gender from iris images by comparing them to VggNet and ResNet. Using the GFI-UND data set, they achieved an average success rate of 75% with ResNet and VggNet. However, they have achieved an 85% success rate by using fewer layers with their own designed network. Morera et al. [15] designed a CNN using the IAM data set with English handwriting and the KHATT data set with Arabic handwriting and achieved an average success rate of 68.90% in the gender prediction success rate. Afifi [16] has developed a model that makes gender estimation with 11.000 hand images. It reached this number by combining many data sets. With 30 epoch and 0.0001 learning rate, it reached 87% in the palm and 91% in the dorsal view of the hand. Although the total number of images is not unique, a hand has many images from various angles. In the data set prepared for this study, each finger is unique. Barbosa et al. [17] designed a temporary biometric system using nail images. The deep learning algorithm was not used, and it was seen in the tests performed that recognition was successful after 1 week and failed after 2 months depending on the shape of the nail. According to the number of data used in the model created in the study was studied with very little data. This study is a precursor to a new biometric recognition system. Ceyhan et al. [18] propose a new method based on ANN model to estimate genders from fingerprints with their study. Modeling operations were obtained by obtaining fingerprints, analyzing the obtained fingerprint images in different dimensions, calculating the peaks, and finding the fingerprints average peak values of individuals. These attributes were then combined into the model. In the study, preparation, adjustment of the model structure, and finally testing of the model were discussed. The results of the proposed model have a 72% success rate.

3. MATERIAL AND METHOD

In the study, many CNN models were designed and the results were compared. The created models are discussed under this title. Layer numbers and hyperparameter values of each model were constantly changed to find the optimum value. Several preprocessing methods were applied to the data.

While the value of the trained model was found to be able to make the most accurate estimation, the number of layers was increased from 3 to 9, and then the hyperparameter adjustments were made. Hyperparameter experiments were made with the model that has 7 convolution layers. First, the mini-batch size was increased from 16 to 64 and the tests were repeated for each value. After the best result was obtained with a value of 32, the learning rate was tried for 0.01,0.001 and 0.0001.

Optimization algorithms were changed after finding the best result layer number, Learning rate, and mini stack size. Training and testing were repeated after each change. Sgdm (Stochastic Gradient Descent with Momentum), Adam (Derived from Adaptive Moment Estimation), and RmsProp (Root Mean Square Propagation) methods have been tried. When Stochastic Gradient Descent with Momentum is used to train a neural network, ‘solverName’ should be specified as 'sgdm'. An

independent variable called 'InitialLearnRate' is used to determine the initial value of the α learning rate [19]. Sgdm algorithm has given the fastest and highest accuracy rate in terms of education-test. The tests made with the sgdm algorithm tried to find the number of epochs that achieved the best prediction success. For this, 6,10,12,15 and 20 epoch values were tried. In all tests, it is aimed to minimize the loss and to have the highest estimation success. Also, the pre-processes applied to the data before training given in Figure 1.

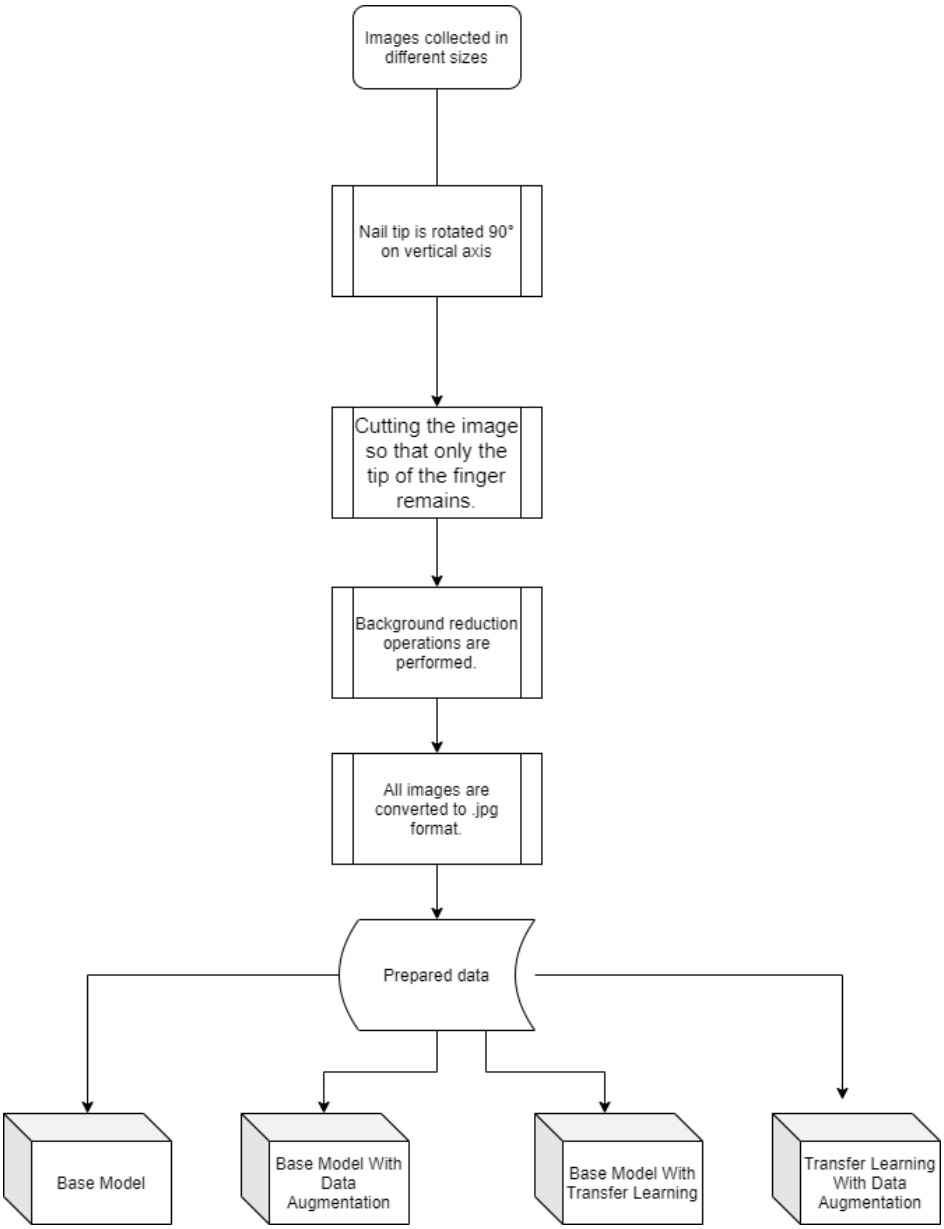

Figure 1. General flow diagram.

3.1. Base Model

The model prepared for the study consists of 7 convolution layers and 2 fully connected layers. Among these layers, layers such as maximum pooling layer, ReLu, and batch normalization are used. Figure 2 shows the proposed CNN model.

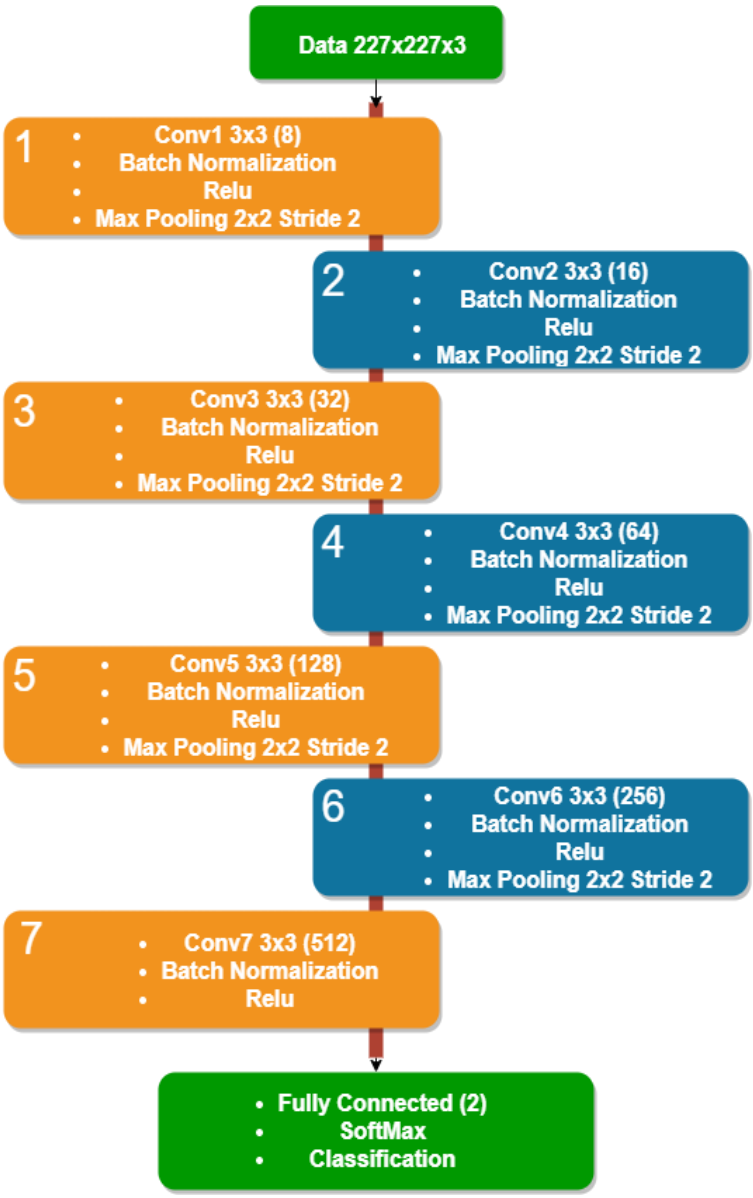

Figure 2. Proposed CNN model for gender prediction.

The sequence of processing and the properties of the layers are as follows:

- Random pictures of 227x227x3 size were cut from the pictures of different sizes at the input.
- In the first convoluted Layer, 8 3x3 filters were applied to the images which were converted to 227x227x3 size. Images that then passed through the batch normalization and ReLu layer were processed at a maximum pooling layer of 2x2 size with 2 strides.
- In the second convolution layer, 16 filters of 3x3 size were applied to the data, and ReLu, 2 stride maximum pooling, and batch normalization layers of 2x2 size were applied.
- 32 filters of 3x3 size were applied to the data from the third convolution layer and ReLu, 2 strides, 2x2 maximum pooling, and batch normalization layers were applied.
- 64 filters of 3x3 size were applied to the data reaching the fourth convolution layer and ReLu, 2 strides 2x2 maximum pooling, and batch normalization layers were applied.
- In the fifth convolution layer, 128 filters of 3x3 size were applied and ReLu, 2 strides 2x2 maximum pooling, and batch normalization layers were applied.
- In the sixth convolution layer, 256 filters of 3x3 size were applied and ReLu, 2 strides 2x2 maximum pooling, and batch normalization layers were applied.
- The seventh convolution layer applied 512 filters in 3x3 size and ReLu, 2 strides 2x2 size maximum pooling, and batch normalization layers were applied. At the end of this layer, 4608 parameters enter the fully connected layer.
- Data from the fully connected layer has been prepared for the training process by connecting SoftMax to the output of the fully connected layer with 2 connections and classification layers to its output.

Of the parameters used in the training, the important ones for this study were that the learning rate is 0,001, mini-batch size is 32 and the maximum epoch is 15. 70% of the data was used for training and 30% for testing. The data allocated for the test is different from the data used in training.

3.2. Model with Data Augmentation

It is the model created with the same parameters by applying data augmentation operations to the Basic Model. For data enhancement, there are techniques such as rotating the image at the desired angle, rotating it on the horizontal or vertical axis, changing color, or adding noise [20]. When generating new images, the random rotation range is specified as [20, -20] degrees. The angle of rotation is randomly selected within the specified range. Also, the horizontal and vertical translation interval applied to the specified input image is specified as [5, -5]. Translation distance is measured in pixels. Random rotation operations are performed on the horizontal and vertical axis at the specified intervals. The reproduced sample images are shown in figure 3.

JSR A
Journal of Scientific Reports

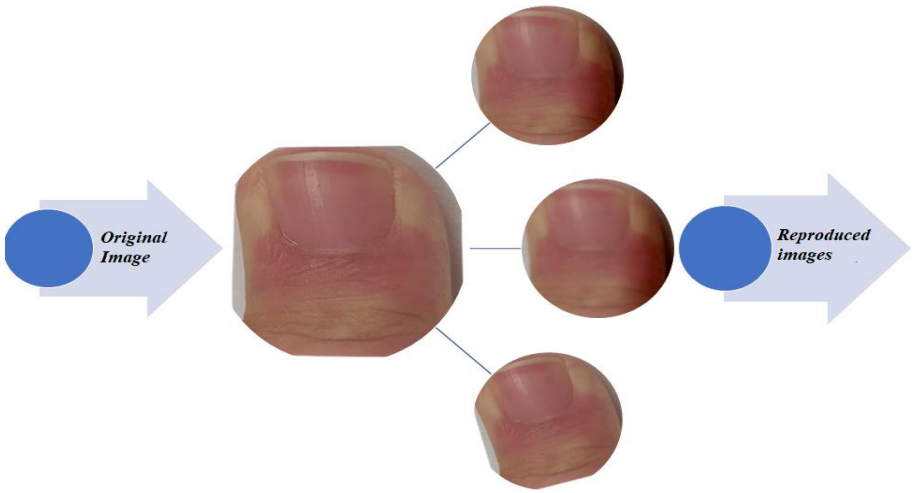

Figure 3. Original and Reproduced Images.

3.3. Model with Transfer Learning

In this model, a transfer learning approach, defined as the transfer of previously trained Evolutionary Neural Network models, was applied to classify genders. It was based on the AlexNet model. The network was retrained with the data set created by changing the 3 layers at the end of this previously trained network. AlexNet has 5 convolution and 3 fully connected layers. In the study, these layers were used as the transfer feature extraction layer. The structure of the new model is given in Figure 4.

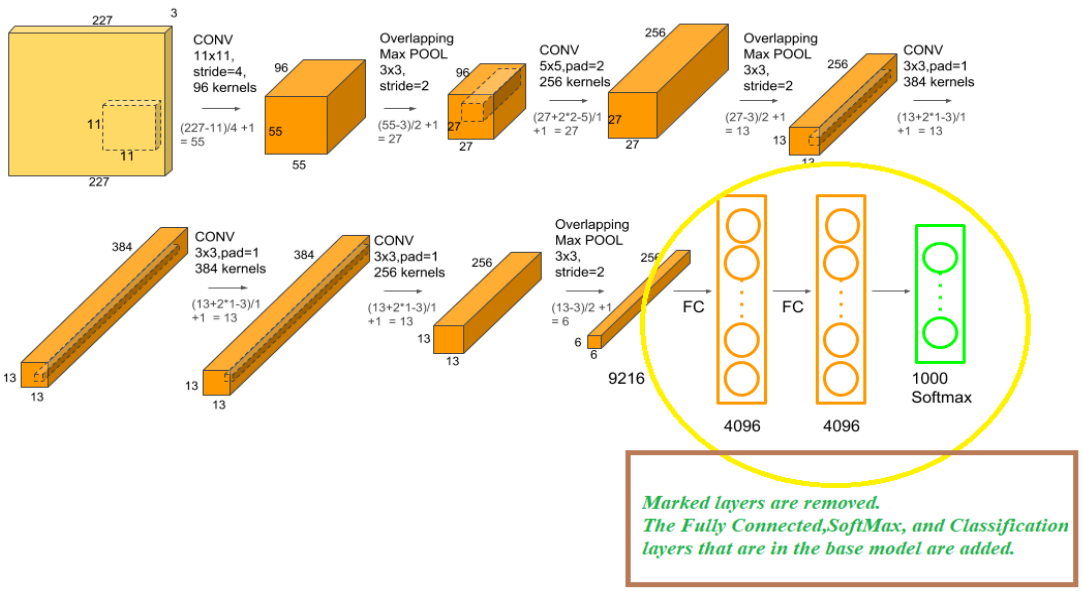

Figure 4. Transfer learning application with AlexNet [21].

JSR A
Journal of Scientific Reports

3.4. Transfer Learning and Data Augmentation Applied Model

The data learning process applied to the base model and the transfer learning model with AlexNet were combined and a new model was created. Instead of the last 3 layers of AlexNet, the parameters defined in the 'Model with Data Augmentation' section have been added by adding the fully connected, SoftMax, and classifier layers of the base model.

4. EXPERIMENTAL EVALUATION

When designing machine learning models based on data such as CNN, the algorithms or techniques used in the model require some parameters that the designer must decide on. The researcher decides what parameters will be such as mini-batch size, epochs, learning rate, and shuffle. In general, the choice of preferences for these parameters initially is not clear and precise; problem, dataset, etc. It varies depending on such factors. Therefore, what to choose is left to the person who designed the network. Parameters that vary depending on the problem, dataset, and similar factors are expressed as hyperparameters [22]. Most models take a long time to train; some models last for days. For this reason, the training process is tried to be shortened as much as possible by changing the hyperparameters and finding optimum values. Hyperparameters that are constantly changed in this study are given in Table 1.

Table 1. Changed parameters and values.

Hyperparameter	**Range**
Learning Rate	[0.001, 0.0001]
Mini-Batch Size	[10 32 64]
Epoch	[6 10 12 15 20]

Apart from the parameters, layer numbers and filter numbers have been changed to achieve the best success rate. The best results yielded a model consisting of 7 convolution layers and 2 fully connected layers. Among these layers, layers such as maximum pooling, ReLu, and batch normalization are used. The training and performance results of the proposed model are given in Figure 5.

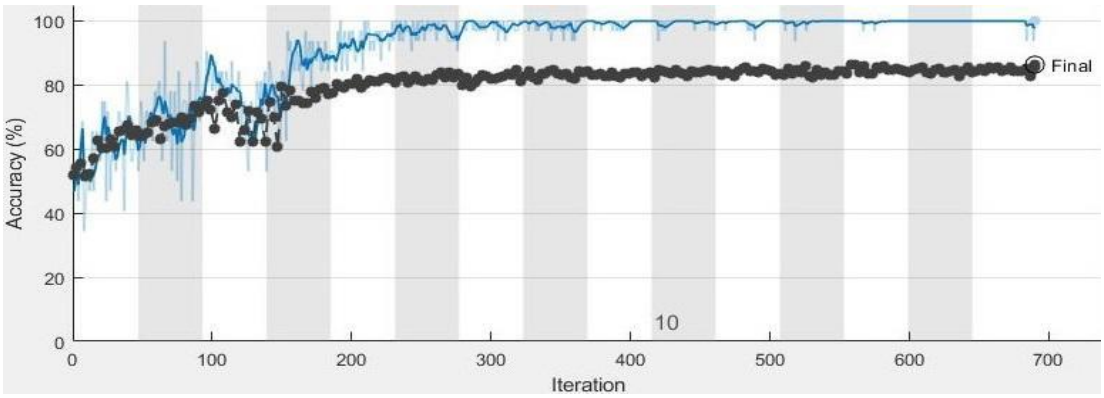

Figure 5. The success rate of the proposed model.

Training has been completed in 15 epochs and 690 iterations. 46 iterations have occurred in each epoch. Training and tests have been completed in 2 hours and 16 minutes.

To understand whether the results are better than real people's estimates, a questionnaire with 100 different fingertip images was applied to 100 people and they were asked to guess their gender. Participants were able to reach an average of 55.34% accuracy rate. The proposed model was able to predict better with an accuracy rate of 86.34%. The sample survey image is given in Figure 6.

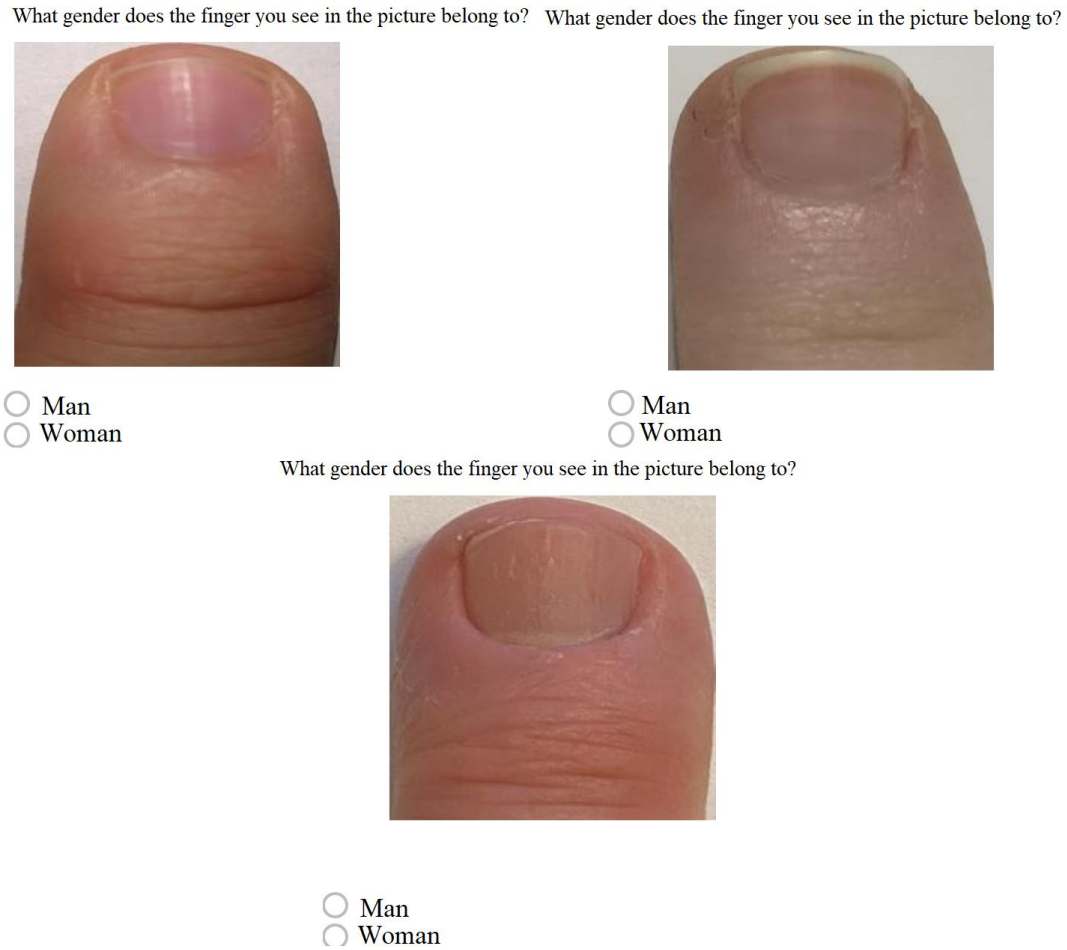

Figure 6. Question samples from the applied questionnaire.

In Figure 6, the top left image belongs to a man and the other 2 images belong to 2 different women. While 80% of the participants were able to answer the male finger in the picture correctly, no one was able to answer the other 2 questions correctly. Values such as average values of the survey, the number of participants, and best estimate results are graphically shared in Figure 7.

JSR A
Journal of Scientific Reports

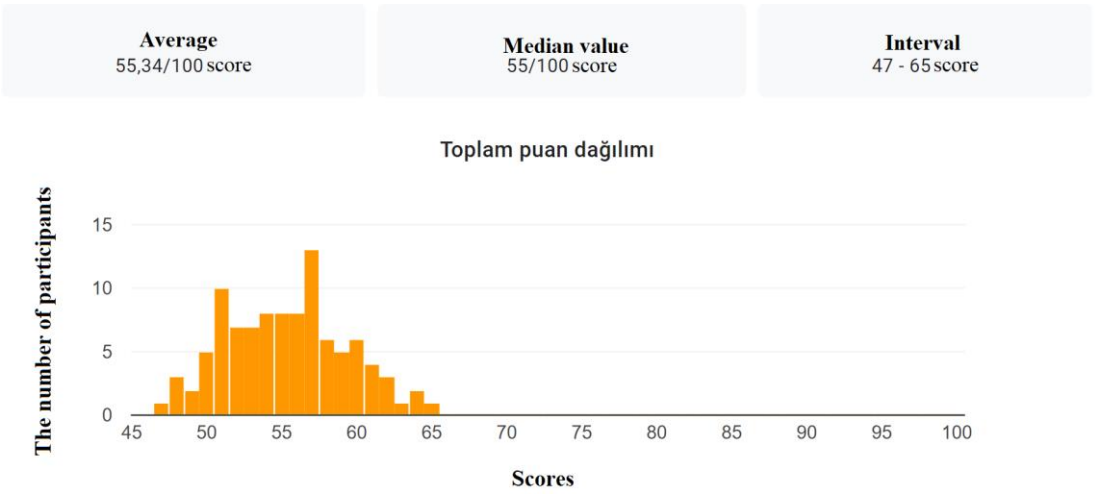

Figure 7. The predicted success of participants.

As the chart shows, 100 participants received an average score of 55.34. As there were no correct answers to all of the questions, only 1 person was able to gather the closest prediction success to the CNN model by answering 65 of the questions correctly. As it is known that the proposed model achieved 86.39% estimated success, it was proved by this survey that it produced much better results than a human being.

Because the collected images were constantly changing, tests were conducted with different data sizes. As a result, the effect of data size on the success rate has also been analyzed. The relation of the number of the epoch, learning rate, mini-batch size, convolution layer numbers with data size was examined with 4 different models. B.M (Base Model), M.D.A (Model with Data Augmentation), M.T.L (Model with Transfer Learning), T.L.D.A.M (Transfer Learning and Data Augmentation Applied Model). Different tests and success rates were shared in Table 2.

Table 2. Effects of Data, Layer and Hyperparameter values on the results.

Model	**Values**							
	1115 Female and 995 male fingertip images			**558 Female and 550 male fingertip images**				
Number of Epoch	15	10	10	6	12	12	12	20
Learning Rate	0.0001	0.001	0.0001	0.0001	0.0001	0.0001	0.0001	0.0001
Mini-Batch Size	32	32	64	10	10	10	10	10
Number of Convolution Layer	7	7	7	3	3	5	7	3
B.M	86,39	76,58	82,59	73,19	76,81	86,75	81,93	78,92

JSR A
Journal of Scientific Reports

Success Rate.								
M.D.A Success Rate.	84,81	75,16	70,32	72,29	79,82	80,72	74,40	72,89
M.T.L Success Rate.	81,65	77,85	75,79	88,25	87,35	75,90	88,55	87,95
T.L.D.A.M Success Rate.	81,26	72,15	65,43	81,63	91,57	86,75	86,45	86,75

The model, which was suggested with full data, obtained the best results with 15 epochs, 0.000.1 learning rate, and 32 mini-batch sizes. In this model, 7 convolution layers have been used and the number of filters has increased gradually to 16,32,64,128,256 and 512, and gradually deepened. As a result of the tests carried out with these values, 86.32% success rate was obtained. The model, which has been applied data augmentation with fewer data sets, has achieved a maximum success of 80.72% with 12 epochs, 0.0001 learning rate, and 10 mini-batch sizes. In this model, 5 convolution layers are used and the number of filters is gradually increased. The model, which was subjected to the Transfer Learning process and used a small amount of data, achieved 88.55% success.7 The convolution layer was used and the number of filters in the proposed model was used. Both the transfer learning process and the data increment process gave the best result with fewer data. In this model, 3 convolution layers were used and 91.57% prediction accuracy was achieved. It can be seen that in studies using less data, the models that increase data yielded better results but did not show the same performance when the original data size was increased. In tests performed with the maximum number of data, all the fitting processes were performed and results with close or better results were found with the tests performed with a small number of data.

In the learning process steps, to analyze whether the color data is important and if it is important, the images were converted to black and white format, and the convolution layer numbers were changed and tests were performed with B.M and M.D.A. In the tests, 995 male and 1115 female fingertip images were used. Mini-Batch size was 32, the learning rate was 0.001, and the epoch was 12. The result of the tests was shared in Table 3.

Table 3. Effect of Black and White Color Conversion on Results.

Model	**Success Rate (%)**		
	3 Conv. Layer	**5 Conv. Layer**	**7 Conv. Layer**
B.M	67,88	70,09	77.85
M.D.A	64,24	58,86	57,65

It was determined that the reason that success rates were lower than the tests performed with color images was due to factors such as henna, nail polish on women's nails, and the difference of colors in the nail flesh.

5. CONCLUSION

Today, the increasingly popular areas of biometric recognition and deep learning have provided researchers with different areas of study. The study also analyzed the performance of CNN models in estimating gender from fingertip images, which yielded very good performance results in estimating gender from facial images. To increase the success rate, layer numbers, filter numbers, and hyper-parameter values have been modified and tested. Four different models were produced and each model was able to detect better than real person estimates.

There has been no previous study of fingertip images in the literature. But some studies show similarities in purpose and technique. For example, Antipov et al. [23] after designing a CNN, they reduced the number of filters in the network's convolution layers and the size of the fully connected layer. These layer and filter reductions achieved both speed and memory gain. Accordingly, there was a negligible decrease in the rate of performance. However, in this study, because the number of data is low and the image sizes are low, the number of filters in each layer was gradually increased and the best estimate success rate was tried to be found. Juefei-Xu et al. [24] instead of using facial images entirely, they blur some areas. Blurring outside the periocular region has made them better use of high-frequency details in the periocular region. In the study, the participants were asked only for fingertip images because they had already been studied in a narrow area and no blurring was applied to a specific part of the fingertip used.

In the literature, some studies use ready-made datasets such as Adience, IMDB, WIKI [25, 26], as well as studies that combine many databases and obtain a new dataset [27, 28]. In this study, the data were collected from the participants one by one, and a new data set was created. The data set has been uploaded to Kaggle for researchers who want to research on this topic [29].

The basic model proposed in the study consists of 7 convolution layers and 2 fully connected layers. Among these layers, 86.39% success was achieved by using layers such as maximum pooling, ReLu, and batch normalization. A transfer learning model was created by removing the last 3 layers of AlexNet architecture and adding the fully connected layer, softMax, and classifier layers in the basic model instead of these layers. With this model, a success rate of 81.65 was achieved. When data enhancement is applied to Transfer Learning model, the success rate decreased and became 81.65%. This data was 84.81% when data increase was applied to the basic model.

According to the results obtained, it has been proven that the proposed model can be used for the gender recognition problem from the fingertip images. Also, even though the original training and test data are limited, it has been demonstrated that CNN structures are a very effective method for solving this problem, with all models created above 80% success. In future researches, it is recommended to increase the success rate with different deep network architectures by expanding the data set created in this study. The method proposed in this study can be used in new biometric recognition systems or as a filter for preprocessing in the existing biometric recognition systems.

REFERENCES

[1] Apaydın, E., (2004), Introduction to Machine Learning (Adaptive Computation and Machine Learning). MIT Press

[2] Bishop, C. M., (2006) Pattern Recognition and Machine Learning. Springer Science + Business Media.

[3] Levi G. and Hassncer, T., (2015), "Age and gender classification using convolutional neural networks," IEEE Comput. Soc. Conf. Comput. Vis. Pattern Recognit. Work., vol. 2015-Octob, pp. 34–42, doi: 10.1109/CVPRW.2015.7301352.

[4] Eidinger, E., Enbar, R., and Hassner, T.,(2014), "Age and gender estimation of unfiltered faces," IEEE Trans. Inf. Forensics Secur., vol. 9, no. 12, pp. 2170–2179, , doi: 10.1109/TIFS.2014.2359646.

[5] Cengil, E., Çinar, A., and Güler, Z., (2017), "A GPU-based convolutional neural network approach for image classification," in International Artificial Intelligence and Data Processing Symposium (IDAP).

[6] Abdulkadir, S., Akbulut, Y., Guo, Y., and Bajaj, V., (2017) "Classification of amyotrophic lateral sclerosis disease based on convolutional neural network and reinforcement sample learning algorithm," Heal. Inf Sci Syst.

[7] Girshick, R., Donahue, J., Darrell, T., and Malik, J., (2014), "Rich feature hierarchies for accurate object detection and semantic segmentation," Proc. IEEE Comput. Soc. Conf. Comput. Vis. Pattern Recognit., pp. 580–587, doi: 10.1109/CVPR.2014.81.

[8] Jialin Pan, S., and Yang, Q., (2010) "A Survey on Transfer Learning," IEEE Trans. Knowl. Data Eng., vol. 22, pp. 1345–1359.

[9] Koçer, B., (2012) "Transfer Öğrenmede Yeni Yaklaşımlar," Selçuk University.

[10] Illouz, E., David, E. and Netanyahu, N.S., (2019), "Handwriting-Based Gender Classification Using End-to-End Deep Neural Networks," vol. 11141, no. October, pp. 613–621, doi: 10.1007/978-3-030-01424-7_60.

[11] Baek, N. R., Cho, S. W., Koo, J. H., Truong, N. Q. and Park, K. R.,(2019), "Multimodal Camera-Based Gender Recognition Using Human-Body Image With Two-Step Reconstruction Network," IEEE Access, vol. 7, pp. 104025–104044, doi: 10.1109/access.2019.2932146.

[12] Liu, T., Ye, X. and Sun, B., (2019), "Combining Convolutional Neural Network and Support Vector Machine for Gait-based Gender Recognition," Proc. 2018 Chinese Autom. Congr. CAC 2018, pp. 3477–3481, doi: 10.1109/CAC.2018.8623118.

[13] Akbulut, Y., Şengür, A. and Ekici, S., (2017), "Gender recognition from face images with deep learning," Int. Artif. Intell. Data Process. Symp., pp. 1–4.

[14] Viedma, I. and Tapia, J., (2018), "Deep Gender Classification and Visualization of Near-Infra-Red Periocular-Iris images," IEEE 3rd Int. Conf. Image Process. Appl. Syst. IPAS, pp. 73–78, 2018, doi: 10.1109/IPAS.2018.8708857.

[15] Van De Wolfshaar, J., Karaaba, M. F. and Wiering, M. A., (2015), "Deep convolutional neural networks and support vector machines for gender recognition," Proc. - 2015 IEEE Symp. Ser. Comput. Intell. SSCI 2015, pp. 188–195, doi: 10.1109/SSCI.2015.37.

[16] Afifi, M., (2019), "11K Hands: Gender recognition and biometric identification using a large dataset of hand images," Multimed. Tools Appl., vol. 78, no. 15, pp. 20835–20854, doi: 10.1007/s11042-019-7424-8.

[17] Barbosa, I.B., Theoharis, T., Schellewald, C. and Athwal, C., (2013)., "Transient biometrics using fingernails," IEEE 6th Int. Conf. Biometrics Theory, Appl. Syst. BTAS 2013, doi: 10.1109/BTAS.2013.6712730.

[18] Ceyhan E.B. and Sağıroğlu, Ş., (2019), "A New Intelligent System for Predicting Gender from Fingerprint," Düzce Univ. J. Sci. Technol., vol. 4, pp. 25–36, doi: 0.29130/dubited.457914.

[19] Liu, X., Li , J., Pan, J.-S., and Hu, C. (2017). Deep convolutional neural networks-based age and gender classification with facial images. 2017 First International Conference on Electronics Instrumentation & Information Systems (EIIS).Matlab Documentation. (2019). MathWorks.

[20] Er, M. B:, (2019), "Emotıon Analysıs In Turkısh Musıc Wıth Machıne Learnıng," Maltepe University.

[21] Vishwesh, S., (2019), "PyTorch for Beginners: Image Classification using Pre-trained models," https://www.learnopencv.com/pytorch-for-beginners-image-classification-using-pre-trained-models/ (accessed May 26, 2020).

[22] Çarkacı, N.,(2018), "Derin Öğrenme Uygulamalarında En Sık kullanılan Hiper-parametreler," https://medium.com/deep-learning-turkiye/derin-ogrenme-uygulamalarinda-en-sik-kullanilan-hiper-parametreler-ece8e9125c4 (accessed May 26, 2020).

[23] Antipov, G., Berrani, S. A. and Dugelay J.L., (2016), "Minimalistic CNN-based ensemble model for gender prediction from face images," Pattern Recognit. Lett., vol. 70, pp. 59–65, doi: 10.1016/j.patrec.2015.11.011.

[24] Juefei-Xu, F., Verma, E., Goel, P., Cherodian, A. and Savvides, M., (2016) "DeepGender: Occlusion and Low Resolution Robust Facial Gender Classification via Progressively Trained Convolutional Neural Networks with Attention," IEEE Comput. Soc. Conf. Comput. Vis. Pattern Recognit. Work., pp. 136–145, doi: 10.1109/CVPRW.2016.24.

[25] Karakaş, E., (2019), "Derin Sinir Ağlarının Füzyonu ile Yüz İmgelerinden Yaş Grubu ve Cinsiyet Sınıflandırma," Atatürk University.

[26] Kabasakal B. and Sumer, E., (2018), "Gender recognition using innovative pattern recognition techniques," 26th IEEE Signal Process. Commun. Appl. Conf. SIU 2018, pp. 1–4, doi: 10.1109/SIU.2018.8404306.

[27] Nistor, S. C., Marina, A. C., Darabant, a. S. and Borza, D.,(2017), "Automatic gender recognition for 'in the wild' facial images using convolutional neural networks," Proc. - 2017 IEEE 13th Int. Conf. Intell. Comput. Commun. Process. ICCP 2017, pp. 287–291, doi: 10.1109/ICCP.2017.8117018.

[28] Afifi, M., (2019), "11K Hands: Gender recognition and biometric identification using a large dataset of hand images," Multimed. Tools Appl., vol. 78, no. 15, pp. 20835–20854, doi: 10.1007/s11042-019-7424-8.

[29] Sırma, K., (2020), "Fingertip Images," https://www.kaggle.com/keremsirma/fingertip-images/ (accessed Aug 1, 2020).

Kütahya Dumlupınar University
Institute of Graduate Studies

Journal of Scientific
Reports-A
E-ISSN: 2687-6167
Number 45, December 2020

RESEARCH ARTICLE

CHARACTERIZATION AND PROCESS OPTIMIZATION OF ULTRASOUND EXTRACTED POLYSACCHARIDES FROM THE "OPUNTIA FICUS INDICA" CLADODES

Tuncay YILMAZ

Manisa Celal Bayar University, Food Engineering Department, Manisa, tuncay.yilmaz@cbu.edu.tr,
ORCID: 0000-0001-8756-2724

Recieved Date:30.06.2020 *Accepted Date: 23.12.2020*

ABSTRACT

Opuntia Ficus Indica (OFI) cladodes are rich in pectin rich polysaccharides can be used nutraceutical, medical and pharmaceutical purposes as a cheap source of raw material. In this study characterization and Response Surface Methodology (RSM) of ultrasonic assisted extraction (UAE) of water-soluble crude polysaccharides (CPS) of OFI cladodes were studied using Box-Behnken Design (BBD). Effect of power intensity, set temperature and processing time investigated, Optimal conditions for yield maximization is found as 345.5 W, 304.5 K and 28.5 min. respectively with the predicted yield as 18.58% dry base polysaccharide extract and this value was validated by experiments at optimal condition having the value as 18.48±0.35%. General composition of the extracts at the optimal condition was 7.5±2.22% moisture content, 14.4±0.87 ash, 0.18±0.05 protein, 82.12±7.2% total sugar content (SC) in glucose, 72.75±6.8% SC in galacturonic acid in dry basis. Degree of esterification was found 40.57±3.11% proving that extracted polysaccharides was low-methoxy (LM) pectin-based material which can be used a good alternative and cheap source for industrial LM pectin. Additionally, this study depicts the importance of the temperature control and temperature rise of UAE systems since depending on power, time and temperature combination, temperature inside the reactor can be increased 7-11.8%.

Keywords: *Opuntia Ficus Indica, Cladode Polysaccharides, Response Surface Methodology, Ultrasound Assisted Extraction*

1. INTRODUCTION

Opuntia Ficus Indica (OFI) is a South American cactus species that comes from the *Cactacea* (cactus) family. Under the *Platyopuntia* species of the *Opuntia* species, it stands out with its altered and flattened branches called cladode which has thorns (1-2 cm) and glochids (0.15-0.2 cm) on the surface [1] OFI; Mexico, Iran, Tunisia, Eritrea, Ethiopia, Argentina, Peru, Bolivia, Brazil, America, Spain, Italy, Israel, Morocco, is grown in semi-arid countries such as South Africa and Turkey. OFI is known as Chumbera in Spain, Higo De Las Indias in India, Fico D in India in Italy, and Barbarie in France. Due to its high degree of ecological adaptation, this plant can be found in almost all climatic conditions [2].

OFI fruit, seed and cladodes are used in commercial areas as nutraceutical and functional products in many countries such as Mexico, Chile and Spain. The fruit part of OFI is consumed fresh or pre-processed; The seed part is used in the cosmetics industry in Morocco and Tunisia in products such as fruit juice, fruit juice concentrate, coloring food, powder products, soft drinks, jam and marmalade [2]. OFI cladodes are characterized by flat bodies with oval or elongated shape and exhibit photosynthetic properties. It can be used for various products such as high dietary fiber powders, juices and nectars, canned cladode products and brine. Young cladodes are consumed in Mexico and Chile as fresh vegetables or added to foods such as sauces, salads and soups. In addition, it is used to protect fresh fruits [3], encapsulating agent for bioactive components, gallic acid and betalains [4–6] and edible film formation [7, 8]. The main components of cladodes are carbohydrate polymers containing a mixture of pectin and mucilage. Looking at the chemical composition of the cladodes; It contains 91% moisture, 4.5% carbohydrates, 1.5% protein, 0.2% fat, 1.3% ash. In addition, it is reported that cladodes contain 11mg \ 100g vitamin C 30 µg \ 100g carotenoid with its rich dietary fiber content up to 43% [9–11] Since ancient times, cactus plants have been used to heal diseases and wounds. Today, it is seen that cactus fruits and the body part called cladodes are still used as therapeutic agents. Scientific data on the medicinal properties of cactus are constantly expanding [4, 12].

OFI has become the focal point of many researches nowadays as it has been involved in the treatment of various diseases such as diabetes, high cholesterol, high blood pressure, stomach diseases, and rheumatic pain in traditional folk medicine and in many countries. OFI contains bioactive components that strengthen the immune and nervous system, reduce oxidative stress-related diseases, sweep free radicals, reduce lipid peroxidation, and increase glutathione level [2, 13, 14].

OFI cladodes are composed of gel part and fiber part where high molecular weight polysaccharides (mucilage) are found. The mucilage in the cladodes; It has been reported to consist of arabinose, galactose, xylose and rhamnose and a small amount of galacturonic acid as neutral sugars. Therefore, cladodes are reported in the literature as rich in polysaccharides as pectin source [15, 16]. Pectin is a common additive in the food industry, which contains different amounts of methyl esters and dissolves in different degrees of neutralization, forming a gel-like structure with sugar and acid under favourable conditions. Apple pulp, orange peel, sunflower tray and sugar beet are the most common raw materials for pectin production. It is stated that the products obtained in the techniques applied in polysaccharide extraction from OFI cladodes are mostly low methoxy (LM) pectin. LM pectin form a gel in a wider pH range (pH: 2-6) with multivalent cations (such as Ca + 2) at sugar-free or low sugar concentrations [12, 17–19].

Extraction phenomenon is the way of obtaining polysaccharide from plant tissue by obeying mass transfer rules. Numerous methods can be applied to extract biological materials such as plant base polysaccharides. Among these methods, besides maceration with hot water or solvent extraction, supercritical fluid extraction, subcritical water extraction, enzymatic extraction, microwave-assisted or ultrasound-assisted extraction or combinations thereof can be said [19–25]. Although this process requires long times, high amount of chemical and energy in conventional techniques, emerging technologies such as ultrasound which eases this process while improving solvent penetration, enhances suspension quality and overcomes mass transfer limiting interface [26–28]. Ultrasound assisted extraction (UAE) is a “Green Chemistry” technique due to requiring minimum amount of chemical, energy and time at lower temperatures while ensuring comparable amount of yield compared to conventional techniques such as hot water or solvent extraction [23, 29].

JSR A
Journal of Scientific Reports

Sonication systems are divided into two application groups associated with applied power and sound frequency called high power low frequency and low power high frequency ultrasound. Industrial applications such as extraction require intensive energy to enhance heat and mass transfer. Applied low frequency high power (around 20kHz) sonicator is used in forms such as bath or probe systems. Probe systems satisfies intensive energy with high efficiency so that these systems are more useful than bath system especially for processes like extraction which requires strong mixing and cell wall disruption. In addition to mass transfer enhancement, in literature it was observed that sonication systems improve heat transfer regardless of changing conditions like viscosity and ensures stable transfer rates in whole reactor unlike conventional heating system which provides limited and diminishing heat transfer rates [30]. Ultrasound-assisted applications play a role in increasing extraction rate and efficiency [25, 31]. Extractable components appear in the tissue by being damaged, and ultrasound applications have been reported to increase the extraction kinetics and the quality of the extract [20]. Studies in the literature show that ultrasound has a positive effect on polysaccharide extract yield [23]. In the literature for the extraction of pectin from OFI cladodes; microwave assisted and ultrasound assisted extraction methods, alkali applications, methods using different solvents to precipitate mucilage such as isopropyl alcohol, ethanol and acetone have been reported in various yields ranging %7-25 (dry base) [10, 15, 17, 18, 32].

System modeling is a useful tool for not only predicting rate and yield but also for understanding the major ultrasound factors and their effects on the extraction process. In this study, correlation among convective heat transfer coefficients and mass transfer rate, which limits concentration in solvent and particle velocity were inspected for selected sonication parameters such as time, temperature and amplitude using experimental observations which were obtained by Response Surface Methodology (RSM).

In this study, polysaccharide of OFI cladodes were extracted by UAE method investigating the effect of applied power, temperature and processing time on the yield of extract. Properties of polysaccharide in optimal condition was investigated by chemical properties of extracts in terms of degree of esterification and total sugar composition.

2. MATERIAL AND METHOD

2.1. Materials

OFI cladodes were freshly harvested obtained in Jun, 2019 from trial lands located in Mersin/Erdemli/Turkey which was set for European Union Project for OFI studies. Average dimensions of the cladodes were 323±7 mm toll, 152±4 mm wide having 10±3 thickness (2:3 of it was skin) with 135±15 g. Average pH of mucilage par of samples were 5.71±0.07. Samples were cleaned in warm water after the thorns and epidermis were removed before treatments. The cleaned parts were cut into small pieces (~ 1cm) and weighed and dried in the oven at 60°C for 24 hours. The dried Cladodes were grounded in a high speed disintegrator (Knife Mill GRINDOMIX GM 200, Retsch GmbH, Haan, Germany) to obtain homogenate bulk which was fine powder (Particle size: 360±45 µm). All samples were kept at 4^{o}C for further treatment. All chemicals used for analyses were purchased from Sigma-Aldrich (St. Louis, MO, USA) in analytical grade.

2.2. Ultrasound Assisted Extraction Procedure

Samples were treated into distilled water satisfying 1:15 solid liquid ratio and pH is adjusted to 2.8 with hydrochloric acid as advised in previous studies [11] which was modification of the method

JSR A
Journal of Scientific Reports

developed by Bagherian et al. [49]. Sonication process was applied using probe (14 mm diameter, 90 mm height) type sonicator (Hielscher UP400S, 24 kHz, Germany) at sonic power up to 400 W. 250 ml volumetric flask was used at the same liquid height of 40±5 mm and merged depth of probe was 35±5 mm. Flask was covered by water jacket for temperature control and additional magnetic stirring was applied in reactor to provide homogeneity. Applied sonication energy was recorded through using wattmeter (VOLTCRAFT Energy Check 3000, Germany) and temperature on the wall (Two) and inside the reactor (Tm) was noted to monitor temperature increase inside the reactor by prolonged extraction (Fig 1).

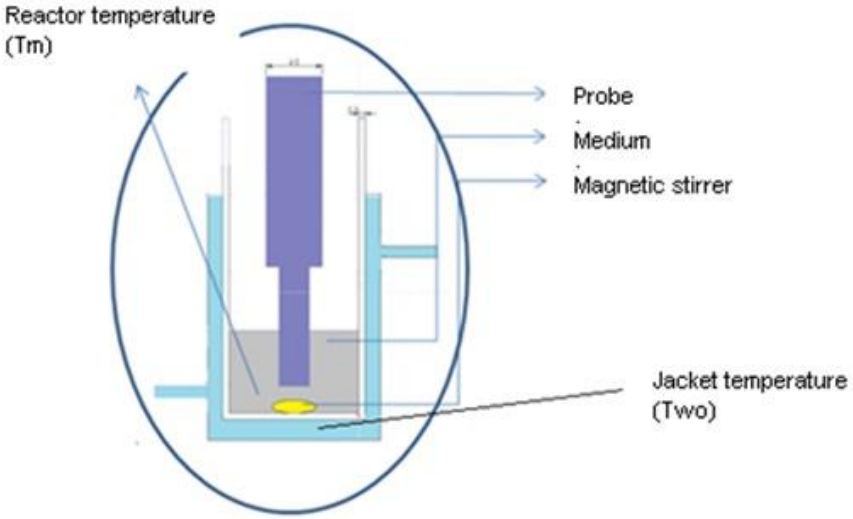

Figure 1. Demonstration of sonication system.

2.3. Calculation of Crude Polysaccharide (CPS) Yield

After sonication, water-sample mixture was centrifuged at 4000 rpm for 15 min. then filtered in order to obtain water soluble part. Settled part was not considered for further calculation. Sevag method was applied to permeate for protein removal [33]. After removal of the Sevag reagent, 200 ml of anhydrous ethanol was added and the mixture was kept 24 h at 4^{o}C to precipitate high molecular weight carbohydrates such as polysaccharides while dissolving mono and oligosaccharides into ethanol. Crude polysaccharide (CPS) was collected after centrifugation at 5000 rpm for 15 min and vacuum drying the final precipitate at 40±5^{o}C. CPS yield was determined by given equation (1) [20].

$$\text{CPS yield} = \frac{\text{weight of crude polysaccharide}}{\text{pretrated sample weight}} x\ 100 \quad (1)$$

2.4. Calculations about Ultrasonic Processors

Applied power was controlled by setting amplitude ratio (%) of equipment. Power level was recorded and it was validated by calorimetric method while measuring the temperature change of water inside the insulated flask by using equation (2) [34]. It was observed that applied sonication power "P" (W) was %80-90 of input power of the equipment that could be read on wattmeter. Further calculations were based on this outcome.

JSR A
Journal of Scientific Reports

$$P = C_P m(\frac{dT}{dt})_{t=0} \quad (2)$$

In equation (2), heat transfer capacity "Cp" and mass of water "m" are constants and their values are 4180 J/kgK and 100 g respectively. (dT/dt)t = 0 is the initial slope of temperature inside water "T" versus time "t" plot. Calculated power levels are comparable to equipment manual and it was correlated with heat transfer calculations. For further calculations, it was thought that determining the exact temperature inside the reactor was vital and effective temperature "T_{eff}" was determined by integrating Tm by processing time for each processing condition at given process time. The purpose was to see the temperature increase and average temperature during reaction.

2.5. Experimental Design, Validation and Data Analysis

In this study a three level three factor Box Behnken Design (BBD) consisting 17 experimental runs with 5 replicates at centre point in Response Surface Methodology (RSM) was developed to optimize UAE conditions. The design variables were ultrasonic power (X1), set temperature (X2), and time of the extraction process (X3) with all other parameters kept constant. Considering the preliminary trials and data in the literature, minimum and maximum values of independent variables were selected as 288-303 K, 10-30 minutes and 150-350 W by adjusting amplitude. Trials were randomized against the risk of unexpected effects occurring in the responses. Independent variables and their coded levels and actual values are shown in Table 1. All experiments were performed in triplicate, but mean values were used for modeling. The data were analysed using analysis of variance (ANOVA) by Design Expert software (Trial version 7.0.0; Stat-Ease, Inc. USA). The confidence level for statistical significance was set at a probability value of 0.05. Best models representing the system within BBD models were used for obtain maximum yield. Obtained results were also compared to the conventional method.

Table 1. Coded actual values used in Box-Behnken Design.

			Coded levels		
Codded	**Variable**	**Unit**	**-1**	**0**	**1**
X1	Power	W	150	250	350
X2	Temperature	K	288	318	303
X3	Time	min.	10	20	30

Linear, squared and interaction terms were investigated for best fitted model by checking lack of fit, R^2, adjusted R^2 and prediction error sum of squares (PRESS). Important independent variables were evaluated by analysis of variance (ANOVA) for each response. Equation validations were controlled by model ANOVA statistics. Response surface plots of selected modes were generated by statistical calculations of regression coefficients. Determined optimal values of the test variables were given as un-coded units after determining coded units [25]. Optimum condition was validated by comparing results of five experiments with predicted result obtained by generated model. For this purpose, t-test was applied.

2.6. Characterization of extracts

2.6.1. Proximate analysis.

Moisture, ash, protein and total carbohydrate content of CPS were analysed. Moisture content was determined by AOAC 930.15, ash content was determined by AOAC 942.05 [35]. Protein

JSR A
Journal of Scientific Reports

concentration was calculated from the nitrogen content (% Nitrogen x 6.25) to be obtained by element analysis (Elemental Analyzer, Perkin-Elmer Model 240) [36]. Total sugar content (SC) was evaluated by the phenol-sulphuric acid colorimetric method [33]. Briefly, 1.0 ml polysaccharide sample solution was mixed with 1.0 ml 5% phenol and 5 ml 98% H2SO4. The absorbance at 490 nm was recorded after standing for 15 min. The sugar content (SC) (%) was then calculated by equation (4) [37, 38]. Where; "C", sugar concentration (mg/mL) calculated using calibration curve, "N", dilution factor, "V_L" is the amount of solution (mL) [39].

$$\text{SC (\%dry weight)} = \frac{\text{C x N x } V_L}{\text{dried sample weight (CPS)}}\ x\ 100 \quad (4)$$

2.6.2. Esterification degree analysis.

Esterification value was one of the most important properties of pectic extracts to identify industrial application area [40]. In this study degree of esterification was determined by using modified method developed by Açıkgöz et al [41] and Bayar et al [17]. Briefly 0.1 g dried pectin dissolved in 1 mL ethanol and then added to 20 mL deionized water by stirring for 2 h at 40^{o}C. Solution was titrated with 0.1 M NaOH for neutralization and this volume was noted as "V1". Then 10 mL 0.1 M HCl was added to sample to disappear pink color. The solution was titrated again with 0.1 M NaOH and volume was noted as "V2". Degree of esterification was calculated by the equation (5) [17, 41].

$$\text{DE (\%)} = \frac{\text{V2}}{\text{V1+V2}}\ x\ 100 \quad (5)$$

3. RESULTS

Polysaccharides of OFI cladodes extracted in water after adjusting pH 2.8 by HCl as advised by previous researchers to maximize yield of pectic polysaccharide [11]. Leflish et al found the best condition by adjusting pH 2.26 [10] with mucilage polysaccharide content while, optimal pH was determined as 1.5 after mucilage removal [17]. In this study UAE was applied to mucilage of OFI cladodes and the effect of extraction conditions were evaluated on pH 2.8 adjusted water- OFI powder suspension.

3.1. UAE extraction and RSM optimization

RSM is helpful method to evaluate statistical models such a complex process as extraction phenomenon. Due to the adequacy tests, it was observed that quadratic model was the best model representing the system among other models while showing lowest and insignificant lack of fit, biggest Fisher's value or lowest p-value, highest R^2, adj-R^2 and pred-R^2 and the lowest predicted residual sum of squares "PRESS" value. ANOVA results (Table 2) of the selected quadratic model showed that correlation value was low enough to be reliable for representing the response, pred-R^2 and R^2 values were close to each other showing the good relation between experiments and predictions.

Table 2. BBD ANOVA table for CPS.

	Sum of	**F**	**p-value**
Source	**Squares**	**Value**	**Prob> F**
Model	79,386	84,849	< 0.0001
X1-Power	33,171	319,077	< 0.0001

X2-Temperature	14,933	143,646	< 0.0001
X3-Time	17,405	167,424	< 0.0001
X1X2	4,818	46,346	0.0003
X1X3	1,664	16,007	0.0052
X2X3	0,240	2,310	0.1724
X1^2	0,040	0,383	0.5556
X2^2	0,386	3,712	0.0954
X3^2	6,582	63,310	< 0.0001
Residual	0,728		
Lack of Fit	0,519	3,321	0.1383
Pure Error	0,208		
Cor Total	80,114		
C.V. %	2,153		
PRESS	8,633		
R-Squared	0,991		
Adj R-Squared	0,979		
Pred R-Squared	0,892		
Adeq Precision	31,173		

Linear effects of parameters were predominant factors on responses while interaction effects and quadratic effect of time were still important ($p<0.05$). Finally, diagnostic analysis (Fig 2) carried on controlling fitness quality of the model because CPS model was important for further modeling steps in order to generate variable during mass transfer calculations. Diagnostic plots (Fig 2) showed that residuals were in normal distribution (Fig 2a), predicted values versus predictions given at Table 3 were laying on 45^{o} trend to each other (Fig 2b), and residuals were staying in reliable limits (Fig 2c-d). Developed BBD quadratic model with codded values are given in equation (6).

$$CPS = 15.66 + 2.04X_1 + 1.37X_2 + 1.48X_3 - 1.10X_1X_2 + 0.65X_1X_3 - 1.25X_3^2 \quad (6)$$

Table 3. Predicted and observed values of CPS.

Run number	**X1**	**X2**	**X3**	**Predicted values**	**Observed values**
1	-1	0	1	13.20	13.33±0.41
2	0	-1	1	14.52	14.75±0.86
3	0	0	0	15.66	15.67±0.33
4	0	1	-1	14.30	13.95±0.83
5	0	1	1	17.26	16.63±0.65
6	-1	1	0	16.09	15.92±0.56

7	1	0	1	18.50	18.41±0.49
8	0	0	0	15.66	15.30±0.25
9	1	1	0	17.97	18.08±0.62
10	0	-1	-1	11.56	11.09±0.76
11	1	-1	0	17.43	17.18±0.43
12	-1	0	-1	11.54	11.89±0.17
13	0	0	0	15.66	15.80±0.30
14	-1	-1	0	11.15	10.63±0.71
15	0	0	0	15.66	15.90±0.35
16	0	0	0	15.66	15.62±0.20
17	1	0	-1	14.32	14.39±0.42

JSR A
Journal of Scientific Reports

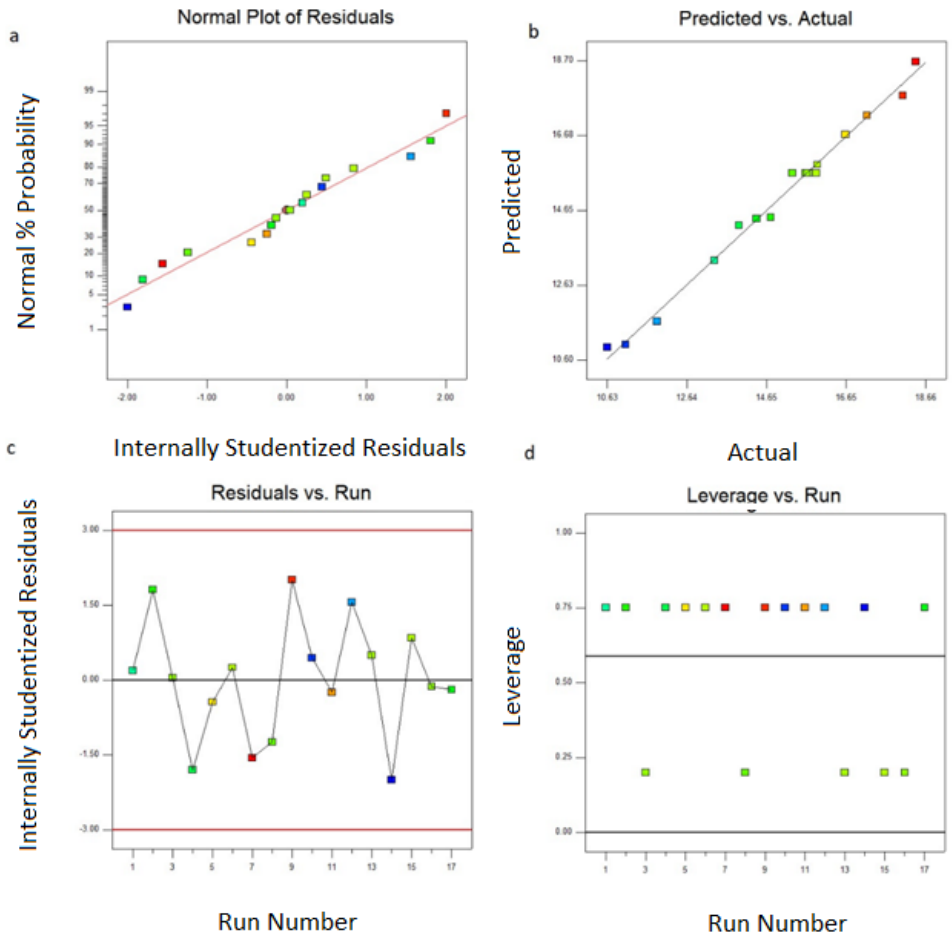

Figure 1. CPS model diagnostic plots.

Polysaccharide yield is highly dependent on extraction condition. Conventionally water soluble pectin rich CPS was extracted from plant tissue by using severe conditions under high temperature (80-90^{o}C) and long processing time (30 min-120 min) [11, 42–44]. Previous researches found the yield of polysaccharide on fresh weight was 1.2% after 80°C for 30 min extraction [44]. In this study the yield in fresh weight was 2.4%±0.46 due to conditions. On the other hand considering moisture content of cladodes 91%±5 and comparing results in dry basis average yield was calculated 14.97%±0.32 and it was still higher than conventional methods which was 12.01% [44], 10.24% [11]. Besides conventional method microwave assisted extraction with several conditions found beneficial to increase the yield up to 25% [32] which is higher than our findings. On the other hand, enzymatic extraction is also promising green method to extract cladode polysaccharides providing 17.91% in previous studies [19] which is lower than UAE yield at 350W, 318K and 30 min extraction providing 18.50% yield (Table 3), however, these variation could be expressed by differences between plant

material (maturity, species, harvesting), pre-treatment and separation technique of CPS and majorly extraction conditions. As given on response plots (Fig 3) positive effect of set temperature on the yield was important. That could be explained by easing cavitation, decrease in surface tension and solvent viscosity, improved solute solubility and enhancing solvent penetration into the solid matrix by means of increasing temperature. As a consequence, mass transfer rate increased and partial-hydrolyzation occurred which breaks weak bonds which are holding polysaccharide intact into the plant cell matrix [45–47]. Although temperature was important, the most affective factor was sonication power which causes cavitation phenomena disturbing cell wall material to ensure leaching of extractable materials [48]. Stronger sonication power caused sharpening in cavitation effect which was responsible for micro streaming and micro jets [29].

For all experiments Tm and Two were recorded and it was observed that set temperature was not reliable although jacket was applied to keep temperature constant during UAE treatment. However, all parameters increase the ambient temperature regardless of how low the set temperature was. As recorded during experiments at least 5 K increment was observed and the maximum temperature increase was recorded as 11.8% after 30 min treatment at 288 K, 350 W treatment. Especially temperature increase was more rapid for low temperature practices. This outcome was important to make further modeling calculation in other temperature sensitive transfer variables such as heat and mass transfer coefficient. On the other hand, in literature, it was investigated that sonication ensures uniform and perfect heat distribution comparing to conventional techniques [30]. Prolonged treatment had positive effect on the yield of extract and in previous studies it was found beneficial up to 25 min but decrease was observed due to structural changes and decomposition of pectic polysaccharides with longer extraction periods [52].

JSR A
Journal of Scientific Reports

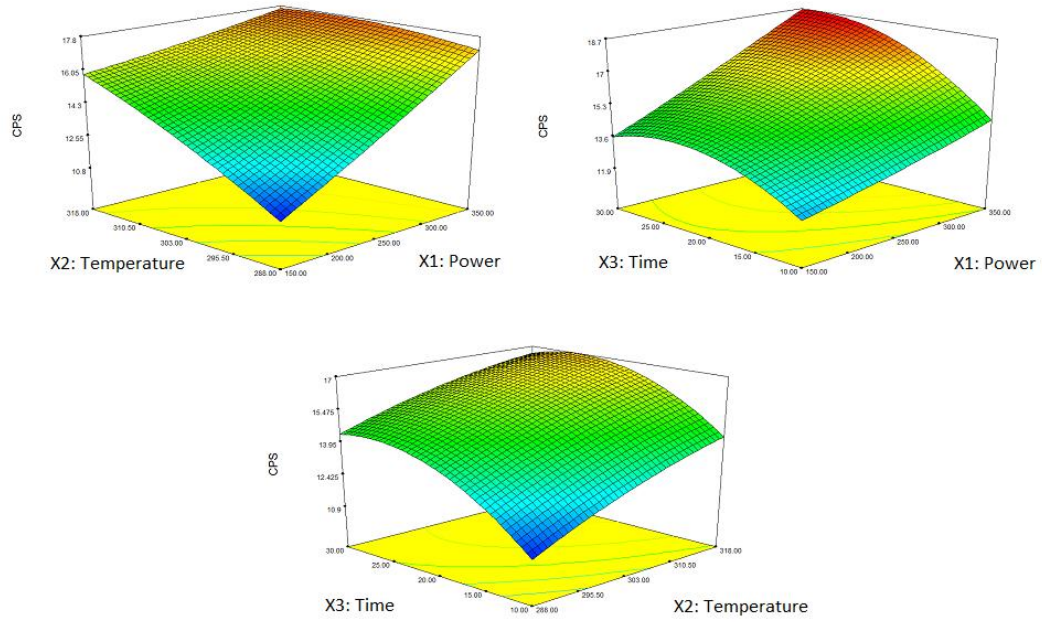

Figure 2. Response plots of CPS yield under ultrasonic conditions.

Optimal conditions were determined to maximize the yield of CPS under given extraction parameters and it was found as 345.5 W, 304.5 K and 28.5 min extraction and predicted yield was 18.58%. Average yield of five experiments run under optimal condition was 18.48±0.35% which was not different from predicted yield statistically ($p>0.05$).

3.2. Characterization of extracted CPS

Extracted CPS were highly fresh having 92±5% moisture content. Therefore, extracts were dried before further characterization. Chemical composition of dried CPS obtained under optimal conditions were 7.5±2.22% moisture content, 14.4±0.87 ash, 0.18±0.05 protein, 82.12±7.2% SC in glucose, 72.75±6.8% SC in galacturonic acid in dry basis. Chemical composition of CPS served similar results as previous researches declared [44]. Protein content was low compared to previous studies which were 0.32% [11, 17, 19], it can be explained by Sevag procedure application in current work to remove protein. Variation on galacturonic acid content was strongly related to extraction condition which had important role on pectin recovery. Ultrasonic extraction and microwave extraction techniques applied previously resulted in 68.8% and 60.66% galacturonic acid and 80.02% and 85.31% total sugar content [19, 17].

Degree of esterification is important property for CPS to identify industrial application. It is known that pectin serves diversified DE (%) due to nature of plant material. It is stated that the products obtained in the techniques applied in polysaccharide extraction from OFI cladodes are mostly LM (low methoxy) pectin [17, 42]. Measured degree of esterification of CPS found as 40.57±3.11% and

this is compatible to previous studies and can be perceived as LM pectin. On the other hand this value is higher than conventionally extracted polysaccharides which was calculated as 30.67% [53].

4. DISCUSSION

In this study, time, temperature and ultrasonic power were selected as optimisation variables. However, it was observed that extract yield was highly affected by various factors as studied plant matrix, application temperature, time, solvent, solid to liquid ratio, pH and process variables as power etc… [51,52]. For ultrasound assisted and microwave extraction procedures of pectic polysaccharides, applied conditions by previous researches were varying as 15-75^{o}C, 10-60 min., pH 1.5-10, 1:5-1:40 (g/ml), 300-900 W microwave power or 50-400 W ultrasonic power while optimisation was applied by RSM design considering three factors of extraction parameters [50-51]. pH was advised to adjust to 2.8 in Bayar et al. [19], since water soluble polysaccharides as pectin in plant material was extracted in acidic conditions as described by previous researchers as well [17,50,51]. It was found that pectin yield was positively affected by increasing pH from 1.5 to 5.5 while considering other parameters as constant [17]. On the other hand, highest pectin yield of plant extracts found between pH 2-3 [52]. Therefore, pH was set to 2.8 in this study to evaluate selected sonication parameters which was also important level to keep protein content low in the extract by keeping away the isoelectric pH of plant protein as discussed in previous studies [11,17]. In water extraction of OFI cladode pectin, solid to liquid ratio was selected as 1:15 g/ml [11,19], while mostly studied ratio was between 1:10-1:30 [50,52]. 1:15 g/ml was found good enough to evaluate the effect of sonication parameters successfully depending on preliminary studies because, dilute concentration requires more chemical usage while high concentration makes extraction difficult to run due to complicating phase separation. For the pectin extraction, solid to liquid ratio was found important factor to ease dissolution of extractable material and formation of cavitation by lowering viscosity and resistant forces for dilute solutions up to 1:30 g/ml [52].

In the present study, UAE was successfully applied to obtain polysaccharide from OFI cladodes by using BBD. Polynomial model was developed to model ultrasonic conditions which were sonic power, set temperature and processing time and optimal conditions in terms of yield maximization were 345.5 W, 304.5 K and 28.5 min extraction respectively. Achieved yield was predicted as 18.58% which was validated by experiments having the average yield 18.48±0.35%. General composition of the extracts at the optimal condition was 7.5±2.22% moisture content, 14.4±0.87 ash, 0.18±0.05 protein, 82.12±7.2% SC in glucose, 72.75±6.8% SC in galacturonic acid in dry basis. In literature Bayar et al studied UAE extraction of OFI cladodes at constant 330 W ultrasonic power and optimal conditions were found as 343 K, 70 min. extraction at pH 1.5 and 1:30 g/ml having yield of 19.06% having chemical composition as 92% dry matter, 16.88% mineral, 0.32% protein 80.02% total sugar, 68.87% uronic acids [17] which were found slightly different from current study due to extraction condition and the nature of the raw material. In this study effect of sonication power was evaluated differing from previous one by studying sonication phenomenon detailly by keeping parameters as pH and solid to liquid ratio constant and the effect of varied sonication power were investigated in terms of yield and temperature increase in the reaction vessel with sonication at various power-temperature combinations. Consequently, it was found that higher sonication power increased the pectin yield but also elevated power increased reactor temperature as well which should be considered for further studies while deciding set temperature and duration.

OFI parts as fruit and cladode have several application areas for medical and food industry with their unique composition. On the other hand, OFI is wild plant and freely available on arid and semi-arid locations without any treatment and practices. Therefore, it is a cheap raw material. Although fruit part is valuable and consumed worldwide, cladodes being high in pectin can be valorised with high added value except for disposing as animal feed. OFI cladodes are mostly LM (low methoxy pectin) pectin. However, research on the use of this product in the field of food needs more research. Degree of esterification was found 40.57±3.11% proving that extracted polysaccharides was low-methoxy (LM) pectin-based material which can be used a good alternative and cheap source for industrial LM pectin.

Another outcome of the study was showing the temperature change while UAE procedure. Although jacketed system was applied to validate constant temperature on the reactor wall, prolonged extraction increased temperature inside the reactor dramatically and the average temperature in reactor media during extraction risen up to 11% for 30 min extraction depending on set temperature and sonication power. This could have additional effect on efficiency and should be considered for UAE designs for better control and prediction.

ACKNOWLEDGMENTS

This research was funded by Scientific Project Department with the project ID: BAP-2019-123 from Manisa Celal Bayar University, Manisa, Turkey. The authors are grateful to the Mediterranean Wildlife Association (NATURELDER) for providing the cladode samples.

REFERENCES

[1] Scalisi A, Morandi B, Inglese P, Lo Bianco R., (2016), Cladode growth dynamics in Opuntia ficus-indica under drought, Environ Exp Bot, 122, 158–167.

[2] Salehi E, Emam-Djomeh Z, Askari G, Fathi M., (2019), Opuntia ficus indica fruit gum: Extraction, characterization, antioxidant activity and functional properties, Carbohydr Polym, 206, 565–572.

[3] Del-Valle V, Hernández-Muñoz P, Guarda A, Galotto MJ., (2005), Development of a cactus-mucilage edible coating (Opuntia ficus indica) and its application to extend strawberry (Fragaria ananassa) shelf-life, Food Chem, 91, 751–756.

[4] Taguchi M, Harinder Makkar F, Mounir Louhaichi F, Duffy R, Moretti D., (2017), CROP ECOLOGY, CULTIVATION AND USES OF CACTUS PEAR Editorial support Book design and layout, 26–30.

[5] Sáenz C, Sepúlveda E., (2001), Cactus-Pear Juices, J Prof Assoc Cactus Dev, 4, 3–10.

[6] Garbelotti ML, Marsiglia DAP, Torres E a. F., (2003), Determination and validation of dietary fiber in food by the enzymatic gravimetric method, Food Chem, 83, 469–473.

[7] Gheribi R, Puchot L, Verge P, Jaoued-Grayaa N, Mezni M, Habibi Y, Khwaldia K., (2018),

Development of plasticized edible films from Opuntia ficus-indica mucilage: A comparative study of various polyol plasticizers, Carbohydr Polym, 190, 204–211.

[8] Allegra A, Sortino G, Inglese P, Settanni L, Todaro A, Gallotta A., (2017), The effectiveness of Opuntia ficus-indica mucilage edible coating on post-harvest maintenance of 'Dottato' fig (Ficus carica L.) fruit, Food Packag Shelf Life, 12, 135–141.

[9] Chaouch MA, Hafsa J, Rihouey C, Le Cerf D, Majdoub H., (2015), Depolymerization of polysaccharides from Opuntia ficus indica: Antioxidant and antiglycated activities, Int J Biol Macromol, 79, 779–786.

[10] Lefsih K, Giacomazza D, Dahmoune F, Mangione MR, Bulone D, San Biagio PL, Passantino R, Costa MA, Guarrasi V, Madani K., (2017), Pectin from Opuntia ficus indica: Optimization of microwave-assisted extraction and preliminary characterization, Food Chem, 221, 91–99.

[11] Bayar N, Kriaa M, Kammoun R., (2016), Extraction and characterization of three polysaccharides extracted from Opuntia ficus indica cladodes, Int J Biol Macromol, 92, 441–450.

[12] Allegra A, Inglese P, Sortino G, Settanni L, Todaro A, Liguori G., (2016), The influence of Opuntia ficus-indica mucilage edible coating on the quality of "Hayward" kiwifruit slices, Postharvest Biol Technol, 120, 45–51.

[13] Khatabi O, Hanine H, Elothmani D, Hasib A., (2016), Extraction and determination of polyphenols and betalain pigments in the Moroccan Prickly pear fruits (Opuntia ficus indica), Arab J Chem, 9, S278–S281.

[14] Lansky EP, Paavilainen HM, Pawlus AD, Newman RA., (2008), Ficus spp. (fig): ethnobotany and potential as anticancer and anti-inflammatory agents., J Ethnopharmacol, 119, 195–213.

[15] Medina-Torres L, Brito-De La Fuente E, Torrestiana-Sanchez B, Katthain R., (2000), Rheological properties of the mucilage gum (Opuntia ficus indica), Food Hydrocoll, 14, 417–424.

[16] Majdoub H, Roudesli S, Deratani A., (2001), Polysaccharides from prickly pear peel and nopals of Opuntia ficus-indica: extraction, characterization and polyelectrolyte behaviour, Polym Int, 50, 552–560.

[17] Bayar N, Bouallegue T, Achour M, Kriaa M, Bougatef A, Kammoun R., (2017), Ultrasonic extraction of pectin from Opuntia ficus indica cladodes after mucilage removal: Optimization of experimental conditions and evaluation of chemical and functional properties., Food Chem, 235, 275–282.

[18] Lefsih K, Delattre C, Pierre G, Michaud P, Aminabhavi TM, Dahmoune F, Madani K., (2016), Extraction, characterization and gelling behavior enhancement of pectins from the cladodes of Opuntia ficus indica, Int J Biol Macromol, 82, 645–652.

[19] Bayar N, Friji M, Kammoun R., (2018), Optimization of enzymatic extraction of pectin from Opuntia ficus indica cladodes after mucilage removal, Food Chem, 241, 127–134.

[20] Yilmaz T, Tavman Ş., (2016), Ultrasound assisted extraction of polysaccharides from hazelnut skin, Food Sci Technol Int. doi: 10.1177/1082013215572415

[21] Chemat F, Zill-e-Huma, Khan MK., (2011), Applications of ultrasound in food technology: Processing, preservation and extraction., Ultrason Sonochem, 18, 813–35.

[22] Chen W, Wang W-P, Zhang H-S, Huang Q., (2012), Optimization of ultrasonic-assisted extraction of water-soluble polysaccharides from Boletus edulis mycelia using response surface methodology, Carbohydr Polym, 87, 614–619.

[23] Hromádková Z, Ebringerová A, Valachovic P., (2002), Ultrasound-assisted extraction of water-soluble polysaccharides from the roots of valerian (Valeriana officinalis L.)., Ultrason Sonochem, 9, 37–44.

[24] Hromádková Z, Ebringerová a, Valachovic P., (1999), Comparison of classical and ultrasound-assisted extraction of polysaccharides from Salvia officinalis L., Ultrason Sonochem, 5, 163–8.

[25] Yılmaz T, Tavman S., (2017), Modeling and Optimization of Ultrasound Assisted Extraction Parameters using Response Surface Methodology for Water Soluble Polysaccharide Extraction from Hazelnut Skin, J Food Process Preserv. doi: 10.1111/jfpp.12835

[26] Benito-Román Ó, Alonso E, Cocero MJ., (2013), Ultrasound-assisted extraction of β-glucans from barley, LWT - Food Sci Technol, 50, 57–63.

[27] García A, Alriols MG, Llano-Ponte R, Labidi J., (2011), Ultrasound-assisted fractionation of the lignocellulosic material., Bioresour Technol, 102, 6326–30.

[28] Xu Y, Zhang L, Bailina Y, Ge Z, Ding T, Ye X, Liu D., (2014), Effects of ultrasound and/or heating on the extraction of pectin from grapefruit peel, J Food Eng, 126, 72–81.

[29] Sivakumar V, Anna JL, Vijayeeswarri J, Swaminathan G., (2009), Ultrasound assisted enhancement in natural dye extraction from beetroot for industrial applications and natural dyeing of leather., Ultrason Sonochem, 16, 782–9.

[30] Feng H, Barbosa-Canovas G V., Weiss J., (2010), Ultrasound Technologies for Food and Bioprocessing. Springer, New York

[31] Patist A, Bates D., (2008), Ultrasonic innovations in the food industry: From the laboratory to commercial production, Innov Food Sci Emerg Technol, 9, 147–154.

[32] Felkai-Haddache L, Dahmoune F, Remini H, Lefsih K, Mouni L, Madani K., (2016), Microwave optimization of mucilage extraction from Opuntia ficus indica Cladodes, Int J Biol Macromol, 84, 24–30.

[33] Dubois M, Gilles KA, Hamilton JK, Rebers PA, Smith F., (1956), Colorimetric Method for Determination of Sugars and Related Substances, Anal Chem, 28, 350–356.

[34] Cheung Y-C, Wu J-Y., (2013), Kinetic models and process parameters for ultrasound-assisted extraction of water-soluble components and polysaccharides from a medicinal fungus, Biochem Eng J, 79, 214–220.

[35] AOAC., (2007), Official Methods of Analysis. 18th edn. AOAC International, Gaithersburg

[36] Hromadkova Z, Ebringerova A., (2003), Ultrasonic extraction of plant materials — investigation of hemicellulose release from buckwheat hulls, Ultrason - Sonochemistry, 10, 127–133.

[37] Albalasmeh A a., Berhe AA, Ghezzehei T a., (2013), A new method for rapid determination of carbohydrate and total carbon concentrations using UV spectrophotometry, Carbohydr Polym, 97, 253–261.

[38] Huang S, Ning Z., (2010), Extraction of polysaccharide from Ganoderma lucidum and its immune enhancement activity., Int J Biol Macromol, 47, 336–41.

[39] Zhang Y, Kong L, Yin C, Jiang D, Jiang J, He J, Xiao W., (2013), Extraction optimization by response surface methodology, purification and principal antioxidant metabolites of red pigments extracted from bayberry (Myrica rubra) pomace, LWT - Food Sci Technol, 51, 343–347.

[40] Thakur BR, Singh RK, Handa AK., (1997), Chemistry and Uses of Pectin - A Review, Crit Rev Food Sci Nutr, 37, 47–73.

[41] Açıkgöz Ç, Poyraz Z., (2006), EXTRACTION AND CHARACTERIZATION OF PECTIN OBTAINED FROM QUINCE(cydonia vulgaris pers.), Dumlupınar Üniversitesi Fen Bilim Enstitüsü Derg, 27–34.

[42] Goycoolea FM, Cárdenas A., (2003), Pectins from Opuntia spp.: A short review, J Prof Assoc Cactus Dev, 5, 17–29.

[43] Di Lorenzo F, Silipo A, Molinaro A, Parrilli M, Schiraldi C, D'Agostino A, Izzo E, Rizza L, Bonina A, Bonina F, Lanzetta R., (2017), The polysaccharide and low molecular weight components of Opuntia ficus indica cladodes: Structure and skin repairing properties, Carbohydr Polym, 157, 128–136.

[44] Dick M, Dal Magro L, Rodrigues RC, Rios A de O, Flôres SH., (2019), Valorization of Opuntia monacantha (Willd.) Haw. cladodes to obtain a mucilage with hydrocolloid features: Physicochemical and functional performance, Int J Biol Macromol, 123, 900–909.

[45] Prakash Maran J, Manikandan S, Vigna Nivetha C, Dinesh R., (2013), Ultrasound assisted extraction of bioactive compounds from Nephelium lappaceum L. fruit peel using central composite face centered response surface design, Arab J Chem. doi: 10.1016/j.arabjc.2013.02.007

[46] Prakash Maran J, Manikandan S, Thirugnanasambandham K, Vigna Nivetha C, Dinesh R., (2013), Box-Behnken design based statistical modeling for ultrasound-assisted extraction of corn silk polysaccharide., Carbohydr Polym, 92, 604–11.

[47] Prakash Maran J, Manikandan S, Mekala V., (2013), Modeling and optimization of betalain extraction from Opuntia ficus-indica using Box–Behnken design with desirability function, Ind Crops Prod, 49, 304–311.

[48] Toma M, Vinatoru M, Paniwnyk L, Mason TJ., (2001), Investigation of the effects of ultrasound on vegetal tissues during solvent extraction, Ultrason Sonochem, 8, 137–142.

[49] Bagherian HZokaee Ashtiani., F., Fouladitajar A., and Mohtashamy M., (2011), Comparisons between conventional, microwave- and ultrasound-assisted methods for extraction of pectin from grapefruit, Chem. Eng. Process. Process Intensif., 50, 1237–1243.

[50] Sundarraj A. A., Thottiam Vasudevan R., and Sriramulu G., (2018), Optimized extraction and characterization of pectin from jackfruit (Artocarpus integer) wastes using response surface methodology, Int. J. Biol. Macromol., 106, 698–703.

[51] Sundarraj A. A. and Ranganathan T. V., (2018), Comprehensive review on ultrasound and microwave extraction of pectin from agro-industrial wastes, Drug Invent. Today, 10, 2773–2782.

[52] Maran J. P. and Priya B., (2015), Ultrasound-assisted extraction of pectin from sisal waste, Carbohydr. Polym., 115, 732–738, 2015.

[53] Forni E, Penci M, Polesello A., (1994), A preliminary characterization of some pectins from quince fruit (Cydonia oblonga Mill.) and prickly pear (Opuntia ficus indica) peel, Carbohydr Polym, 23, 231–234.

Kütahya Dumlupınar University
Institute of Graduate Studies

Journal of Scientific
Reports-A
E-ISSN: 2687-6167
Number 45, December 2020

RESEARCH ARTICLE

EXPERIMENTAL ANALYSIS OF THE AIR DEFROST PROCESS IN AN INDUSTRIAL COOLING SYSTEM

Süleyman ERTEN[1], Meltem KOŞAN[2,*], Furkan İŞGEN[3], Mustafa AKTAŞ[4]

[1] Nurdil Technical Cooling, Ankara, suleymanerten@nurdil.com.tr,
ORCID: 0000-0002-7811-6148
[2] Gazi University, Technology Faculty, Energy Systems Engineering, Ankara, mltmkosan@gmail.com
ORCID:0000-0001-7311-9342
[3] Gazi University, Technology Faculty, Energy Systems Engineering, Ankara, isgenfurkan@gmail.com,
ORCID:0000-0002-3299-6485
[4] Gazi University, Technology Faculty, Energy Systems Engineering, Ankara, mustafaaktas@gazi.edu.tr,
ORCID: 0000-0003-1187-5120

Received Date:02.07.2020 *Accepted Date: 19.11.2020*

ABSTRACT

Keeping product temperatures homogeneous is an important problem in defrosted industrial coolers. In this study, it is aimed to obtain findings that will shed light on researchers and producers by analyzing the defrosting process of the industrial cooler. For these reasons, the system was designed using R290 (propane), a new generation refrigerant with a single evaporator, double condenser and double compressor, in order to ensure homogeneous cooling. By keeping the cooled products in the range of – 1 ℃ and +5 ℃ as required by the standard, during the experiment, temperature-pressure measurements of the refrigerated products and cooling system equipment were taken from certain points every minute and test data were recorded. The average temperature and relative humidity values measured minute of the environment where the experimental setup is located was calculated as 25℃ ±1℃ and 60% ± 0.02%, respectively. During the experiment, eight defrost operations were performed, and it was observed that the average temperature values taken from the products during the 24 hours during defrosting changed to 3.07℃. During the experiment, the highest and lowest temperatures of the cooled products were measured as 4.22℃ and 2.02℃. Increased product temperatures and cooling stopped during defrosting increased the power consumption in the system. In order to observe the effect of the power consumption on system performance, COP values after each defrost time were calculated as 2.31, 2.30, 2.29, 2.60, 3.36, 3.29, 3.30, 3.49, respectively. When the defrost process of cooling system analyzed, it was seen that the products were successfully cooled at desired temperature ranges in the scope of TS EN ISO 23953-2.

Keywords: *Defrost, Industrial Cooling, Efficiency, Heat Pump*

1. INTRODUCTION

Vapor compression refrigeration systems are frequently used in terms of both energy efficiency and ease of application [1]. According to the source of the heat, there are vapor compression heat pump systems originating from ground, air and water. Among these, air-source heat pumps (ASHPs) are

widely used in industrial systems. In an environment with 25℃ ± 1℃ temperature and 60% ± 0.02% relative humidity, the dew thermometer temperature of the air is 16.7℃. In this context, ice formation on the surface of the evaporator with a temperature of -10℃ is inevitable. When using an air-borne evaporator with a surface temperature of -10℃ in industrial refrigerators, icing is inevitable in the evaporator. The humid and hot air affects the ice formation rate and the ice thickness formed [2].

Zhu et al. (2015) observed that the ice formation rate increased with the increase of the temperature and relative humidity values of the environment whereas the relative humidity of the environment rather than temperature had a greater effect on the ice formation rate. In addition, they separated frost formation as light, medium and severe ice formation regions, respectively [3]. During the ice formation phase on the evaporator surface, Guo et al. (2008) have shown that the relative humidity of the ambient air develops at a constant rate of 10-15 minutes at an ice formation rate above 65%. They stated that there was a decrease in the ice formation rate in the next 5 minutes and that it developed very rapidly in the next time period [4].

The defrost layer, which increases over time in the evaporator wall, adversely affects the heat transfer due to the high heat transfer resistance of the ice. The increase in the thickness of the defrost layer causes Coefficient of Performance (COP) values of the ASHP unit to decrease and prevent the airflow outside the evaporator, causing high-pressure losses on the airside. Wang et al. (2019) observed that when the ice formation reached the severe ice formation zone, the defrosting time ranged from 20 minutes to 60 minutes in different temperature experiments and the air-side pressure drop varied between 36% to 86% [5]. High pressure drops occurring on the airside will cause an increase in fan power and will cause irregularities in the air circulation in the environment. Defrosting applied towards cooling systems will increase the system performance with heat transfer.

One of the methods commonly used for defrosting is to perform defrosting by operating the system in reverse with the 4-way valve to be used in the cooling system [6]. Although such an application seems to eliminate the problem, the interruption of the cooling process, changes in the ambient temperature during defrosting and the thermal loads released during defrosting cause a decrease in COP value in the cooling system. Therefore, different applications are encountered in the literature that aims to eliminate such effects occurring during defrosting. Byun et al. (2008) applied the defrost operation with by passing hot gas at 0%, 20%, 30%, and 40%, respectively, and examined the effects of these ratios on the system. The highest COP value was obtained when the hot gas by-pass rate was 20% [7].

In the cooling systems, there are also defrost applications performed by placing the external electrical resistance directly on the serpantine or by placing on the fan blowing air to the serpantine [2,8]. Long et al. (2014) carried out the defrosting process by making use of the waste heat of the compressor and achieved a 1.4% increase in the COP value [9]. Liu et al. (2017) stated that the defrost operation to be performed by storing the heat discharged from the condenser in the phase-changing material in the home type refrigerators will create 71% less energy consumption compared to the electric defrost application [10]. Ice melting in the evaporator where icing occurs, passing over other ice masses with the effect of gravity, both prolongs the defrost time and reduces the performance of the cooler. For this reason, proper removal of water dissolved during defrosting also increases cooling efficiency [11, 12].

In this study, analyzes were made that will shed light on the solution of the problems caused by the application of defrosting of the vapor compression refrigeration system, which is becoming

increasingly common in food storage and industrial cooling and heating applications. However, in order to provide a homogeneous cooling in the system, a single evaporator, double condenser and double compressor are used. At the same time, the cooling system is designed using R290 (propane), which is one of the new generation refrigerants.

2. MATERIAL AND METHOD

In this study, it is aimed to investigate the defrosting process in the air source industrial cooling system. Vapor compression industrial cooling system operating with vertical type open, positive, R290 (Propane) refrigerant was designed, manufactured and tested by calculating the cooling load. The cooling system has a single evaporator, double compressor and double condenser, as can be seen in Figure 1a. Thus, it was desired to provide homogeneous cooling on the products. The tests were carried out in the test room under Class-3 at 25 ℃±1℃ temperature and 60% ± 0.02% relative humidity (% RH). A visual of the experimental setup is shown in Figure 1b.

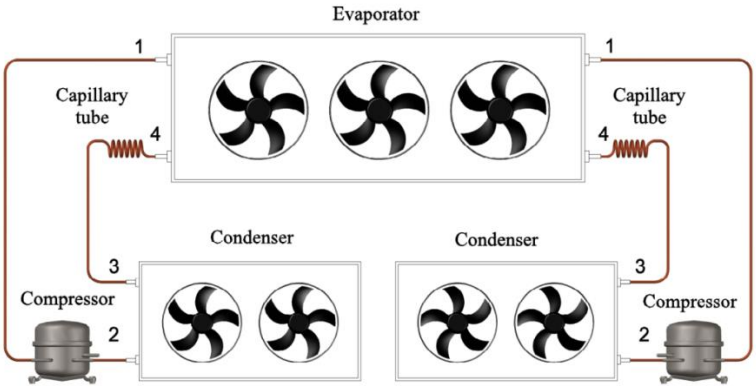

Figure 1a. Vapor compression refrigeration system.

Figure 1b. Experimental setup.

JSR A
Journal of Scientific Reports

In the defrost system, it is planned to direct the ambient air to the evaporator surface through the fans for a period determined at certain time intervals, and defrosting is performed. In general, defrosting is repeated 8 times a day for 15-25 minutes in this type of cooler. In this experimental study, defrost was performed in the system every three hours. The experimental set-up and measurement points are shown in Figure 2.

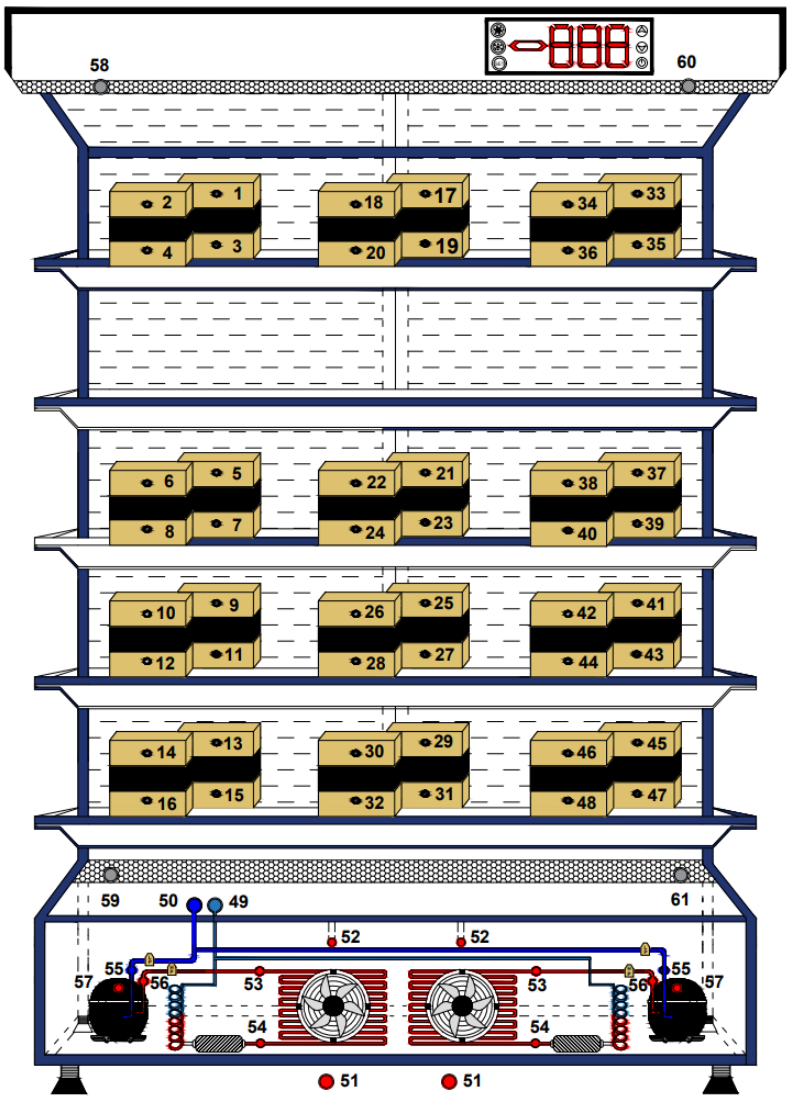

Figure 2. Cooling system and measuring points.

1-48	Test package temperature values	**56**	Compressor discharge line temperature value
49	Evaporator inlet temperature value	**57**	Compressor body temperature value
50	Evaporator output temperature value	**58**	Left side blowing air temperature value

JSR A
Journal of Scientific Reports

51	Condenser air inlet temperature value	**59**	Left side intake air temperature value
52	Condenser air outlet temperature value	**60**	Right side blowing air temperature value
53	Condenser gas inlet temperature value	**61**	Right side intake air temperature value
54	Condenser liquid output temperature value	**HP**	High pressure value
55	Compressor suction temperature value	**LP**	Low pressure value

The experiments were carried out in the test room with calibrated test devices within the scope of TS EN ISO 23953-2 standard. Cooling performance of the system, energy consumption amount measurement, temperature measurements, pressure measurements and energy efficiency tests were performed. While performing these tests, temperature measurements were taken every minute by means of thermocouples from certain points of cooling systems equipment (compressor, condenser and evaporator inlet-outlet temperature values). Information on measurement equipment used in prototype production and tests is given in Table 1.

Table 1. Measurement devices and their technical features used in prototype production and tests.

Device	**Model**	**Unit**	**Measuring Range**	**Accuracy**
Thermocouple	Omega, CL-23A	$°C$	-40 / +150	$\pm$ % 0.02
Pressure transmitter	Eliwell, HP	bar	0-30	$\pm$ 0.1
Pressure transmitter	Eliwell, LP	bar	0,5-8	$\pm$ 0.01
Thermohygrometer	Rotronic, M23W2HT-1X	$°C$ / $\%RH$	0 / +50 0-100 %	$\pm$ % 1.5 $\pm$ 0.03
Anemometer	E+E Electronic, EE66-VA3 EE660-V7	m/s	0-2	$\pm$ 0.01
Vacuum pump	Value, VP2200	Pa	0,04-0,8	$\pm$0.02
Digital scales	Value, VES-100B	g	0-100	$\pm$ % 0,05
Digital manifold	Testo, 550	bar	-50 / +150 -1 / +60	$\pm$ 0.1 $\pm$ 0.01
Energy analyzer	Janitza, UMG508	$Ampere$ $Volt$	-	$Current$ $\pm$ % 0.2 $Voltage$ $\pm$ % 0.1
Flowmeter	Siemens, SITRANS FC MASS 6000	kg/h	0-1000	$\pm$ % 0.1

2.1. Defrost Process

Defrost is the name given in the cooling technique for the elimination or melting of the icing and snowing formed by the water vapor condensing on the cool surfaces of the coolers (evaporator). Ice or snow accumulating on the evaporator surface is undesirable and causes loss of efficiency while making heat transfer difficult. At the same time, the amount of energy spent on defrosting to solve ice or snowing in cooling systems reaches large sizes, as it is not effectively controlled. An additional

JSR A
Journal of Scientific Reports

cooling load is created by consuming energy for defrosting or by sending hot fluid from the outside to the cold room.

Defrost methods that can be applied in solid-state cooling systems of water vapors condensed on the cool surfaces (evaporator) of coolers; It can be classified as air (with fans), hot gas, electric resistance (resistance), water. The aqueous method is not very common. In practice, defrost methods with hot air fans, hot gas and electrical resistance are frequently used [2-12].

In industrial cooling systems, the heat is given to defrost during the defrosting process, the interruption of the cooling process causes heat to be stored on the ambient air and products. As these thermal loads are met, the compressor consumes more energy than it should be, increasing the energy consumption of the cooling system and thus the energy costs. The following practical approaches can be made in the selection of defrost methods.

Especially for positive cabinets with an ambient temperature above 0 ℃, air defrost can be preferred. In this method, when the compressor is stopped by the digital thermostat, the fans do not stop and defrost is performed with ambient air.

Hot gas defrost method can be preferred in cabinets with an ambient temperature of -10 ℃. However, in this method, a liquid trap should be added to the compressor return line to prevent the liquid refrigerant that will accumulate in the evaporator after defrosting.

In negative freezer cabinets with an ambient temperature of -18 ℃, hot gas may not be sufficient for defrosting and may become inefficient due to prolonged time. Therefore, in deep cooling applications, electric resistance defrosting should be preferred [13].

2.2. Theoretical Analysis

The amount of energy to be stored in the ice accumulated on the evaporator coil of the industrial cooler is calculated with the equation given below [14,15]:

$$Q = m_{ice.} . L \tag{1}$$

Evaporator capacity of the cooler can be calculated with the following equation:

$$\dot{Q}_e = \dot{m}_r . (h_1 - h_4) \tag{2}$$

The compressor power that will meet the cooling load in the industrial cooler and create the desired pressure difference in the cooling system can be determined with the following equation:

$$\dot{W}_c = \dot{m}_r . (h_2 - h_1) \tag{3}$$

Cooling coefficient of performance of the industrial refrigeration cycle [16,17]:

$$COP = \frac{\dot{Q}_e}{\dot{W}_c} \tag{4}$$

JSR A
Journal of Scientific Reports

Carnot coefficient of performance of the industrial refrigeration cycle can be calculated as below:

$$COP_{car} = \frac{T_L}{T_H - T_L} \tag{5}$$

The second law efficiency of the industrial cooling system can be found by the ratio of the coefficient of performance of cooling the system to the carnot coefficient of performance at the same conditions [18]:

$$\eta = \frac{COP}{COP_{car}} \tag{6}$$

Fan power to circulate the cool air blown through the evaporator [18]:

$$\dot{W}_f = \frac{\dot{V} \ . \ \Delta p}{\eta_f} \tag{7}$$

In calculating the total heat transfer coefficient in the evaporator, the Eq. (8) was created by taking into account the thermal resistances formed by the cooling fluid passing through the evaporator, the evaporator coil thickness, the ice increasing over time and the external air (Fig 3). Using this equation, the total transfer coefficient (U) can be calculated from the interior wall of the evaporator until ambient air is reached.

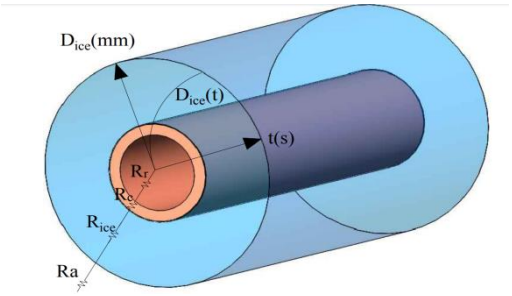

Figure 3. The icing on the evaporator and representation of the thermal resistance network.

$$\frac{1}{U.A} = \frac{1}{A\,.h_r} + \frac{ln\left(\frac{D_o}{D_i}\right)}{2.\pi.l.k} + \frac{ln\left(\frac{\int_{t_i}^{t_s} D_{ice}(t)dt}{t\,.D_{ice\,i}}\right)}{2.\pi.l.k_{ice}} + \frac{1}{A.h_{air}} \tag{8}$$

The logarithmic temperature difference can be calculated with the following equation [15]:

$$\Delta T_{ln} = \frac{\Delta T_1 - \Delta T_2}{\ln\left(\frac{\Delta T_1}{\Delta T_2}\right)} \tag{9}$$

The equation used in determining the amount of heat extracted from the air per unit time with the evaporator is given below [15]:

JSR A
Journal of Scientific Reports

$$\dot{Q}_e = U.A.[\Delta T_{ln}] \quad (10)$$

3. RESULTS AND DISCUSSIONS

In the experimental setup shown in Figure 2 within the scope of TS EN ISO 23953-2 standard, the air defrost process was observed and tested 8 times. During the experiment, average air temperature and relative humidity values of the test room were measured as 25 ℃±1℃ and 60%±0.02%, respectively. Despite this measured temperature and relative humidity, the dew thermometer temperature was found to be 16.7 ℃ from the psychrometric diagram. This value indicated that the air with the measured conditions could create dehumidification on the surface where the water in the air hit when it hit a surface with a temperature of 16.7 ℃ or lower.

The variation of the evaporator inlet and outlet air temperature over time is shown in Figure 4. In the system, the change in the instantaneous power consumption of the compressor until the first defrost time is given in Figure 5, and the time-dependent change of the refrigerant's evaporator inlet temperature is given in Figure 6. As seen in Figure 4, the evaporator surface was below the dew point temperature with a temperature of 10.19℃ from the beginning, so dehumidification started on the surface. Despite the condensation of water, it is seen in Figure 7 that the formation of ice occurred after the evaporator surface temperature dropped below the freezing temperature of the water as a result of a 2-minute period in the experiment.

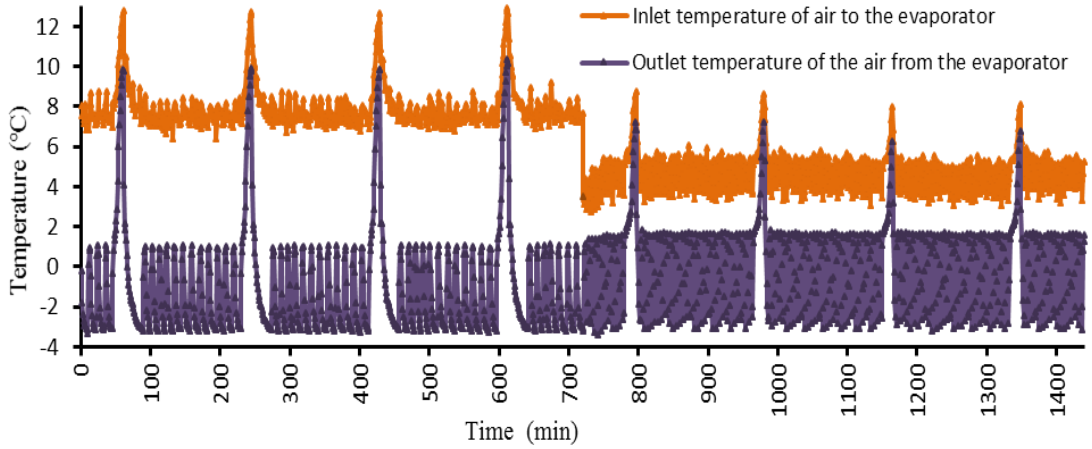

Figure 4. The variation of evaporator inlet and outlet air temperature over time.

As can be seen in Figure 4, the air passing through the evaporator has been subjected to temperature fluctuations caused by the start-stop of the compressor by controlling of the cooling system set temperature value. The effect of increased thermal resistance caused by ice formation in the experiment is understood by the increase in the temperature of the evaporator outlet air at the end of each cooling period. However, since the increased ice thickness on the evaporator surface could decrease the cross-sectional area where the air passed, it could increase the differential pressure in the airflow.

JSR A
Journal of Scientific Reports

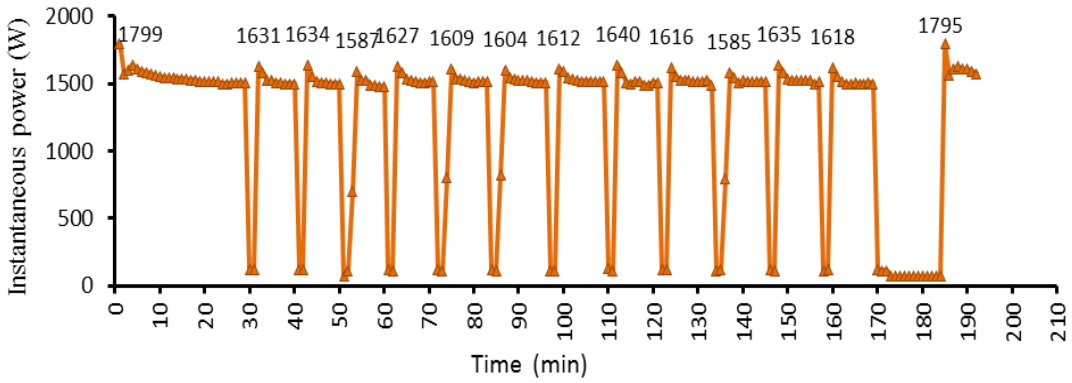

Figure 5. The change in the instantaneous power consumption of the compressor during the first defrost period.

Increased temperatures of the products during defrost require more cooling power due to the increased temperatures. For this reason, as seen in Figure 5, after the defrosting of the compressor, it peaked in the power consumption at 185 minutes to meet the cooling load.

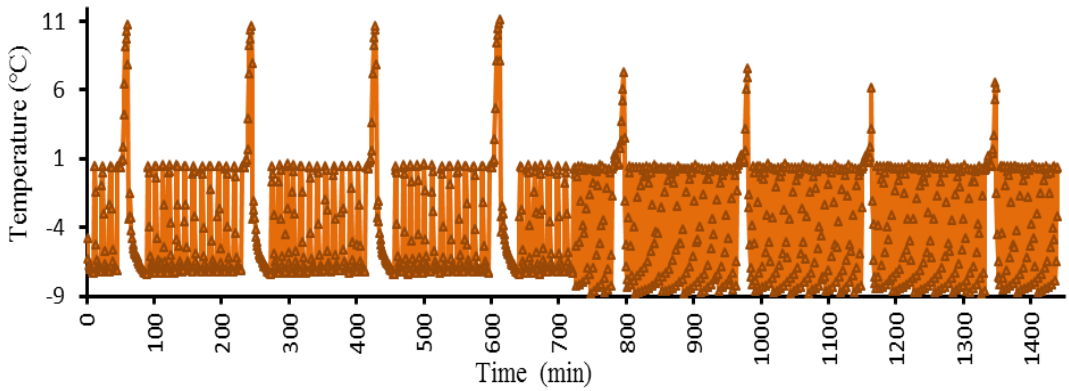

Figure 6. Time-dependent change of refrigerant temperature entering the evaporator.

It is noteworthy that in Figure 6 and Figure 7, where the inlet and outlet temperature values of the evaporator surface are given, the formation of ice on the evaporator surface increased rapidly as the temperature drops to -6 ℃ within a period of 10 minutes after the first defrost operation. The heat conduction coefficient of ice was low compared to the heat conduction coefficient of the material used in the evaporator. For this reason, it is known that the formation of ice, which increases the thickness of the surface over time, will be negatively affected by reducing the total heat transfer.

JSR A
Journal of Scientific Reports

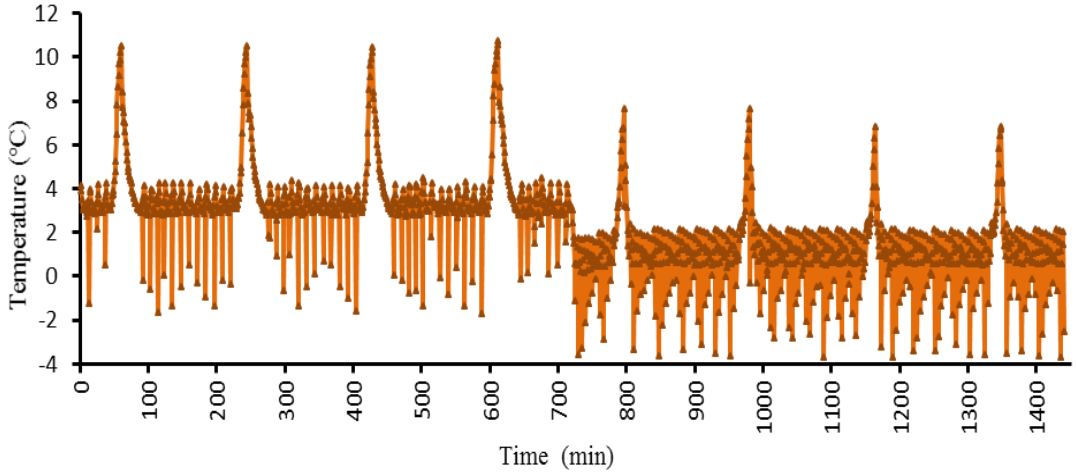

Figure 7. Time dependent change of refrigerant outlet temperature from evaporator.

In the experiment, package temperatures of 48 products, which were located in different compartments of the industrial cooler, were measured with thermocouples. As a result of these measurements, the average temperature values of the products in the left, middle and right compartments were calculated as 2.92℃, 2.74℃ and 2.34℃, respectively. As can be seen in Figure 8, it is observed that the temperature values of the products in different compartments in the industrial cooler increased overtime during the defrosting process and then decreased again. This temperature change was measured as an average 3.07 ℃ on products.

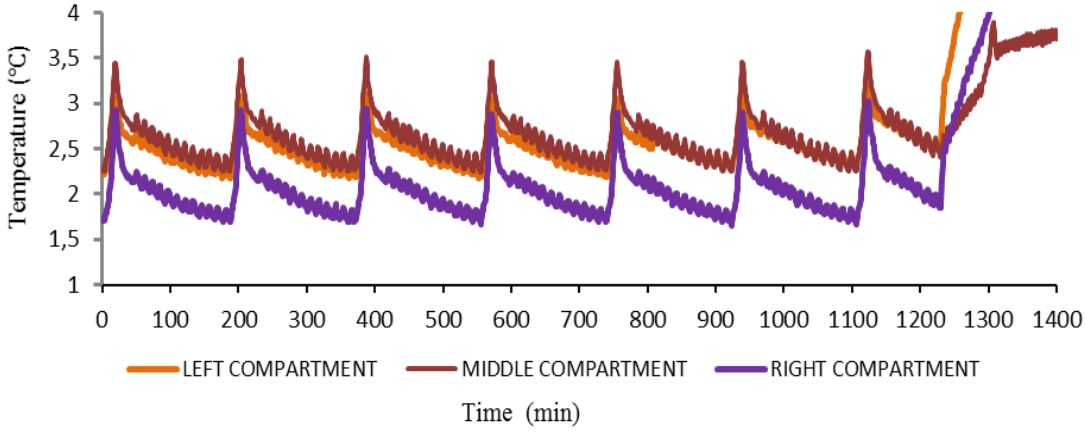

Figure 8. Variations of the temperature values of the products placed in the industrial cooler over time.

Increasing power consumption after defrost operations can be seen in Figure 9 whereas COP value decreases as seen in Figure 10. When Figure 9 and Figure 10 are examined in more detail, it is seen that the power consumption and COP values change with each defrosts operation compared to the

JSR A
Journal of Scientific Reports

previous defrost operation. The reason for this is thought to be the most appropriate defrost time not being achieved in every defrost period.

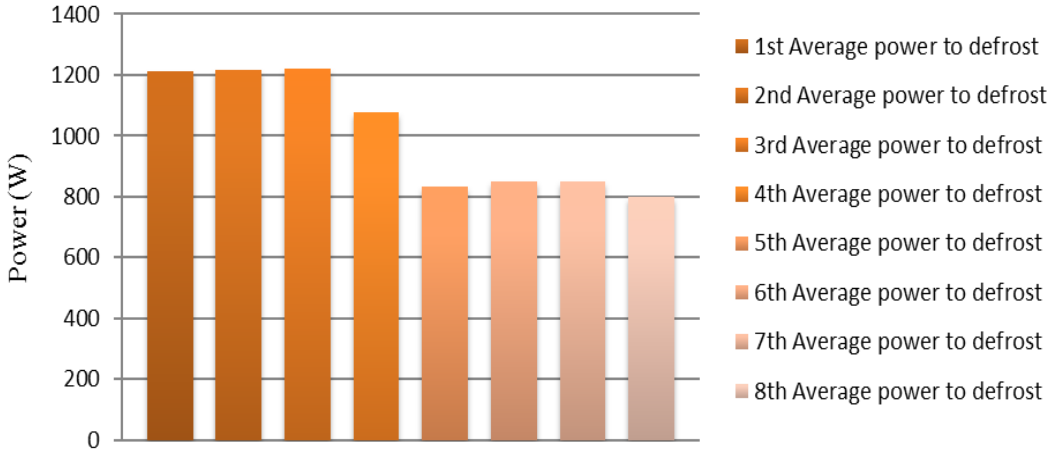

Figure 9. Average power values calculated after each defrost.

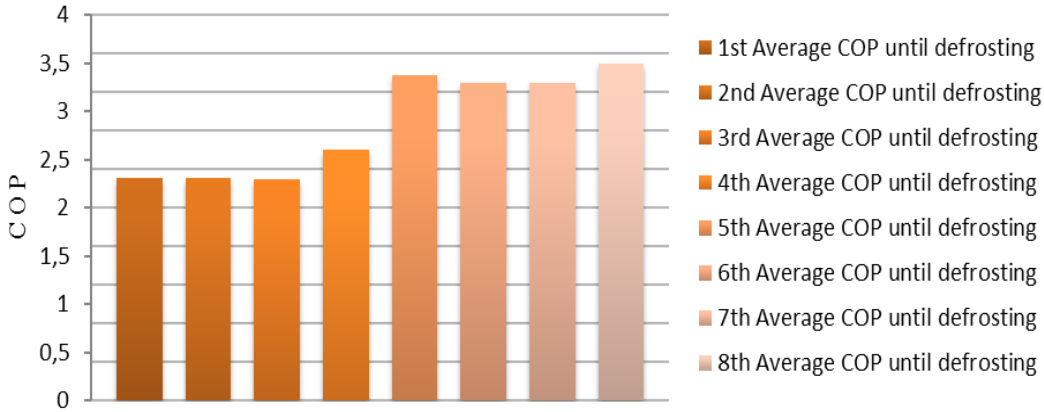

Figure 10. Variations of COP values calculated after each defrost time.

In Figure 9, when the power value of the cooling system is evaluated an increase in the average power consumption is observed after the first defrost operations. This situation was caused by a 15-minutes interruption of cooling with the defrosting process; however, unmet heat gains during defrosting could be caused. It was observed that there was an increase in power value in the parts up to the fourth defrost operation of the compressor while a decrease in power value was seen in the final defrost operations. In the scope of TS EN ISO 23953-2standard, this, situation was caused that in the experimental setup, the first 12 hours of lighting and night curtains remained open, and in the next 12 hours, the power value of the system decreased as a result of closing the night curtain and lighting. Considering the changing values in the power value of the cooling system, as shown in Figure 10, the coefficient of performance of the system was affected by this change.

4. CONCLUSION

In this study, an industrial refrigerant using R-290 refrigerant and air defrost method has been designed, manufactured and tested. It is aimed to obtain findings that will shed light on researchers and manufacturers by analyzing the effect of defrosting on cooling performance and on refrigerated products. As a result of the temperature measurements taken from 48 points on the experimental setup, the average temperature values of the cooled products in the left, middle and right compartments are 2.92 ℃, 2.74 ℃ and 2.34 ℃, respectively, and the average product temperature is 2.664 ℃. From the test data, an average of 3.07 ℃ changes in the temperature of the products cooled during the defrosting process was observed. Eight defrost operations were performed during the system operation, and the COP values calculated before each defrost operation were found as 2.13, 2.31, 2.30, 2.29, 2.60, 3.36, 3.29, 3.30, 3.49, respectively. In the designed and tested system, the products cooled in terms of the cooling technique of the defrosting process measured the highest temperature of 4.22℃ and the lowest 2.02℃ in the products during the experiment, and the results were found to comply with the TS EN ISO 23953-2 standard M1 class. The suggestions given below can be presented regarding the air defrost process.

- Despite the changing ambient conditions in cooling systems, performing defrosting at the appropriate defrost time will increase the COP value of the cooling system while reducing energy consumption. Intelligent systems that can determine the defrost time according to the conditions of the defrost application in the cooling system will increase the performance of the cooling system.

- Energy efficiency can be achieved for defrosting by using the heat delivered in the condenser to the environment with the usage of this heat during defrost. Evaporator design is important for the melting of ice and the flow of air. With its vertical or horizontal positioning the design of the evaporator coil can significantly affect the heat transfer, which will shorten the defrost time. In future studies, more effective defrost methods can be developed instead of stopping the compressor during defrost.

ACKNOWLEDGEMENTS

We would like to thank Nurdil Teknik Cooling Inc. for its contributions to this work.

REFERENCES

[1] Qu, M., Xia, L., Deng, S., & Jiang, Y. (2012). An experimental investigation on reverse-cycle defrosting performance for an air source heat pump using an electronic expansion valve. Applied Energy, 97, 327–333.

[2] Kwak, K. and Bai, C., (2010), A study on the performance enhancement of heat pump using electric heater under the frosting condition: Heat pump under frosting condition, Applied Thermal Engineering, 30(6-7), 539–543.

[3] Zhu, J.H., Sun, Y.Y., Wang, W., Deng, S.M., Ge, Y.J. and Li, L.T., (2015), Developing a new frosting map to guide defrosting control for air-source heat pump units, Applied Thermal Engineering, 90, 782-791.

[4] Guo, X.M., Chen, Y.G., Wang, W.H. and Chen, C.Z, (2008), Experimental study on frost growth and dynamic performance of air source heat pump system, Applied Thermal Engineering, 28 (17-18), 2267–2278.

[5] Wang, W., Zhang, S., Li, Z., Sun, Y., Deng, S. and Wu, X., (2019), Determination of the optimal defrosting initiating time point for an ASHP unit based on the minimum loss coefficient in the nominal output heating energy, Energy, 191, 116505.

[6] Hewitta, N. and Huang, M.J., (2008), Defrost cycle performance for a circular shape evaporator air source heat pump, International Journal of Refrigeration, 31, 444–452.

[7] Byun, J.S., Lee, J. and Jeon, C.D., (2008), Frost retardation of an air-source heat pump by the hot gas bypass method, International Journal of Refrigeration, 31, 328–334.

[8] Egelandsdal, B., Abie, S.M., Bjarnadottir, S., Zhu, H., Kolstad, H., Bjerke, F., Martinsen, O.G., Mason. A. and Münch, D., (2019), Detectability of the degree of freeze damage in meat depends on analytic-tool selection. Meat Science, 152, 8-19.

[9] Long, Z., Jiankai, D., Yiqiang, J. and Yang, Y., (2014), A novel defrosting method using heat energy dissipated by the compressor of an air source heat pump, Applied Energy, 133, 101–111.

[10] Liu, Z., Li, A., Wang, Q., Chi, Y. and Zhang, L., (2017), Experimental study on a new type of thermal storage defrosting system for frost-free household refrigerators, Applied Thermal Engineering, 118, 256–265.

[11] Song, M., Pan, D., Li, N. and Deng, S., (2015), An experimental study on the negative effects of downwards flow of the melted frost over a multi-circuit outdoor coil in an air source heat pump during reverse cycle defrosting, Applied Energy, 138, 598–604.

[12] Mengjie, S., Deng, S., Pan, D. and Ning, M., (2014), An experimental study on the effects of downwards flowing of melted frost over a vertical multi-circuit outdoor coil in an air source heat pump on defrosting performance during reverse cycle defrosting, Applied Thermal Engineering, 67(1-2), 258–265.

[13] Green T, Luckmann E, The secret behind danfoss adaptive defrost (BE327320541044en-000101). Danfoss: 2020.

[14] Aktaş, M., Koşan, M., Arslan, E. and Tuncer, A.D., (2019), Designing a novel solar-assisted heat pump system with modification of a thermal energy storage unit, Proc IMechE Part A: J Power and Energy, 233(5): 588-603.

[15] Tuncer, A.D., Mavuş, R., Gökçe, C., Koşan, M. and Aktaş, M., (2019), Efficient Energy Systems Models for Sustainable Food Processing, Turkish Journal of Agriculture: Food Science and Technology, 7, 1138-1145.

[16] Koşan, M., Demirtaş, M., Aktaş, M. and Dişli, E., (2020), Performance analyses of sustainable PV/T assisted heat pump drying system, Solar Energy, 199: 657-672.

[17] Caner, M., Duman, N., Buyruk, E. and Kılınç F., (2019), Performance Analysİs of Horizontal Ground Source Heat Pump System in Sıvas, Journal of Science and Technology of Dumlupinar University, 42, 47-53.

[18] Cengel, Y.A. and Boles, M.A., (2014), Thermodynamics: An Engineering Approach, McGraw-HillHigher Education.

NOMENCLATURE

Acronyms

ASHP	Air source heat pump
COP	Coefficient of Performance

Symbols

Q	Energy required to melt ice (kJ)
$\dot{Q}$	Evaporator capacity (kW)
m	Mass of melting ice (kg)
L	Latent heat of melting (kJ/kg)
$\dot{m}$	Refrigerant mass flow rate (kg/s)
$\dot{W}$	power input (kW)
T	temperature (^{o}C)
η	efficiency
$\dot{V}$	Volumetric flow rate of air (m^3/s)
Δp	Air side pressure drop across an evaporator (Pa)
RH	Relative humidity (%)
HP	Compressor discharge pressure (Pa)
LP	Compressor suction pressure (Pa)
U	Total heat transfer coefficient ($W/m^2.K$)
h	Heat transfer coefficient ($W/m^2.K$)
l	Serpantine length of evaporator condition (m)
t	Defrosting time (s)
ΔT	Temperature difference (^{o}C)
A	Area (m^2)
h	Enthalpy (kJ/kg)
k	Heat conduction coefficient (W/m.K)
D	Diameter (m)
R	Thermal resistance (W/m.K)

Subscripts

a	air
s	surface
lm	logarithmic mean
L	low
H	high

4	evaporator refrigerant inlet
1	evaporator refrigerant outlet or compressor refrigerant inlet
2	compressor refrigerant outlet
o	outer
i	inner
r	refrigerant
ice	ice formed in the evaporator$ice\ o$ ice outer diameter
$ice\ i$	ice inner diameter
c	compressor
e	evaporator
f	fan
car	carnot

Kütahya Dumlupınar University
Institute of Graduate Studies

Journal of Scientific
Reports-A
E-ISSN: 2687-6167
Number 45, December 2020

RESEARCH ARTICLE

EXPERIMENTAL ANALYSIS OF THE OUTPUT PERFORMANCE OF THE ABRASIVE EFFECT OF DUST ON PHOTOVOLTAIC CELLS

Hüseyin BENLİ[1,*], Mert GÜRTÜRK[2], Neslihan Koçdemir ERTÜRK[3]

[1]Technical Vocational School, Fırat University, 23119 Elazig, hbenli@firat.edu.tr,
ORCID:0000-0002-4057-8750
[2]Department of Energy Systems Engineering, Technology Faculty, Fırat University, 23119 Elazig, m.gurturk@gmail.com,
ORCID:0000-0003-0380-5704
[3]Department of Energy Systems Engineering, Technology Faculty, Fırat University, 23119 Elazig,
neslihan23kocdemir@hotmail.com, ORCID:0000-0003-4523-6984

Received Date: 24.08.2020 *Accepted Date: 23.12.2020*

ABSTRACT

This article presents an evaluation of the power-voltage (P-V) and I-V characteristics of PV cells after exposure to artificial dust spraying. The dusted cells and other clean cells have been to the tested, exposed to five different radiation ranges, and used a solar simulator. In the experiment, a solar simulator analyzer was used to define the PVs' electrical performance, meantime a Sandblasting Cabinet and Atomic Force Microscope were used to inspect the properties abrasive of the dust on the cells. A significant reduction in both I-V and P-V properties was observed when dust accumulation on the surface of photovoltaic solar cells was compared to the same parameters of the clean cells. The average yield loss rate of solar cells exposed to dust spraying has decreased by 5-25% compared to clean cells, considering the inclination angle of the cells.

Keywords: *Photovoltaic cell; dust effect; solar energy; dust spraying; renewable energy.*

1. INTRODUCTION

The solution to the world's energy deficit problem is in renewable energy sources, and it is an undoubted fact that these resources are sustainable and clean, when besides being used correctly and rationally. PV panels are now one of the most realistic, fast, and clean renewable energy sources accepted by many countries. The reason for the rapid growth of solar panels in many countries is the price reduction, ease of maintenance, and installation. Although Turkey is a developing country, with insufficient energy resources, and excessive energy consuming it is a country that entirely dependent on foreign energy sources. Based on Turkey's geological location and economic conditions solar energy has a significant market compared to other renewable energy sources. In 2017, 37% of Turkey's electricity production obtained from natural gas, 33% from coal, 20% from hydraulic energy, 6% from wind, 2% from geothermal energy, and 2% from other sources. Turkey's energy consumption and production are approximately equal to each other. In 2017, consumption was 294.9 billion kWh and electricity generation was 295.5 billion kWh. As of the end of June 2018, the total installed capacity of the PV solar power plant is 4,726 MW. All sources except renewable energy sources, including solar, biomass, and wind, for example, hydro (dam) and geothermal resources are

completely in use. The last established power cycle plants are natural gas conversion plants, fed by Iran and Russia. The country almost pays 40% of its total exports for energy. Therefore, this situation makes it dependent on the neighbors. Currently, the government in power is trying to increase the diversity of energy and increase the rate of clean and renewable energy [1].for this reason, besides the construction of two numbers 4800 MWe nuclear power plants, it also aims to increase the use of wind and PV potential.

In recent years, very detailed and sensitive researches on the effect on PV modules have been conducted on dust accumulation [2–4]. Gholami et al. [5] examined the factors that constituted the accumulation of dust and the decrease in power loss in PV panel applications. Gholami et al. [6] have shown that the accumulation of dust on the panel in an arid environment for 70 days was 6,0986 g/m^2 and this deposition caused a power reduction of 21.47% in Tehran, Iran. The factors affecting the accumulation of dust were investigated to research the PV performance effect of dust accumulation. Fountoukis et al. [7] have shown that decreasing the atmospheric pollution value, for example, decreasing the density of the particulate matter, decreased the PV energy losses in Doha, Qatar for a year, Saidan et al. [8] have investigated the loss of efficiency due to dust accumulation on PVs, daily, weekly and monthly in Baghdad, Iraq. Dust accumulation resulted in a decrease in the yield of PV at 6.24%, 11.8%, and 18.74%. Al Shehri et al. [9] have investigated the effect of dust accumulation on solar panels in an environment where dust and sandstorms are common in a dry climate where solar radiation is highest. They have shown that cleaning with using nylon brushes, as a different cleaning method is not effective when compared to water and fine cleaning. They showed that the nylon brushes did not provide adequate cleaning. Mehmood et al. [10] have shown that the accumulation of dust and mud in a damp environment negatively affects the optical, tissue, and mechanical properties of PVs. Researchers showed the morphological and elemental analysis of total dust and examined the micro-level adhesion forces between protective transparent substrates and dust particles. Jiang et al. [4] have created considering the wind cleaning process, building a more accurate model to estimate energy output for PV modules due to accumulated dust. Lu and Zhao, [11] have conducted a numerical study to investigate the dust accumulation on a PV system and its effect. They carried out their work using experimental and fluid dynamics simulation. Menoufi et al. [12] have studied the electrical performance of PV panels exposed to artificial dust in Nile, Egypt. Ahmed and Mohammed, [13] have investigated the thermal and electrical performance of the dust on a hybrid solar collector. They investigated the effects of the dust particles of different sizes, the amounts of different released dust particles, and the effects of gravitational force based on the dust accumulation rate on PV panels. Fountoukis et al. [14] have investigated both the modeling and experimental study of dust accumulation of the loss of energy efficiency in PV panels in a dry climate. Lay-Ekuakille et al. [15] have studied the possibility of modeling and experimental efficiency by using the relevant parameters which allow the deposition of dust and pollutant on the PV panels. Mejia et al. [16] have investigated the efficiency losses between concentrated solar power and flat PV due to dust accumulation. They showed that CPV caused losses greater than flat PV due to contamination. They calculated that this loss was 71%. Tanesab et al. [17] have investigated the seasonal effects of dust on the performance of PV panels in two different climate zones, Perth, Western Australia, and tropical climate zone Teygana Timur (NTT) Indonesia. Wang et al. [18] have shown that dust accumulation in PV modules is dependent on environmental and weather conditions, resulting in a decrease in energy production over time.

As mentioned above, many types of researchers describe how the dust factor that accumulated on the photovoltaic panels affects the yield. In this study, it was investigated how the dust particles in high

JSR A
Journal of Scientific Reports

wind velocities adhered to the cells, and the damage on the cell surface affected the P-V and I-V values in PV cells. The cells were tested at different tilt angles and measurements were made. For the homogeneous and balanced distribution of dust particles in the cells used in the experiments, a sandblasting device was used in particular. As a result of the experiments, it was found that the sand particles caused a significant decrease in the efficiency at high tilt angle values with the impact effect. A special device used for cleaning metal parts was used to ensure homogenous sandblasting in PV cells during operation. The device used for this purpose is the SK-1400 product of SAYKAR company, (www. saykar.net). The cells placed in the device were kept at 20^0,30^0,40^0,50^0,60^0,70^0,80^0 and 90^0 tilt angles and were sprayed fine glass sand for two minutes. The material used in the air pressurized sandblasting systems is grade C, 310-400-micron glass grit particles. Photographs of the sandblasting Cabinet (SK-1400) are given in Figure 1.

Figure 1.Sandblasting Cabinets (SK 1000) Saykar.net.

2. EXPERIMENTAL PROCEDURE

There are four methods commonly used to clean the surface of the solar panel: natural, mechanical, electromechanical, and electrostatic. Further research and ideas are needed to reduce the negative impact of dust accumulation on PVs. In this study, the reason for using the sandblasting device to measure dust accumulation and its effect is that wood resins frequently encountered in this region of Turkey are adhered to the panels as a result of encountering dust and insects and carried away by the wind. It is a very demanding and long process to remove them. Dust last long in panels. The most precise and optimum form of calculating the abrasive effect of the dust sprayed on photovoltaic cells is to design an experiment in which the dust particles adhered regularly. Then the process performed, the power output of the cells (directly exposed to the glass sand spray) was measured. The power output was then compared with similar clean (dust-free) cells for comparison. The photographing of the cells after sand spraying was done by Atomic Force Microscopy. The photographs are given in Figure 2.

JSR A
Journal of Scientific Reports

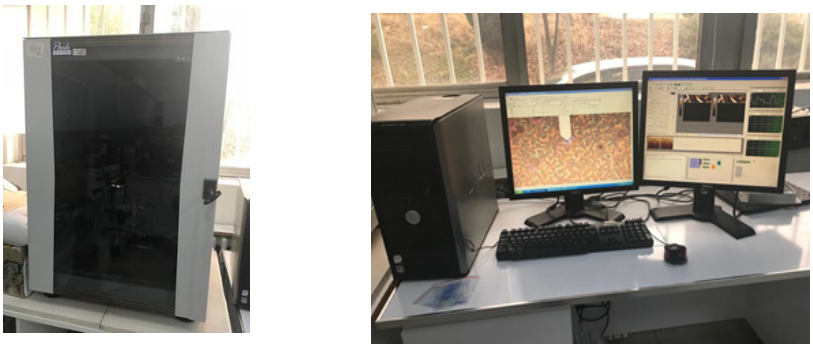

Figure 2 Atomic Force Microscope XE-100E (Park System).

To perform measurements under outdoor actual test conditions, a solar analyzer "Model 4200-SCS" is used. The model of the device manufactured and marketed by Keithley Company is 4200-SCS. A photograph of the solar analyzer is given in Figure 3. Detailed information about the solar simulator is given in ref. [19], (www.keithley.com) is used which allows to trail the P-V and I-V curves and let the main parameters of the PV cell: Short circuit current (I_{sc}), Fill Factor (FF), Maximum power ($P_{\max}$), Open circuit voltage (V_{oc}), and $I_{\max}$ $V_{\max}$ respectively.

The basic equations used in this experimental study are as follows [20]:

$$I = I_{pv} - I_0\left(\exp\left(\frac{q\left(V + IR_s\right)}{akT}\right) - 1\right) \tag{1}$$

$$V_{oc} = \left(a\frac{kT}{q}\right)\ln\left(\frac{I_{sc}}{I_0}\right) \tag{2}$$

Based on the I-V curve constituted by Eqs. (1) and (2), $P_{\max}$, V_{oc} and I_{sc} were composed and then filling factor (FF) can be calculated using the following equations 3 and 4 [20].

$$P_{\max} = V_{oc} I_{sc} FF \tag{3}$$

$$FF = \frac{I_{\max} V_{\max}}{I_{sc} V_{oc}} \tag{4}$$

Studies were performed five different solar radiations which are 200-400-600-800-1000 W/m^2.

JSR A
Journal of Scientific Reports

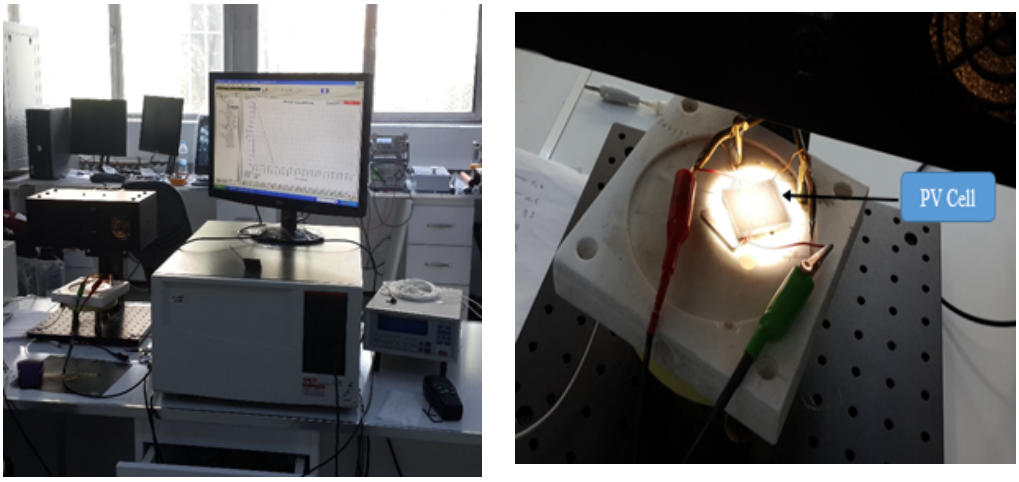

Figure 3 Solar simulator and experiment of PV cell.

2.1. Properties of Dust Used in Spraying

Glass sand is also known as glass grit or glass powder in the market. It is more suitable to be used at air pressurized sandblasting systems. Glass Sand, which is used in applications, is made of 100% consumer post, recycled bottle glass. Glass Sand has very low particles, giving a whiter, cleaner result in the applications using. The cornered particles in the crushed glass allow a thrusting surface profile to be formed and to remove coatings such as paint, alkyds, epoxy, polyurea vinyl, elastomers, and coal tar. Table 1 shows the physical and chemical properties of the glass sand. The photograph of the glass sand is given in Figure 4.

Table 1 Glass sand Physical and chemical characteristics.

GLASS SAND PHYSICAL CHARACTERISTICS	
Glass Sand - Specific Gravity	2,45 g/cm3
Glass Sand - Average Bulk Density	1,50 g/cm3
Glass Sand's Hardness	47 HRC
Glass Sand's Durability	Low
Glass Sand's Free Flow Feature	97 % minimum
Glass Sand's Moisture Absorption	High
Glass Sand's Radioactivity Characteristic	No
Glass Sand's Magnetic Characteristic	No
GLASS SAND CHEMICAL CHARACTERISTICS	
SiO2 >% 65	Glass Sand does not enter a reaction with oxygen.
Al2O3 : % 0,5-2	Glass Sand does not contain free silica.
CaO : %8-11	Glass Sand has inert structure.
MgO : % 3-5	Glass sand does not cause corrosion.

JSR A
Journal of Scientific Reports

Fe2O3 < % 0,2	Glass Sand is not flammable.
K2O < %1,5	Glass Sand does not contain cancerogenic substances.
Na2O : %13-15	
GLASS SAND ABRASIVE GRADES	
Grade C	310-400 micron glass grit particles

Figure 4 The view of glass sand.

3. RESULT AND DISCUSSION

Due to increasing oil prices and the high exchange rate, Turkey's energy production costs are constantly increasing. In January and December of 2018, the Turkish lira depreciated by about 58% against the US dollar. In recent days, electricity and natural gas usage prices have increased by about 50%. However, due to the rational use of renewable energy sources, a steady downward trend is observed in energy costs in many countries. The emergence of new firms and technologies in the production of PV panels and the increase in efficiency led to a decrease in costs and thus a significant increase in its use. The success of many countries in panel production has also made it easier to reach them. The same success was not achieved in the production of wind turbines. Because the production of wind turbines requires higher technology, which limits its use and production. The use of PVs which has a very high demand in our country, due to the increasing exchange rate and inflation since 2018, investments in this field have completely stopped except for previous investments. However, there is a rapid return to clean energy in the world, especially renewable energy.

As previously described, the power output of the cells varies depending on both the current and the voltage. The curves of the change and abrasive effect of sand spraying on PV cells, Figs. 5 and 6 are given. The abrasive effect of the dust on the cells was investigated in two separate sections (P-V and I-V).

3.1. Effect of Abrasive Effect of Dust on the Power output of PV Cell

As mentioned before, experiments were conducted using five different solar irradiance values; 200, 400, 600, 800, and 1000 W/m^2. Many researchers have shown that the accumulation of dust on PV panels is one of the most important reasons for the decrease in the power output that can be achieved. Power losses in PV cells were examined in two parts. Firstly, individual cells were measured, and then the cells having different properties were subjected to glass sand spraying in the sandblasting chamber. At low radiation intensities (200, 400 and 600 W/m^2) the power drop is very low, and the power drop at 800 and 1000 W/m^2 radiation values increases. This decrease is between 10-20%. The ratio of power output drop on cells 80^0,70^0 and 60^0 is carried out at a low rate. The reason for this is that as the angle of inclination becomes smaller, a portion of the sprayed glass sand cannot hold on to

JSR A
Journal of Scientific Reports

the cell. Consequently, it is a decrease in the amount of dust falling to a lower area. It should be remembered that each cell used before the experiments has different characteristics. The power output tilt angle of 40^0 and 50^0 is quite high, this loss which is between 10-20 percent.

As the tilt angle value increases, the power output is low except for a 90^0 angle of inclination. The power output value increases after 50^0 of the tilt angle because the accumulation of dust is more likely to accumulate in the lower part of the cells, and the cells do not have any contact with the sand sprayed in any amount. This is something to be expected. In each cell subjected to sand blasting, the spray gun is held upright. At low inclination angles, the amount of sand contacting the cell decreases. The power drop at the tilt angle of 20^0 was very low.

The reason for the further drop in this angle range is since sand spraying is concentrated in a restricted area. Briefly, the P-V curves vary considerably between before and after each cell. The P-V exchange curves were given before and after the experiment in Figure 5.

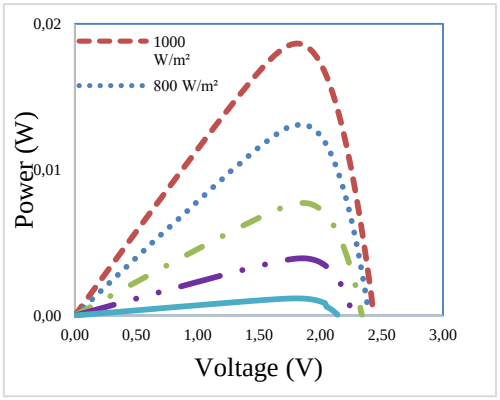

Non using dust spraying (Before 90^0)

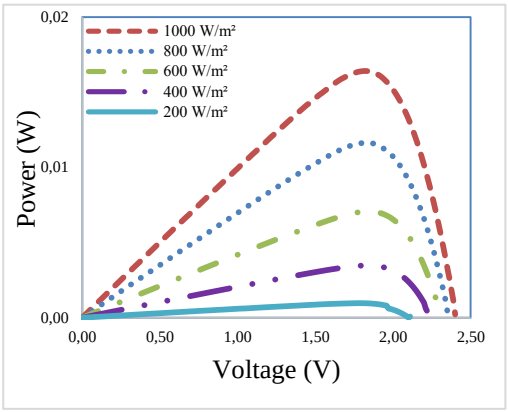

Using dust spraying (After 90^0)

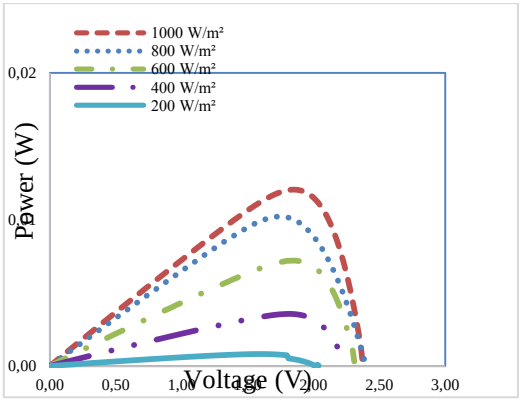

Non using dust spraying (Before 80^0)

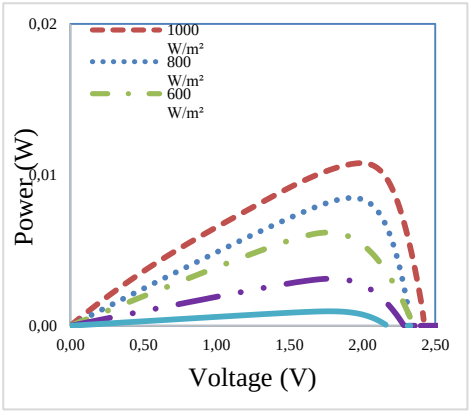

Using dust spraying (After 80^0)

JSR A
Journal of Scientific Reports

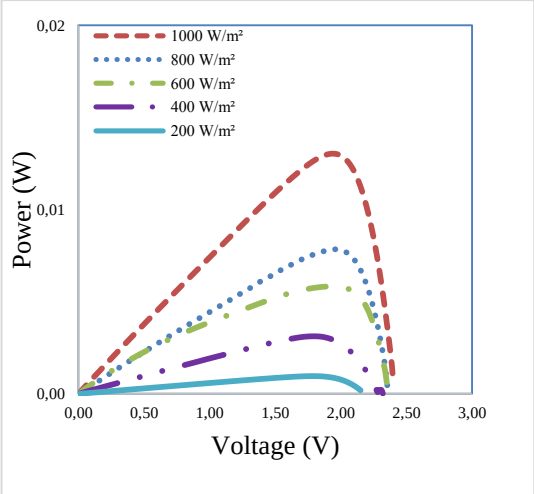

Non using dust spraying (Before 70^0)

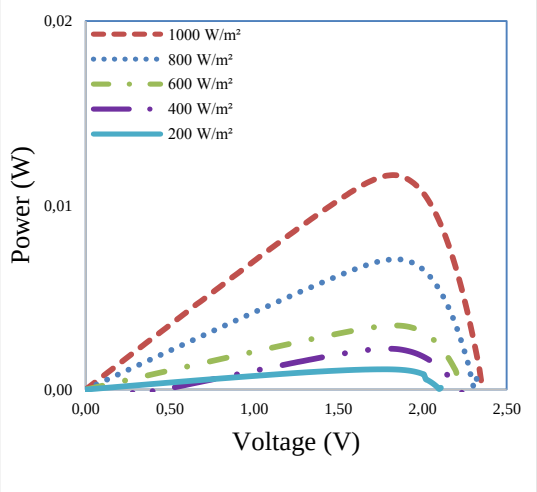

Using dust spraying (After 70^0)

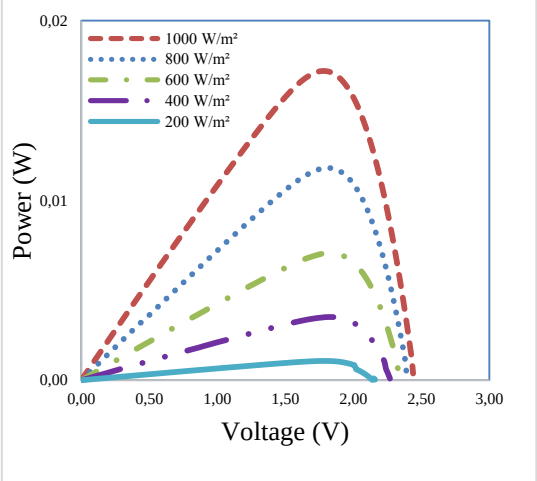

Non using dust spraying (Before 60^0)

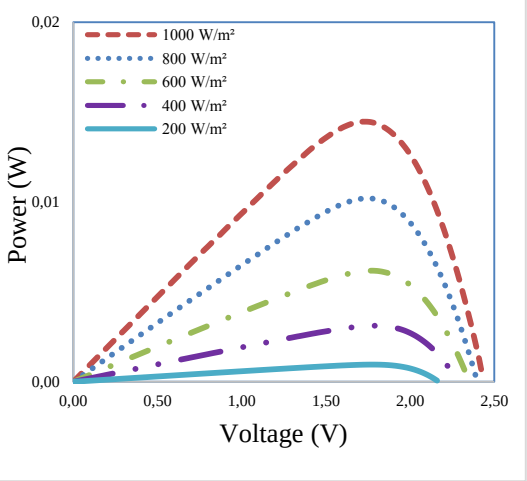

Using dust spraying (After 60^0)

JSR A
Journal of Scientific Reports

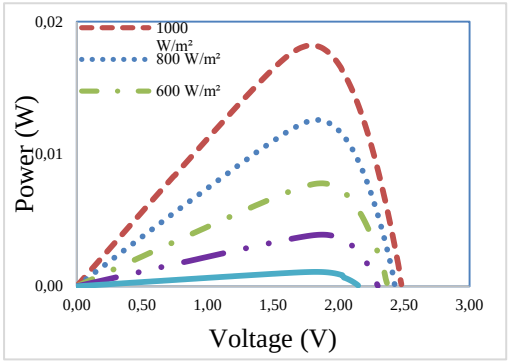

Non using dust spraying (Before 50^0)

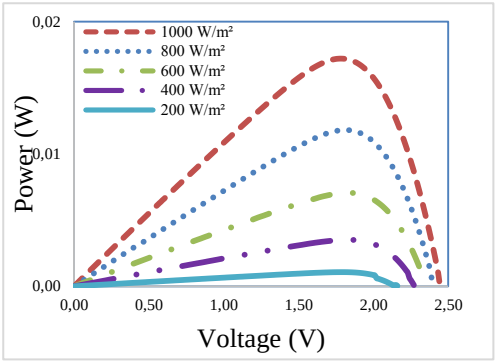

Using dust spraying (After 50^0)

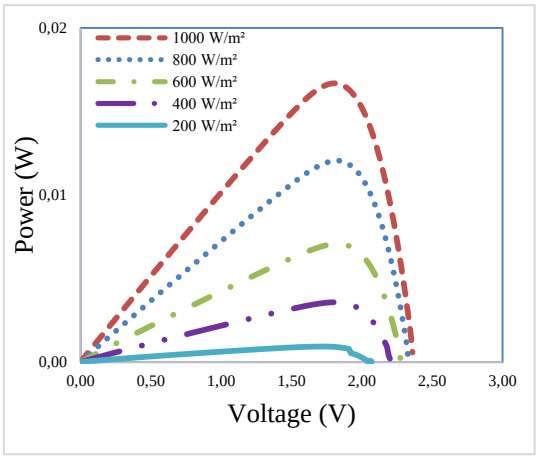

Non using dust spraying (Before 40^0)

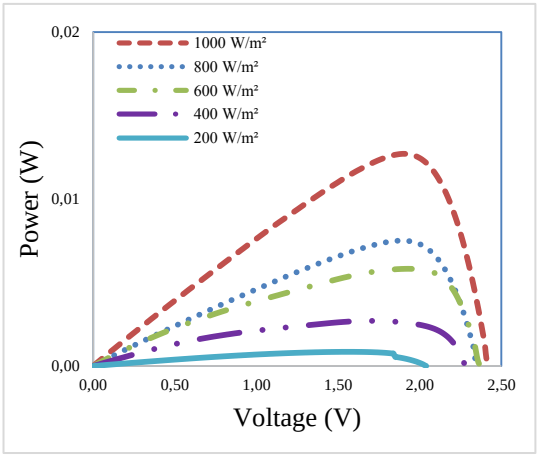

Using dust spraying (After 40^0)

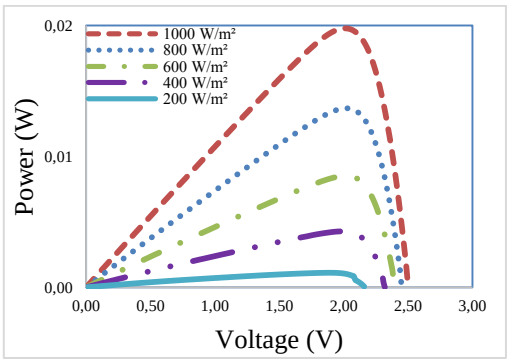

Non using dust spraying (Before 30^0)

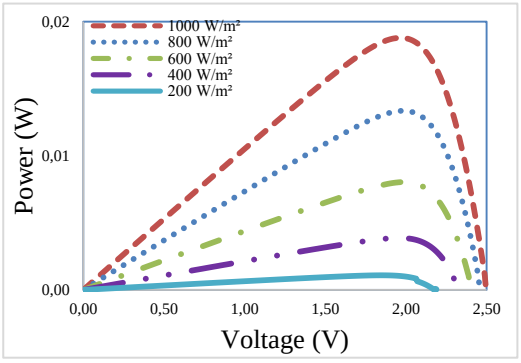

Using dust spraying (After 30^0)

JSR A
Journal of Scientific Reports

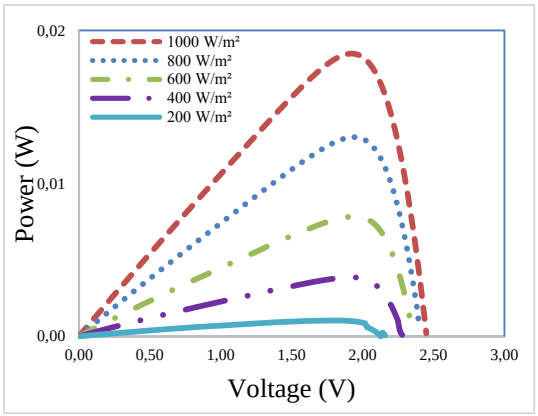

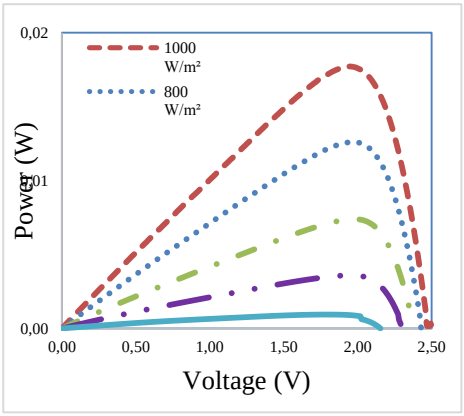

Non using dust spraying (Before 20^0)

Using dust spraying (After 20^0)

Figure 5 Change of P-V curves of dust spraying.

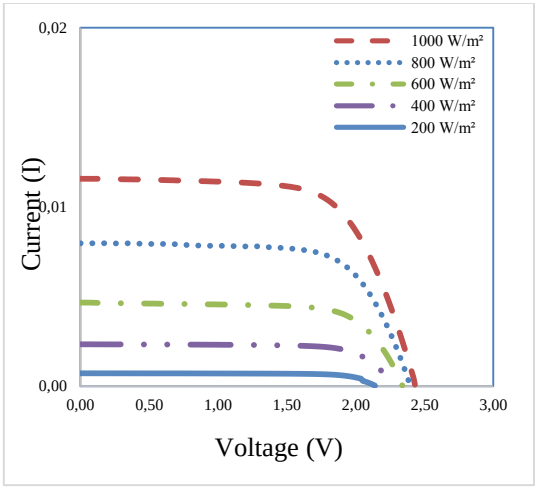

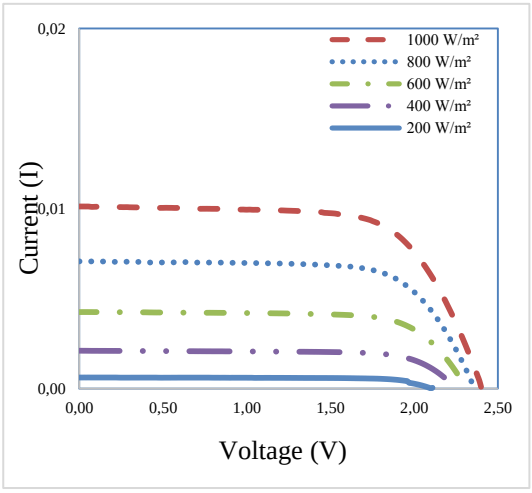

Non using dust spraying (Before 90^0)

Using dust spraying (After 90^0)

JSR A
Journal of Scientific Reports

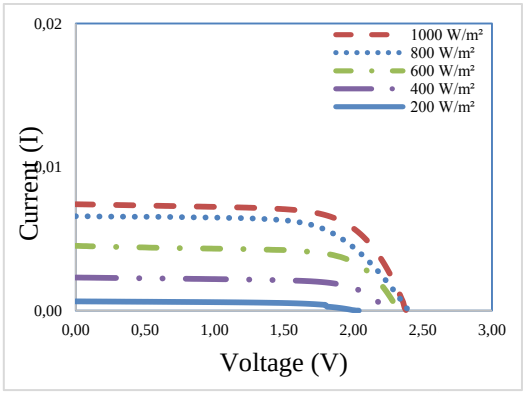

Non using dust spraying (Before 80^0)

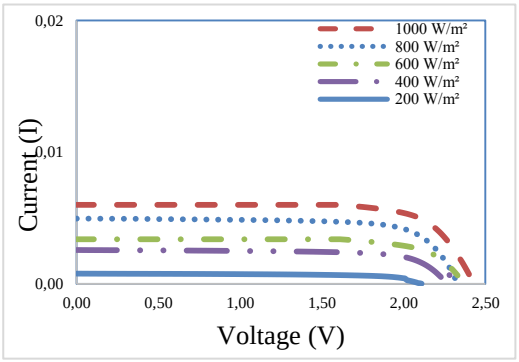

Using dust spraying (After 80^0)

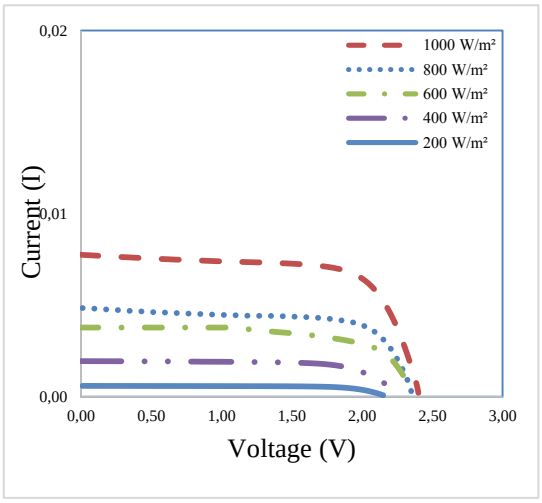

Non using dust spraying (Before 70^0)

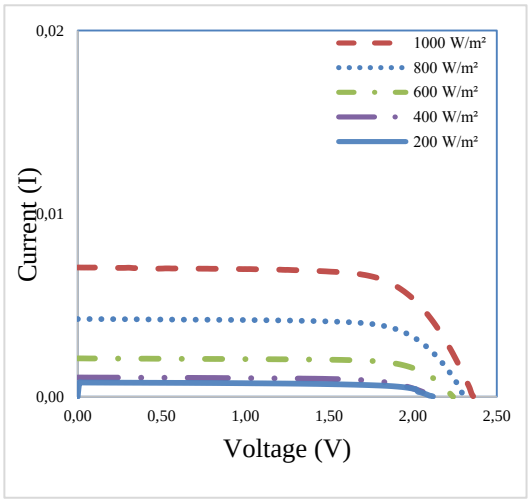

Using dust spraying (After 70^0)

JSR A
Journal of Scientific Reports

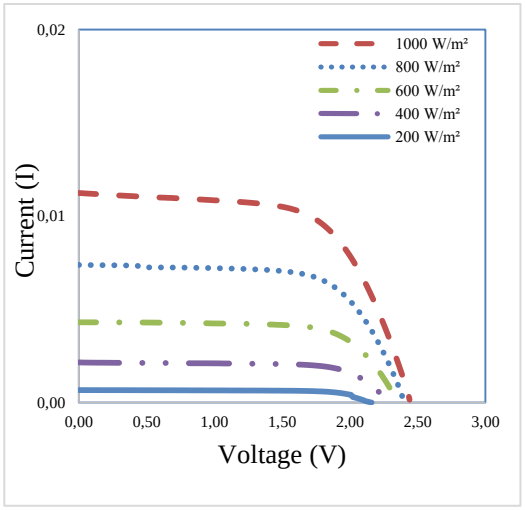

Non using dust spraying (Before 60^0)

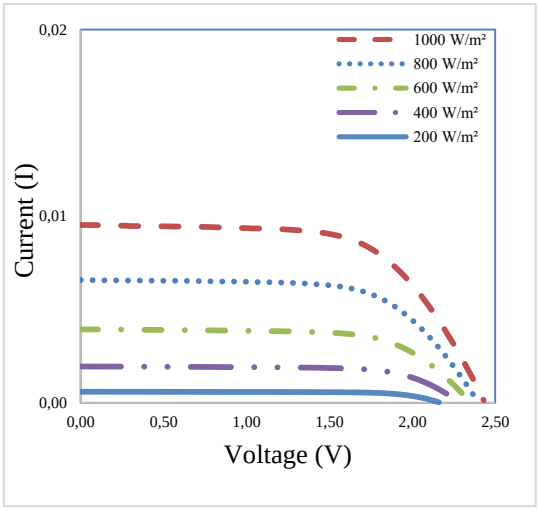

Using dust spraying (After 60^0)

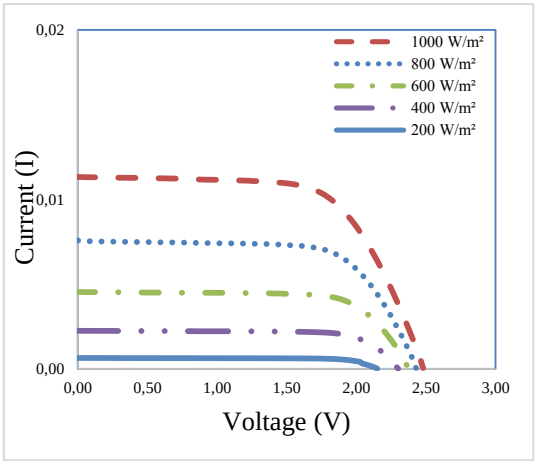

Non using dust spraying (Before 50^0)

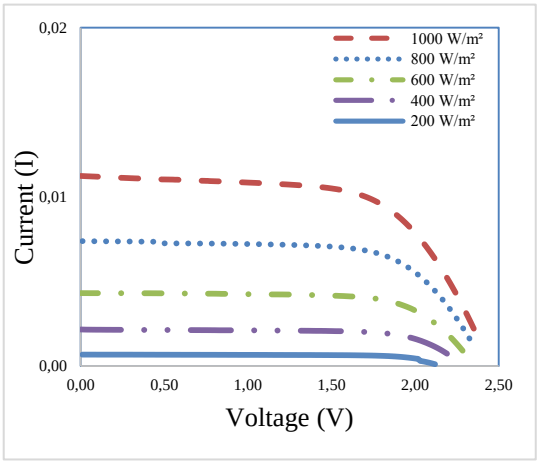

Using dust spraying (After 50^0)

JSR A
Journal of Scientific Reports

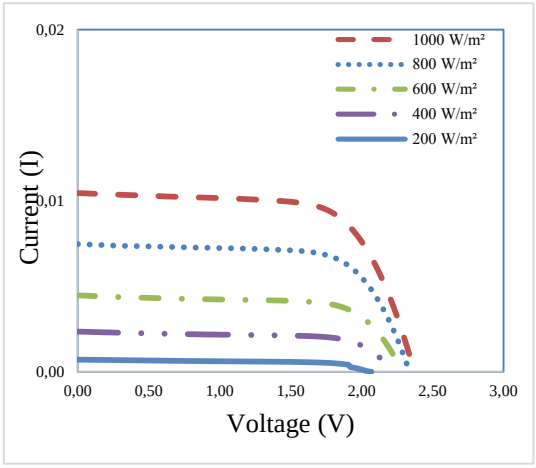

Non using dust spraying (Before 40^0)

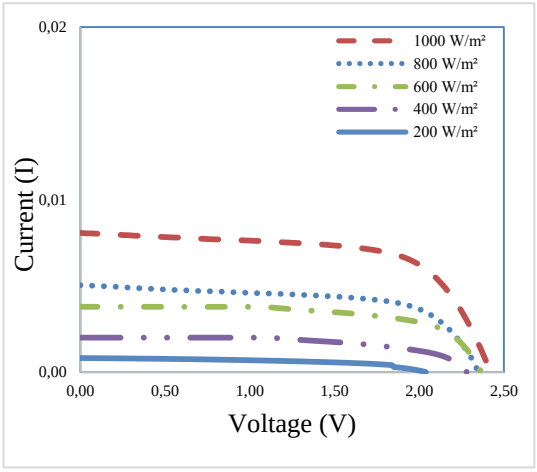

Using dust spraying (After 40^0)

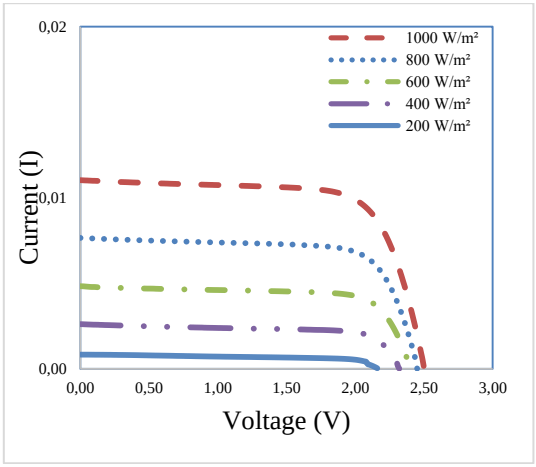

Non using dust spraying (Before 30^0)

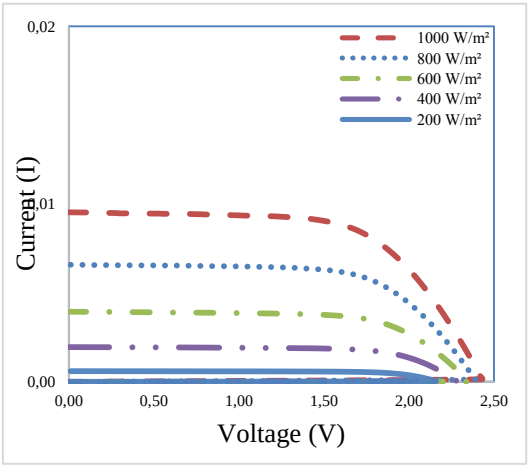

Using dust spraying (After 30^0)

JSR A
Journal of Scientific Reports

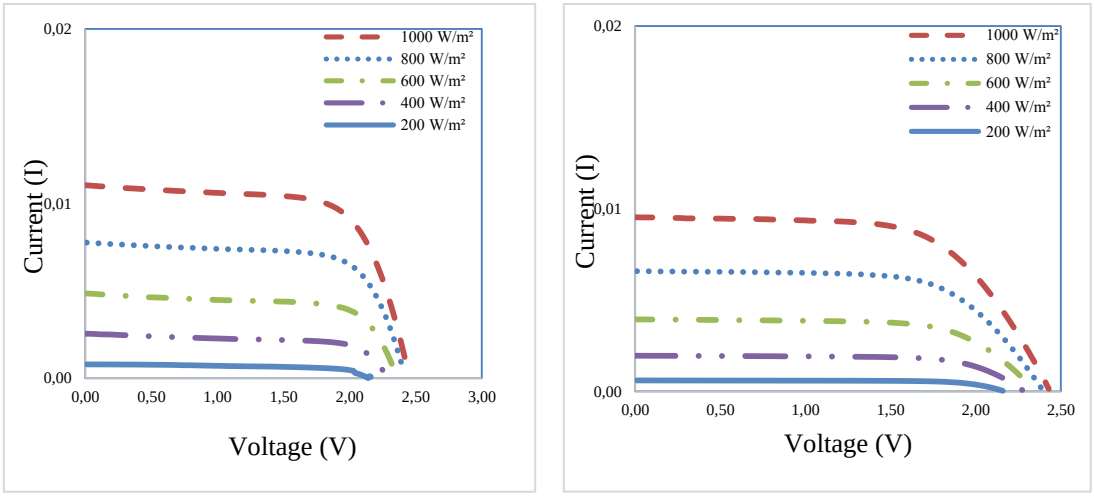

Non using dust spraying (Before 20^0)

Using dust spraying (After 20^0)

Figure 6. Change of I-V curves of dust spraying.

3.2. Effect of Abrasive Effect of Dust on I-V Characteristic of PV Cell

When the I-V curves are taken into consideration, the highest loss occurs similarly to the P-V curves. At low radiation intensities (200, 400 and 600 W/m^2), the reduction in I-V curves is very low, this change is between 0-10%, and this change is increased at 800 and 1000 W/m^2 radiation values, this change occurs 10-20 %. At the 80^0 and 70^0 tilt angles, a small reduction in I-V curves was observed in the low radiation values after sand blasting (200,400,600 W/ m^2). The I-V curves show a decrease in the radiation values of 800 to 1000 W/m^2 and this change varies between 5-15%. In the same way, the decreases in the 60^0 and 50^0 tilt angles in the I-V curves and the high radiation values (800 and 1000 W/m^2) are in the 5-15% range. The decrease in low irradiation values is very limited. The I-V exchange curves were given before and after the experiment in Figure 6. Two photographs of every one cell photographed by electron microscopy are given in Figure 7.

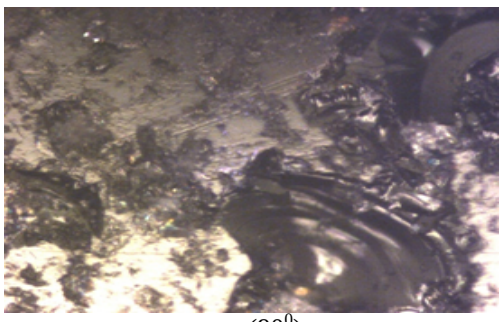

a (90^0)

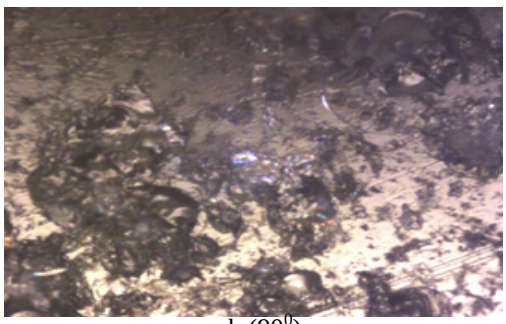

b (90^0)

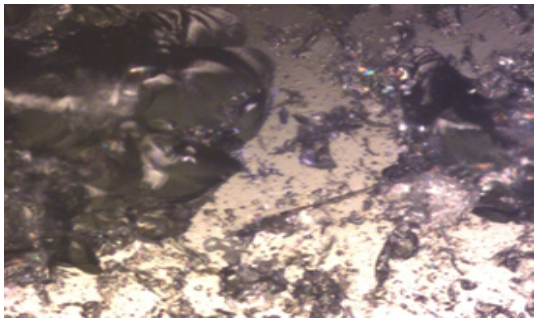

a (80^0)

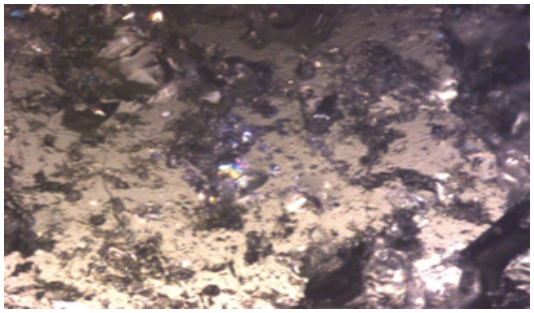

b (80^0)

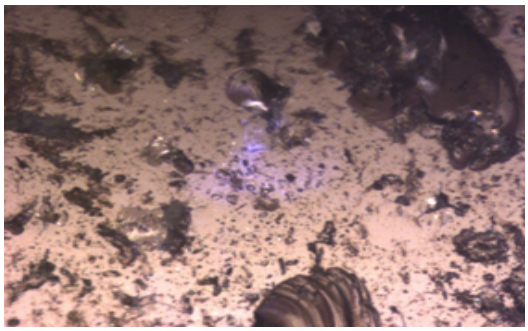

a (70^0)

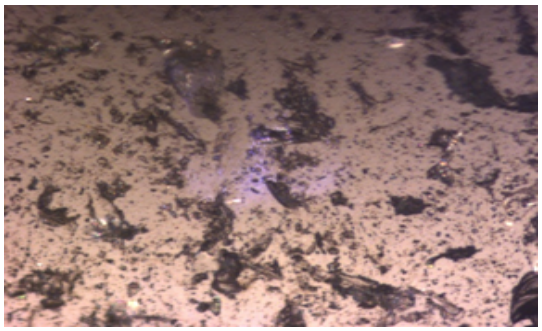

b (70^0)

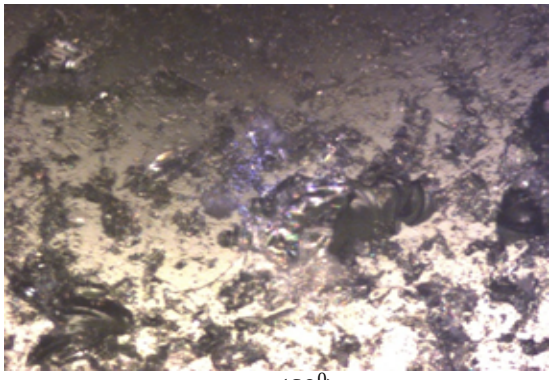

a (60^0)

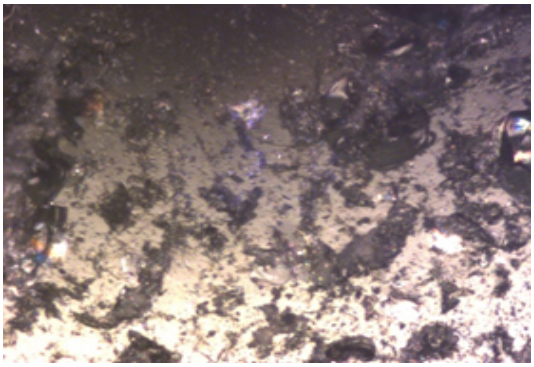

b (60^0)

JSR A
Journal of Scientific Reports

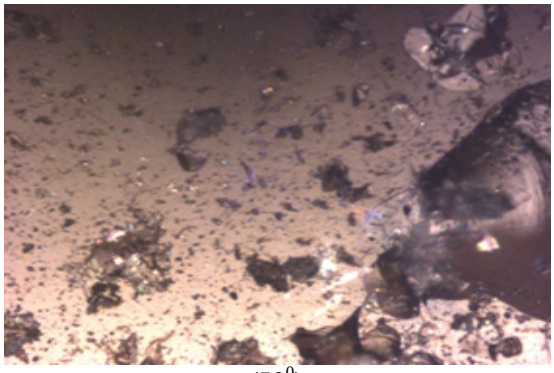

a (50^0)

b (50^0)

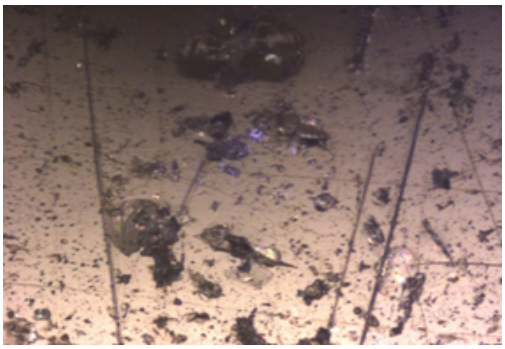

a (40^0)

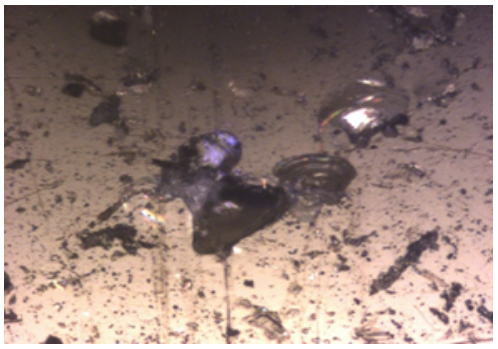

b (40^0)

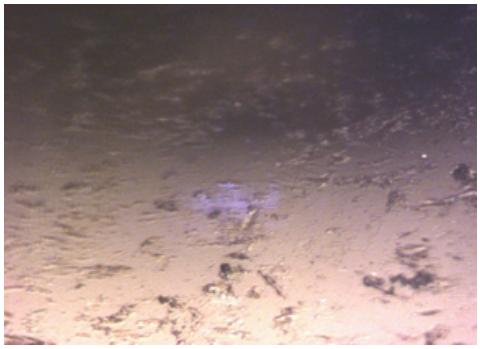

a (30^0)

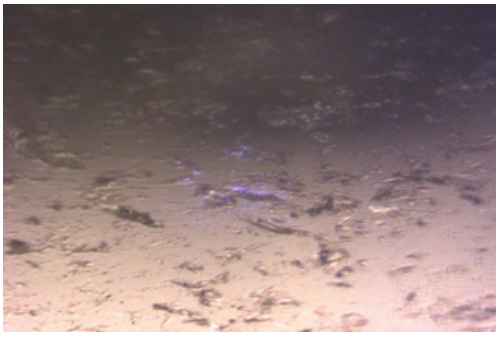

b (30^0)

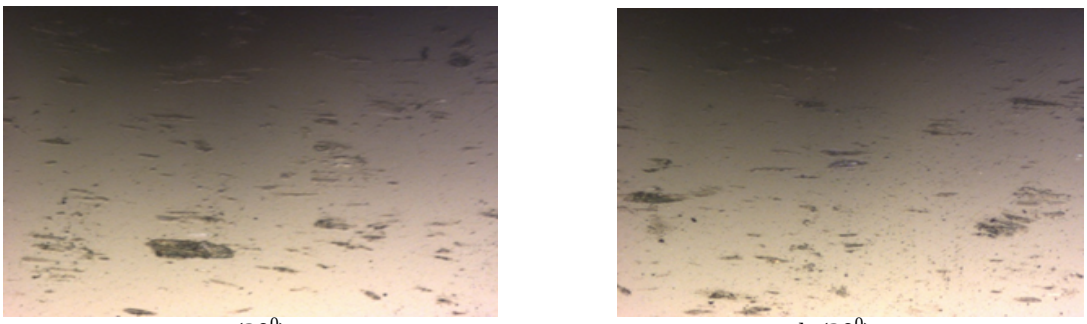

a (20^0) b (20^0)

Figure 7 The views of the cells after the dust spraying in different tilt angles.

4. CONCLUSIONS

The use of solar energy, known as the cleanest energy source in the world, contributes to the reduction of greenhouse gas emissions while at the same time meeting a significant part of the world's energy needs. The emergence of new, cheaper and more efficient products with PV panel technology is considered to be the most useful source for countries that have energy deficit problems. The frequent use of PV Panel technologies has brought many problems such as use, cleaning, maintenance, operation, and pollution. At present, the biggest problem experienced by many enterprises is the loss of power and efficiency due to pollution. Most of the recent studies are related to the identification and elimination of the factors causing these losses.

In this study on different tilt angles, the effect of dust spraying on the transmittance of PV cells have been investigated. Dust particles were uniform and in the same form, all of them being special sand with a spherical shape. In this study, the effects of dust spraying on the cells at different tilt angles were photographed by electron microscopy. It was also evident from the photographs and the results that the effect of the sprayed dust on the surface of the cells increased as the angle of inclination increased, and I-V and P-V curves decreased as a result.

These dust deposits indicate a deterioration of the panel surfaces and consequently prevent a certain part of the incoming solar radiation. In this study, the sands used was the same properties and the cells were subjected to real sand spraying at the determined angle values.

- At low radiation intensities (200, 400 and 600 W/m^2) the power drop is very low, and the power drop at 800 and 1000 W/m^2 radiation values increases. This decrease is between 10-20%.

- At low radiation intensities (200, 400, and 600 W /m^2), the reduction in I-V curves is very low, this change is between 0-10%, and this change is increased at 800 and 1000 W/m^2 radiation values, this change occurs 10-20 %.

- The average degradation rate of efficiency of the solar cells exposed to the dust spraying is 5-25 % compared to exposure periods of the clean cells.

As a result, the increased inclination angle decreased the accumulation of dust and the experiments in

this study show that the increased inclination angle increases the damage on the PV cell. All of them are permanent on the cell, which also reduces solar permeability.

ACKNOWLEDGMENTS

The authors would like to acknowledge the support of Fırat University. Nu. TBMYO.17.01.

REFERENCES

[1] Kok, B., Benli, H. (2017), Energy diversity and nuclear energy for sustainable development in Turkey. Renew. Energy, 111, 870–877. https://doi.org/10.1016/j.renene.2017.05.001

[2] Jiang Y., Lu L. (2016), Experimentally investigating the effect of temperature differences in the particle deposition process on solar photovoltaic (PV) modules. Sustainability. 8 (11),1091. https://doi.org/10.3390/su8111091

[3] Darwish, ZA., Kazem, HA., Sopian, K, Al-Gou, M.A., Alawadhi, H. (2015), Effect of dust pollutant type on photovoltaic performance. Renew. Sustain. Energy Rev. 41, 735–744. https://doi.org/10.1016/j.rser.2014.08.068

[4] Jiang, Y., Lu, L., Ferro, A.R., Ahmadi, G. (2018), Analyzing wind cleaning process on the accumulated dust on solar photovoltaic (PV) modules on flat surfaces. Solar Energy. 159, 1031–1036. https://doi.org/10.1016/j.solener.2017.08.083

[5] Gholami, Aslan., Ahmad, Saboonchi A.A.A., (2017), Experimental study of factors affecting dust accumulation and their effects on the transmission coefficient of glass for solar applications. Renewable Energy. 112, 466–473.

[6] Gholami, A., Khazaee, I., Eslami, S., Zandi, M., and Akrami E. (2018). Experimental investigation of dust deposition effects on photo-voltaic output performance. Solar Energy. 159, 346–352. https://doi.org/10.1016/j.solener.2017.11.010

[7] Fountoukis, C., Figgis, B., Ackermann, L., and Ayoub, M.A. (2018). Effects of atmospheric dust deposition on solar PV energy production in a desert environment. Solar Energy. 164, 94–100. https://doi.org/10.1016/j.solener.2018.02.010

[8] Saidan, M., Albaali, A.G, Alasis, E., and Kaldellis, J.K. (2016). Experimental study on the effect of dust deposition on solar photovoltaic panels in desert environment. Renewable Energy. 92, 499–505. https://doi.org/10.1016/j.renene.2016.02.031

[9] Al Shehri, A., Parrott, B., Carrasco, P., Al Saiari, H., and Taie, I. (2016). Impact of dust deposition and brush-based dry cleaning on glass transmittance for PV modules applications. Solar Energy. 135, 317–324. https://doi.org/10.1016/j.solener.2016.06.005

[10] Mehmood, U., Al-Sulaiman, F.A., and Yilbas, B.S. (2017). Characterization of dust collected from PV modules in the area of Dhahran, Kingdom of Saudi Arabia, and its impact on protective

transparent covers for photovoltaic applications. Solar Energy. 141, 203–209. https://doi.org/10.1016/j.solener.2016.11.051

[11] Lu, H., Zhao, W. (2018). Effects of particle sizes and tilt angles on dust deposition characteristics of a ground-mounted solar photovoltaic system. Applied Energy. 220, 514–526. https://doi.org/10.1016/j.apenergy.2018.03.095

[12] Menoufi, K., Farghal, H.F.M., Farghali, A.A., and Khedr, M.H. (2017). Dust accumulation on photovoltaic panels: A case study at the East Bank of the Nile (Beni-Suef, Egypt). Energy Procedia. 128, 24–31. https://doi.org/10.1016/j.egypro.2017.09.010

[13] Ahmed, O.K., Mohammed, Z.A. Dust effect on the performance of the hybrid PV/Thermal collector. *Therm. Sci. Eng. Prog.* 2017; 3, 114–122. https://doi.org/10.1016/j.tsep.2017.07.003

[14] Fountoukis, C., Ackermann, L., Ayoub, M.A., Gladich, I., Hoehn, R.D., and Skillern, A. (2015). Impact of atmospheric dust emission schemes on dust production and concentration over the Arabian Peninsula. Model Earth Syst. Environ. 2, 115. https://doi.org/10.1007/s40808-016-0181-z

[15] Lay-Ekuakille, A., Ciaccioli, A., Griffo, G., Visconti, P., and Andria, G. (2018). Effects of dust on photovoltaic measurements: A comparative study. Meas. J. Int. Meas. Confed. 113, 181–188. https://doi.org/10.1016/j.measurement.2017.06.025

[16] Mejia, F., Kleissl, J., and Bosch, J.L. (2013). The effect of dust on solar photovoltaic systems. Energy Procedia. 49, 2370–2376. https://doi.org/10.1016/j.egypro.2014.03.251

[17] Tanesab, J., Parlevliet, D., Whale, J., and Urmee, T. (2017). Seasonal effect of dust on the degradation of PV modules performance deployed in different climate areas. Renewable Energy. 111, 105–115. https://doi.org/10.1016/j.renene.2017.03.091

[18] Wang, P., Xie, J., Ni, L., Wan, L., Ou, K., Zheng,L., and Sun, K. (2018). Reducing the effect of dust deposition on the generating efficiency of solar PV modules by super-hydrophobic films. Solar Energy. 169, 277–283. https://doi.org/10.1016/j.solener.2017.12.052

[19] Gürtürk, M., Benli, H., and Ertürk, N.K. (2018). Effects of different parameters on energy - Exergy and power conversion efficiency of PV modules. Renewable and Sustainable Energy Reviews. 92, 426–439. https://doi.org/10.1016/j.rser.2018.04.117.

[20] Sze, S.M. (1969). Physics of semiconductor devices, John Wiley and Sons NY.

NOMENCLATURE

A	area (m^2)
a	ideality factor
FF	fill factor
G	solar intensity (W/m^2)

I	current (A)
k	Boltzmann's constant (1.381 x 10^{-23} J/K)
P	power (W)
q	electron charge (1.602 x 10^{-19} C)
R	resistance (Ω)
T	temperature (K)
V	series voltage (V)

Greek letters

η	efficiency (%)

Subscripts

amb	ambient
en	energy
pv	photovoltaic
s	series
sc	short circuit
sun	Sun's surface
0	saturation

Kütahya Dumlupınar University
Institute of Graduate Studies

Journal of Scientific
Reports-A
E-ISSN: 2687-6167
Number 45, December 2020

RESEARCH ARTICLE

A NEW MOBILE APPLICATION FOR PHYSICAL MEASUREMENT IN A CELLULAR NETWORK

Aygün VAROL[1], Bilge KARTAL ÇETİN[2]

[1] Isparta Applied Science University, Faculty of Technology, Electrical Electronic Engineering, Isparta,
aygunvarol@isparta.edu.tr, ORCID: 0000-0002-4029-7676
[2] Ege University, Faculty of Engineering Electrical Electronic Engineering, İzmir,
bilge.kartal@ege.edu.tr, ORCID: 0000-0002-3338-1538

Received Date:22.04.2020 *Accepted Date:12.08.2020*

ABSTRACT

Mobile cellular network operators make network parameter measurements called 'driving test' at regular intervals to understand the service quality and plan the network capacity. In order to reduce the man power and the cost required for the driving test, these measurements can be obtained with a mobile application which runs on the user equipment. Moreover, end user measurements of the cellular network parameters can be used to improve network performance in many ways, such as troubleshooting problems in network or determining the number and capacity of base stations.

In this paper, existing smartphone applications for network parameter measurement in the literature has been investigated and a new Andoid based application CoverME (Coverage of My Environment) has been developed. CoverME provides all the measurements performed by existing applications and supports four more additional measurements. The developed application makes the measurement accuracy to be analyzed with the help of the return time (RTT-round trip time) parameter and monitor the battery level. In addition, it limits the energy consumption as it is designed to operate in a semi-autonomous. CoverME keeps a record that contains key performance parameters of LTE communication systems; RSRP, RSRQ, RSSI, CQI values. These values matched with cell ID, download speed, latency and current location for the consistency of the application. As a case study, the measurements were made on a route determined in Isparta province with the developed application. Utilizing obtained measurements, the relationship of these values with each other and the relationship with the download speed were examined.

Keywords: *LTE, Android, Measurement Application, RSRP, RSRQ, RSSI, CQI, Download Speed*

1. INTRODUCTION

Today, it is possible to find smartphone applications developed for all activities of daily life such as health, sports, eating and drinking. As these applications and their diversity are rising, the network requirements of mobile users are increasing and varying day by day. The increase in mobile user's demand for data usage has accelerated the service providers' efforts to provide more capacity and improve the network according to current requirements. LTE (Long Term Evolution) is the most current communication technology offering mobile users high data download speed and high network

capacity [1]. In order to find out the quality of the service provided to the users in LTE, physcical measurements are made regularly in the field. With regular monitoring, the user expectation and the quality of service experienced by users can be understood.

The signal values experienced by the end user in communication are necessary to understand the performance of the network and to evaluate the quality of service offered by the operator. Operators use a method called 'drive test' to obtain these values. The drive test involves downloading and uploading data with user equipment or measuring various signal values while a vehicle is travelling on a previously determined route. The measurement results obtained by driving tests are used to determine the coverage area, the capacity of the system, and the quality of service. Through the analysis of the data obtained, operators maintain and improve the quality and performance of the network. However, this test is costly because it requires manpower and cannot fully reflect the real user experience. The desired network parameters can be obtained with a measurement application instead of the driving test [2]. With such a measurement application, operators can reduce the work force and cost required for driving testing. Service providers can obtain data that better reflects the user experience rather than a driving test by offering their customers a number of rewards or discounts in exchange for using this app and sharing the data with the operator.

3GPP (3rd Generation Partnership Project) has defined a standard called Minimization of Drive Tests (MDT) to reduce the workload and expenditure required for driving testing and to achieve the true values experienced by users [3]. MDT uses the operating, management, and maintenance system to collect radio measurements from user hardware along with their location. This system allows recording messaging signals between user equipment and base station [3].

Obtaining information about network parameters on the user side can be usefull for users as well as the operators. For example, the mobile user can choose the service provider that is best for their usage habits based on the measurements they perform with the application. For example, high data download and upload speed might be more important selection criteria for a company that shares visual contents with its customers over a mobile network, but for a frequent traveler coverage in rural areas becomes the key selection criteria rather than the data speed.

JSR A
Journal of Scientific Reports

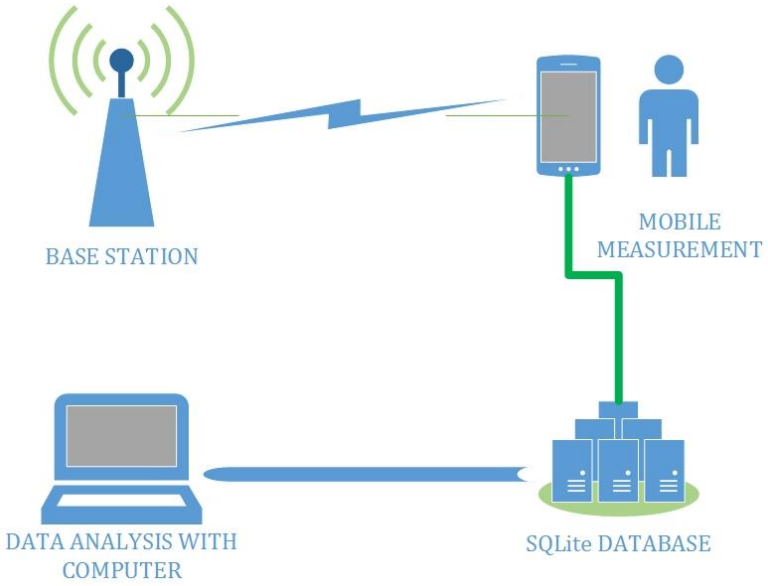

Figure 1. Required components for the measurements.

The most used operating system at smartphones is Android [4]. Android's open-source structure and configurability have made it popular for the application developers. In this study, Android software was used to develop a measurement application due to its widespread use and open source.

When the applications developed for this purpose are examined in the literature, it was seen that the highest number of parameter measurements belong to the Advanced signal status [2] application. In this study, a new application was developed that contains all of the parameters measured by Advanced signal status application, in addition to measuring four different parameters. In the literature, RTT measurement is used to confirm the consistency of the values obtained by the measurement application [5]. It is ensured that the consistency of the measured values in the application is tested with RTT measurement. This application can also measure battery level, network type and data download speed.

As a case study for the developed application, a route was determined in the province of Isparta and the desired data was collected with an Android-based smartphone while travelling at a constant speed in a vehicle. The selected parameters were measured and saved in the SQLite database, and the measurement data was then transferred to the computer and analyzed. Figure 1 shows the main components of the measurements. .

2. EXISTING PHYSICAL MEASUREMENT APPLICATIONS

Mobile networks have become dominant in internet access. Therefore, measuring the end user's network performance has gained interest from developers, users, and network operators. There are many applications in the literature that perform these performance measurements. The parameters and objectives of these applications are briefly explained. The parameters measured by the applications in

JSR A
Journal of Scientific Reports

the literature are shown in Table 1. A detailed literature review of current practices can be found in [6].

Table 1. Measurement applications and the parameters they measure.

	RSRP	RSRQ	RSSI	RSSNR	CQI	Cell Location	Handover	RTT or PING	Download Speed	Upload Speed	Network Type	Battery Level
Netmap	X							X				
NetworkCoverage	X					X		X			X	
Netradar	X							X		X		
Advanced Signal Status	X	X	X	X	X	X	X					
Mobilyzer								X	X	X		
MobiPerf								X	X	X	X	
OpenSignal	X	X		X					X			
MopEye								X				
Napplytics	X		X						X			
NetMap	X					X			X	X		
CoverME	X	X	X	X	X	X	X	X	X		X	X

Netmap is a community-sourced android application used to measure network key performance indicators such as received power, latency, and data rate. Measurements are made in four different scenarios, including inside, in the city and on the highway. Netmap measures data rate, network connection status, RTT and received power [7].

NetworkCoverage was developed with a focus on multi-source data collection. The measurements are collected on the central server after being performed in different regions on smart devices. The collected data is made available by mobile devices to estimate network performance in certain regions. Thanks to the data, it is possible to improve mobile energy consumption and service quality. They are concerned with the signal strength of the cellular network, RTT and available output parameters in the given region. NetworkCoverage is used to visualize the quality of the cellular network. Signal strength measurements are performed automatically, without user interaction. RTT measurements are usually done manually [8]. However, this application only measures RSRP from LTE signal parameters.

Netradar consists of a client specifically designed for smartphones and tablets and a number of servers that will serve those clients. Clients perform measurements about the network infrastructure. This system, which collects measurements from users around the world, is called Netradar [9]. Netradar measures download speed, upload speed, RTT and signal strength [10].

Advanced Signal Status shows the possibilities of optimizing measurement operations using widely available Android devices. The application measures RSRP, RSSI, SNR, CQI, RSRQ, SINR, Cell Handover parameters using Android's celllocation, NeighboringCellInfo, CellInfo, PhoneStateListener, ServiceState, SignalStrength, TelephonyManager libraries [2].

Mobilyzer is a platform created for conducting mobile network measurement experiments. Mobilyzer is designed around three main parameters: the isolation of network measurement, the realization of measurements, and the platform can be deployed as a library and easily adaptable by other applications [11]. Mobilyzer is a library used by measurement applications rather than a measurement application. It can be integrated into measurement applications using Mobilyzer's API. It can be used for TCP data rate, RTT and ping measurements.

MobiPerf is an open source application for measuring network performance on mobile platforms. MobiPerf measures at regular intervals in the background. MobiPerf is one of the applications that uses the Mobilyzer library. The application works on Android and iOS devices for 2-3 minutes to obtain basic network information, network performance information. As a mobile network measurement system MobiPerf, contains two major components: one is the user application running on mobile devices and the other is the Linux server under their control. Measurement parameters: network characteristics, carrier name, network type, Cell ID, signal strength, Local IP address, GPS, downlink and uplink tests [12].

OpenSignal is a measurement platform that performs an accurate and current measurement of the user experience using the crowdsource measurement technique. The app collects and reads crowdsource signal information. LTE signal parameters measured by the application are RSRP, RSRQ and RSSNR [13].

Mopeye is a passive-active permanent monitoring application, as opposed to active measuring applications. This method does not generate separate network traffic to the devices. MopEye stops all network traffic and makes the measurement then transfers the collected information. Thus, MopEye can accurately measure RTT (round trip time) without the need for additional network traffic. MopEye monitors network traffic initiated by other apps available on the phone using a VPN service. App measures RTT between the application where the network traffic is created and the server [14].

Napplytics is designed as an Android library, with the goal of being a measurement network tool that can be easily incorporated into any Android application. This library selects the most appropriate application protocol, depending on the network conditions experienced by the user. For example, for LTE technology, the network parameters used are selected as RSRP, RSSI and download speed [15].

NetMap is designed to capture specific parameters that affect network performance and user experience at the application layer. The app collects information for 2G, 3G and 4G, while recording user position with GPS. Netmap measures data rate, network connection status, RTT, and received power [16].

3. MEASUREMENT PARAMETERS FOR LTE CELLULAR NETWORK

In the design of the measurement application, it is necessary to determine the parameters that best represent the performance of LTE communication systems. The four basic radio resource management (RRM) metrics in LTE are CQI, RSRP, RSRQ, and RSSI. The channel quality measurement represented by the SINR measurement is used in link adaptation and packet planning. RSRP and RSRQ are used in handover (switching between networks using different radio technology) decision making [17].

In smartphones, the factors affecting the performance perceived by users are listed as: TCP data rate, RTT, retransmission rate, TCP handshake time, Ping [18]. Signal quality and strength, network operator factors are required to determine channel capacity. None of the LTE-specific signal parameters sufficient enough to determine the download speed without other parameters. Only when all parameters used together, by gathering, they can explain some of the variability in the model. Understanding the factors that determine download speed is valuable for both users and operators. With these factors, users wish for the best performance services and devices that are practically possible. And the network operators can understand how to increase and improve their infrastructure.

It is not easy to achieve signal strength criteria in LTE connections. In 2G and 3G technologies, there was the metric called the Received Signal Strength Indicator (RSSI), which specifies the received signal strength, which is always precise and easy. The RSSI metric was useful in the case that frequencies were not reused in multiple cells. In a single cell, the signal strength could be described directly with a single frequency. Due to the increasing number of users, it was necessary to use the same frequencies again at regular intervals. With the advancement of digital modulation technologies, network operators were able to develop increasingly complex and overlapping cell topologies. Since reuse of the same frequencies led to interference between neighboring cells, it became difficult to obtain information about network performance by using the RSSI metric alone. Instead of the RSSI value used in 2G and 3G, three LTE-specific signal criteria that can be measured on Android-based devices are RSRP, RSRQ and RSSNR parameters [13]. Key performance parameters for a cellular network introduced below.

3.1. Key Performance Parameters

The most important metric on the user side for evaluating the service quality of a network is the data rate and latency. In addition, key performance parameters that must be monitored by operators in order to use network resources efficiently and ensure service quality can be listed as RSRP, RSRQ, RSSNR, RSSI, CQI, SINR, and RTT.

- **RSRP**
  Reference Signal Received Power (RSRP), is a cell-specific signal strength-dependent metric used as an input for cell selection and handover decisions. RSRP for a given cell is defined as the average power (Watt) of the source elements carrying cell-specific reference signals within the bandwidth [17]. The RSRP value range is from -140 to -44 dBm.

- **RSRQ**
  Reference Signal Received Quality (RSRQ) measurement is a cell-specific signal quality metric. Similar to RSRP measurement, this metric is used to sort between different cells based on their signal quality. This metric can be used as input in scenarios where RSRP measurements are not sufficient to make reliable cell selection / handover decisions [17].

- **RSSNR**
  Reference Signal Signal to Noise Ratio (RSSNR), is a measure of the signal-to-noise ratio of the reference signal and therefore provides an indication of the quality of the link. This metric can be used to assess the interference effect, and therefore in urban areas RSRP may be high [13].

- **RSSI**
  Reference Signal Strength Indicator (RSSI), is the total power received by the source element in dBm. Although not critical for LTE, its measurement is important to understand its relationship with other parameters. RSSI is a combination of signals from all sources, including power from the serving cell, the non-serving cell, the common channel, and the adjacent channel interference [19].

- **CQI**
  Channel Quality Indicator, carries information about how good or bad the communication channel quality is. There are 15 different CQI values in LTE and it maps between CQI and modulation scheme. For example, the CQI's 10 value corresponds to the 64QAM modulation scheme [20].

- **RTT**
  Round-Trip Time (RTT), is the time it takes for a signal packet to reach and return to a specified target from the source. The measurement of this parameter is done to ensure the consistency of the application.

  The importance of these parameters varies according to the requirements of the application. For example, broadcasting video requires high data rate and low packet loss hence RTT has less impact on quality. In contrast, audio connections require low RTT, but low data rate and high packet loss are acceptable [21].

3.2. Other Measured Parameters

- **Network Type**
  This parameter is used to determine if the base station is exchanged horizontally or vertically between two networks using different radio technology or within the same network. When the cell location changes while in the same network type, it is concluded that this handover is horizontal, if the network type and the cell location change, this handover is vertical.

- **Location**
  Required for the location where the signal values will be recorded. In this way, the coverage map can be created.

- **Cell Location and Cell ID**
  Returns the identity of the cell the user is in. Required to capture the handover event.

- **Battery Level**
  Battery level monitoring is necessary to determine the effect of the battery on the measurements. It is also used to determine the energy consumption of the application .

  The received signal level (RSL) from each cell in the network is one of the basic RF measurements. In LTE networks, this measurement is provided from the reference sequence and is called RSRP. The reference signal is transmitted at constant power. Signal strength measurements determine the received cell strength and cell coverage. For this reason, RSRP is used to identify holes in the coverage area. In addition, RSRP measurement is essential in troubleshooting and establishing correlation with other key performance indicators (data rate and latency). This measurement determines the allocated modulation scheme and encoding rate. To measure received power,

professional tools including receivers and channel carriers are used. Alternatively, RSRP can be measured using the app on an ordinary smartphone [22].

In addition to these parameters, the application measures the parameters EVDO (Evolution Data Optimized) RSSI, EC/IO (the Ratio of the Received Energy to the Interference Energy), SNR (Signal-to-Noise Ratio), CDMA (Code Division Multiple Access) RSSI, EC/IO which are 3G technology, and GSM RSSI, BER which are 2G technology. The purpose of these measurements is to capture signal parameters when a collapse occurs in the network .

4. MEASUREMENT CONSISTENCY

As smartphone used for the measureument, the results have been exposed to many factors, therefore, these measurements may not be the values that users expected. In order to be able to rely on the measurement results of the application, first of all the factors affecting these measurements should be known and their effects should be minimized. For this purpose, the factors affecting the measurement results were examined in this section.

One of the factors affecting the measurement results is the delay. To see the effect of the delay , the RTT measurement is performed and the consistency of the measurement is tested by using the obtained RTT results. RTT measurement are defined based on RFC 2681 [23] and contains a time stamp immediately before sending the packet and immediately after receiving the packet [24].

Although there are many measurement applications available, the consistency of measurements is not efficient. Using RTT as a metric, the performance of smartphone-based network metrics can be evaluated [5]. Other factors affecting measurement results might be listed as application models, Android architecture and network protocols. Detailed information about these effects can be found in [24].

5. ENERGY CONSUMPTION OF MEASUREMENTS IN SMARTPHONES

This section describes some situations that cause energy consumption in mobile networks. Thus, the energy required by the developed application per measurement can be determined.

- **Location Measurement**
  Location-based apps have become increasingly popular on smartphones in recent years. Using these applications actively may drain the battery due to intensive location-sensing operations.

  GPS energy consumption is between 400mW – 600mW. Using GPS continuously on a smartphone with a battery of 1000mAh will end battery life in 6 hours. GPS location detection and reporting times are 4 to 5 and 10 to 12 seconds, respectively [25].

- **Connection Speed**
  The increase in data rates of cellular 3G/4G networks, coupled with the growth of mobile application use, is significantly affecting the quality of service the user perceives. QoE can be affected in two ways: first, data rates on networks decrease when multiple users take turns requesting content; second, data transfer on slow connections consumes considerable energy over fast connections. Both can be avoided by better management of available resources [21].

- **Handover**
  It is the name given to the transition between two networks using different radio technologies or between base stations on the same network. In a heterogeneous network environment, vertical and horizontal handover is a very desirable feature. An effective handover solution provides fixed connectivity to mobile users and allows seamless transition between different networks. Thus, by improving the user experience, it enables the best quality of service. But changing the network requires more device energy.

  Handover can be between base stations with the same technology (horizontal Handover) or it can trigger change in radio technology, such as 2G to 3G or 3G to LTE (vertical Handover). Horizontal Handover usually occurs from the movement of the user. To study the effect of move, measurements at different speeds are required [26], [10].

After investigating the parameters to be measured, the factors affecting these parameters and the energy consumption of the measurements, the CoverME application was designed by considering all these parameters.

6. PROPOSED NEW MOBILE APPLICATION: COVERME

In this section, the libraries and tools used in the design of the measurement application and the parameters measured by the application and overall operating principle of the application are explained.

Android Studio is an IntelliJ IDEA-based, formal Integrated Development Environment (IDE) environment for developing Android applications. The application can be developed for all Android devices thanks to the editor and developer tools of Android Studio. Utilizing its emulator, the designed application can be tested. With Android-enabled libraries and external libraries, applications can be created for various purposes.

The developed measurement app CoverME detects the performance of the cellular network the smartphone is in its coverage. To this end, it measures RSRP, RSRQ, RSSI, RSSNR, Download Speed, Cell ID and location. These values are stored in the internal memory of the phone with SQLite for analysis. Utilizing the obtained measurement a coverage map is created for the cellular network. Measurement parameters can be accessed through the libraries provided by Android. Three Android classes (TelephonyManager, LocationManager and BatteryManaer), one library (Sqlite) and one external class (facebook network connetion class) that are used to make these measurements are listed below.

1)android.telephony TelephonyManager
2)android.os BatteryManager
3)android.location LocationManager
4)android.database.sqlite SQLiteOpenHelper
5)facebook network-connection-class

The measurement application can be used on API 27 Android 8.1 Oreo devices or latter version devices. CoverME performs two different measurements, active and passive measurements. Active measurements are download speed and RTT measurements that require internet and generate additional network traffic. Passive measurement performs LTE signal parameters, cellular network

type, cell location, battery, GPS measurements that do not require internet and do not generate additional network traffic. Figure 2 shows the screenshots during the passive and active measurements.

The application automatically performs passive measurements every time one of the values changes, without the need for the user to press the button, and saves it to the SQLite database with a timestamp. When the data is successfully saved, the user is informed via a (Toast) notification message. For the active measurement, the active measurement button must be clicked by the user. In the active measurement, the application downloads a 100 MB file and divides it by the processing time to achieve the download speed. To obtain RTT, measurements performed in the active mode and the application pings the website 'google.com'. In this ping process, the application sends 4 packets to 'google.com'. The time that these packets reach and return to the target is determined. The minimum / average / maximum / standard deviation RTT values of the 4 packets that sent, packet loss and total processing time are displayed in the terminal. RTT is used to confirm accuracy in active measurement, but is not stored in the database. Flowchart for the measurement process is given in Figure.3. TelephoneyManager class is used to obtain Network Types, Cell Location and Signal Parameters. D To obtain batterly level and location BatteryManager and LocationManager classes are used, respectively.
General Mobile GM 8 smartphone was used for measurements. As seen in Figure 2, the value of LTE CQI data is '2147483647' which is the maximum value of the 32-bit String variable. CoverME measurement application has the ability to measure CQI, but this false CQI value seen because the smartphone used in the measurements does not support CQI measurement. The measurements supported by smartphones differ by models and brands. The ability of the phone to measure the desired measurement needs to be considered before using any app for physical measurements.

CoverME measurement application can be developed for IOS devices. However, this is not possible with Android Studio. Although IOS and Android devices look similar on the outside, operating systems on the inside are very different. The codes used in the IOS application design are in different languages and different structures. IOS developers use Mac-supported Xcode as a program. The programming language used by these developers is Swift. The IOS library with the signal parameters is Core Telephony. Since the market share of mobile operating systems is 74.14% for Android and 25.26% for IOS, the platform on which the application will run is selected Android [4].

JSR A
Journal of Scientific Reports

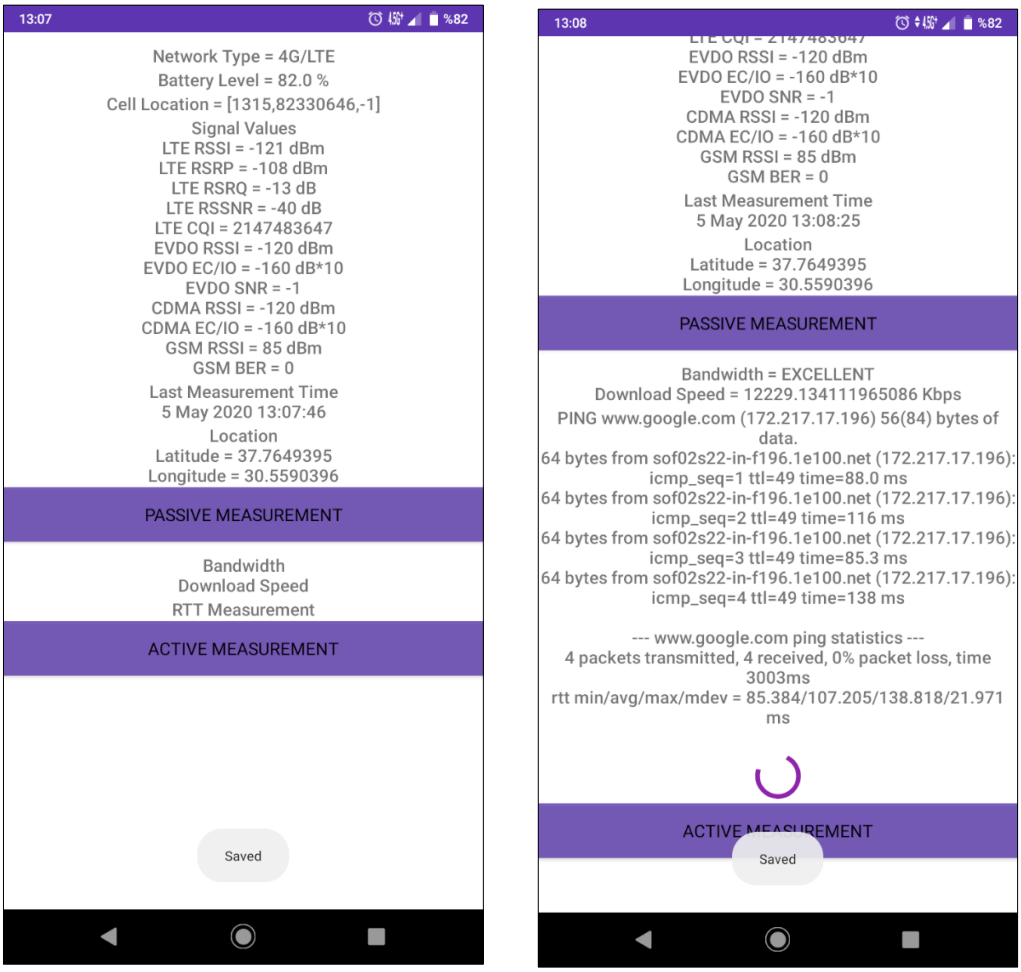

a) Passive Measurments **b) Active Measurements**

Figure 2. CoverME Passive/Active Measurement Interface.

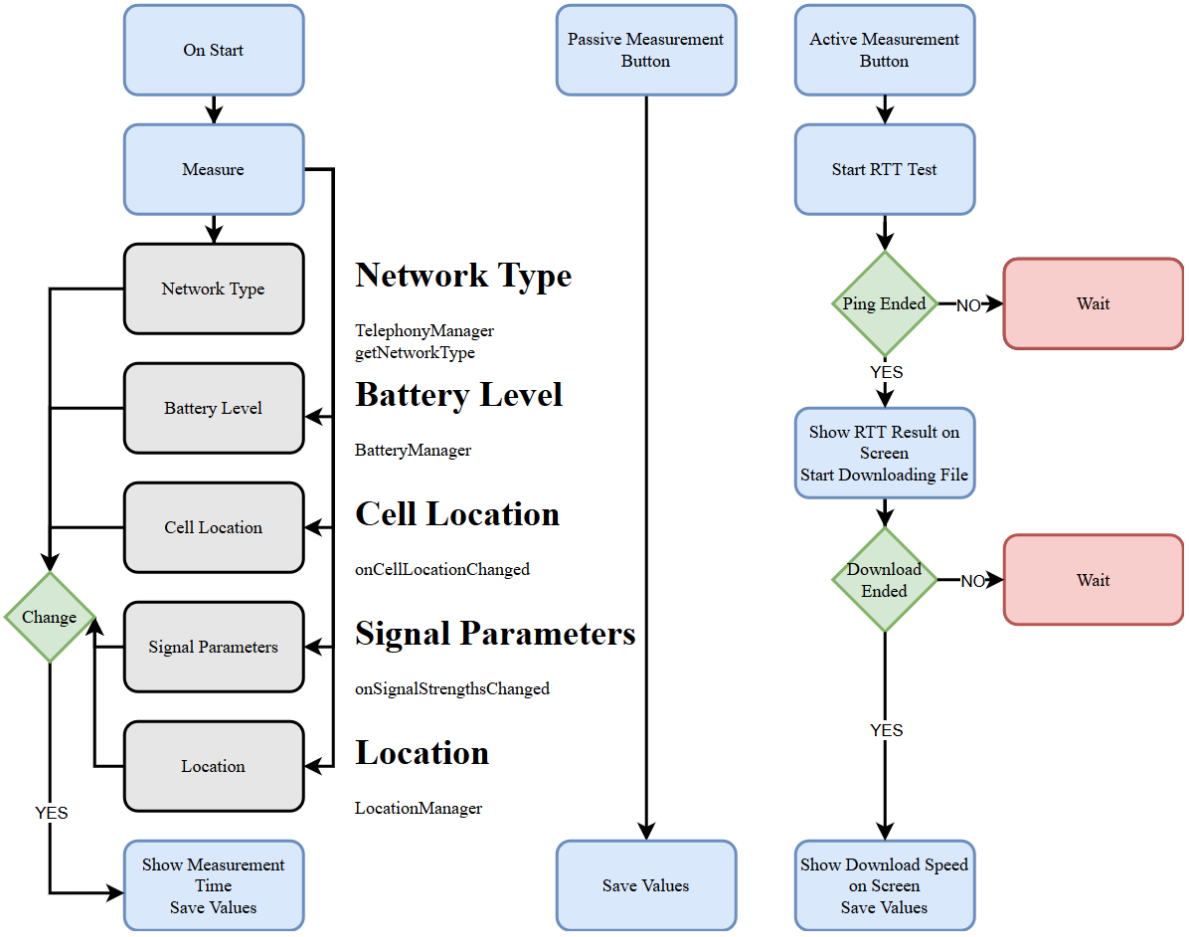

Figure 3. Flowchart of the Measurement Process

7. MEASUREMENTS AND DISCUSSIONS

Using the developed measurement application CoverME, 1186 measurements were carried out in different neighborhoods of Isparta. 85% of the measurements were made on foot, and 15% were carried out on the vehicle with an average of 40 km/h. 838 of the measurements are available since they have both location and download speed values. With these measurements, a coverage area has been created in Google My Maps. Each marker on the map represents a measurement. By clicking on the marker, the performance of the cellular network of its location can be accessed.

JSR A
Journal of Scientific Reports

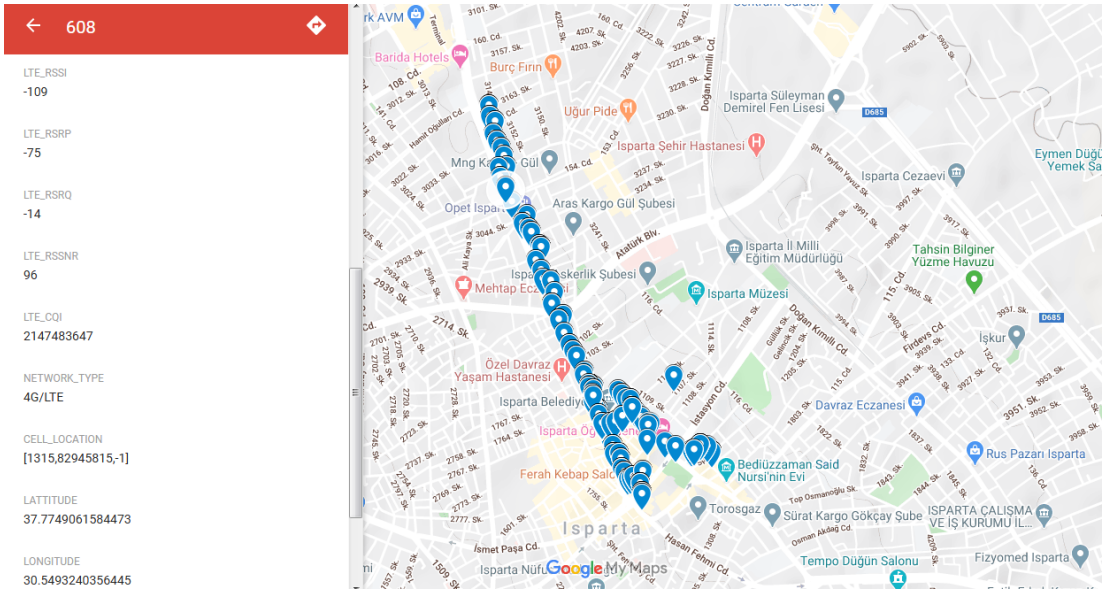

Figure 3. Isparta MyMaps Image.

Measurements are made by the end user via smartphone and stored in the database in its internal memory. The data collected were analyzed on the computer, and the correlation between LTE signal values and download speed was plotted. To determine whether the battery level has an effect on the measurements, the download speed is also plotted by the battery percentage.

The graphics were created with the Curve Fitting tool. Exponential model for two-dimensional graphics and Polynomial model with a grade 2 for three-dimensional graphics were used.

7.1.Correlation of LTE RSRP value with download speed

Figure 5 shows the relationship of RSRP value with download speed. High download speeds (60 Mbps>) occurred when the LTE RSRP value was -70 dBm and above. When the graphic in Figure 5 is examined, different download speeds can be seen at the same RSRP values. This indicates that the download speed is not only dependent on RSRP. There are different RSRP values for the same download speed values. However, it can be concluded that a certain RSRP value must be exceeded in order to increase the download speed. The highest download speed value was measured between -60 and -50 dBm of LTE RSRP. The lowest value of LTE RSRP was measured between -110 and -100 dBm. Measurements below 10 Mbps continued up to -60 dBm. In general, according the measurement results it was concluded that the increase in RSRP value has a positive effect on the download speed.

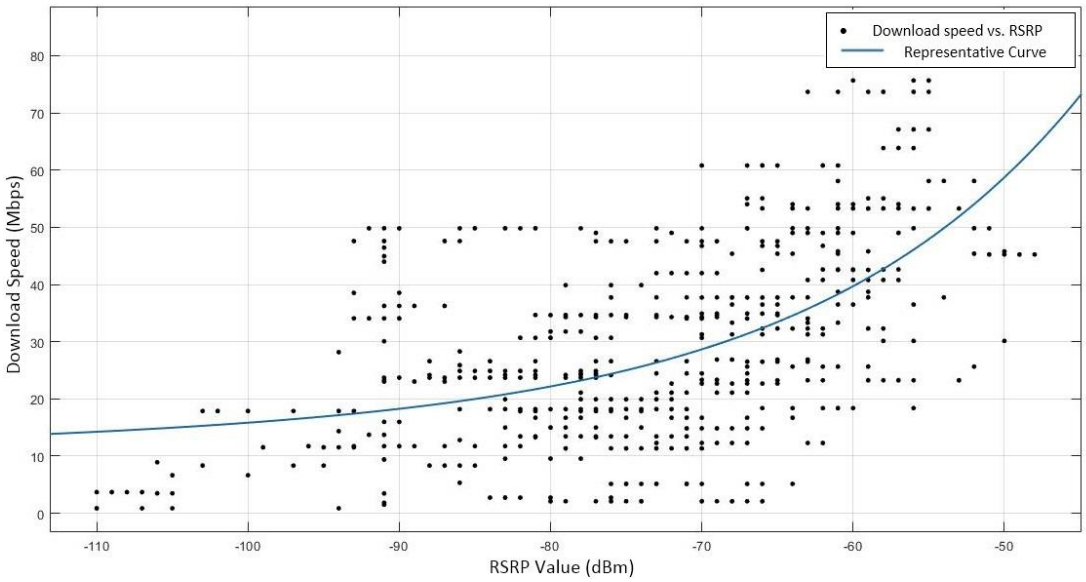

Figure 4. RSRP graph.

7.1.1. Correlation of LTE RSRQ value with download speed

Figure 6 shows the download speed according to the RSRQ change. Based on the curve we obtained with Curve fitting, the increase of LTE RSRQ also increased the download speed. The highest download speed measurement was realized at -12 dB of RSRQ. Measurements were made at different speeds at the same value of RSRQ. This is due to the effect of other parameters on download speed. Low download speed measurements were taken even at high values of RSRQ. For measurements made at values less than -14 dB for LTE RSRQ, the download speed could not exceed 50 Mbps. High download speeds were achieved only after this level of RSRQ. Also, for measurements with RSRQ values greater than -9 dB, the download speed has always been above 15 Mbps. Although the increase in RSRQ value increases the average data rate, it is not enough to evaluate network performance alone.

JSR A
Journal of Scientific Reports

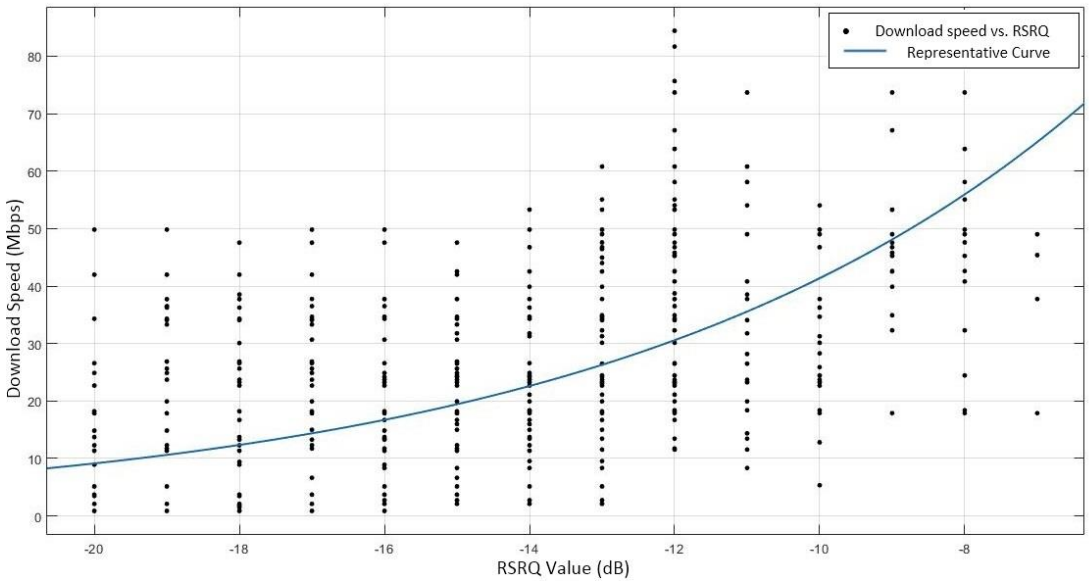

Figure 5. RSRQ graph.

7.1.2. Correlation of LTE RSSI value with download speed

Figure 7 shows the effect of RSSI on download speed. The graph in Figure 7 shows that high download speeds are achieved at high RSSI values. Download speed measurements of 50 Mbps and faster performed LTE RSSI values greater than -110 dBm. In general, LTE RSSI value has been found to affect download speed in a linear way, but this effect is limited.

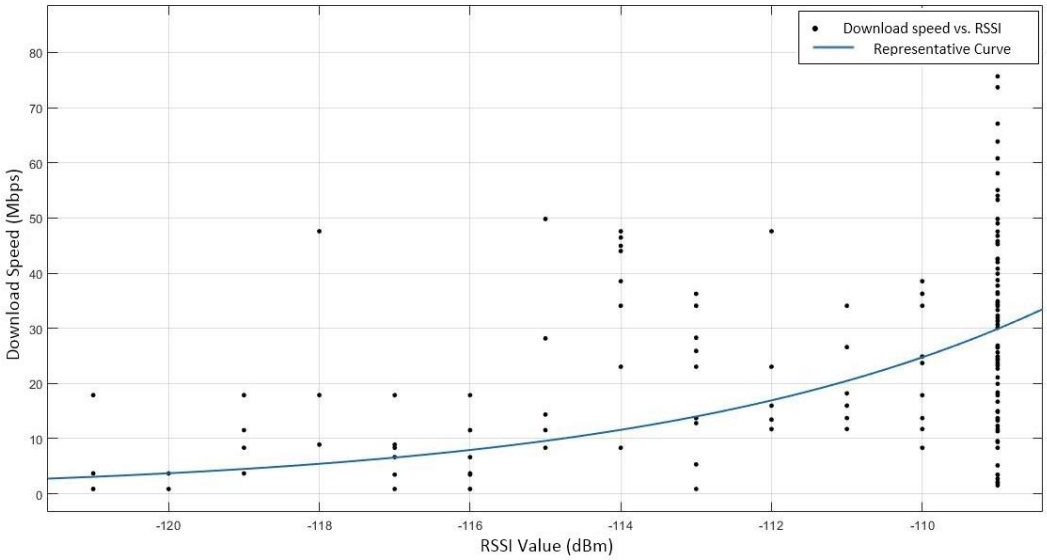

Figure 6. RSSI graph.

JSR A
Journal of Scientific Reports

7.1.3. Correlation of LTE RSSNR value with download speed

Figure 8 shows the relationship between download speed and RSSNR value. The highest download speed measured between 200 dB and 250 dB of RSSNR value. It is seen that it is possible to reach high download speeds after 50 dB of RSSNR. For measurements greater than 120 dB of RSSNR, the download speed is not less than 10 Mbps. In some cases where RSSNR is less than -100 dB, there are exceptions that can reach the download speed of 50 Mbps. The reason for this is that other parameters that affect the download speed are partially good (when the measurements are examined, it has observed that the RSSI value is high in these values). Based on the measuremets, RSSNR has a positive correlation with the download speed most of the time. This can also be seen from the representative curve obtained with curve fitting. However, as can be seen from the graph same download speed might be obtained for a large range of RSSNR values.

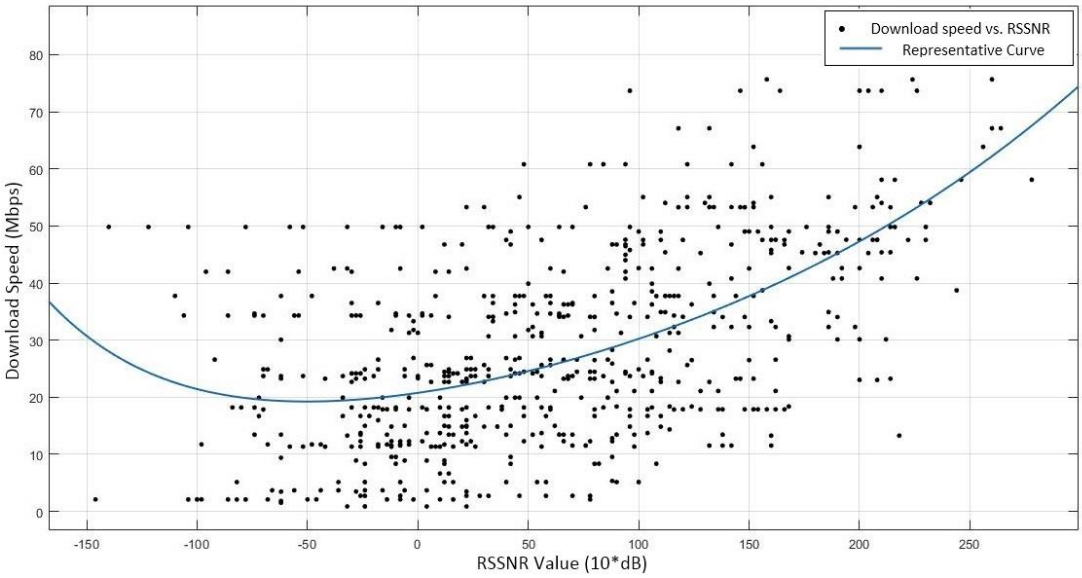

Figure 7. RSSNR graph.

7.1.4. Correlation of battery level with download speed

Figure 9 shows the effect of the percentage of the battery on the download speed. High download speeds are achieved when the battery is almost fully charged. In cases where the battery is less than 80%, the download speed could not exceed 60 Mbps. The lower the battery level, the lower the download speeds in the measurements. This can be understood from the peak values of the download speed in the measurement groups that occur in battery percentages.

JSR A
Journal of Scientific Reports

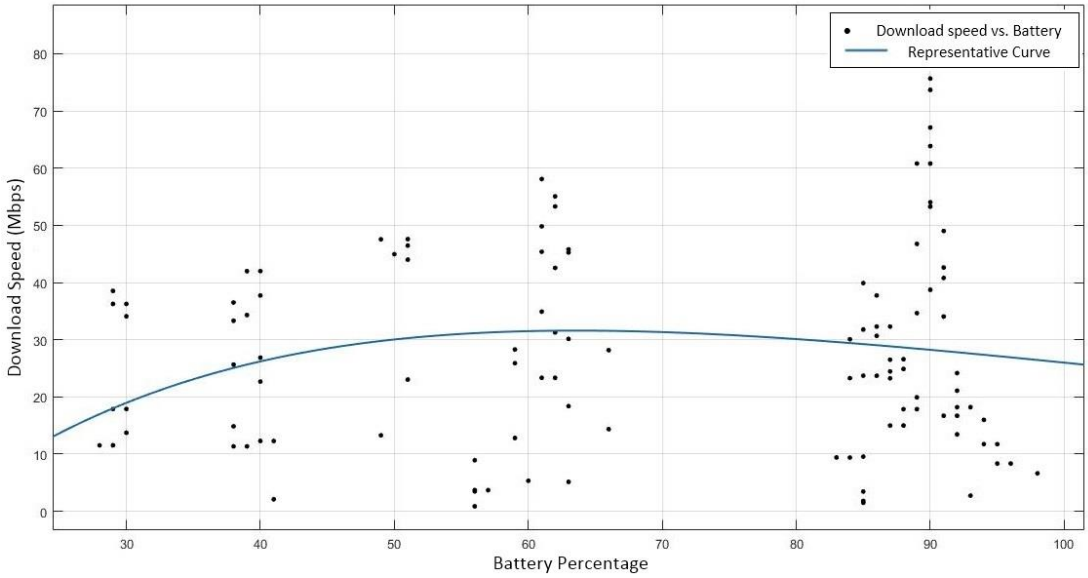

Figure 8. Battery graph.

Since the download speed does not change depending on a single parameter, different speed values are observed at the same points in two-dimensional graphics. In order to better explain this situation, the variation of the download speed depending on two parameters has also been drawn in three dimensions. These drawings were created using the Matlab Curve Fitting tool using Polynomial, x and y with grades 2.

7.2. Correlation of LTE RSRP and LTE RSRQ values with download speed

Figure 10 shows the relationship of download speed to both RSRQ and RSRP. Low download speed measurements are observed even at high values of RSRQ. Hence, it was concluded that the effect of RSRQ value on download speed is limited. However, it is seen that both RSRQ and RSRP should be high in order to reach high download speeds. At the very large values of the RSRQ value, even though the RSRP value is very small, the data download speed has been found to be around 15 Mbps. However, when the RSRQ and RSRP values are compared, it can be said that the RSRP value plays a more decisive role in the download speed compared to the RSRQ value.

JSR A
Journal of Scientific Reports

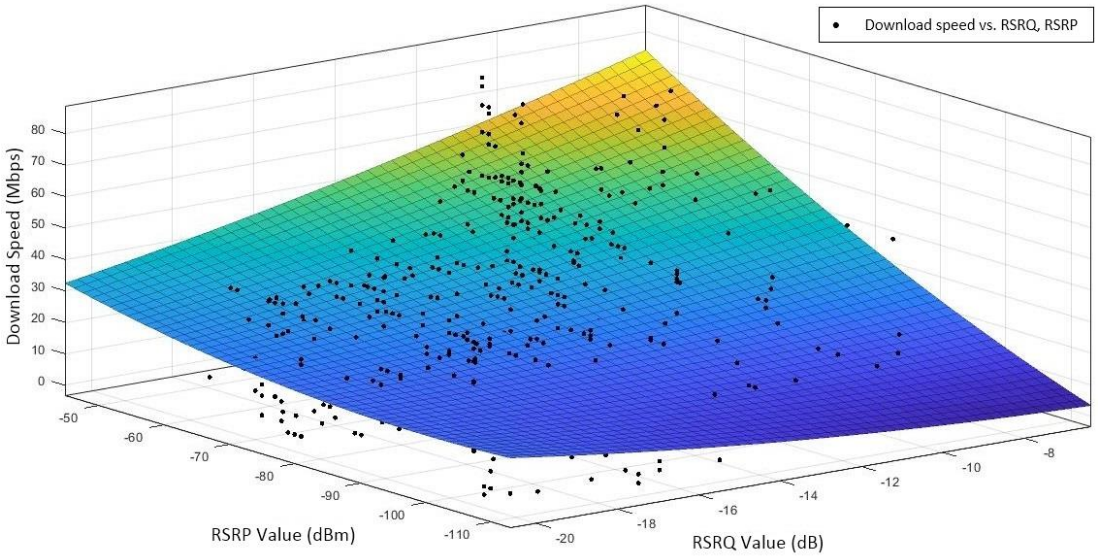

Figure 9. RSRP and RSRQ graph.

7.2.1. Correlation of LTE RSRP and LTE RSSNR values with download speed

Figure 11 shows how the download speed changes according to RSRP and RSSNR values. When RSRP is very small (<-100 dB) RSSNR values greater than 0 dB, a small increase in download speed has occurred. The high download speed is achieved only if these two values are high.

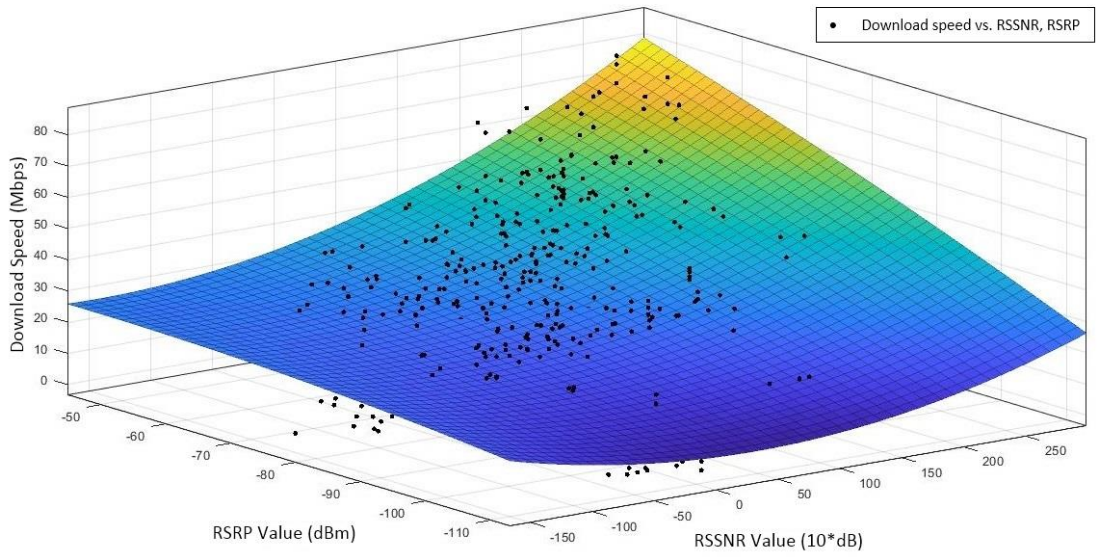

Figure 10. RSRP and RSSNR graph.

7.2.2. Correlation of LTE RSSI and LTE RSRQ values with download speed

When the graph in Figure 12 is examined, it is observed that the RSSI value has no effect on the data download speed. As can be seen form the graph, even RSSI is at very low value, the data download speed takes a wide range of values. For example, for the same RSSI value, the data rate can be 10 Mbps or 70 Mbps. According to obtained results, it is observed that there is no positive or negative corelation between RSRQ and RSSI.

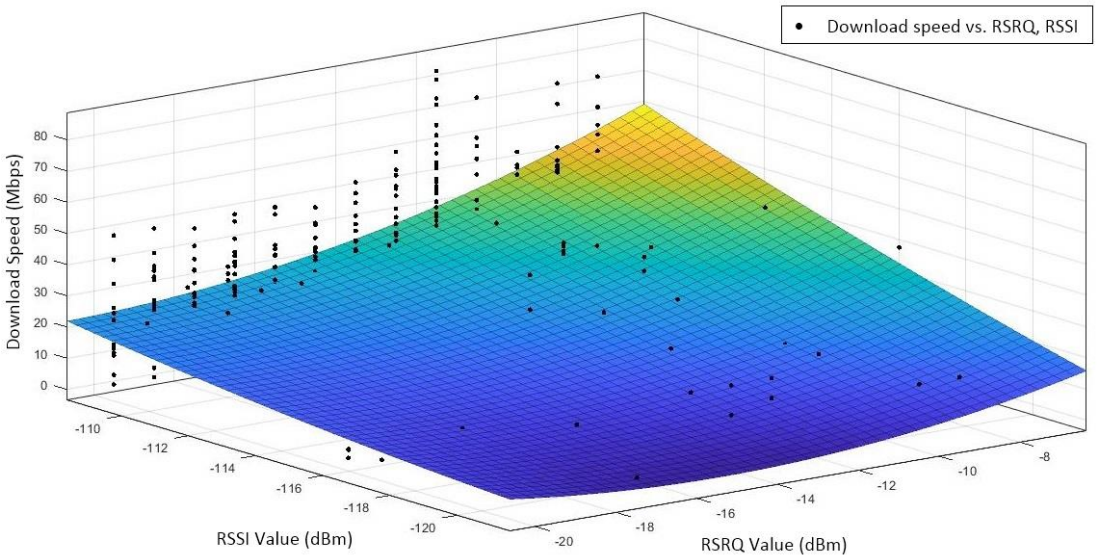

Figure 11. RSSI and RSRQ graph.

7.2.3. Correlation of LTE RSSI and LTE RSSNR values with download speed

Figure 13 shows how both RSSI and RSSNR affect the download speed. As can be seen from the figure, it is observed that RSSNR has a positive effect on the download speed regardless of RSSI value. It can be concluded that the RSSNR value must necessarily be high to achieve high data rates. For example, if the point where the RSSNR value is 50 dB is examined in the figure, it can be seen that even at the lowest value of the RSSI, the data rate of 20 Mbps can be exceeded.

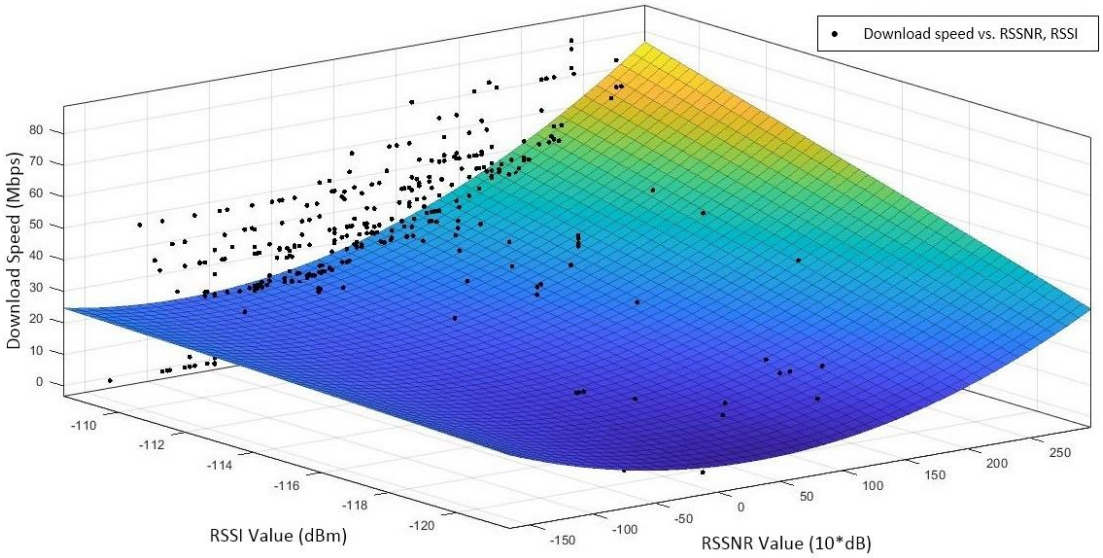

Figure 12. RSSI and RSSNR graph.

8. CONCLUSION

In this study, a smartphone application was developed in order to measure specific parameters in the LTE communication network. The relationship between RSSI, RSSNR, RSRQ and RSRP values measured in the field and correlation of these values with the download speed was analyzed. Based on the analyses, it is seen that measured parameters RSSI and RSRQ increase the average data download speed, but they do not provide accurate information about network performance or instantaneous data rate. In other words, a good data rate value can be obtained at a measured point where the RSRQ value is too small, whereas the opposite can occur in a case where the data rate value at a very high RSSI or RSRQ value can be quite low. In addition, RSSNR and RSRP values enable accurate inferences about data rate performance below and above certain values. For example, a specific threshold value for RSRP and RSRQ can be mentioned in order to exceed a specific data rate value.

Measurement application CoverME is an application that covers all the parameters measured by measurement applications in literature. Cell location, network type, signal parameters, download speed and delay are measured with this application. In the next phase of the study, measurements will be made in different field classifications (Stadium, campus, concert area, intercity roads etc.) and will be classified for different movement speeds of the mobile user. In addition, by transforming the application into a crowd-sourcing application, gaining the ability to collect large amounts of data in a short time and determining the uploading speed is the next step in the work.

REFERENCES

[1] Cisco Annual Internet Report (2018–2023)

[2] Albero, F. M., Štern, A., & Kos, A. (2013). Mobile network measurements using Android. In ERK-2013 International Electrotechnical and Computer Science Conference (pp. 97-100).

[3] Johan J, Wuri A. H., Sean K., Gyula B. (2012). Minimization of Drive Tests in3GPP Release 11, IEEE Communications Magazine.

[4] https://gs.statcounter.com/os-market-share/mobile/worldwide, Feb 2019 - Feb 2020, Son Erişim 21.04.20.

[5] Li, W., Mok, R. K., Wu, D., & Chang, R. K. (2015, April). On the accuracy of smartphone-based mobile network measurement. In 2015 IEEE Conference on Computer Communications (INFOCOM) (pp. 370-378). IEEE.

[6] Goel, U., Wittie, M. P., Claffy, K. C., & Le, A. (2015). Survey of end-to-end mobile network measurement testbeds, tools, and services. IEEE Communications Surveys & Tutorials, 18(1), 105-123.

[7] Lauridsen, M., Rodriguez, I., Mikkelsen, L. M., Gimenez, L. C., & Mogensen, P. (2016, April). Verification of 3G and 4G received power measurements in a crowdsourcing Android app. In 2016 IEEE Wireless Communications and Networking Conference (pp. 1-6). IEEE.

[8] Kaup, F., Jomrich, F., & Hausheer, D. (2015, March). Demonstration of NetworkCoverage–A Mobile Network Performance Measurement App. In International Conference on Networked Systems (NetSys) (Vol. 77, No. 7, pp. 228-230).

[9] Sonntag, S., Schulte, L., & Manner, J. (2013, April). Mobile network measurements-It's not all about signal strength. In 2013 IEEE Wireless Communications and Networking Conference (WCNC) (pp. 4624-4629). IEEE.

[10] Sonntag, S., Manner, J., & Schulte, L. (2013, May). Netradar-measuring the wireless world. In 2013 11th International Symposium and Workshops on Modeling and Optimization in Mobile, Ad Hoc and Wireless Networks (WiOpt) (pp. 29-34). IEEE.

[11] Nikravesh, A., Yao, H., Xu, S., Choffnes, D., & Mao, Z. M. (2015, May). Mobilyzer: An open platform for controllable mobile network measurements. In Proceedings of the 13th Annual International Conference on Mobile Systems, Applications, and Services (pp. 389-404).

[12] Huang, J., Chen, C., Pei, Y., Wang, Z., Qian, Z., Qian, F., ... & Bahl, P. (2011). Mobiperf: Mobile network measurement system. Technical Report. University of Michigan and Microsoft Research.

[13] Cainey, J., Gill, B., Johnston, S., Robinson, J., & Westwood, S. (2014, September). Modelling download throughput of LTE networks. In 39th Annual IEEE Conference on Local Computer Networks Workshops (pp. 623-628). IEEE.

[14] Wu, D., Li, W., Chang, R. K., & Gao, D. (2016). MopEye: Monitoring per-app network performance with zero measurement traffic. arXiv preprint arXiv:1610.01282.

[15] Alepuz, I., Cabrejas, J., Monserrat, J. F., Perez, A. G., Pajares, G., & Gimenez, R. (2017, June). Use of mobile network analytics for application performance design. In 2017 Network Traffic Measurement and Analysis Conference (TMA) (pp. 1-6). IEEE.

[16] Lauridsen, M., Rodriguez, I., Mikkelsen, L. M., Gimenez, L. C., & Mogensen, P. (2016, April). Verification of 3G and 4G received power measurements in a crowdsourcing Android app. In 2016 IEEE Wireless Communications and Networking Conference (pp. 1-6). IEEE.

[17] Afroz, F., Subramanian, R., Heidary, R., Sandrasegaran, K., & Ahmed, S. (2015). SINR, RSRP, RSSI and RSRQ measurements in long term evolution networks. International Journal of Wireless & Mobile Networks.

[18] Huang, Junxian & Xu, Qiang & Tiwana, Birjodh & Mao, Zhuoqing & Zhang, Ming & Bahl, Paramvir. (2010). Anatomizing Application Performance Differences on. 165-178. 10.1145/1814433.1814452.

[19] Almohamedh, H., Al Qurashi, F., & Kostanic, I. (2014). Mobile videos quality measurements for long term evolution (LTE) network. vol. I, 505-509.

[20] https://www.sharetechnote.com/html/Handbook_LTE_CQI.html, Son Erişim 21.04.20.

[21] Kaup, F., & Hausheer, D. (2013, October). Optimizing energy consumption and qoe on mobile devices. In 2013 21st IEEE International Conference on Network Protocols (ICNP) (pp. 1-3). IEEE.

[22] Hazza A.S., Humaid A.S., Ivica K., Josko Z. (2018). Verifying Measurements of Reference Signal Received Power (RSRP)on LTE Network using an App on Android Smartphones, 2018 IEEE 9th Annual Information Technology, Electronics and Mobile Communication Conference (IEMCON), Canada.

[23] https://tools.ietf.org/html/rfc2681, Son Erişim 21.04.20.

[24] Xue, L., Ma, X., Luo, X., Yu, L., Wang, S., & Chen, T. (2017, May). Is what you measure what you expect? factors affecting smartphone-based mobile network measurement. In IEEE INFOCOM 2017-IEEE Conference on Computer Communications (pp. 1-9). IEEE.

[25] Zhuang, Z., Kim, K. H., & Singh, J. P. (2010, June). Improving energy efficiency of location sensing on smartphones. In Proceedings of the 8th international conference on Mobile systems, applications, and services (pp. 315-330).

[26] Apoorva Prakash M V, Dr. MC Padma (2014). Battery-Bandwidth Based Handover Framework for 3G/WLAN Using Android Handheld Devices, Journal of Engineering Research and Applications

ABBREVIATIONS

2G	Second Generation
3G	Third Generation
3GPP	The 3rd Generation Partnership Project
4G	Fourth Generation

BER	Bit Error Rate
CDMA	Code Division Multiple Access
CQI	Channel Quality Indicator
EC/IO	The Ratio of the Received/Good Energy to the Interference/Bad Energy
EVDO	Evolution Data Optimized
GPS	Global Positioning System
GSM	Global System for Mobile Communication
LTE	Long Term Evolution
MDT	Minimization of Drive Tests
QoE	Quality of Experience
RF	Radio Frequency
RFC	Request For Comments
RRM	Radio Resource Management
RSL	Received Signal Level
RSRP	Reference Signal Receive Power
RSRQ	Reference Signal Received Quality
RSSI	Received Signal Strength Indicator
RSSNR	Reference Signal Signal to Noise Ratio
RTT	Round-Trip Time
SINR	The Signal-to-Interference-Plus-Noise Ratio
SNR	Signal-to-Noise Ratio
TCP	Transmission Control Protocol
VPN	Virtual Private Network

INFORMATION

This study is partially supported by a research project with number of 16-muh-033 at the Ege University.

Kütahya Dumlupınar University
Institute of Graduate Studies

Journal of Scientific
Reports-A
E-ISSN: 2687-6167
Number 45, December 2020

RESEARCH ARTICLE

INVESTIGATION OF SOMA REGION COALS WITH RESPECT TO SPONTANEOUS COMBUSTION SUSCEPTIBILITY

Hasan Hüseyin ILICA[1], Özer ÖREN[2], Cem ŞENSÖĞÜT[3]

[1]Kütahya Dumlupinar University, Mining Engineering Dept., 43100, Kütahya, hasanhuseyinilica@outlook.com;
ORCID: 0000-0001-9975-2699
[2]Kütahya Dumlupinar University, Mining Engineering Dept., 43100, Kütahya, ozer.oren@dpu.edu.tr;
ORCID: 0000-0002-4629-1718
[3]Kütahya Dumlupinar University, Mining Engineering Dept., 43100, Kütahya, cem.sensogut@dpu.edu.tr;
ORCID: 0000-0001-9192-8813

Recieved Date:08.08.2020 *Accepted Date:30.10.2020*

ABSTRACT

One of the factors that make coal mining difficult is the spontaneous combustion of coal. Spontaneous combustion including various parameters is not only met in underground mining, but also in surface mining, stockyards and long-distance transport of coal by land and sea. This event, which threatened the occupational safety in mines, has effects of causing loss of lives and defecting human health. In mining enterprises, it causes production losses along with economic losses. It is a serious matter that requires good planning and supervision in order not to cause irreversible damages. Spontaneous combustion of coals develops depending on internal, environmental factors and production methods. In order to eliminate the problems caused by spontaneous combustion, the spontaneous combustion conditions of coals must be determined and classified beforehand. In this study, spontaneous combustion tendencies of Soma Region coals were generally determined with samples taken from Işıklar Colliery, İmbat Mining and Eynez Colliery of Demir Export. Using the crossing point method, a total of 30 experiments were carried out with 10 samples taken from each colliery to find out the risk of spontaneous combustion of the Soma Region coals. Based on the values obtained, it has been determined that the coals of the Soma Region have a "high" tendency to spontaneous combustion.

Key words: *Coal, Crossing point method, Oxidation, Spontaneous combustion*

1. INTRODUCTION

Spontaneous combustion of coals is a natural phenomenon that causes serious losses especially in the mining area and causes environmental pollution as a result of toxic gases released from burning of coal [1]. This problem can be encountered in long-term storage in thermal power stations, including coal stocks, surface mining, underground old production areas, dump sites and even in transport conditions such as long-distance cargo ships or trains [2]. Spontaneous combustion phenomenon has been tried to be enlightened by many researchers and scientists from different disciplines since the 17th century due to the complex structure of coal. Different theories have been developed to explain this phenomenon. Some of these theories; pyrite theory, bacterial theory, phenyl reaction, free radical reaction, hydrogen reaction, activation group reaction and coal - oxygen interaction theory. Among

JSR A
Journal of Scientific Reports

these theories, the most accepted approach by researchers is the theory of coal-oxygen interaction [3]. According to this theory, the reactions between coal and oxygen take place in two main stages as "direct combustion" and "chemisorption". In the stage called "direct burning"; oxidation products such as CO, CO_2 and H_2O are released as a result of the reaction between coal and oxygen [4]. "Chemisorption stage" consists of 4 consecutive sub-stages. These stages can be summarized as follows: 1) physical adsorption of oxygen, increase in temperature; 2) chemical adsorption (above 50°C), production of oxygenetic hydrocarbons or peroxy compounds; 3) decomposition of oxygenetic hydrocarbons when the spontaneous combustion temperature is reached (above 70°C) with simultaneous oxidation of unaltered coal; and 4) the occurrence of the phenomenon called spontaneous combustion when all of the processes in the first three substances cause temperatures higher than 150°C, typically defined as the ignition threshold [5]. Figure 1 shows the general reaction steps in coal oxidation [6].

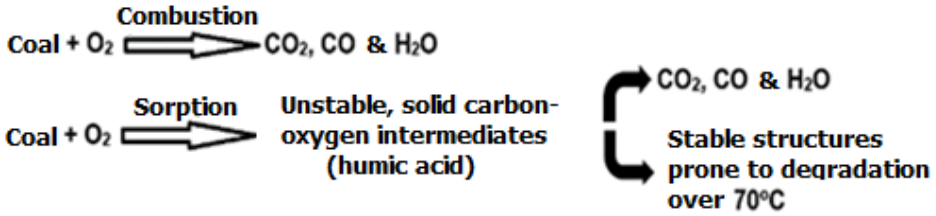

Figure 1. Reaction steps taking place in coal oxidation.

Many factors can affect the spontaneous combustion of coals. In the literature, these factors are divided into two as internal and external factors. While internal factors are mostly related to the physical properties of coal or rocks with organic content; External factors concern the geological characteristics of the coal seam and the site where the seam is located and the framework of the production method applied during mining. The parameters effective in spontaneous combustion are shown in detail in Table 1 [7]. In general, since low-rank coals contain more reactive moisture, oxygen and volatile matter, they are more prone to spontaneous combustion than high-rank coals [8]. Different opinions are put forward on the effects of moisture content in coal on oxidation and spontaneous combustion.

Table 1. Parameters effective in spontaneous combustion of coal.

Internal (endogenous) factors		External (exogenous) factors	
Coal features	Geological features	Atmospheric conditions	Factors related to mining
Carbonization degree	Seam thickness	Temperature	Production method
Petrographic structure	Seam slope	Moisture	Advance rate
Moisture content	Collapse feature	Oxygen concentration	Pillar conditions
Mineral matter content	Tectonic faults		Roof conditions
Particle size	Depth		Main gate conditions
Pyrite content	Geothermic gradian		Air leakage
Physical features			Coal losses
Bacteria			Mined out areas
			Filling conditions
			Ventilation pressure
			Air moisture

JSR A
Journal of Scientific Reports

It was found by the researchers that there is a critical humidity range value for the value at which coal's oxygen consumption is maximum; it has been stated that oxygen consumption rates decrease for coals below or above this humidity range [9]. Considering coal oxidation and the spontaneous combustion process is an event that occurs on the surface and pores of the coal. In the researches to date; it has been stated that the surface area increases as a result of the decrease in the particle size of the coal and it has the role of increasing spontaneous combustion since it allows the formation of additional surfaces that will come into contact with oxygen [10]. It is possible to say that high mineral substance content will reduce the spontaneous combustion of coal, since the increase of mineral substance in coal will decrease the amount of carbon in its structure. Apart from that, in the past studies, the oxidation accelerator of lime, soda and iron compounds in the coal structure; it is stated that minerals such as aluminum and silica have an effect that slows down the process in concern [11]. Especially in the literature, it has been stated that this ratio should be above 2% for pyrite to play an effective role in spontaneous combustion [12]. Contrary to this view, there are also studies suggesting that pyrite does not mean anything on its own and requires a certain amount of moisture to function as a catalyst in oxidation, and that pyrite alone does not contribute to oxidation in tests on dry samples [13]. The effects of coal petrography on spontaneous combustion are also among the topics that attract the attention of researchers in the literature. It is generally accepted that coals with high reactivity macerals such as liptinite and vitrinite are prone to spontaneous combustion [14]. Apart from internal factors, other factors that are effective in spontaneous combustion are external factors. External factors such as seam thickness and depth, ventilation and production method and advance rate stand out among external factors when evaluated in terms of the effect level. As the thickness of the coal seam increases, the thermal conductivity of the coal decreases and the heat accumulation in the coal may increase. In the block caving methods, which are frequently used in the excavation of thick coal seams, coal pieces with a fractured structure that have been abandoned without being produced in the goaf prepare the ground for spontaneous combustion [15]. It is stated in the literature that coal deposits with a thickness of more than 5 m are more prone to spontaneous combustion [16]. With the increasing depth, the risk of spontaneous combustion of coal increases in parallel. Rock pressure on coal in deep coal mines leads to breaking and cracking of the pillars left and especially the coal pieces at the coal face. These fractures and cracks form free surfaces for the coal to contact with oxygen [17]. Apart from this, it is stated in the literature that the geothermal gradient will increase as a result of the increase in the depth, the temperature of the coal and the surrounding rocks will increase as a result of this increase, and this will prepare a suitable environment for spontaneous combustion [11]. In general, as a result of the temperature increase of every 10°C at temperatures between 30-100°C, the oxidation rate of coal increases on average 2.2 times [18]. When examined in terms of atmospheric conditions in the mine, the effect of the amount of moisture in the air on spontaneous combustion is also shown among the parameters affecting spontaneous combustion. It is stated that humid air acting on the coal surface produces 2.5 times more heat than dry air [19]. If the partial pressure of the humidity in the air is high, moisture exchange between coal and atmospheric air, and the heat released during condensation may cause the temperature of the coal to increase and the risk of spontaneous combustion to increase [20]. The advanced longwall method is a more dangerous method for spontaneous combustion compared to the retreating longwall method due to the continuous air flow of the coals behind the goaf. In retreating longwall method, since the main gate roads are in the coal, air cannot find any way to escape and thus air leaks can be reduced to a minimum. In addition, different chemicals called inhibitors can be used to prevent the spontaneous combustion of coals and basically limit the contact of oxygen with coal. The inhibitors in wide range from inorganic salts such as NaCl, $MgCl_2$, $CaCl_2$ to antioxidants that can also be used in food products [21, 22].

JSR A
Journal of Scientific Reports

Mine fires caused by spontaneous combustion events in our country have caused a great loss of life and property in important enterprises such as the Turkish Hard Coal Enterprises and the Western Lignite Corporation [23, 24]. Studies of the determining to spontaneous combustion liability carried out by many researchers on various coals in our country have gained momentum after these events. Spontaneous combustion studies carried out by different researchers in different institutions, especially in the Zonguldak region, have given important ideas in terms of the oxidation characteristics of coal in the region [25-29]. In addition, in studies conducted at the Western Lignite Corporation, the ignition temperature of coals was determined as 138-146ºC and they were included in the high-risk coal [30]. Kadıoğlu ve Varamaz [31] examined the effects of moisture and dried air on the ignition temperatures of Aşkale and Balkaya lignites, found that the moisture content increased the ignition temperature values, while the ignition temperatures of coals passed through dry air decreased. Şensöğüt ve Çınar [32] determined the ignition temperatures of coals of Konya – Ermenek region as 151–160ºC and the liability index values as 4,4–7,3.

The center of the studies from the past to the present is the determination of the factors affecting the spontaneous combustion process, their prevention at the beginning of the combustion process or their disposal afterwards, and the determination of the spontaneous combustion tendency of the coal or organic rocks. Considering that spontaneous combustion is an actual process and the seam depth and coal structure may change with the production processes, it is important to carry out susceptibility measurements and risk assessments periodically. With this study, spontaneous combustion risks of coal samples taken from underground production faces of three separate private enterprises that continue their activities in the Soma region were determined.

2.MATERIAL AND METHOD

2.1. Preparation of Samples

Examples of lignite used in the study have been obtained from the production panels of three different private enterprises operating in the field of underground mining in Soma district of Manisa province (Demir Export / M2 panel, İmbat Mining / D11 panel and Soma Coal Enterprises / panel 8) (Figure 2).

Figure 2. Location map of the region where coal samples were taken.

JSR A
Journal of Scientific Reports

The samples obtained from the underground coal mines were covered with aluminum foil and stretch film in order to avoid oxidation and were quickly brought to the Mining Engineering Laboratories of Kütahya Dumlupinar University in closed containers. Subsequently, all samples were reduced to -75 µm in size and placed in airtight bags of approximately 200 g and preserved in the deep freezer until the test processes. The chemical analysis results of the samples have been obtained from the enterprises and are given in Table 2.

Table 2. Chemical analysis results of coal samples.

Analysis	**Soma Coal Enterprises**	**İmbat Mining**	**Demir Export**
Original total moisture (%)	10,0	11,7	10,6
Dried ash (%)	40,07	46,21	44,52
Dried volatile matter (%)	39,60	37,49	38,54
Dried fixed carbon (%)	19,43	18,89	17,81
Dried total sulphur (%)	1,07	0,78	1,85
Dried upper cal. val. (cal/g)	3127	2698	3461
Dried lower cal. val. (cal/g)	2959	2544	3281

2.2. Experimental Studies

Many methods and experimental devices have been developed in different countries of the world in determining the spontaneous combustion behavior of coals. Among the most commonly used of these experimental systems are isothermal and adiabatic calorimeter method [33, 34], dinamic oxidation method [26], basket heating method [35], Olpinski's method [36], TGA/DTA (thermogravimetric analysis/differential thermogravimetric analysis) [37, 38] ve crossing point temperature method [39]. The crossing point temperature method has advantages over other methods due to reasons such as ease of installation of the experimental set, low cost and widespread use in major coal producing countries such as China, India. In determining the spontaneous combustion tendency of the coals that are the subject of the present study, the set up that is currently operating in Kütahya Dumlupinar University, Mining Engineering Department, Spontaneous Combustion Test Laboratory was used (Figure 3). The set up in concern consists of an oven (Carbolite PF120, England) allowing to program and ramp at different temperature and time intervals, a chromium-nickel alloy reactor in which the coal sample is placed and the combustion takes place, thermocouple and data recorder (Testo 175-T3, Germany) for measuring the temperature of the coal in the reactor and flow meter (Cole Parmer, Dual-Float SN-32466-04, USA) that provides air to the coal at desired flow rates and oxygen and nitrogen cylinders.

JSR A
Journal of Scientific Reports

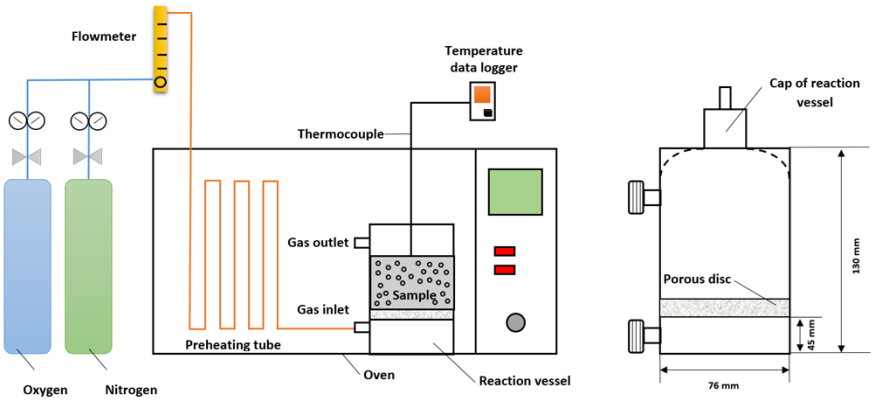

Figure 3. Spontaneous combustion test set up.

The crossing point method, which is widely used in the literature, was used to determine the spontaneous combustion susceptibility of the coals. In the experiments, 100 g coal samples reduced to -75 µm size were used.

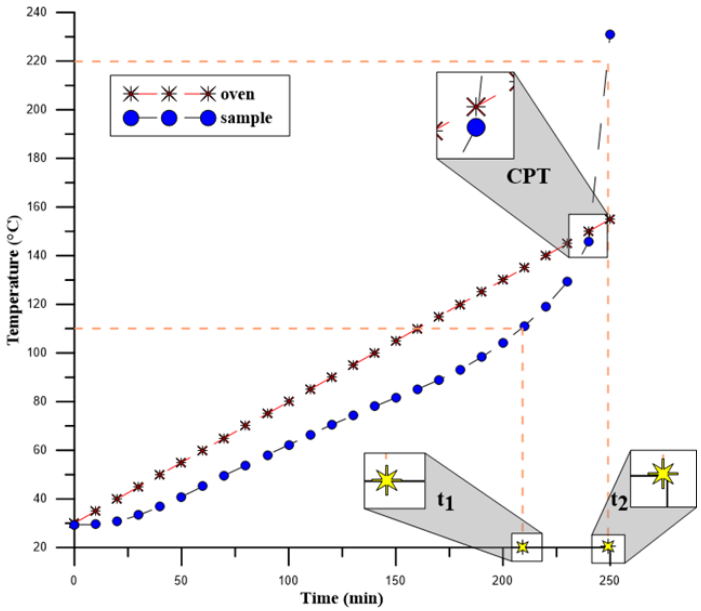

Figure 4. A typical spontaneous combustion curve.

At the beginning of the experiment, the coal sample was put into the reactor and the gas inlet and outlet connections of the reactor were made, and oxygen was not given into the reactor until the temperatures of the oven and coal sample equaled to 30°C during the equilibrium time period. Nitrogen gas was introduced into the reactor during the equilibrium time to prevent the coal from oxidizing. At the point where the process was completed and the temperatures of the coal and oven

JSR A
Journal of Scientific Reports

were equalized, oxygen was introduced to the reactor at a flow of 200 cc/min with 99.6% purity, and after this stage, the temperature values of the coal and oven were recorded every 10 minutes. In the experimental process, the temperature increase of the oven was set as 0.5°C/min and the temperature changes in the coal and oven were observed until the end of the experiment. The temperature of the coal sample oxidized over time reaches the temperature of the oven, which increases linearly, and the temperature of the oven and coal intersect at one point. While this point is called the "crossing point" in the literature, the temperature at that point is expressed as the "ignition temperature" (Figure 4).

2.3. Determination of Spontaneous Combustion Liabilities of Coals.
Spontaneous combustion tendencies of coals were determined by using the data obtained during the experiment. Empirical equation developed by Feng, Chakravorty and Cochrane [40] was used when making susceptibility classification (Equation 1 & 2). The formulation of the mentioned index and the explanations of the variables used in the formulation are given below.

$$I_{FCC} = \frac{\text{Average Heating Rate (AHR)}}{\text{Crossing Point Temperature (CPT)}} \times 1000 \quad (1)$$

Here;

I_{FCC} : Feng, Chakravarty, Cochrane index, min^{-1}.
AHR : Average Heating Rate between 110 - 220°C, °C min^{-1}

Average heating rate (AHR) is calculated by the formula given below;

$$AHR = \frac{110}{t_2 - t_1} \quad (2)$$

Where;

t_2: time when the coal sample reaches a temperature of 220°C, min
t_1: Time when the coal sample reaches a temperature of 110°C, min

By using the index (I_{FCC}), the spontaneous combustion tendencies of coals are classified as shown in Table 3.

Table 3. Liability classification of coals according to I_{FCC} index.

Susceptibility index	Risk category
0-5	low
5-10	medium
>10	high

3. CONCLUSION

In this study, spontaneous combustion characteristics of the coals procured from Soma Coal Enterprises (SK), Imbat Mining (IM) and Demir Export (DE) which continue their coal production activities in the Soma region were determined using the crossing point method. For each coal sample belonging to each enterprise, 10 crossing point tests were conducted and the results were examined.

JSR A
Journal of Scientific Reports

The test results and intersection graphs of all coals are given in detail in Table 4 and Figure 5-7, respectively.

When the experimental results are examined, the ignition temperatures of the samples taken from Panel 8, Soma Coal Enterprises are between 151 - 160°C; average heating rates ranged from 1.64 - 4.07°C min-1 and susceptibility indices ranged from 10.87 - 26.28 min-1.

Ignition temperatures of samples taken from D11 panel, Imbat Mining are 142 - 149°C; While average heating rates were determined between 2.07 - 4.23°C min-1, the susceptibility index values were determined between 14.6 - 28.78 min-1.

Ignition temperatures of the sample taken from M2, Demir Export panel are 142 - 151°C; average heating rates were found between 2.04 - 4.4°C min-1, whereas susceptibility indices were determined as 14.27 - 30.3 min-1.

In the light of the data obtained, Soma Basin lignite coals were identified as "high risk" in terms of spontaneous combustion. Although these results support the studies carried out in previous years; considering the parameters on spontaneous combustion and changes in production processes, it is vital to repeat spontaneous combustion susceptibility measurements and to evaluate production plans according to the risk scale in question.

Table 4. Spontaneous combustion results for all coal samples.

Sample	CPT (°C)	AHR (°C min^{-1})	I_{FCC} (min^{-1})	Risk classification
SK-1	151	1,64	10,87	High
SK-2	155	4,07	26,28	High
SK-3	153	2,75	17,97	High
SK-4	153	2,39	15,6	High
SK-5	159	3,24	20,38	High
SK-6	159	3,24	20,38	High
SK-7	160	3,44	21,5	High
SK-8	159	2,39	15,03	High
SK-9	155	3,33	21,48	High
SK-10	154	2,44	15,84	High
IM-1	142	2,07	14,6	High
IM-2	142	2,16	15,19	High
IM-3	142	2,619	18,44	High
IM-4	143	3,14	21,95	High
IM-5	144	2,82	19,58	High
IM-6	145	2,62	18,07	High
IM-7	146	2,62	17,88	High
IM-8	149	3,93	26,38	High
IM-9	148	4,07	27,5	High
IM-10	147	4,23	28,78	High
DE-1	145	4,4	30,3	High
DE-2	142	3,66	25,77	High
DE-3	143	2,04	14,27	High
DE-4	146	3,33	22,8	High

DE-5	150	3,33	22,2	High
DE-6	149	3,7	24,83	High
DE-7	148	2,82	19,05	High
DE-8	149	3,06	20,54	High
DE-9	149	3,24	21,74	High
DE-10	151	3,93	26,03	High

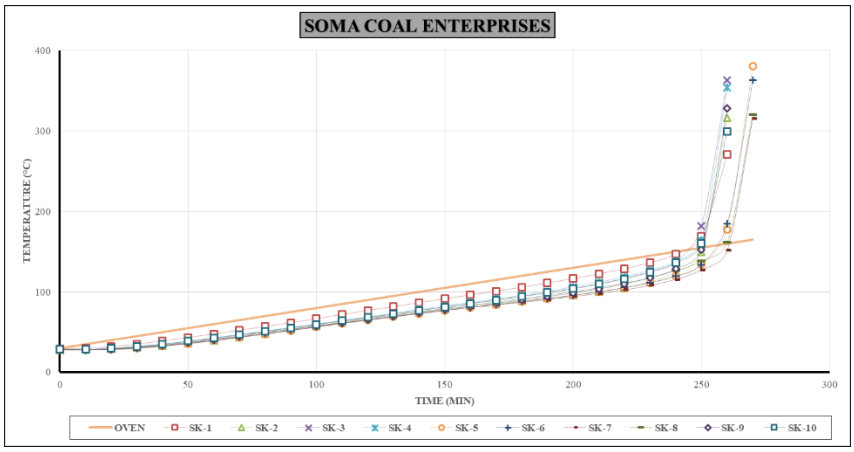

Figure 5. Time-temperature curves of experiments belonging to Soma Coal Enterprises (SK).

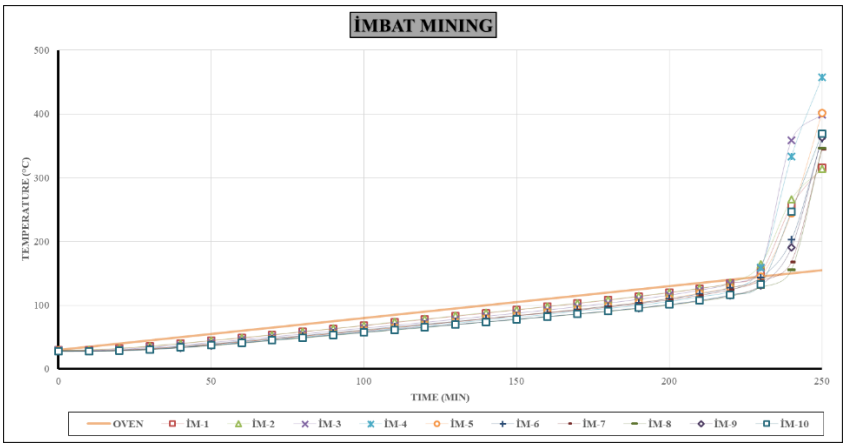

Figure 6. Time-temperature curves of experiments belonging to İmbat Mining (İM).

JSR A
Journal of Scientific Reports

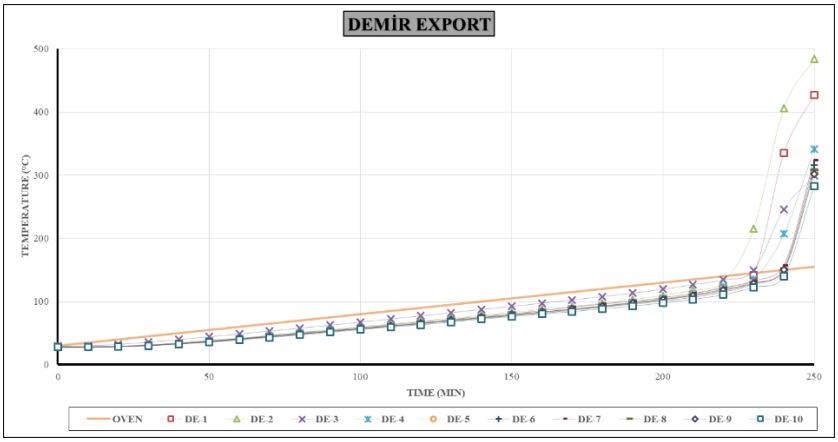

Figure 7. Time-temperature curves of experiments belonging to Demir Export (DE).

In addition, the relations between the proximate analysis values of coals and the ignition temperatures are given in Figure 8. During the investigation of this relationship, the average ignition temperatures obtained in 10 experiments for each coal sample were taken and the correlation between them was investigated. According to the results obtained, it is possible to say that the most significant relationship with the ignition temperatures of coals is with the ash content in coal. In general, as the amount of ash in coal increases, the ignition temperature values decrease. It is believed that this condition is caused by the content of mineral substances that accelerate oxidation found in the ash of coal, as revealed in some studies conducted in the past [41].

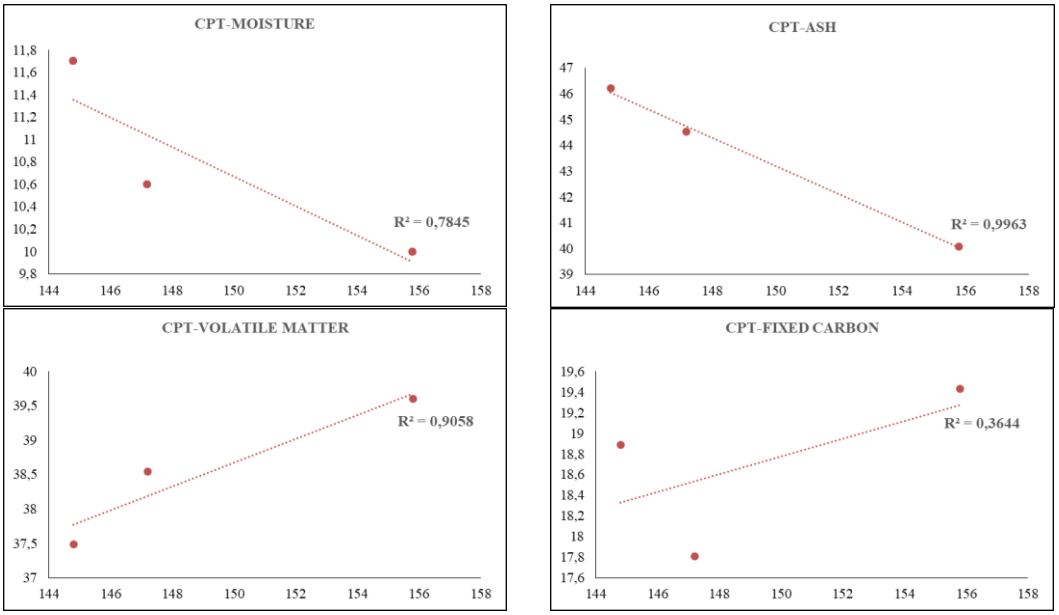

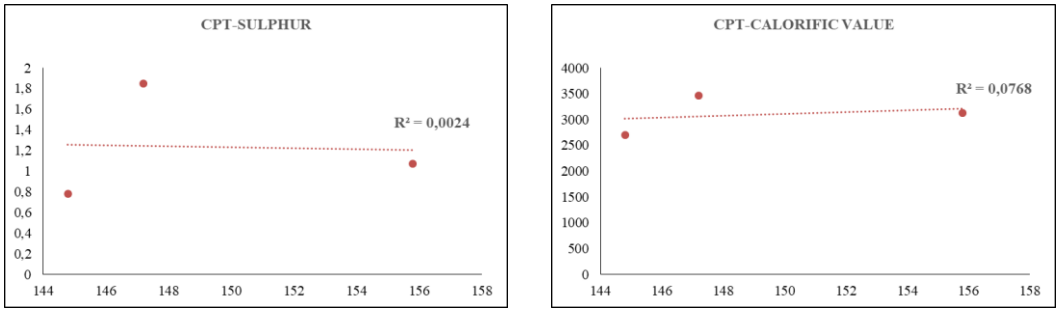

Figure 8. Relationship between proximate analysis values of coals and ignition temperatures.

ACKNOWLEDGEMENT

The authors give endless thanks to the authorities of Soma Coal Enterprises, Imbat Mining and Demir Export due to the help and conveniences they showed during the sample procurement stage.

REFERENCES

[1] Carras, J. N., Day, S. J., Saghafi, A. and Williams, D. J. (2009). Greenhouse gas emissions from low-temperature oxidation and spontaneous combustion at open-cut coal mines in Australia. Int. J. of Coal Geology, 78(2), 161–168.

[2] Fierro, V., Miranda, J. L., Romero, C., Andrés, J. M., Arriaga, a., Schmal, D. and Visser, G. H. (1999). Prevention of spontaneous combustion in coal stockpiles: Experimental results in coal storage yard. Fuel Processing Technology, 59(1), 23–24.

[3] Qi, X., Wang, D., Zhong, X., Gu, J. and Xu, T. (2010). Characteristics of oxygen consumption of coal at programmed temperatures. Mining Science and Technology (China), 20(3), 372–377.

[4] Carras, J. N., Young, B. C. (1994). Self-heating of coal and related materials: Models, application and test methods. Progress in Energy and Combustion Science, 20(1), 1–15.

[5] Gürdal, G., Hoşgörmez, H., Özcan, D., Li, X., Liu, H. and Song, W. (2015). The properties of Çan Basin coals (Çanakkale—Turkey): Spontaneous combustion and combustion by-products. Int. J. of Coal Geology, 138, 1–15.

[6] Wang, H., Dlugogorski, B. Z. and Kennedy, E. M. (2003). Coal oxidation at low temperatures: oxygen consumption, oxidation products, reaction mechanism and kinetic modelling. Progress in Energy and Combustion Science, 29(6), 487–513.

[7] Güney, M., (1968). Certain factors affecting the oxidation and spontaneous combustion of coal. University of Nottingham, Mining Dept. Magazine, 20, 71 – 80.

[8] Ramlu, M.A., (1991). Mine disastersand mine rescue. A.A. Balkema, Rotterdam, p.397

[9] Wang, H., Dlugogorski, B. Z. and Kennedy, E. M. (2003). Analysis of the mechanism of the low-temperature oxidation of coal. Combustion and Flame, 134(1–2), 107–117.

[10] Akgün, F., Arisoy, A. (1994). Effect of particle size on the spontaneous heating of a coal stockpile. Combustion and Flame, 99(1), 137–146.

[11] Didari, V. (1986). Yeraltı ocaklarında kömürün kendiliğinden yanması ve risk indeksleri. Madencilik Dergisi, 25(4), 29-34.

[12] Arisoy, A., Beamish, B. (2015). Mutual effects of pyrite and moisture on coal self-heating rates and reaction rate data for pyrite oxidation. Fuel, 139, 107-114.

[13] Beamish, B., Lin, Z. and Beamish, R. (2012). Investigating the influence of reactive pyrite on coal self-heating. Proc. of the Twelfth Coal Operators Conference (pp.294-299), Wollongong, Australia.

[14] Stracher, G.B.,Prakash, A. and Ellina, V.S. (2010). Coal and peat fires – A global perspective. vol.I: coal, geology and combustion, p.343

[15] Gill, F., Browning, E. (1971). Spontaneous combustion in coal mines. Colliery Guardian, 219, 79-85.

[16] Banerjee, S.C. (1985). Spontaneous combustion of coal and mine fires. A.A. Balkema / Rotterdam, 167 s.

[17] Kural, O. (1988). Kömür kimyası ve teknolojisi.

[18] Erkan, H. (1964). Kömürün depolanması. Madencilik, 3, 12-13.

[19] Karpuz, C., Güyagüler, T., Bağcı, S., Bozdağ, T., Başarır, H. ve Keskin, S. (2000). Linyitlerin kendiliğinden yanmaya yatkınlık derecelerinin tespiti: Bölüm I – Risk sınıflaması derlemesi. Madencilik Dergisi, 3-13.

[20] Kural, O. (1998).Kömür özellikleri, teknolojisi ve çevre ilişkileri. Özgün Ofset Matbaacılık A.Ş.

[21] Wang, D.; Dou, G.; Zhong, X.; Xin, H.; Qin, B. (2014). An experimental approach to selecting chemical inhibitors to retard the spontaneous combustion of coal. Fuel, 117, 218-223.

[22] Li, J., Li, Z., Yang, Y., Zhang, X., Yan, D. and Liu, L. (2017). Inhibitive Effects of Antioxidants on Coal Spontaneous Combustion. Energy Fuels, 31(12), 14180-14190.

[23] Saraç, S. (1992). Yeraltı Kömür Ocaklarında Kendiliğinden Yanma. Anadolu Üniversitesi Mühendislik – Mimarlık Fakültesi Yayınları, 106-118.

[24] Soytürk, T. (1992). Tunçbilek Kömürlerinin Kendiliğinden Yanmaya Yatkınlıklarının Araştırılması. Yüksek Lisans tezi Anadolu Üniversitesi Fen Bilimleri Enstitüsü, 77.

[25] Şahin, N., Didari, V. (2002). Zonguldak Kömürlerinde Kendiliğinden Yanmanın Erken Saptanması Amacıyla Yanma Ürünü Gazların İncelenmesi. Madencilik, 41, (4) 37– 51.

[26] Ayvazoğlu, E., 1978; EKİ Kozlu bölgesi Çay ve Acılık Kömürlerinin Oksidasyonunun Erken Tespiti Yönünden İncelenmesi. Türkiye 1. Kömür Kongresi, 539 – 563.

[27] Karaçam, E., Didari, V., Atalay, T. (1988). Zonguldak Kömürlerinin Kendiliğinden Yanmaya Yatkınlıklarının Araştırılması. Türkiye 6. Kömür Kongresi, 91 – 100.

[28] Yılmaz, A.O., Atalay, T. (1990). TTK Armutçuk Müessesesinde Kendiliğinden Yanma Olayının Araştırılması. Türkiye 7. Kömür Kongresi, 399–410.

[29] Kaymakçı, E. (1998). Zonguldak Havzası Kömür Damarlarına Uygulanabilecek bir Kendiliğinden Yanmaya Doğal Yatkınlığı Değerlendirme Tekniğinin Geliştirilmesi. Doktora tezi Zonguldak Karaelmas Üniversitesi Fen Bilimleri Enstitüsü.

[30] Saraç, S., Soytürk, T. (1992). Tunçbilek Kömürlerinin Kendiliğinden Yanmaya Yatkınlıklarının araştırılması. Türkiye 8. Kömür Kongresi, 141–152.

[31] Kadioglu, Y., Varamaz, M. (2003). The Effect of Moisture Content and Air – Drying on Spontaneous Combustion Characteristics of Two Turkish Lignites. Fuel, (82) 1685-1693.

[32] Sensogut, C., Cinar, I. (2000). A Research on the Tendency of Ermenek District Coals to Spontaneous Combustion. Mineral Resources Engineering, 9(4), 421– 427.

[33] Beamish, B.B., Barakat, M.A., St.George, J.D. (2000. Adiabatic testing procedures for determining self-heating propensity of coal and sample ageing effects. Thermochimica Acta, 362, 79-87.

[34] Zubíček, V., Adamus, A. (2013). Susceptibility of coal to spontaneous combustion verified by modified adiabatic method under conditions of Ostrava-Karvina coalfield, Czech Republic. Fuel Processing Technology, 113, 63-66.

[35] Chen, X.D. (1999). On basket heating methods for obtaining exothermic reactivity of solid materials: The extent and impact of the departure of the crossing-point temperature from the oven temperature. Process Safety and Environmental Protection, 77(4), 187-192.

[36] Zubíček, V. (2008). Assessment of susceptibility of coal to spontaneous combustion in OKR. Geoscience Engineering, 4, 1-9.

[37] Avila, C., Wu, T., Lester, E. (2014). Estimating the spontaneous combustion potential of coals using thermogravimetric analysis. Energy&Fuels, 28, 1765-1773.

[38] Pis, J.J., de la Puente, G., Fuente, E., Moran, A., Rubiera, F. (1996). A study of the self-heating of fresh and oxidized coals by differantial thermal analysis. Thermochimica Acta, 279, 93-101.

[39] Oren, O., Sensogut, C. (2010). Spontaneous combustion liability of Kutahya (Turkey) region

lignites. Energy Sources, Part A: Recovery, Utilization and Environmental Effects, 32, 877-885.

[40] Feng, K.K., Chakravorty, R.N. and Cochrane, T.S. (1973). Spontaneous combustion – a coal mining hazard. The Canadian Mining and Metall. Journal, 66(738), 75–84.

[41] Beamish, B. B., Blazak, D.G. (2005). Relationship Between Ash Content and R70 Self-heating Rate of Callide Coal. International Journal of Coal Geology, 64, 126-132.

Kütahya Dumlupınar University
Institute of Graduate Studies

Journal of Scientific
Reports-A
E-ISSN: 2687-6167
Number 45, December 2020

RESEARCH ARTICLE

RECOVERY OF COAL SLIME BY USING THE KNELSON CONCENTRATOR

Ali UÇAR[1,*], Oktay ŞAHBAZ[2], Nezahat EDİZ[3], Sevgi KARACA[4], İ.Göktay EDİZ[5]

[1] Kütahya Dumlupınar University, Faculty of Engineering, Department of Mining Engineering, Kütahya, ali.ucar@dpu.edu.tr, ORCID: 0000-0002-5220-8829
[2] Kütahya Dumlupınar University, Faculty of Engineering, Department of Mining Engineering, Kütahya, oktay.sahbaz@dpu.edu.tr, ORCID: 0000-0003-0945-9048
[3] Kütahya Dumlupınar University, Faculty of Engineering, Department of Mining Engineering, Kütahya, nezahat.ediz@dpu.edu.tr, ORCID: 0000-0001-9619-7589
[4] Kütahya Dumlupınar University, Faculty of Engineering, Department of Mining Engineering, Kütahya, sevgi.karaca@dpu.edu.tr, ORCID: 0000-0001-7478-2437
[5] Kütahya Dumlupınar University, Faculty of Engineering, Department of Mining Engineering, Kütahya, goktay.ediz@dpu.edu.tr, ORCID: 0000-0003-0874-1113

Received Date:05.10.2020 *Accepted Date: 15.12.2020*

ABSTRACT

The coal slimes are formed during the gravity processes applied at the coal preparation plant (Coal Washery). After the washing process of coal, large amounts of fine coals with a high calorific value is being discharged to the abandoned open cast spaces causing economic losses and significant environmental problems. A re-processing of these coal slimes by using the newcomer separation devices, such as Knelson concentrator, is a necessity due to the filling up of ponds, requirements of new legislation, and so on. In this study, the recovery of fine coal slimes of Tuncbilek Washery in Kutahya-Turkey was carried out by using the Knelson Concentrator (KC). Besides, the effect of particles sizes on the recoverability of fine coals was also investigated to reach optimum recovery. According to the particle size analysis made for this purpose, the maximum particle size of the samples was found as 4 mm while the ratio of material below 0.038 mm was found as 69.66%. From the chemical analysis made (ash, calorific value), it was also found that the ash content and the upper calorific value of the waste material 68% and 1603 kcal/kg, respectively. After the coal processing studies carried out using the KC for two different particle size groups, it was realized that the recovery rate was highly reduced at carbon content which is the indicator of the valuable substance while it was slightly decreased at lower particle sizes. When all the coal processing results were considered, it could be concluded that clean coal with 70% carbon content and an upper calorific of 4807,9 kcal/kg could be obtained through a combustible recovery of 57.4%.

Keywords: *Coal Recovery, Knelson Concentrator, Slime Pond, Western Lignite Corporation*

1. INTRODUCTION

Coal, an organic sedimentary rock, contains minerals and combustible organic substances in the maceral structure. Coal is heterogeneous at certain levels. At its simplest level, it is a mixture of organic and inorganic phases. However, the mineral material of the coal is composed of inorganic

constituents of the plant, other organic substances and the inorganic constituents which have different structures and liberation characters carried to coal bed [1].

Coal preparation and enrichment is a process in which the value of raw coal is increased by reducing the content of impurities such as inorganic matter. The quality of the operation depends on many parameters, and particle size is one of the most important parameters. The finer the particle size is, the harder the separation will be. Therefore, it very hard to separate coal slimes from the gangue. Increased fine size coals called as slimes caused due to the fragile nature of the coals and the increased mechanized production methods cannot be enriched using the existing methods. These fine coals not only cause economic loss but also cause environmental problems. Such causes necessitate the evaluation of the coal in the fine fractions. Besides, slimes, are problematic for coal washeries.

Coal slimes processing plants have higher water content and are generally stored in a waste dam near the coal mine. These slimes are problematic in terms of processing due to the fine size, oxidization, and so on [2]. Many researchers have investigated to find the most appropriate method to separate coal slimes from the inorganic materials due to the environmental and economical concerns. Types of equipment that make the separation between organic and inorganic components of coal (+0.1 mm) for the enrichment purposes such as heavy media, jig, shaking table, spirals, cyclone, etc. are effectively used for mining industry efficiently with low cost. However, the recovery decreases for fine size by using these types of equipment, and if the size is less than 0.1 mm, the enrichment is rather difficult and costly [3, 4]. Advanced gravimetric enrichment, based on centrifugal forces, and flotation methods have become more effective in the separation of such fine size coal [5, 6, 7, 8]. However, in the flotation process, environmental problems arise together with the costs of the reagents, and the oxidization of coal [4, 9, 10, 11]. Therefore, centrifugal force-based gravity concentrator seems higher potential to separate coal slimes from gangue minerals.

Centrifugal separators using the gravity-based separation mechanism can be divided into three basic types: vertical axis machines (Knelson, Falcon etc.), centrifugal jigs (Altar jig, Kelsey jig) and horizontal axis machines (Multi-Gravity separator). By using high gravitational force of these devices, efficient and effective separation of ultra-fine free particles is made possible [6, 10, 11, 12].

Based on the aforementioned trends, it is clear that there is a need for a highly effective physical coal cleaning technology to recover fine coals present in modern coal preparation plants. One of these separators is the Knelson Concentrator (KC) with a vertical axis conical bowl type that performs the concentration process using the fluidized bed mechanism. The different series of KCs are used for different application purposes, such as base metals and coal industries all over the world. KC has the advantages of simple construction, small installation space, high capacity, recovery for large particle sizes, and most importantly the benefits of having very large enrichment rates up to 1000: 1 in a single step. The separation principle of KC is based on the difference between centrifugal forces applied to heavy and light particles and separation bed fluidization [4, 6, 9, 10, 12, 13, 14].

The movement of a particle in a centrifugal fluid bed depends on the number of parameters, such as the geometry of the conical reservoir, the physical properties of the particles, and the operational conditions of the concentrator. The efficiency of the KC also depends on some basic parameters such as the size of the feed particles, the feed type, the feed particle class, the feed rate, the centrifugal force density, the concentration cycle, the bed fluidizing water flow rate and pressure. Minor changes

in these parameters can cause significant variations in the effectiveness of the separation process [13, 14].

Previous studies on the enrichment of coal in different sizes and properties have been carried out by some researchers. In these studies, the effect of fluidizing water rate, centrifugal force and feed rate on the separation was investigated.

Sabah and Koltka (2014) obtained a clean coal containing 30.51% ash with a amount of 81.18% for the particle size of -0.5+0.038 mm having 42.6% ash content from Aegean Lignite Corporation (ALC) waste pond [15].

Honaker et al. (1996) obtained a clean coal with 8% ash and 85% combustible recovery by using the KC. In this study feed size is -0.6 + 0.210 mm and an ash content of the feed is 21% [6]. Honaker and Das (2004) also obtained a clean coal with 8% ash content and 90% combustible recovery from the feed of 22% ash content with a size range of -0.150 + 0.044 mm by using a pilot scale KC [16].

According to a study carried out by Oney and Tanriverdi (2016) on the enrichment of Amasra coals containing 34.30% ash with a size of -1 + 0.15 mm, a clean coal with 16.28% ash content was obtained with a combustible recovery of 67.82% [14].

In another work carried out by Uslu et al. (2012), oxidized coal with a high-sulphur content was classified by the size ranges of -0.106, -0.300 + 0.106 and -0.500 + 0.300 mm and then enriched with KC. 99.13% combustible recovery and 60.94% carbon content were achieved in the range of -0.500 + 0.300 mm [4].

Tunçbilek coal processing plant of Western Lignite Corporation (WLC) was taken into operation in 1952 while Ömerler coal washery of the same corporation has been in service since 1993 in Tunçbilek, Kütahya (Turkey). Coal processing is carried out by the use of gravity methods in both plants and fine wastes arise at significant amounts. These wastes have been stored in abandoned open cast spaces of the No. 4 and Beke Yörgüç for a long time. However, the slimes of both coal washing plants are still being discharged to the pond of 6/C worked out open cast panel, since these spaces are already filled up (Figure 1).

It was reckoned by the WLC administration that safe storage of slimes in ponds according to the new "Mineral Waste Regulation" will increase the storage costs considerably. Therefore, alternative approaches such as partial or total enrichment of coals from the wastes or isolating the wastes after dewatering process in suitable deposits to prevent environmental negative effects should be considered. However, the main obstacles for the use of fine coal wastes in the nearby power station after dewatering were considered to be the high dewatering costs, insufficient thermal value (1300-1800 kcal/kg) and the high humidity value (30-35%).

The protocol values agreed for the raw coal/mix fed to the Celikler Tunçbilek B Group Thermal Power Plant by the corporation are given in Table 1. According to the values listed in Table 1, it is impossible to comply with these base values by only dewatering. Therefore, there is a necessity of enrichment to obtain these base values.

JSR A
Journal of Scientific Reports

Figure 1. Location of the ponds No. 4, Beke-Yorguc and 6/C panel and Tuncbilek Coal Processing Plant.

Table 1. Protocol values of raw coal/mix fed Celikler Tunçbilek B Group Thermal Power Plant.

Base value of lower calorific value (kcal/kg)	Highest lower calorific value (kcal/kg)	Lowest lower calorific value (kcal/kg)	Moisture (%)	Ash (%)	Particle size (mm)
2 350	3 000	1 900	24 (± %10)	42 (± %10)	0-1000

In this study, the beneficiation of fine size coals in No. 4 slime pond of WLC was investigated by using the Knelson concentrator. The optimum conditions have been tried to achieve by taking into considerations of various parameters includes particle size, rotation speed and water flow rate. Thus, we tried to figure out the possible application of KC for Turkish coal industry.

2. EXPERIMENTAL STUDIES

2.1. Material and Method

The samples used in the experiments were taken from the No. 4 slime pond of WLC. The material taken from the field was then brought to Mineral Processing Laboratory of Mining Engineering

JSR A
Journal of Scientific Reports

Department of Dumlupinar University, Turkey. The sample was homogenized systematically. The sample was then stored for use in experimental studies after reduction by cone and quartering, and sample divider. Russell sieve was used for size classification of the sample.

Sieve analysis was performed for the samples taken from the slime pond to determine the size distribution of the material by using the Retsch type laboratory sieves. The particle size analysis results of the samples are shown in Table 2.

The maximum particle size is 4 mm and the material ratio of -0.038 mm is 69.55% when Table 2 is examined for original particle sizes, The ash and upper calorific value (UCV) analyses have been made according to the particle size groups of the same sample. Ash analysis was carried out in a Nuve brand ash oven and calorimetric measurements on the Ika Werke instrument. The results obtained from these analyses are also given in Table 2.

Table 2. Particle size and ash-calorific value analysis of the slime pond sample .

Particle size (mm)	Fractional			Cumulative		
	Weight (%)	**Ash (%)**	**UCV (kcal/kg)**	**Weight (%)**	**Ash (%)**	**UCV (kcal/kg)**
+4	0.24	27.25	5191	0.24	27.25	5191
-4+2	1.50	24.83	5441	1.74	25.16	5407
-2+1	2.87	20.41	5731	4.61	22.20	5609
-1+0.85	0.24	25.45	5170	4.85	22.36	5587
-0.85+0.5	5.16	23.46	5403	10.01	22.93	5492
-0.5+0.3	2.75	30.52	4936	12.76	24.57	5372
-0.3+0.15	6.64	39.41	4561	19.40	29.65	5095
-0.15+0.075	4.41	47.38	3757	23.81	32.93	4847
-0.075+0.038	6.63	48.26	2255	30.44	36.27	4282
-0.038	69.56	81.91	431	100.00	68.02	1603
Total	100	68.02	1603			

Depending on the particle size decrease, an increase in the ash values and a decrease in the calorific values is expected. It is also seen that the ash value of the feed material is high.

The materials in the -1 + 0.212 and -0.212 + 0.038 mm size groups obtained from the sample of No 4 slime pond were subjected to enrichment process with the laboratory type Knelson Concentrator (KC-MD3). Experiments were carried out with the rotation speed of 150, 430, 700, 1000 rpm, and the bed fluidizing water flow rate of 2, 3 and 4 L/min, respectively. The overflow product (clean coal) formed by feeding the KC at a rate of 10% solids and 0.75 L / min of flowrate was collected in a bucket and the downstream (residue) remained in the reservoir. The contents of the bowl were taken by washing into the bucket. After dewatering with a vacuum filter, the products were dried, weighed and analyzed in terms of ash content.

JSR A
Journal of Scientific Reports

Combustible recovery values of the experiments were calculated using Equation 1.

$$\%Combustible\ Recovery = \frac{C(100-c)}{F(100-f)} \times 100 \quad (1)$$

where C and F are concentrate and feed amount, c and f are concentrated and feed ash, respectively.

3. EXPERIMENTAL RESULTS

In this study, KC, which is a newcomer gravity separator, was used to clean fine coals effectively. Although KC has not yet been applied to industrial scale for coal cleaning, different researches have been carried out in recent years on this subject [4, 6, 9, 10, 11, 13, 16] . In this study, oxidized coal samples from No. 4 slime pond of WLC were used. In the first tests, the sample was classified in two different size groups which were -1 + 0.212 and -0.212 + 0.038 mm, and then the sample was subjected to KC experiments. Experimental variables were rotation speed of the conical bowl and flow rate of the fluid. The results obtained in these experiments are given in Figures 2 and 3.

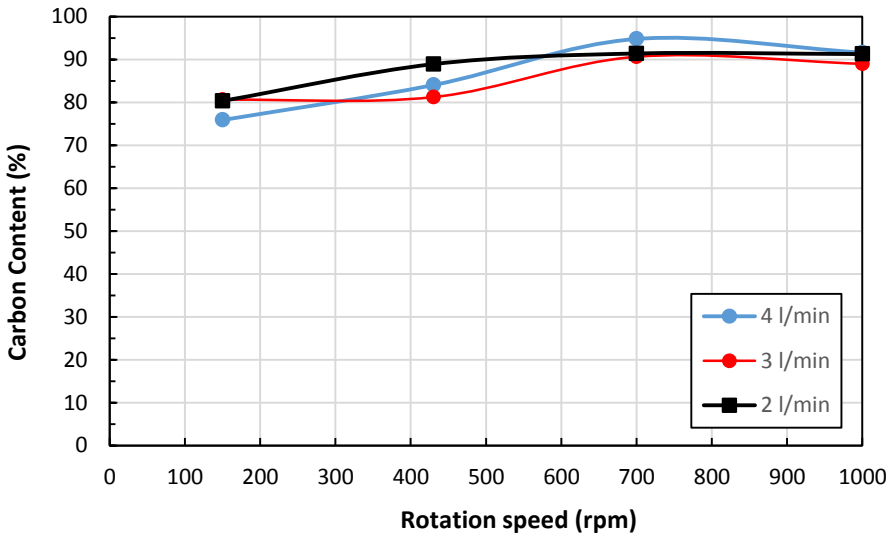

Figure 2. The effect of rotation speed on carbon content of -1.0 + 0.212 mm particle size group.

JSR A
Journal of Scientific Reports

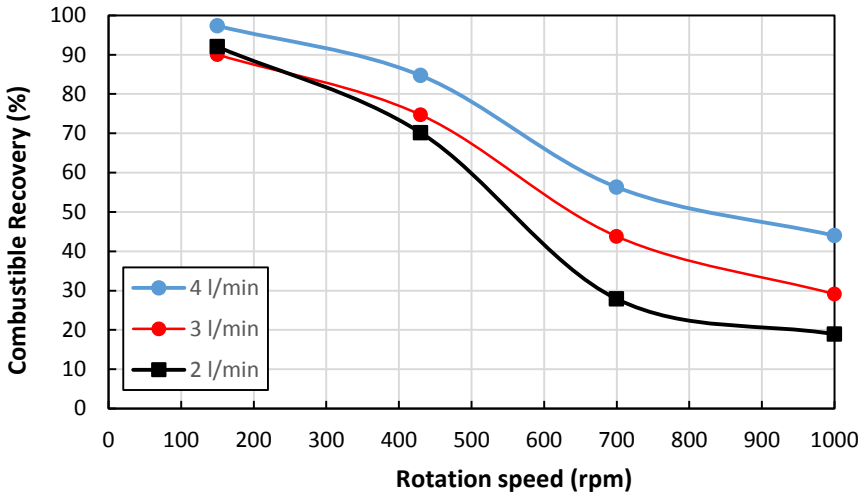

Figure 3. The effect of rotation speed on combustible recovery of -1.0 + 0.212 mm particle size group.

According to Fig. 2, the carbon content slightly increases with the increase of rotational speed of KC's bowl. However, the combustible recovery diminished significantly with the increase in rotation speed and water flow rate. The increase in rotation speed causes the increase of centrifugal force. Therefore, light particles, which are coal here, tend to remain in the bowl of knelson concentrator with the heavy minerals. Thus the combustible recovery decreases with the increase of rotation speed (Figure 3). Clean coal having 80.36% carbon content with 95.29% combustible recovery was obtained at 150 rpm and 2 L/min water flow rate

.

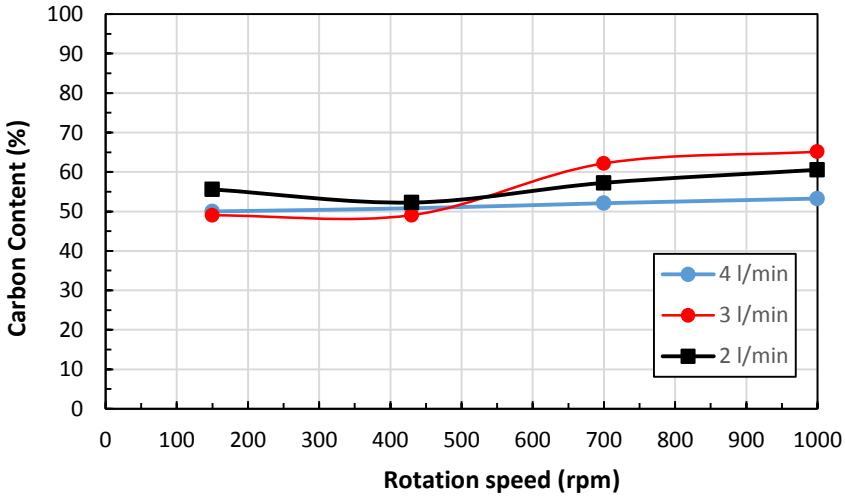

Figure 4. The effect of rotation speed on carbon content of -0.212+0.038 mm particle size group.

JSR A
Journal of Scientific Reports

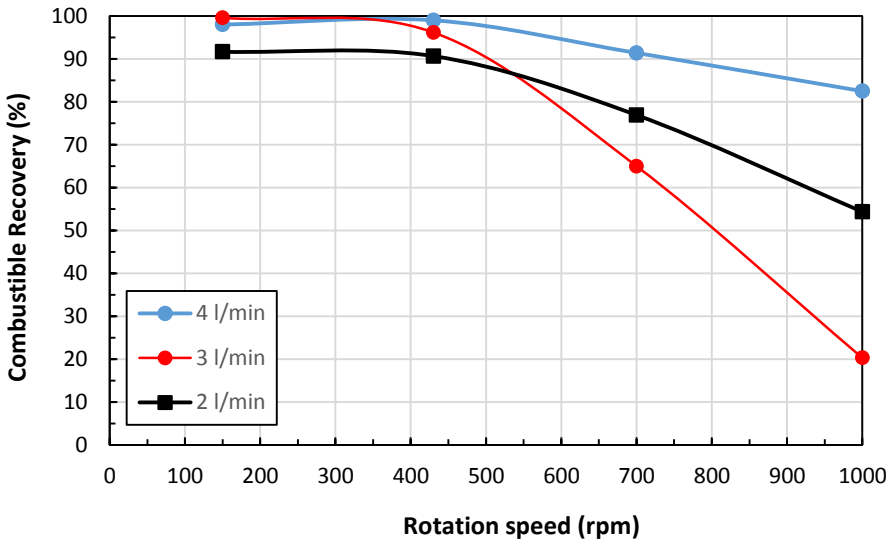

Figure 5. The effect of rotation speed on combustible recovery of -0.212+0.038 mm particle size group.

In the fine-size group of -0.212 + 0.038 mm, the values obtained were rather low with regarding to the coarse size group even though there was a slight increase depending on the rotation speed (Fig 4). The combustible recovery remained constant at high rates up to 430 rpm while it was decreased above it (Fig 5). However, the combustible recovery was not significantly different at 150 rpm when compared with the coarse size group, while the dramatic decrease was obtained after 430 rpm.

In this size group, clean coal with 55.58% carbon content and 91.66% combustible recovery was obtained at 150 rpm and 2 L/min.

Table 3. Combined results of the sample obtained from the slime pond.

Particle size (mm)	Product	Weight (%)	Carbon Content (%)	Combustible Recovery (%)	UCV (kcal/kg)
+1		4.62	77.84	11.30	5521
-1+0.212	Concentrate	11.05	80.36	27.92	5641
	Tailing	1.88	23.37	1.38	
-0.212+0.038	Concentrate	10.40	55.58	18.17	3606
	Tailing	2.50	21.06	1.65	
-0.038		69.55	18.09	39.56	
Feed		100.00	31.80	100.00	1603

By increasing the centrifugal force at high rotational speed, it was observed that the coal remained between the ribs with mineral substances, in spite of the lower specific gravity. That is, the light

particles are particularly retained due to the centrifugal force, especially at fine sizes. Thus, there was a decrease in combustible recovery and carbon content values.

The combined mass balance of the products obtained by classification and enrichment of the slime pond sample is given in Table 3. Table 3 indicates that the combining the concentrates of size groups with the size fraction of +1 mm, clean coal with 70% carbon content was obtained with 57.4% combustible recovery.

4. RESULTS

In this study, it was tried to enrich the coal sample, which was obtained from No-4 slime pond of WLC-Turkey, by using the KC. According to the sieve analysis results of the slime pond sample, the largest particle size is 4 mm and the ratio of material below 0.038 mm is determined as 69.66%. The ash and upper calorific value of the sample were determined as 68.01% and 1603 kcal/kg, respectively.

The experiments were carried out at below conditions for two samples, having the size of -1+0.212 mm with 70% carbon content and the size of 0.212+0.038 mm with 48% carbon content, by using the KC.

Solid ratio (%): 10
Feed flowrate (L/min): 0.75
Rotation speed (rpm): 150
Water flowrate (L/min): 2

The results of the enrichment experiments conducted are summarized below:

- Clean coal with 80.36% carbon content, 95.29% combustible recovery and 5641 kcal/kg upper calorific value was obtained from the -1 + 0.212 mm while clean coal with 55.58% carbon content, 91.66% combustible recovery and 3606 kcal/kg upper calorific value was produced from the material was -0.212 + 0.038 mm.
- It was determined that a clean coal with 70% carbon content, 57.4% combustible recovery and 4807.9 kcal/kg upper calorific value could be obtained by the enrichment of slime pond samples as a whole.
- It was also found that a decrease in particle size causes dramatic diminish in the carbon content of the clean coal whilst there is no significant change in combustible recovery.

ACKNOWLEDGEMENT

The authors of the paper would like to thank the authorities of the Western Lignite Corporation (WLC) Directorate for their understanding and for providing necessary data during the research.

REFERENCES

[1] Meyers R.A., Laskowski, J.S., Walters, A.D., (2001), Coal Preparation, Encyclopedia of physical science and technology, Energy, Editor-in-Chief: Robert A. Meyers, 277.

JSR A
Journal of Scientific Reports

[2] Anonim, (2017), http://www.sourcewatch.org/index.php/Environmental_impacts_of_coal, İndirme Tarihi: 25.05.2017.

[3] Kemal, M., Arslan, V., (1999), Kömür teknolojisi, Dokuz Eylül Üniversitesi Mühendislik Fakültesi Yayınları, 33, 373.

[4] Uslu, T., Sahinoglu, E., Yavuz, M., (2012), Desulphurization and deashing of oxidized fine coal by Knelson concentrator, Fuel Processing Technology, 101, 94–100.

[5] Aktaş, Z., (2002), Some Factors Affecting Spherical Oil Agglomeration Performance of Coal Fines, International Journal of Mineral Processing, 65, 177-190.

[6] Honaker, R.Q., Wang, D., Ho, K., (1996), Application of the falcon concentrator for fine coal cleaning, Minerals Engineering, 9, 1143-1156.

[7] Osborne, D.G., (1988), Coal Preparation Technology (1st ed.), London: BP Coal Ltd.

[8] Özbayoğlu, G., Mamurekli, M., (1988), Zonguldak Kömürlerinden Süper Temiz Kömür Üretimi, Türkiye 6. Kömür Kongresi, TMMOB, Zonguldak, 159-170.

[9] Ghaffari, A., Farzanegan, A., (2017), An investigation on laboratory Knelson Concentrator separation performance: Part 1: Retained mass modelling, Minerals Engineering, 112, 57–67.

[10] Kökkılıc, O., Langlois, R., Waters, K.E., (2015), A design of experiments investigation into dry separation using a Knelson Concentrator, Minerals Engineering, 72, 73–86.

[11] Peer, F., Mongwe, A., Van Heerden, J.H.P., (2002), A preliminary investigation into the metallurgical efficiency of an enhanced gravity separator, The Journal of South African Institute of Mining and Metallurgy, 251-254.

[12] Xiao, J., (1998), Testing A New Gold Centrifugal Concentrator, Department of Mining and Metallurgical Engineering, McGill University, Montréal, Canada, Master's thesis.

[13] Fatahi, M.R., Farzanegan, A., (2017), DEM simulation of laboratory Knelson concentrator to study the effects of feed properties and operating parameters, Advanced Powder Technology, 28, 1443–1458.

[14] Öney, Ö., Tanrıverdi, M., (2016), Zonguldak İnce Kömürlerinin Knelson Ayırıcıda Zenginleştirilebilirliğinin Araştırılması, Türkiye 20. Kömür Kongresi, TMMOB, Zonguldak, 375-383.

[15] Sabah, E., Koltka, S., (2014), Separation Development Studies on the Beneficiation of Fine Lignite Coal Tailings by the Knelson Concentrator, Energy Fuels, 28(7), 4819–4827.

[16] Honaker, R.Q., Das, A., (2004), Ultrafine Coal Cleaning Using a Centrifugal Fluidized-Bed Separator, Coal Preparation, 24, 1–18.

Kütahya Dumlupınar University
Institute of Graduate Studies

Journal of Scientific
Reports-A
E-ISSN: 2687-6167
Number 45, December 2020

RESEARCH ARTICLE

THE EFFECT OF PH AND CURRENT DENSITY IN THE REMOVAL OF ALUMINUM COBALT, CHROMIUM, AND ZINC FROM METAL PROCESSING WASTEWATER BY ELECTROCOAGULATION METHOD

Nevzat BEYAZIT[1,*] and Banu TÜRK[2]

[1] Ondokuz Mayıs University, Faculty of Engineering, Department of Enviromental Engineering, Samsun, nbeyazit@omu.edu.tr, ORCID: 0000-0002-8396-5996
[2] Ondokuz Mayıs University, Faculty of Engineering, Department of Enviromental Engineering, Samsun, turkbanu61@gmail.com, ORCID: 0000-0002-7809-3468

Recieved Date:29.10.2020 *Accepted Date: 16.12.2020*

ABSTRACT

In this study, the effects of initial pH (3, 5, 7, 9) and current density (25, 50, 75, 100, 125, 150, 175, 200 A/m^2) on the removal of Al^{3+}, Co^{2+}, Cr^{6+} and Zn^{2+}ions from metal processing wastewater by electrocoagulation method were examined. Iron and stainless steel electrodes were used as anode and cathode materials. All of the removal efficiencies were insignificant at the initial pH value of 1.32. As the initial pH values were increased the removal efficiencies increased in all stages of the experiments. With increasing the pH from 3 to 9, removal efficiencies increased from 67.4% to 99.2% for Al, from 18.1% to 99.7% for Co, and from 36.6% to 99.9% for Zn, while removal efficiencies for Cr were over 99% for each pH. Although the inital concentration of Co was relatively low, it was only removed with over 99% efficiency at long electrocoagulation times or at relatively high final pH values. A similar trend was determined for Zn, but this case was explained by a relatively high concentration of Zn. While the maximum removal efficiency was achieved with a current density of 50 A/m^2 for Cr, the efficiency increases were more obvious with increasing current density for Al, Co, and Zn.

Keywords: *Electrocoagulation, pH, Current Density, Metal Processing*

1. INTRODUCTION

Most of the metals such as aluminium, cobalt, chromium, and zinc are toxic or carcinogenic and cause toxic effects. Therefore, it is very important to treat metal-containing wastewaters before discharging into receiving environments.The most used heavy metal removal from wastewaters containing metal ions is precipitation with $Ca(OH)_2$, NaOH, and coagulation with $FeSO_4$ or $Al_2(SO_4)_3$ compounds [1,2,3,4]. Other technologies include chemical precipitation [5], ion-exchange [6], adsorption [7], biosorption [8] membrane filtration [9], coagulation-flocculation [3], flotation [10] and electrocoagulation (EC) [4,11]. Although chemical precipitation of these methods seems appropriate in terms of applicability, it produces a large amount of sludge [12]. The electrocoagulation method is more economical because of low sludge production [11]. EC is a method that can be easily applied without the need for additional chemicals [13,14,15]. The fact that the sludge flocs formed in this method are relatively large, contain less bound water, and are stable, allowing them to be separated easily by filtration [16-18]. Also, it is known that sludge flocs formed in this method are effective in

JSR A
Journal of Scientific Reports

removing the smallest colloidal particles. In most of the studies reported in the literature [11,19-24] except that of Heidmann and Calmano [25], the metal concentrations in their wastewaters were relatively low.

Unlike these studies, the wastewater used in the present study contained Zn in high concentrations. In this context, this paper deals with the mechanisms influencing heavy metal removal performance from original real wastewater by electrocoagulation method. It was studied the effects of initial pH and current density on the removal of Al, Co, Cr, and Zn.

2. MATERIALS AND METHODS

2.1. Wastewater characterization

The wastewater samples were collected from an aluminum-zinc metal processing facility located in Sinop city. In this facility, using the alloy obtained by adding aluminum and copper to pure zinc, the production of the door handle, window handle, decorative aluminum products (Furniture and Table Leg, etc.), hinges, fittings, and auxiliary accessories are carried out. Using the electro galvanizing method, the materials produced are subjected to zinc and chromate coating to prevent corrosion that may occur on product surfaces. The annual consumption of aluminum and its alloys are 7891 tons. The amount of wastewater consisting of metal coating effluents is 83 m^3 per day. Wastewater samples were collected from this facility and filtered through a coarse filter to separate the soluble solids before use in experiments. The composition of the wastewater is presented in Table 1. It is pointed out that very high zinc concentration in wastewater characterization was due to zinc solutions used extensively in the facility.

Table 1. Composition of the wastewater.

Characteristics	Value
Al (mg/L)	29.33
Co (mg/L)	37.72
Cr (mg/L)	64.89
Zn (mg/L)	2385.9
Suspended solids (g/L)	6.36
pH	1.32
Conductivity (mS/cm)	75.2

2.2. Experimental apparatus and procedure

The experiments were carried out in an 8.95 x 8.95 x 8.85 cm (width x length x depth) plexiglass reactor. EC experiments were evaluated for 30 minutes of electrolysis time. As the anode and the cathode, iron and stainless steel electrodes of rectangular shape with 4.5 cm width x 5.7 cm length x 0.3 cm thickness were used in all experiments. The EC reactor, which contained 3 anodes and 3 cathodes connected in monopolar parallel with a total active anode surface area of 148.60 cm^2, was connected to a direct current power source (GW GPC-3060D DC Power Supply 0-30 V, 0-6 A), which was operated at a galvanostatic mode. In other words, even if the resistance against the current changed, constant current flow was provided in all conditions. pH and conductivity measurements were made with a Thermo Scientific Orion 4-Star Plus Portable pH/Conductivity Meter. The experiments were carried out with 600 mL of wastewater at 200 rpm mixing speed. The metal oxide layers formed on the anode and cathode surfaces during the experiments were cleaned with

hydrochloric acid (37% HCl) and dried at 110 °C for 30 minutes. Metal analysis in treated wastewater samples taken at 5 mL periodically was performed using inductively coupled plasma optical emission spectroscopy (Perkin ELMER ICP-OES, Optima 7000 DV) according to the standard methods for the examination of water and wastewater [26]. Wastewater was used in all experiments in original conductivity (75.2 mS/cm) to prevent current resistance, which was enough for transferring the electrons from the anode, without the addition of electrolyte was made [4]. Although the effects of experimental parameters were determined without optimization, at the end of the experimental studies, by using the optimum experimental values obtained for each experimental stage, the maximum achievable removal efficiencies were determined with electrical energy consumptions.

2.2.1. Calculations

In the EC reactor, the anode and the electrical energy consumption were calculated according to Faraday's law [27] and (Eq. 1) to the mathematical expression [28] given in Eq. (2), respectively.

$$m = \frac{I.t.M}{z.F.V} \quad (1)$$

where m is the amount of the dissolved anode material (g), I is the current (A), t is the electrolysis time (s), M is the molar mass of aluminum and iron (g/mol), z is the number of electron transfer, F is the Faraday's constant (96,485.34 As/mol), and V is the volume of wastewater (m^3)

$$E = \frac{I.t.U}{V} \quad (2)$$

Where E is the electrical energy consumption, I is the current (A), t is the electrolysis time (s), U is a voltage (v), V is the volume of wastewater (m^3).

3. RESULTS AND DISCUSSION

3.1. Effect of pH

pH is a very effective operating parameter in removing pollutants in EC systems [22]. The initial pH values ranging from 1.32 (original) to 9 were studied under constant experimental conditions (current density: 100 A/m^2, stirring speed: 200 rpm, inter-electrode gap: 0.6 cm) as shown in Fig (1-4). After 30 minutes of EC, the removal efficiencies of Al, Co, Cr, and Zn were insignificant at an initial pH of 1.32. Fig. 5 shows the variations in final pH values concerning their initial values.

JSR A
Journal of Scientific Reports

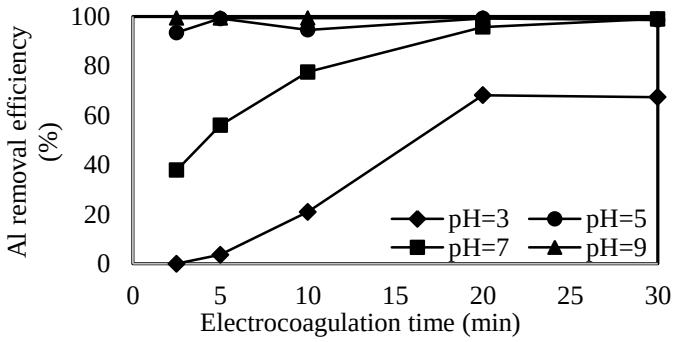

Figure 1. Effect of initial pH on Al removal efficiency.

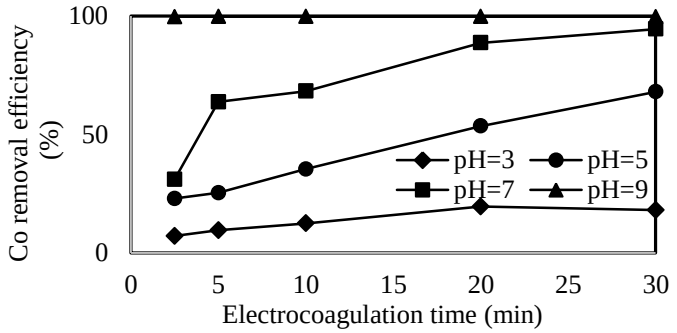

Figure 2. Effect of initial pH on Co removal efficiency.

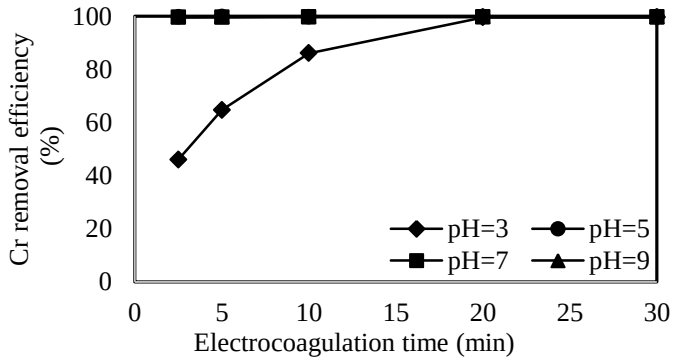

Figure 3. Effect of initial pH on Cr removal efficiency.

JSR A
Journal of Scientific Reports

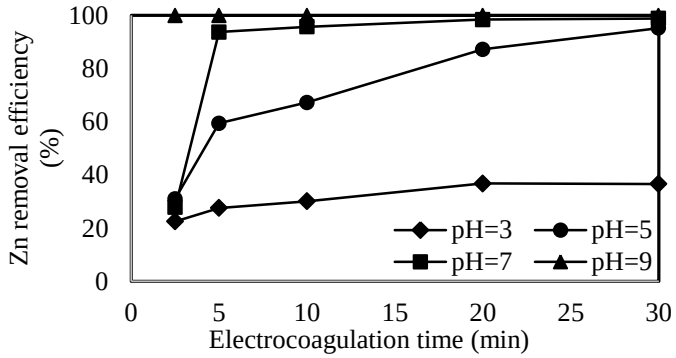

Figure 4. Effect of initial pH on Zn removal efficiency.

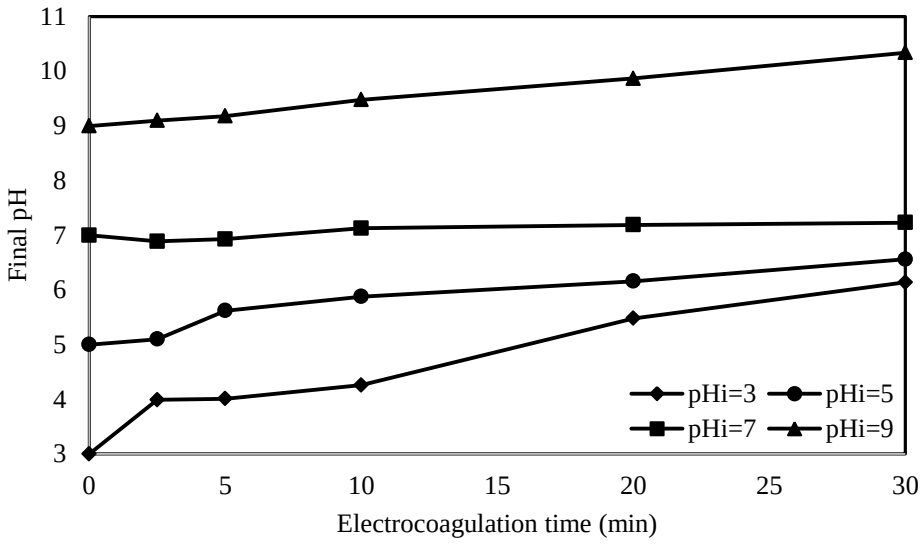

Figure 5. Variations of the final pH values at the end of electrolysis time.

With the increase of the initial pH to 3, a maximum of 99.6% Cr removal was achieved in 20 minutes of electrolysis time, while the maximum removal of Al, Co, and Zn was 68.2%, 19.6%, and 36.6%, respectively. The highest pH increase rate was determined at an initial pH of 3, and the final pH achieved to 6.14 after 30 min of electrolysis time. These fast increases in pH were attributed to the occurred hydroxyl ions at the cathode, which increases the ambient pH until consumed by the Fe^{2+} ions formed at the anode [27]. At an initial pH of 5, over 99% Cr removals were obtained at all times of the EC while the removal efficiencies of Al, Co, and Zn were 93.5-99.3%, 23-68%, and 31-95.2% were achieved at electrolysis times ranging from 2.5 to 30, respectively. At an initial pH of 7, by increasing the electrolysis time from 2.5 to 30 minutes, the removal efficiencies increased from 37.9 to 99.1% for Al, from 31% to 94.5 for Co, from 99.6 to 99.7% Cr, and from 27.8 to 98.8% for Zn with

JSR A
Journal of Scientific Reports

electrolysis time, respectively. At the initial pH of 9, all of the metal ions were removed over 99% over the entire EC period. At high pH, the removal of the high initial concentration of Zn with high efficiency indicates that the hydroxide precipitation was dominant [4). Long electrolysis times were required for Zn removal at high concentrations. This result was also observed by Chen et al. [28]. Particularly in Zn removal, it was understood that specific adsorption on Fe(OH)n flocs was effective in combination with the hydroxide precipitation of Zn ions. The removal of Zn ions over 99% at all electrolysis times for the first 2.5-30 minutes can be attributed to the change in the final pH between 9.1 and 10.14 in this period time since the precipitation of Zn $(OH)_2$ is significant at pH 8.6 [29]. Providing high removal efficiencies at high pH indicated that metal ions were removed by precipitation, mainly in the form of their hydroxides [19]. It was found that the initial pH and final pH (Fig. 5) values were high enough for the metal removal, especially for Co ions. The removal of Co at efficiencies of over 99% at an initial pH of only 9 can be explained by the precipitation in the form of hydroxides of Co ions at final pH values of 8 to 9. $Fe(OH)_2$ or/and $Fe(OH)_3$ flocs in the EC cell were found not to be significantly effective at lower initial or final pH values when removing Co at close to an efficiency of 100%. As the time of EC increased, significant increases in the removal efficiencies were observed at pH of 7 for Al, Co, and Zn, pH of 3 for Cr. With the increase of electrolysis time from 2.5 to 30 minutes, the removal rates of Al, Co, and Zn were up from 37.9% to 99.1%, 31.5% to 94.5%, and 27.8% to 98.8% respectively, at pH 7, while the Cr removal increased from 46% to 99.6% at pH 3. In varied times of EC between 2.5 to 30 minutes the electrical energy consumptions for initial pH values of 3, 5, 7 and 9 were 0.154-1.973, 0.154-1.850, 0.164-1.973 and 0.175-2.220 kWh/m^3. Anode consumption increased from 0.107 to 1.285 kg/m^3 by Faraday's law, with the EC period increasing from 2.5 to 30 minutes. The electrical conductivity values decreased from 75 to 38.9 mS/cm at initial pH values ranging from 3-9 after 30 minutes of electrolysis time. In varying times between 2.5-30 minutes of EC, the final pH values for initial pH values of 3, 5, 7, and 9 varied between 3.99-6.14, 5.10-6.56, 6.89-7.23, and 9.10-10.34.

3.2. Effect of current density

The current density directly affects the formation of coagulant formation rate, bubble size, and large flocs that provide removal of pollutants [12]. To determine the effect of current density on the removal of Al, Co, Cr, and Zn ions a series of experiments were carried out with the current density ranging from 50 to 200 A/m^2 under constant experimental conditions (pH: 3, stirring speed: 200 rpm, inter-electrode gap: 0.6 cm). The effects of current densities on the metal removal efficiency are given in Fig. 6-9 as a function of the electrolysis time. The final pH values are shown in Fig. 10.

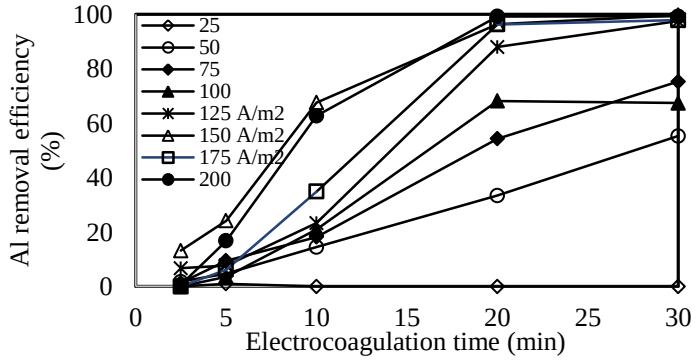

Figure 6. Effect of current density on Al removal efficiency.

JSR A
Journal of Scientific Reports

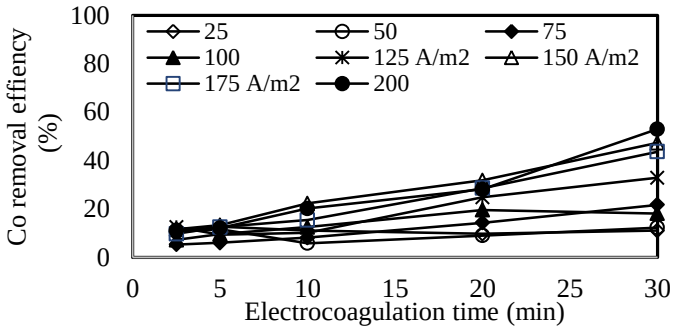

Figure 7. Effect of current density on Co removal efficiency.

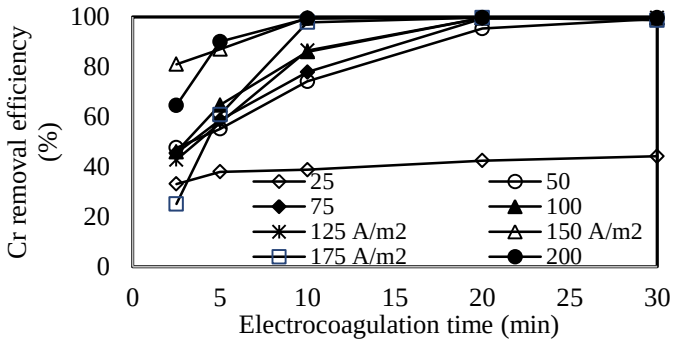

Figure 8. Effect of current density on Cr removal efficiency.

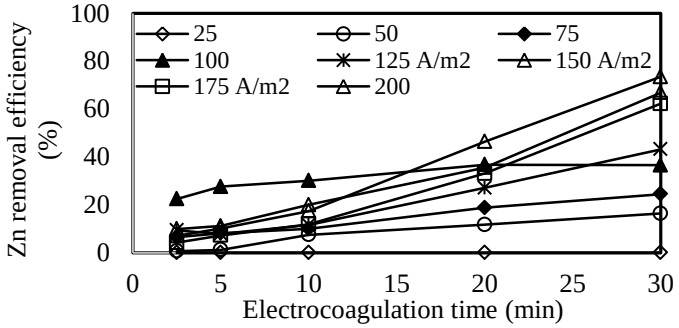

Figure 9. Effect of current density on Zn removal efficiency.

As shown in Fig. 6-9, as the current density increased, the metal removal efficiencies increased for all electrolysis times. After 30 minutes of EC exposure with increasing current density from 25 A/m^2 to 200 A/m^2, the removal efficiencies increased from 0.0% to 99.3% for Al, from 11% to 53% for Co, from 44.2% to 99.7% for Cr and from 0.0% to 73.5% for Zn. As shown in Fig. 6-9, sudden increases in the removal of Al, Cr, and Zn were observed after 30 minutes of EC exposure with increasing current density from 25 A/m^2 to 50 A/m^2. Al was removed above 99% at 150 A/m^2 and Cr was also removed above 99% at 50 A/m^2. There were no significant changes in Cr removal efficiencies

JSR A
Journal of Scientific Reports

obtained for different current densities ranging from 25-200 A/m^2 after 30 minutes of EC. The effect of current density on the removal of ions other than Co was higher. Co and Zn reached their maximums of 53% and 73.5% at 200 A/m^2 respectively and at 5.920 kWh/m^3 and 2.570 kg/m^3 after 30 minutes of EC, respectively. As can be seen in Fig. 7 and Fig. 9, at initial pH 3, the high removal of Co and Zn could not be achieved at any current density. Because the fixed initial pH value of 3 increased between 25 and 200 A/m^2, in 150 A/m^2 and increased to a maximum value of 6.65 after 20 minutes of EC. This pH value was not sufficient to precipitate in the form of Co and Zn hydroxides. Thus, the high initial concentration of Zn (2385.9 mg/L) in the wastewater caused low Zn removal. Also, it was concluded that the iron hydroxide flocs formed in the EC cell were not significantly effective for the removal of Co and Zn in high concentrations, and low removal efficiencies were due to the relatively low final pH values achieved after 30 minutes of EC.

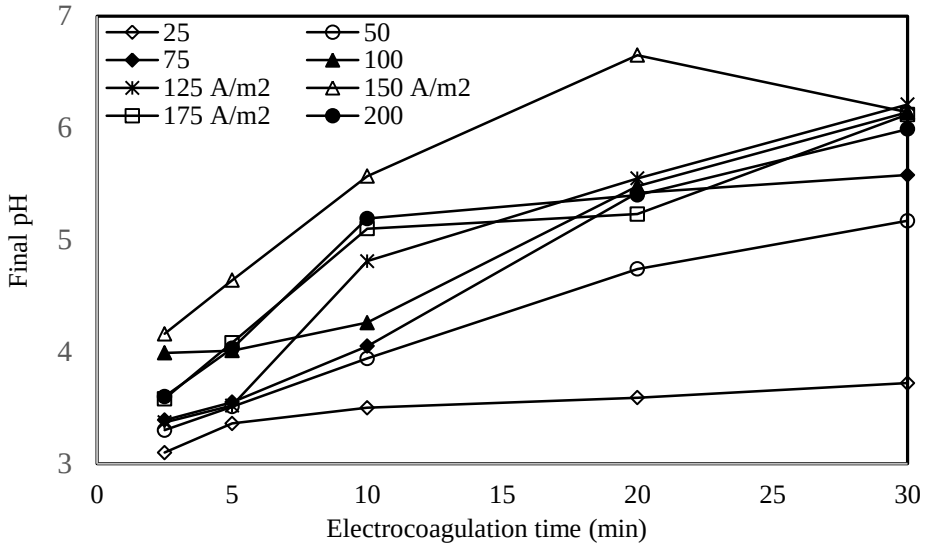

Figure 10. Variations of the final pH values at the end of electrolysis times.

Fig. 10 shows the change of final pH values with current densities as a function of the electrolysis time. The final pH values also increased with increasing the current density from 25 to 100 A/m^2. The final pH changes after 100 A/m^2 were insignificant. In 25, 50, 75, 100 A/m^2, the initial pH values increased to 3.72, 5.17, 5.58 and 6.14, while in 125, 150, 175 and 200 A/m^2 had it on 6.21, 6.14, 6.12 and 5.99. The amount of anodes consumed at current densities ranging from 25 to 200 A/m^2 was calculated as 0.321, 0.422, 0.964, 1.285, 1.606, 1.927, 2.249, and 2.570 kg/m^3 after 30 minutes of EC period according to the Faraday law (Eq. 1) The initial electrical conductivity values of 39.2 mS/cm at pH 3 varied from 38-39 mS/cm at current densities of 25-200 A/m^2. It was observed that the high initial conductivity values of the wastewater did not affect the increase in the amount of flocs that formed due to the increases in the current densities.

4.CONCLUSION

The removal efficiency of metal ions from real wastewater was directly dependent on the initial pH and current density. The obtained experimental results revealed that initial wastewater pH was a

much more effective parameter on the removal efficiencies of metal ions when compared to applied current density into electrodes in the reactor. Despite its low concentration in wastewater, it was difficult to remove cobalt ions efficiently except for the relatively high final pH of the wastewater, which was due to increased hydroxyl ions with increasing electrolysis time. This means that cobalt ions were mainly removed by its hydroxide precipitation. It was concluded that it is much more important to provide sufficient electrolysis time rather than high current densities for achieving high removal efficiencies. Also, the EC method can be used efficiently and economically in the treatment of real metal processing wastewaters containing very high concentrations of metal ions as long as sufficient electrolysis time is provided.

ACKNOWLEDGEMENT

This study was supported by Ondokuz Mayıs University with a project number of PYO.MUH.1904.14.003. The authors thank for their financial support.

REFERENCES

[1] Vasudevan, S., J. Lakshmi, J. and Sozhan, G., (2012), Simultaneous removal of Co, Cu, and Cr from water by electrocoagulation, Toxicological & Environmental Chemistry, 94, 1930-1940.

[2] Fu, F. and Wang, Q., (2011), Removal of heavy metal ions from wastewaters: A review, Journal of Environmental Management, 92, 407-418.

[3] Heidmann, I. and Calmano, W., (2008), Removal of Cr(VI) from model wastewaters by electrocoagulation with Fe electrodes, Separation and Purification Technology, 61 (1), 15-21.

[4] Matlock, M., Howerton, B., and Atwood, D., (2002), Chemical precipitation of heavy metals from acid mine drainage, Water Research 36, 4757-4764.

[5] Inglezakis, V.J., Loizidou, M.D. and Grigoropoulou, H.P., (2002), Equilibrium and kinetic ion exchange studies of Pb^{2+}, Cr^{3+}, Fe^{3+} and Cu^{2+} on natural clinoptilolite, Water Research, 36, 2784-2792.

[6] Hong, M., Yu, L.,Wang, Y., Zhang, J., Chen, Z., Dong, L., Zan, Q. and Li, R., (2019), Heavy metal adsorption with zeolites: The role of hierarchical pore architecture, Chemical Engineering Journal, 359, 363-372.

[7] Sarioglu, M., Guler, U. and Beyazit, N., (2009), Removal of copper from aqueous solutions using biosolids, Desalination, 239, 167-174.

[8] Blocher, C., Dorda, J., Mavrov, V., Chmiel, H., Lazaridis, N.K. and Matisc, K.A., (2003), Hybrid flotation—membrane filtration process for the removal of heavy metal ions from wastewater, Water Research, 37, 4018-4026.

[9] Taseidifar, M., Makavipour, F., Pashley, R.M. and Rahman, A.F.M., (2017), Removal of heavy metal ions from water using ion flotation, Environmental Technology and Innovation, 8, 182-190.

[10] Yadav, A., L. Singh, A. Mohanty, S. Satya and Sreekrishnan, T.R., (2012), Removal of various pollutants from wastewater by electrocoagulation using iron and aluminum electrode, Desalination and Water Treatment, 46, 352-358.

[11] Al Aji, B., Yavuz, Y. and Koparal, S., (2012), Electrocoagulation of heavy metals containing model wastewater using monopolar iron electrodes. Separation and Purification Technology, 86, 248-254.

[12] Wang, C. and Chou, W., (2009). Performance of COD removal from oxide chemical mechanical polishing wastewater using iron electrocoagulation, Journal of Environmental Science and Health Part, A44, 1289-1297.

[13] Mansouri, K., Elsaid, K., Bedoui, A., Bensalah, N. And Abdel-Wahab, A., (2011), Application of electrochemically dissolved iron in the removal of tannic acid from water, Chemical Engineering Journal, 172, 970-976.

[14] Ozyonar, F. and Karagozoglu, B., (2014), Investigation of technical and economic analysis of electrocoagulation process for the treatment of great and small cattle slaughterhouse wastewater, Desalination and Water Treatment, 52, 74-87.

[15] Bazrafshan, E., Mohammadi, L., Ansari-Moghaddam, A. and Mahvi, A., (2015), Heavy metals removal from aqueous environments by electrocoagulation process- a systematic review, Journal of Environmental Health Science and Engineering, 13, 1-16.

[16] Khandegar, V. and Saroha, A.K., (2013)., Electrocoagulation for the treatment of textile industry effluent - A review, Journal of Environmental Management, 128, 949-963.

[17] Yousuf Mollah, M., Schennach, R., Parga, J. and Cocke, D., (2001), Electrocoagulation (EC)-science and applications, Journal of Hazardous Materials, B84, 29-41.

[18] Akbal, F. and Camci, S., (2011), Copper, chromium and nickel removal from metal plating wastewater by electrocoagulation, Desalination, 269, 214-222.

[19] Beyazit, N., (2014), Copper(II), Chromium(VI) and Nickel(II) Removal from Metal Plating Effluent by Electrocoagulation, International Journal of Electrochemical Science, 9, 4315- 4330.

[20] Al-Shannag, M., Al-Qodah, Z., Bani-Melhem, K., Rasool Qtaishat, M. and Alkasrawi, M., (2015), Heavy metal ions removal from metal plating wastewater using electrocoagulation: Kinetic study and process performance. Chemical Engineering Journal, 260, 749-756.

[21] Gatsios, E., Hahladakis, J. and Gidarakos, E., (2015), Optimization of electrocoagulation (EC) process for the purification of a real industrial wastewater from toxic metals, Journal of Environmental Management, 154, 117-127.

[22] Oden, M.K. and Erkan, H.S., (2018), Treatment of metal plating wastewater using iron electrode by electrocoagulation process: Optimization and process performance, Process Safety and Environmental Protection, 119, 207-217.

[23] Mamelkina, M.A., Vasilyev, F., Tuunila, R., Sillanpa, M. and Hakkinen, A., (2019), Investigation of the parameters affecting the treatment of mining waters by Electrocoagulation. Journal of Water Process Engineering, 32, 100929.

[24] Heidmann, I. and Calmano, W., (2010), Removal of Ni, Cu and Cr from a galvanic wastewater in an electrocoagulation system with Fe-and Al-electrodes, Separation and Purification Technology, 71, 308-314.

[25] Rice, E.W., Baird, R.B., Eaton, A.D. and Bridgewater, L.L., (2012), Standard Methods in Examination of Water and Wastewater, twenty-three ed. Water Environment Federation, American Public Health Association, American Water Works Association (APHA-AWWA).

[26] Moussa, D., El-Naas, M., Nasser, M. and Al-Marri, M., (2017), A comprehensive review of electrocoagulation for water treatment: Potentials and challenges, Journal of Environmental Management, 186, 24-41.

[27] Chen, X., Ren, P., Li, T., Trembly, J. and Liu, X., (2018), Zinc removal from model wastewater by electrocoagulation: Processing, kinetics and mechanism, Chemical Engineering Journal 349, 358-367.

[28] Hussin, F., Abnisa, F., Issabayeva, G. and Aroua, M., (2017), Removal of lead by solar-photovoltaic electrocoagulation using novel perforated zinc electrode, Journal of Cleaner Production, 147, 206-216.

Kütahya Dumlupınar University
Institute of Graduate Studies

Journal of Scientific
Reports-A
E-ISSN: 2687-6167
Number 45, December 2020

RESEARCH ARTICLE

PERFORMANCE COMPARISON OF UV, UV/H_2O_2, UV/Fe^{2+}, H_2O_2/Fe^{2+}, UV/H_2O_2/Fe^{2+} PROCESSES IN THE REMOVAL OF COD AND COLOR FROM TEXTILE WASTEWATER

Nevzat BEYAZIT[1,*] and Hande KARACA[2]

[1] Ondokuz Mayıs University, Faculty of Engineering, Department of Enviromental Engineering, Samsun, nbeyazit@omu.edu.tr, ORCID: 0000-0002-8396-5996
[2] Ondokuz Mayıs University, Faculty of Engineering, Department of Enviromental Engineering, Samsun, hkaraca03@outlook.com, ORCID: 0000-0001-5868-0625

Recieved Date: 29.10.2020 *Accepted Date: 11.12.2020*

ABSTRACT

In this study, the removal of chemical oxygen demand (COD) and color from textile industry wastewater were investigated in comparison with UV, UV/H_2O_2, UV/Fe^{2+}, H_2O_2/Fe^{2+}, UV/H_2O_2/Fe^{2+} processes. Initial pH, hydrogen peroxide dosage, ferrous iron dosage, and UV radiation were selected as variables. A maximum of 95.65% COD and 98.52% color removal were achieved by the photo-Fenton method. Another effective method was Fenton process by which 83.76% COD and 80.44% color removal efficiencies were obtained. It was concluded that the Fe^{2+}/H_2O_2 process (Fenton) with UV light (photo-Fenton) can provide higher removal efficiencies in shorter process times in the treatment of textile wastewater.

Keywords: *Textile wastewater, COD, Color, Photo-Fenton, UV/H_2O_2/Fe^{2+}*

1. INTRODUCTION

The textile industry generally creates large volumes of wastewater containing highly concentrated organic dyes, inorganic ions such as chlorides and sulfates, soaps, oils, solvents, salts, and many other soluble compounds. The complex structure of these wastewaters can prevent their biodegradation. For this reason, they must be treated with appropriate methods to avoid environmental risks before being introduced into the receiving environment [1,2]. The main source of COD and color parameters in textile wastewater is dyestuff and polyvinyl alcohol, and they are characterized by high concentrations of COD (150-10,000 mg/L), BOD (100-4000 mg/L), and color content (50-2500 Pt-Co). Also, these wastewaters are considered toxic and carcinogenic [3, 4]. BOD/COD ratios of textile wastewaters are mostly in the range of 0.1–0.25 and are resistant to biodegradation [5,6,7,8]. Physico-chemical processes such as coagulation/flocculation, precipitation, adsorption, ion exchange, membrane separation, and oxidation or biological methods have been applied in most cases. Because of the toxicity possibilities of textile wastewaters, biological methods are seen inefficient especially if the pollutants are present in high concentrations. In physicochemical methods, sludge formation occurs relatively more [4,5]. Recently, electrochemical Technologies such as Advanced Oxidation Processes (AOPs) have been considered as efficient and practical alternatives for the removal of pollutants from textile wastewaters [9]. By using the hydroxyl radicals ($^{\bullet}OH$) produced in advanced oxidation

JSR A
Journal of Scientific Reports

processes, organic pollutants are converted into carbon dioxide and water quickly and efficiently [10]. Among these methods, especially H_2O_2/Fe^{2+} and $UV/H_2O_2/Fe^{2+}$ (photo-Fenton) processes attract attention. In the Fenton reaction, a highly reactive hydroxyl radical is formed by the H_2O_2 ferrous reaction (Eq. 1). In addition, the ferric iron formed can be oxidized by H_2O_2 to form a hydroperoxyl radical ($^{\bullet}O_2H$) (Eq. 2)

$$Fe^{2+} + H_2O_2 \longrightarrow Fe^{3+} + OH^- + {}^{\bullet}OH \quad (1)$$

$$Fe^{3+} + H_2O_2 \longrightarrow Fe^{2+} + {}^{\bullet}O_2H + H^+ \quad (2)$$

Eq. 3 shows that $Fe(OH)^{2+}$ complexes formed Fenton reactions can transform into hydroxyl radicals by UV light, also ferrous ions can be occurred, which is used in fenton process. This situation creates much less sewage sludge. Eq. 4 show that hydrogen peroxide can be convert to two hydroxyl radicals under exposure to UV light. Thus, the efficiency of fenton processes can be improved by UV radiation [11,12,13].

$$Fe(OH)^{2+} + hv \longrightarrow Fe^{2+} + {}^{\bullet}OH \quad (3)$$

$$H_2O_2 + hv \longrightarrow 2\ {}^{\bullet}OH \quad (4)$$

For removing several pollutants from synthetic or real textile wastewaters, advanced oxidation methods such as electro-Fenton (2), photo-Fenton (4), UV, UV/H_2O_2, $UV/H_2O_2/Fe^{2+}$ (5) ve peroxi-coagulation were used (6). Most of them were a comparison of one or two methods. In this study, COD and color removal from real textile wastewater by UV, UV/H_2O_2, UV/Fe^{2+}, H_2O_2/Fe^{2+}, and $UV/H_2O_2/Fe^{2+}$ methods were investigated in detail.

2. MATERIAL AND METHODS

2.1. Wastewater Characterization

The textile industry wastewater used in the experiments was supplied from the dyeing process effluent of an enterprise operating in the fields of printing services (including clothing) on fabrics and textile products in the organized industrial zone of Fatsa district of Ordu. Wastewater characterization is given in Table 1.

Table 1. Characteristics of untreated textile wastewater.

Analytical parameter	Value
pH	6.8-8.2
Total suspended solids (mg/L)	77.8
Turbidity (NTU)	872
Conductivity (µS/cm)	7960
COD (mg/L)	2962-4412
Color (Pt-Co)	1426-1779

2.2. Apparatus and Procedure

All experiments were carried out in a plexiglass column with an inner diameter of 7.8 cm, an outside diameter of 8.35 cm, and a height of 48.5 cm (Fig. 1). A 16W UV-C (254 nm) low-pressure mercury-vapor lamp mounted in a quartz tube was placed vertically in the center of the reactor. At the base of

JSR A
Journal of Scientific Reports

the reactor, a 2 cm vertical space was left for the magnetic stirrer to rotate. The mixing of the wastewater in the reactor was provided by the magnetic stirrer at the bottom.

Figure 1. Experimental setup.

All experiments were carried out with 2.1 L wastewater volume at room temperature (22 ± 2 ℃). Before each experiment, the wastewater was filtered through 2 coarse filter papers. H_2SO_4 and NaOH solutions were used for pH adjustments. The reactor was covered with aluminum foil to prevent light from coming out. With the help of the tap placed in the reactor, samples of treated wastewater were taken at certain time intervals. Final pH values were recorded after each experiment. The treated wastewater samples taken after the experiments were centrifuged at 5000 rpm for 10 minutes to remove the flocs. Thermoreactor (Spectroquant TR 4220) and photometer (Merck Spectroquant NOVA 60A) were used for COD analysis. This photometer was also used for color measurements. COD measurements were carried out according to the closed-reflux colorimetric method (5520-D). Color measurements were made according to the visual comparison method (2120-B) [14]. H_2SO_4 (98%), potassium dichromate ($K_2Cr_2O_7$), mercury sulfate ($HgSO_4$), silver sulfate (Ag_2SO_4), potassium hydrogen phthalate ($C_8H_5KO_4$) were used for COD analysis. Ferrous sulfate heptahydrate ($FeSO_4.7H_2O$) was used as the Fe^{2+} source. H_2O_2 (35%) was used in Fenton experiments. All reagents used were analytical grade.

3. RESULTS AND DISCUSSION

3.1. UV Process

3.1.1. Effect of pH

The effect of UV was examined for a process time of 120 minutes. As can be seen from the Fig. 2 and Fig. 3, COD and color removal efficiencies obtained at the initial pH values of 4, 7, and 10 increased

JSR A
Journal of Scientific Reports

with increases in the process time. While the maximum efficiencies achieved were 7.78%, 11.56%, and 8.61% for COD at pH 4, 7, and 10, they were 10.50%, 13.72%, and 11.02% for color. As can be seen from Fig. 2 and Fig. 3, pH 7 was optimal for both COD and color removal. By increasing the initial pH from 4 to 7, the efficiency for COD increased from 7.78% to 11.56% after 120 minutes, while for the color it was slightly increased from 10.50% to 13.72%. This indicates that initial pH is very effective in removing COD and color removal. On the other hand, UV radiation alone was not effective in COD and color removal from real textile wastewater. Concerning the UV effect, a similar result was obtained in the dye removal study by Bali (2004).

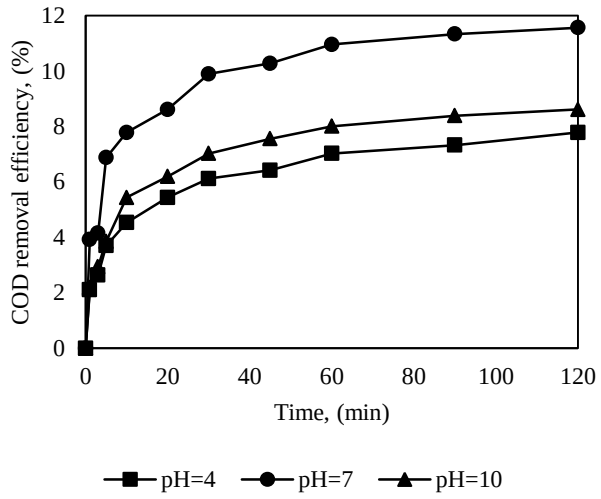

Figure 2. Effect of initial pH on COD removal efficiency in UV process.

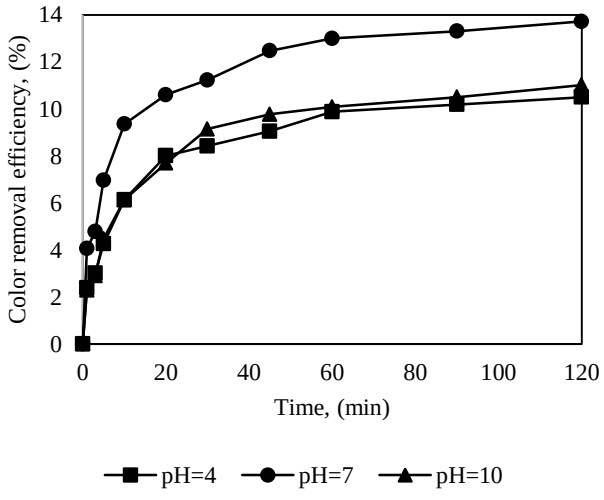

Figure 3. Effect of initial pH on Color removal efficiency in UV process.

JSR A
Journal of Scientific Reports

3.2. UV/H_2O_2 Process

3.2.1. Effect of pH

The change over time of the effects of initial pH values varying between 4 and 9, in which H_2O_2 concentration was kept constant at 25 mM, on COD and color removal efficiencies is shown in Fig. 4 and Fig. 5. With the increase of pH from 4 to 7, COD and color removal efficiencies increased from 20.58 to 26.70%, and from 37.32 to 49.87%, respectively. Increasing pH from 7 to 9 decreased COD and color removal efficiencies from 26.70% to 25.49%, and from 49.87% to 44.90, respectively. Initial pH values of 7 and 9 reached 7.12 and 9.10, respectively, at the end of 120 minutes. No significant changes occurred in other pH values.

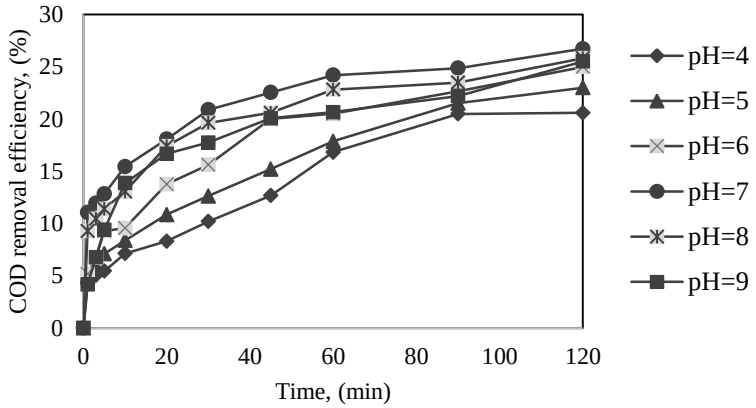

Figure 4. Effect of initial pH on COD removal efficiency in UV/H_2O_2 process.

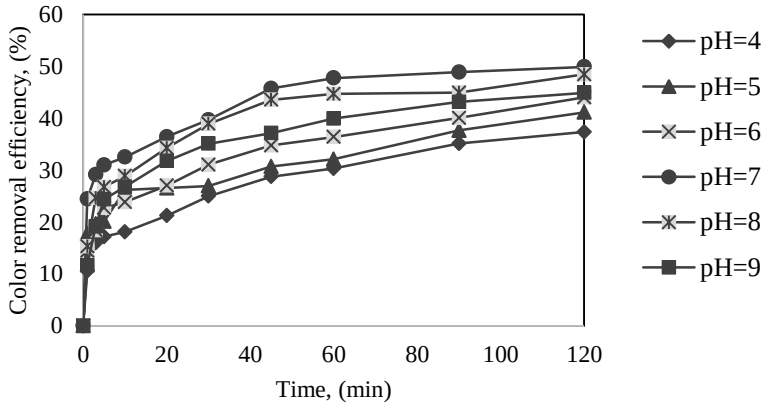

Figure 5. Effect of initial pH on Color removal efficiency in UV/H_2O_2 process.

3.2.2. Effect of H_2O_2

The change over time of the effects of H_2O_2 concentrations varying between 5 and 100 mM, in which pH was kept constant at 7, on COD and color removal efficiencies is shown in Fig. 6 and Fig. 7. With the increase of H_2O_2 concentration from 5 mM to 100 mM, COD and color removal efficiencies

JSR A
Journal of Scientific Reports

reached 33.08% and 61.21%, respectively, which are the maximum values for both. As can be seen from Fig. 6 and Fig. 7, while the COD removal efficiencies were dependent on different H_2O_2 concentrations after 60 minutes, the observed dependence for color removal efficiencies was over the entire experiment period. The initial pH value of 7 varied between 7.07 and 7.40 for 5 and 100 mM H_2O_2 concentrations, respectively.

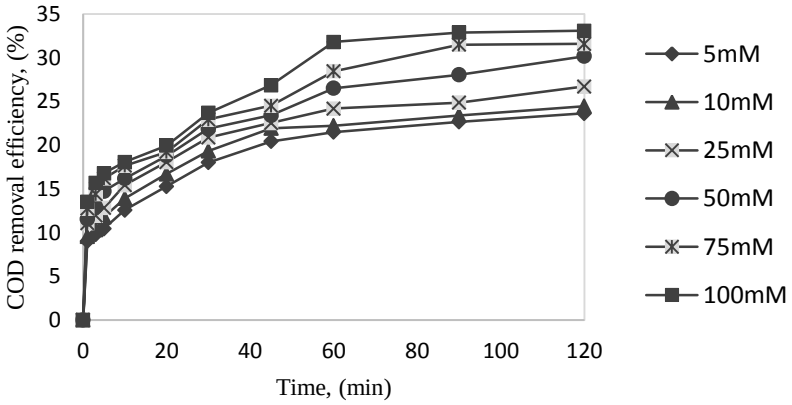

Figure 6. Effect of H_2O_2 concentration on COD removal efficiency in UV/H_2O_2 process.

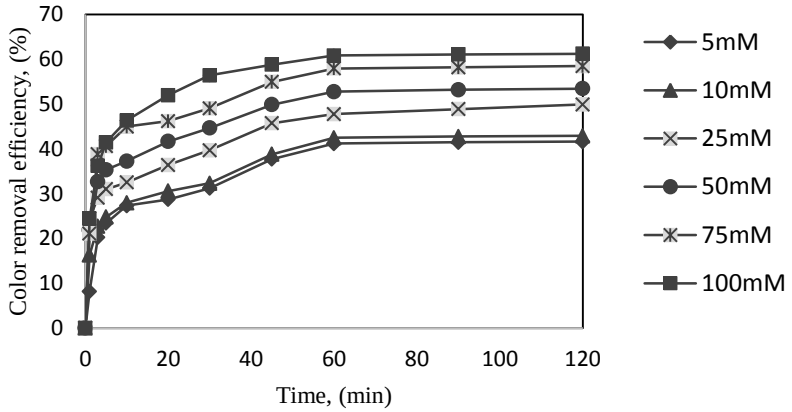

Figure 7. Effect of H_2O_2 concentration on Color removal efficiency in UV/H_2O_2 process.

3.3. UV/Fe^{2+} Process

3.3.1 Effect of pH

The change over time of the effects of initial pH values varying between 4 and 9, in which Fe^{2+} was kept constant in 2 mM, on both COD and color removal efficiency is shown in Fig. 8 and Fig. 9. Maximum of 44.02% COD and 55.42% color removal efficiencies were obtained at pH 4 at the end of 120 minutes, while COD removal of 43.21% and color removal of 54.86% were obtained in the first 60 minutes. By increasing the pH from 4 to 9, COD and color removal efficiencies decreased from 44.02% to 29.30% and from 55.42% to 41.09, respectively. Initial pH values between 4 and 9 changed between 4.07 and 9.05 at the end of 120 minutes.

JSR A
Journal of Scientific Reports

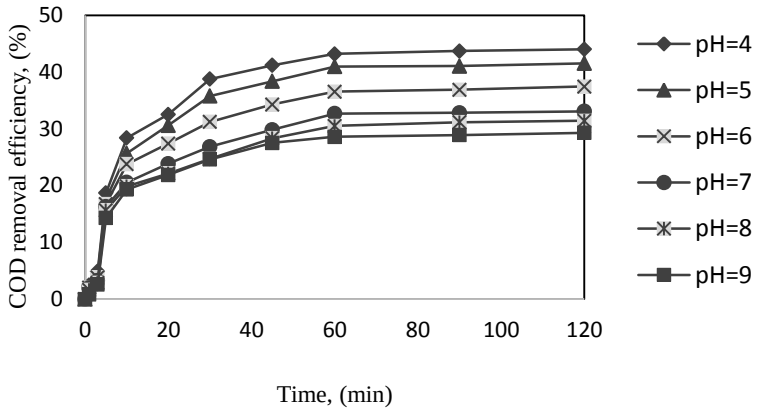

Figure 8. Effect of initial pH on COD removal efficiency in UV/Fe^{2+} process.

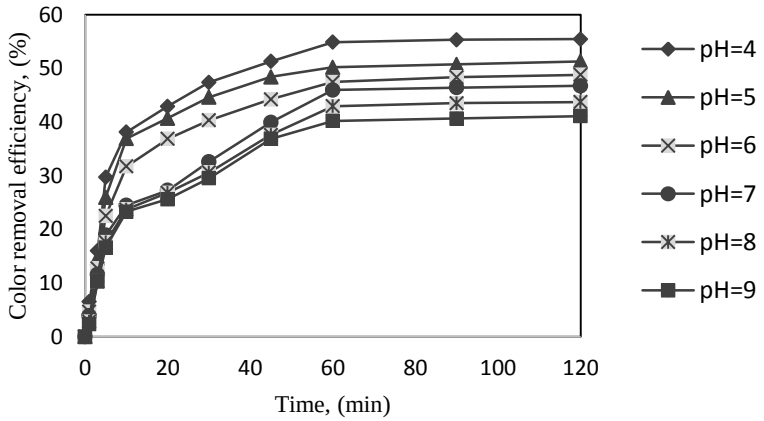

Figure 9. Effect of initial pH on Color removal efficiency in UV/Fe^{2+} process.

3.3.2. Effect of Fe^{2+}

The change over time of the effects of initial Fe^{2+} concentrations varying between 0.25 and 3 mM, in which pH was kept constant at 4, on both COD and color removal efficiencies is shown in Fig. 10 and Fig. 11. A maximum COD of 19.62% and 33.74% color removals obtained at the 0.25 mM Fe^{2+} concentration increased to 49.89% and 59.44%, respectively, by increasing the Fe^{2+} concentration to 3 mM. The initial pH 4 value changed between 4.03 and 4.04 at the end of 120 minutes.

JSR A
Journal of Scientific Reports

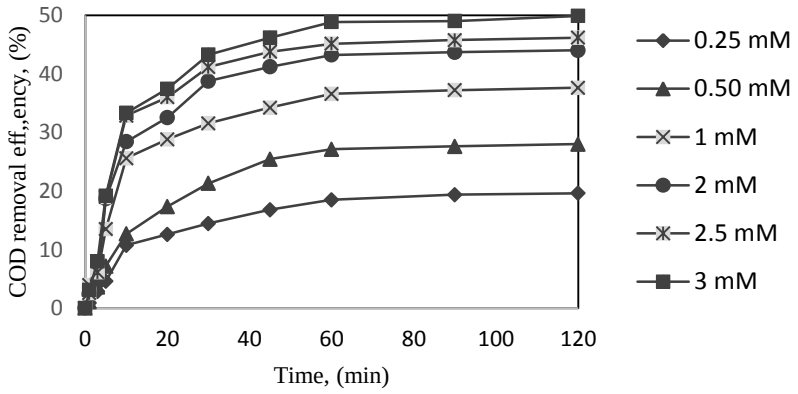

Figure 10. Effect of initial Fe^{2+} concentration COD removal efficiency in UV/Fe^{2+} process.

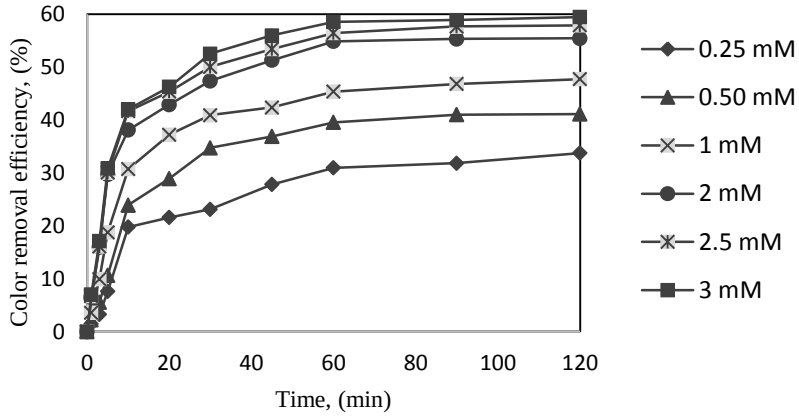

Figure 11. Effect of initial Fe^{2+} concentration Color removal efficiency in UV/Fe^{2+} process.

3.4. H_2O_2/Fe^{2+} Process

3.4.1.Effect of pH

The effect of initial pH values varying between 2 and 4.5 on COD and color removal efficiencies by keeping the 60 mM H_2O_2 concentration and the 2 mM Fe^{2+} concentration constant (H_2O_2/Fe^{2+} molar ratio: 30) is shown in Fig. 12 and Fig. 13. The maximum COD of 83.76% and color of 80.44% were obtained in the first 30 minutes at pH 2. With increasing pH from 2 to 4.5, COD and color removal efficiencies decreased to 48.54% and 55.42%, respectively, after 30 minutes. Initial pH values varying between 2 and 4 varied between 2.09 and 4.56.

JSR A
Journal of Scientific Reports

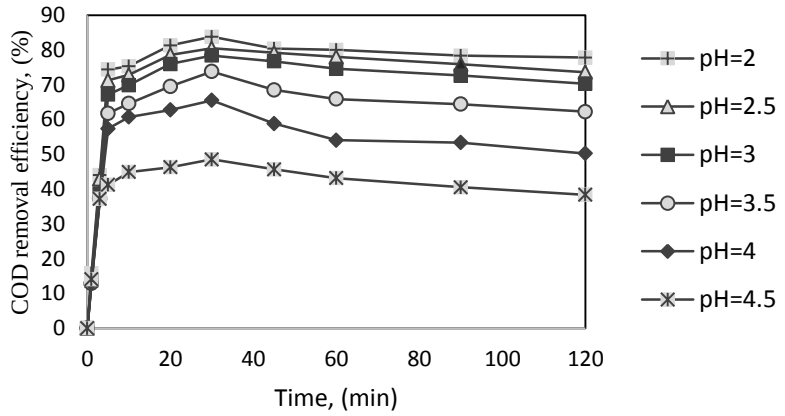

Figure 12. Effect of initial pH on COD removal efficiency in H_2O_2/Fe^{2+} process.

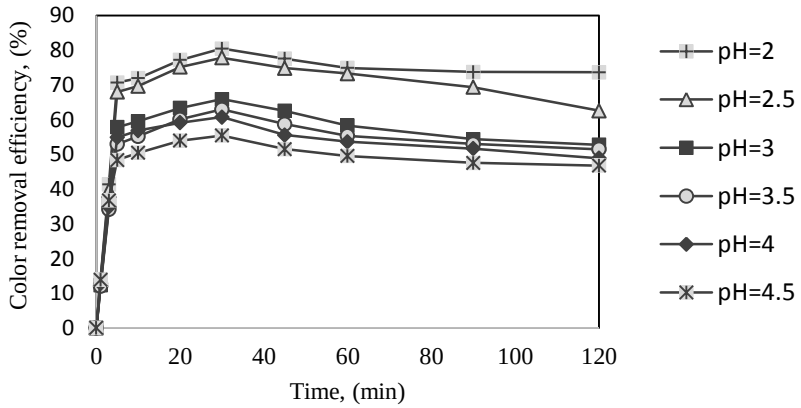

Figure 13. Effect of initial pH on Color removal efficiency in H_2O_2/Fe^{2+} process.

3.4.2. Effect of H_2O_2

The effects of H_2O_2 concentrations varying between 5 and 100 mM on COD and color removal efficiencies by keeping the pH 2 and 2 mM Fe^{2+} concentration constant are shown in Fig. 14 and Fig. 15. As can be seen from Fig. 14 and Fig. 15, COD removal of 83.76% and color removal of 80.44% was obtained at H_2O_2 concentration of 60 mM in the first 30 minutes. The efficiencies obtained with 50, 75 and 100 mM H_2O_2 in the first 30 minutes were 78.38%, 76.34%, and 72.71% for COD, while these values were 77.87%, 67.72%, and 59.25% for color removal. The results indicated that the H_2O_2/Fe^{2+} molar ratio should be at least 25 (50 mM H_2O_2/2 mM Fe^{2+}) in the conditions of this study. Initial pH values of 2 varied between 2.08 and 2.10 at the end of 120 minutes.

JSR A
Journal of Scientific Reports

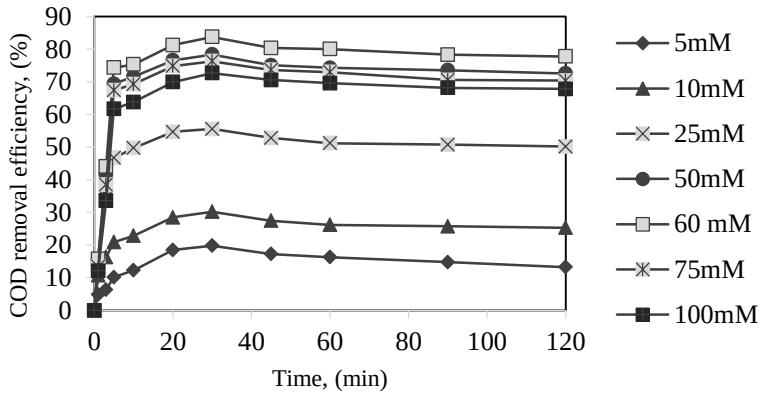

Figure 14. Effect of H_2O_2 concentration on COD removal efficiency in H_2O_2/Fe^{2+} process.

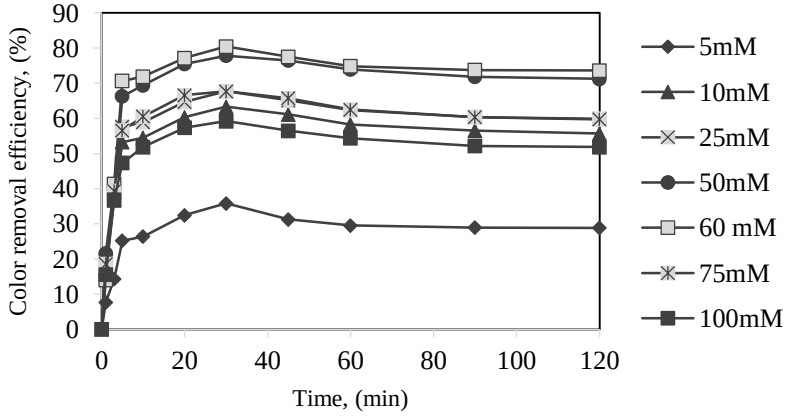

Figure 15. Effect of H_2O_2 concentration on Color removal efficiency in H_2O_2/Fe^{2+} process.

3.4.3. Effect of Fe^{2+}

The effects of Fe^{2+} concentrations varying between 0.25 and 3 mM, in which pH was kept at 2 and H_2O_2 was kept in 60 mM, on both COD and color removal efficiency are shown in Fig. 16 and Fig. 17. The maximum of 83.76% COD and 80.44% color removal efficiencies obtained at Fe^{2+} concentration of 2 mM decreased to 76.54 for COD at the end of 30 minutes when the Fe^{2+} concentration was increased to 3 mM and decreased to 67.81 for color. Initial pH 2 value varied between 2.03 and 2.02 at the end of 120 minutes.

JSR A
Journal of Scientific Reports

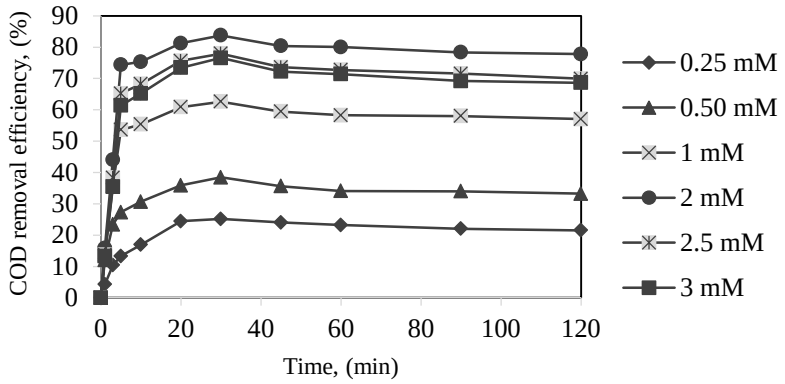

Figure 16. Effect of Fe^{2+} concentration on COD removal efficiency in H_2O_2/Fe^{2+} process.

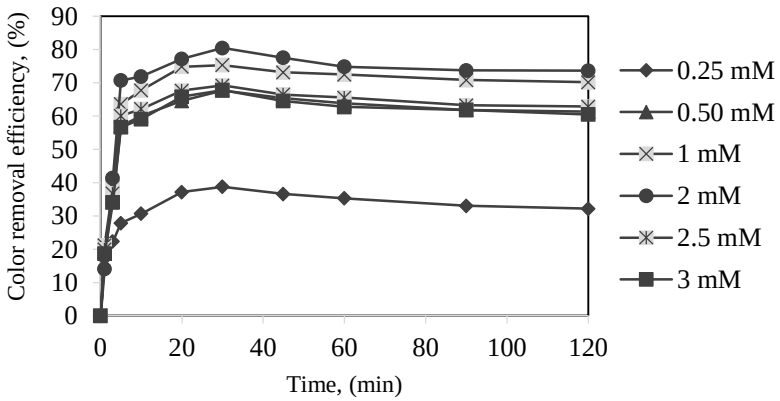

Figure 17. Effect of Fe^{2+} concentration on Color removal efficiency in H_2O_2/Fe^{2+}.

3.5. UV/H_2O_2/Fe^{2+} Process

3.5.1. Effect of pH

The effect of initial pH values varying between 2 and 4.5, in which H_2O_2 was kept constant in 60 mM and Fe^{2+} was kept in 2 mM, on both COD and color removal efficiencies is shown in Fig. 18 and Fig. 19. COD of 49.86% and color of 53.21% removal efficiencies at pH 2 in the first 3 minutes, increased to 71.27% and 82.74%, respectively at the end of the 5 minutes. While the maximum values of 88.60% and 93.95%, of COD and color, are reached after 60 minutes, these values decreased to 79.57% and 83.42 when the pH increased from 2 to 4.5. Initial pH values between 2 and 4.5 varied between 2.08 and 4.53 in parallel with increasing pH values.

.

JSR A
Journal of Scientific Reports

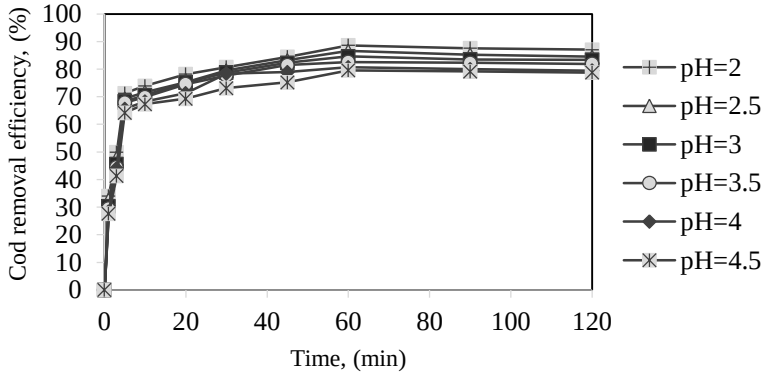

Figure 18. Effect initial pH on COD removal efficiency in UV/H_2O_2/Fe^{2+} process.

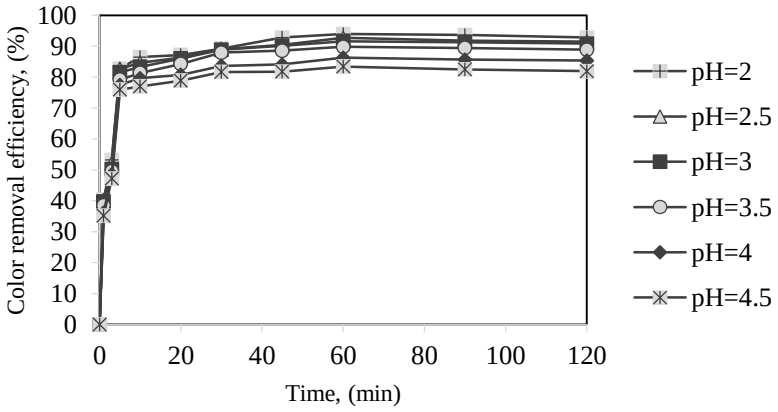

Figure 19. Effect initial pH on Color removal efficiency in UV/H_2O_2/Fe^{2+} process.

3.5.2. Effect of H_2O_2

The effects of H_2O_2 concentrations varying between 5 and 100 mM, in which pH was kept at 2 and Fe^{2+} was kept in 2 mM, on both COD and color removal efficiencies are shown in Fig. 20 and Fig. 21. By increasing the H_2O_2 concentration from 5 to 50 mM, COD removal efficiency increased from 42.29% to 90.30% in the first 60 minutes and color removal increased from 57.79% to 95.83% at the end of the same period time. With increasing the concentration to 100 mM, the efficiencies increased to 84.87% and 92.86% for COD and color, respectively. No significant differences were determined after the first 60 minutes between efficiencies achieved with H_2O_2 concentrations other than 5 and 10 mM. The initial pH of 2 varied between 2 and 2.08 for 5 and 100 mM H_2O_2 concentrations, respectively.

JSR A
Journal of Scientific Reports

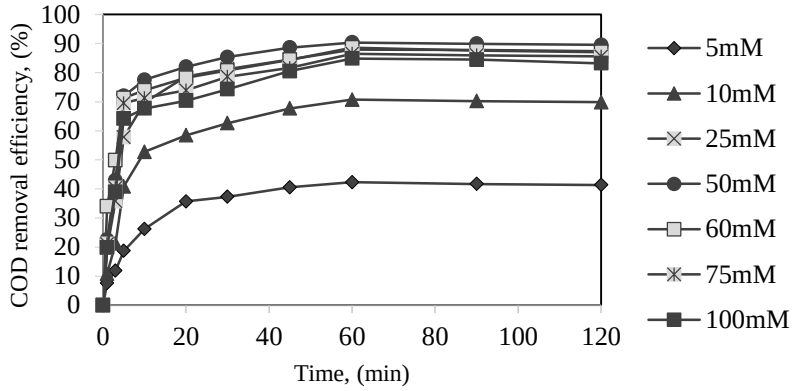

Figure 20. Effect of H_2O_2 concentration on COD removal efficiency in UV/H_2O_2/Fe^{2+} process.

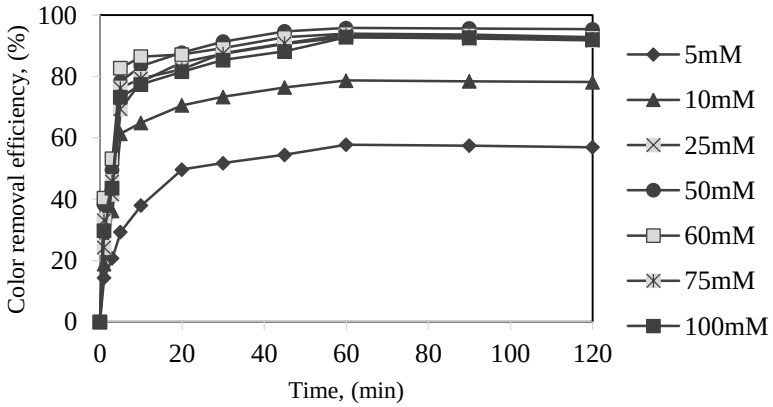

Figure 21. Effect H_2O_2 concentration on Color removal efficiency in UV/H_2O_2/Fe^{2+} process.

3.5.3. Effect of Fe^{2+}

The effects of Fe^{2+} concentrations varying between 0.25 and 3 mM, in which pH was kept at 2 and H_2O_2 was kept in 50 mM, on both COD and color removal efficiency are shown in Fig. 22 and Fig. 23. Maximum COD and color removal efficiencies of 95.65% and 98.52% were achieved in the first 60 minutes with 3 mM Fe^{2+} concentration. Fe^{2+} concentrations of 0.25 and 0.50 mM were not sufficient for COD removal. While relatively high Fe^{2+} concentrations were required for high COD removals, this was not determined for color removal. For example, the COD and color removal efficiencies of 95.65% and 98.52%, respectively, at a concentration of 3 mM Fe^{2+} at the end of 60 minutes were 59.97% and 82.36%, respectively, at 0.25 M Fe^{2+} concentration. The initial pH 2 changed between 2 and 2.03. By examining all experimental conditions, pH: 2, H_2O_2: 50 mM, Fe^{2+}: 3 mM, and process time: 60 minutes were determined as optimum operating conditions.

JSR A
Journal of Scientific Reports

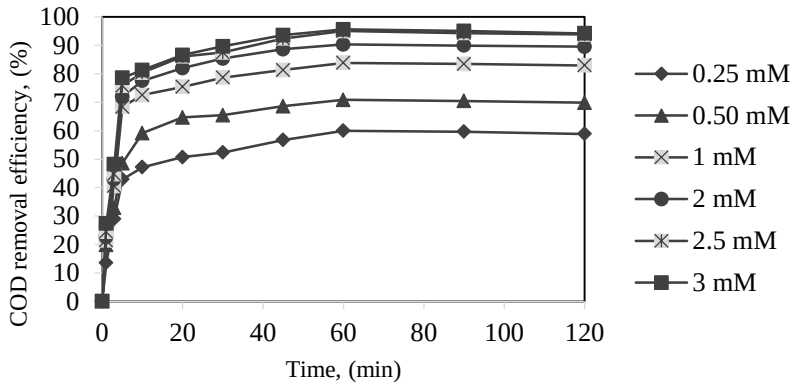

Figure 22. Effect Fe^{2+} concentration on COD removal efficiency in UV/H_2O_2/Fe^{2+} process.

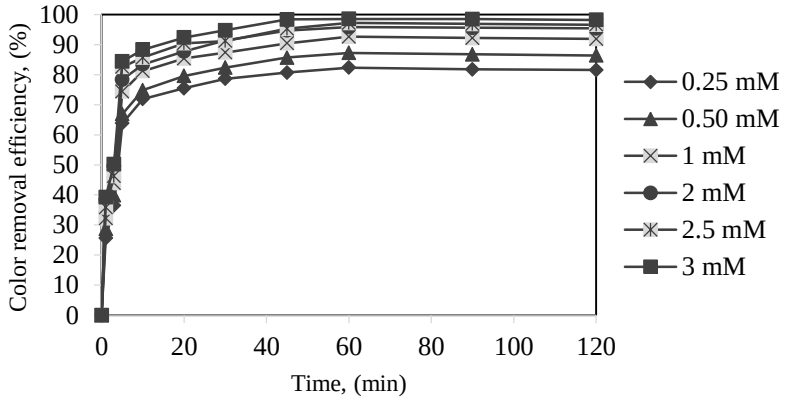

Figure 23. Effect Fe^{2+} concentration on Color removal efficiency in UV/H_2O_2/Fe^{2+} process.

3.6. Comparison of Processes

Under the optimum conditions determined for each process (UV: pH 7; UV/H_2O_2: pH 7 and 100 mM H_2O_2; UV/Fe^{2+}: pH 4 and 3 mM Fe^{2+}; H_2O_2/Fe^{2+}: pH 2 and 60 mM H_2O_2; UV/H_2O_2/Fe^{2+}: pH 2, 50 mM H_2O_2 and 3 mM Fe^{2+}) obtained COD and color removal efficiencies are given in Fig. 24 and Fig. 25, respectively. As can be seen from Fig. 24 and Fig. 25, a maximum of 95.65% COD and 98.52% color removal efficiencies were obtained at the end of 60 minutes by the photo-Fenton method. It was understood that a combination of UV radiation with Fenton process caused an increase of 9.99% and 18.08%, respectively in 83.76% COD and 80.44% removal efficiencies obtained by Fenton process. In the H_2O_2/Fe^{2+} process, the decreases in COD and color efficiency after 30 minutes indicated that no H_2O_2 could react and the remaining Fe^{2+} ions created color and COD. Also, the UV process was not effective alone. UV/H_2O_2 and UV/Fe^{2+} processes were relatively efficient only in color removal.

JSR A
Journal of Scientific Reports

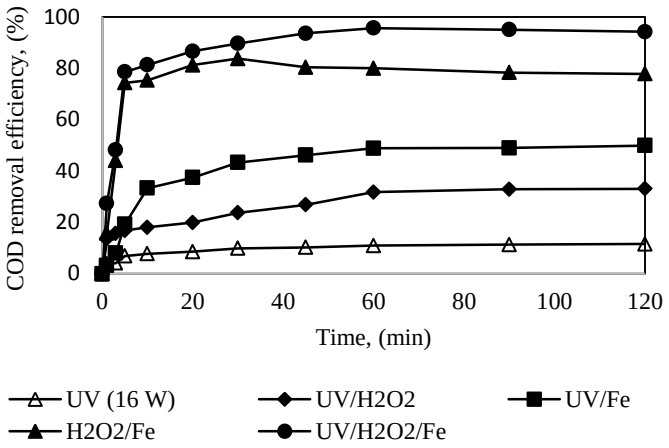

Figure 24. Comparison of UV, UV/H_2O_2, UV/Fe^{2+}, H_2O_2/Fe^{2+}, UV/H_2O_2/Fe^{2+} processes on COD removal efficiency.

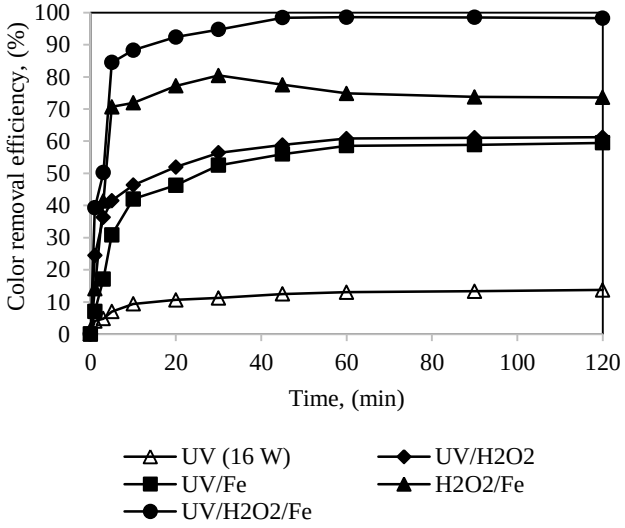

Figure 25. Comparison of UV, UV/H_2O_2, UV/Fe^{2+}, H_2O_2/Fe^{2+}, UV/H_2O_2/Fe^{2+} processes on Color removal efficiency.

4. CONCLUSION

- UV process alone was not effective in COD and color removal. Maximum of 11.56% COD and 13.72% color removal efficiencies were achieved at the optimum conditions.

- While UV/H_2O_2 process achieved a maximum of 33.08% COD and 61.21% color removal efficiency, a maximum of 49.89% COD and 59.44% color removal efficiency were achieved with the UV/ Fe^{2+} process.
- While the maximum COD and color removal was 83.76% and 80.44% in the first 30 minutes in the Fenton process, these values were reached in a short time like 10 minutes in the photo-Fenton process. For the photo-Fenton process, a maximum of 95.65% COD and 98.52% color removal efficiencies were achieved within 60 minutes.

- In UV, UV / H_2O_2, UV/Fe^{2+}, H_2O_2/Fe^{2+}, and UV/H_2O_2/Fe^{2+} processes, maximum COD and color removal efficiencies were achieved at ph values of pH 7, 7, 4, 2, and 2, respectively.

- It has been determined that the textile wastewater treated only with the photo-Fenton method met the COD and color discharge standards of Water Pollution and Control regulation in force in our country.

ACKNOWLEDGMENTS
This study was supported by the Scientific Research Project Fund of Ondokuzmayis University (Project No: PYO.MUH.1904.19.008). We would like to thank for the financial support.

REFERENCES

[1] Silva, G.M., Moreira, F.C., Alice, M., Mazur, L.P., Souza, A.U., Boaventura, A.R., Vilar, J.P, (2020), Integration of Fenton's reaction based processes and cation exchange processes in textile wastewater treatment as a strategy for water reuse, Journal of Environmental Management, 272, 111082.

[2] Pereda, B.R., Gallegos, A.A., Terrones, Y.A, Silva, S., Perez, A.H., (2020), Effective Electro-Fenton Treatment for Real Textile Effluent. A Case Study, Journal of Water Engineering, 37, 101434.

[3] Asghar, A., Raman, A.A. and Daud, W.M., (2015), Advanced oxidation processes for in-situ production of hydrogen peroxide/hydroxyl radical for textile wastewater treatment: a review, Journal of Cleaner Production, 87, 826-838.

[4] Kang, S.F., Liao, C.H. and Po, S.T., (2000), Color removal of textile wastewater by photo-fenton oxidation technology, Chemosphere, 41, -1287-1294.

[5] Bali, U., Çatalkaya, E. and Şengül, F., (2004), Photodegradation of Reactive Black 5, Direct Red 28 and Direct Yellow 12 using UV, UV/ H_2O_2 and UV/ H_2O_2/Fe^{2+}: a comparative study, Journal of Hazardous Materials, B-114, 159-166.

[6] Ghanbari, F. and Moradi, M., (2015), A comparative study of electrocoagulation, electrochemical Fenton, electro-Fenton and peroxi-coagulation for color removal of real textile wastewater: Electrical energy consumption and biodegradability improvement, Journal of Environmental Chemical Engineering, 3, 499-506.

[7] Perez, M., torrades, F., Domenech, X. and Peral, J., (2002), Fenton and photo-Fenton oxidation of textile effluents, Water Research, 36, 2703-2710.

[8] Gilpavas, E., Gomez, I.D. and Garcia, M.A.G., (2018), Optimization of solar-driven photo-electro-Fenton process for the treatment of textile industrial wastewater, Journal of Water Process Engineering, 24, 49-55.

[9] Gilpavas, E., Gomez, I.D. and garcia, M.A.G., (2019), Optimization and toxicity assessment of a combined electrocoagulation, H_2O_2/ Fe^{2+}/UV and activated carbon adsorption for textile wastewater treatment, Science of the Total Environment, 651, 551-560.

[10] Sreeja, P.H. and Sosamony, K.J., (2016), A Comparative Study of Homogeneous and Heterogeneous Photo-Fenton Process for Textile Wastewater Treatment, Procedia Technology, 24, 217-223.

[11] Rott, E., Minke, R., Bali, U. and Steinmetz, H., (2017), Removal of phosphonates from industrial wastewater with UV/Fe(II), Fenton and UV/Fenton treatment, Water Research, 122, 345-354.

[12] Zhang, H., Choi, H.J. and Huang, C.P., (2005), Optimization of Fenton process for the treatment of landfill leachate, Journal of Hazardous Materials, B125, 166-174.

[13] Umar, M., Aziz, H.A. and Yusoff, M.S., (2010), Review: Trends in the use of Fenton, electro-Fenton and photo-Fenton for the treatment of landfill leachate, Waste Management, 30, 2113-2121.

[14] Rice, E.W., Baird, R.B., Eaton, A.D., and Bridgewater, L.L., (2012), Standard Methods in Examination of Water and Wastewater, twenty-three ed. Water Environment Federation, American Public Health Association, American Water Works Association (APHA-AWWA).

Kütahya Dumlupınar University
Institute of Graduate Studies

Journal of Scientific
Reports-A
E-ISSN: 2687-6167
Number 45, December 2020

REVIEW ARTICLE

TISSUE CULTURE TECHNIQUES OF MEDICINAL AND AROMATIC PLANTS: HISTORY, CULTIVATION AND MICROPROPAGATION

Betül AKIN

Kütahya Dumlupinar University, Faculty of Arts and Sciences, Department of Biology, Kütahya, betul.akin@dpu.edu.tr, ORCID: 0000-0002-2325-7496

Received Date:06.08.2020 *Accepted Date: 30.10.2020*

ABSTRACT

Medicinal aromatic plants, which are source of secondary metabolites, have been used for treatment and other purposes since ancient times. In recent years, people have preferred medicinal and aromatic herbs to be healthy. Plant tissue culture methods have the potential to produce medicinal compounds such as secondary metabolites from plants as an alternative to traditional agriculture. Increasing population and increasing demand for herbal products, unconscious collection and illegal trade cause the extinction of medicinal plants in natural habitats. Therefore, it is important to cultivate medicinal and aromatic plants to protect biodiversity and endangered species. As a result, plant tissue culture methods are an alternative way for propagation of medically and economically important plants, the production of bioactive components for the pharmaceutical industry, and the production of medically important secondary metabolites.

Keywords: *Cultivation, Medicinal and aromatic plants, Plant tissue culture, Propagation, Secondary metabolite.*

1. HISTORICAL DEVELOPMENT, DEFINITION AND USE OF MEDICINAL AND AROMATIC PLANTS

Medicinal and aromatic plants undoubtedly have been widely used in many fields such as food, paint, cosmetics, perfume and medicine for centuries. In traditional systems, drugs have been obtained using various plant species grown in different parts of the world. Medicinal plants have been intriguing for humans since ancient times, and the first humans often used aromatic herbs. Medicinal and aromatic plants were frequently used in the prevention and treatment of diseases in traditional medicine during the Neolithic periods, and medicinal plants still continue to be the main types of drugs used in the world. Information about medicinal plants used by humans for therapeutic purposes in ancient times has been transferred to this day and this information is still valid today. Despite the decrease in interest in medicinal plants with the production of synthetic drugs in the 20th century, medicinal products of herbal origin regained importance towards the end of the 20th century [1-6,7].

In ancient times, people were in search of medicine in nature to combat diseases. Since there was not sufficient information about diseases and treatment methods with plants at that time, people learned how a plant could be used in treatment by experience [8,9]. In 3000 B.C., Egyptians used 500 wild

JSR A
Journal of Scientific Reports

and cultured plant species in medicine and thus “Phytotherapy”, namely, treatment methods using plants, emerged. However, in 2700 B.C., people in China used cinnamon and the Ancient Greeks referred to the spices as "fragrant aromatic herbs". In the past, methods of obtaining ethereal oil from fragrant plants were developed by humans. In fact, methods of obtaining rose oil were mentioned in ancient sources and in 3500 B.C., people obtained dye from plant roots. More than 600 medicinal plants were examined in a study of 5 volumes titled “De Materia Medica” by Dioskorides, and the use, side effects, dosages and plant growing techniques of drugs were discussed in detail. Some of the drugs that Dioskorides studied are still used today [2,6,10,11]. Medicinal and aromatic plants are generally defined as herbal medicines used as components of natural health products in such areas as pharmacy, cosmetics, nutrition, medicine and perfumery. Medicinal and aromatic plants can also be defined as plants used to prevent diseases, maintain a healthy life and cure diseases [12-15]. The use of herbal medicines is growing rapidly in developed countries and complementary-alternative medicine and herbal medicines are widely used by people with higher education and income levels. With the rapid growth of the population in recent years, people prefer herbal remedies or products to improve their health conditions. Approximately 40% of the compounds used in the pharmaceutical industry are obtained from plants directly or indirectly. Medicinal plants are globally valuable herbal resources, and the majority of these plants are obtained by harvesting from nature and some by cultivation. Therefore, many plant species showing medicinal properties are threatened with extinction due to excessive collection from nature [9, 16-18]. In the last century, as well as the rapid development and increasing side effects of synthetic substances, the advances in knowledge of chemistry and biology, which allow new molecules to be isolated from plants, animals and microorganisms, have led to increased interest in traditional medicines today. With the growing demand from consumers for herbal medicines, natural health products and secondary metabolites, the use of medicinal plants is growing rapidly worldwide. The use of medicinal plants has become important in recent years due to their low side effects [7,18,19,20].

2. CULTIVATION AND PROPAGATION OF MEDICINAL AND AROMATIC PLANTS IN TURKEY AND IN THE WORLD

Located in the temperate zone, Turkey, with the influence of geographical factors, is rich in plant diversity compared to many other countries and the number of plants distribution in Turkey is close to the number of plants distribution in the whole of the European continent. People have used plants for various purposes since ancient times, especially for their health benefits and especially since the 1990s, demand for medicinal and aromatic plants has increased. Many plant types widely used in Anatolia are still used as therapeutic today [10,11,21,22,23]. However, significant parts of medicinal and aromatic plants in the world and in our country are collected from nature, and the rest are cultivated. Although some of the economically important medicinal and aromatic plants used in many fields can be produced easily, there are difficulties in production of some. Thus, only approximately 10% of these plants are cultivated. In Turkey, also the plant cultivation rate is not adequate [14,24]. Accordingly, production area and production amount of medicinal and aromatic plants in Turkey are given by years in Table 1 [25]. According to Table 1 showing the production area and production amount of some medicinal and aromatic plants in Turkey between 2012-2018, opium poppy ranks first among cultivated plants as of 2018 with 26 991 tons of production, followed by thymus with 15 895 tons of production and rose with 14 773 tons of production respectively.

It is stated that 28,187 plant species are used medically in the world; however, only 4478 of the species used in plant-based medicines are shown in the publication as a medicinal regulatory. The

JSR A
Journal of Scientific Reports

global herbal medicine market is growing rapidly every year. Today, commercial production of some anticancer drugs from herbal sources is carried out successfully [6,26]. Worldwide, the production amounts of medicinal and aromatic plants cultivated for commercial purposes in 2017 and the producer countries are given in the FAO statistics. According to the production amounts of medicinal and aromatic plants worldwide are examined, garlic, ginger, anise, badian, fennel, coriander are among the top places. On the other hand, when the producer countries are evaluated, India and China, which are rich in biodiversity, are at the forefront (Table 2) [27].

Table 1. Production area (decare) and production amounts (ton) of some medicinal and aromatic plants in Turkey by years [25].

Item	**Unit**	**2012**	**2013**	**2014**	**2015**	**2016**	**2017**	**2018**
Anise	Area (Decare)	194430	152431	140506	138118	136552	121833	124455
	Production (Ton)	11023	10046	9309	9050	9491	8418	8664
Thyme	Area (Decare)	94283	89137	92959	104863	121127	121472	139061
	Production (Ton)	11598	13658	11752	12992	14724	14477	15895
Black Cumin	Area (Decare)	2299	3261	1717	4681	23160	32560	33864
	Production (Ton)	161	352	140	425	2527	3094	3322
Fennel	Area (Decare)	15775	13848	15848	15512	17503	16525	23400
	Production (Ton)	1862	1994	2289	1461	2464	2022	3067
Coriander	Area (Decare)	11	11	11	150	503	410	405
	Production (Ton)	1	1	1	11	42	29	29
Caper	Area (Decare)	-	-	15	15	3	-	-
	Production (Ton)	-	-	-	-	-	-	-
Opium poppy (Capsule)	Area (Decare)	135106	322773	266212	615919	299217	237314	451226
	Production (Ton)	3497	19244	16223	30730	16550	13836	26991
Stinging nettle	Area (Decare)	3	3	3	0	5	5	5
	Production (Ton)	0.42	0.42	0.42	0	1	1	1

Sage tea	Area (Decare)	54	30	130	536	3681	4123	3951
	Production (Ton)	7	4	19	80	411	557	428
Rose (Oil)	Area (Decare)	30832	28012	28359	28243	29753	33277	34205
	Production (Ton)	10225	10769	10831	9483	12267	13372	14773
Lavender	Area (Decare)	509	709	3189	3218	5700	6606	8684
	Production (Ton)	123	105	297	400	747	845	1040

Table 2. Production amounts (ton) of some medicinal and aromatic plants in the world in 2017 [27].

Items	**Area**	**Production amount (ton)**
Anise, badian, fennel, coriander	India Mexico Iran	646 000 132 565 64 788
Cinnamon (canella)	Indonesia China Viet Nam	87 130 79 486 37 126
Garlic	China India Bangladesh	22 160 465 1 693 000 425 401
Ginger	India China Nigeria	1 070 000 557 303 349 895
Jojoba seed	Mexico	143
Maté	Brazil Argentina Paraguay	619 003 290 950 105 005
Mustard seed	Nepal Canada Russian Federation	159 710 121 600 98 319
Pepper (piper ssp.)	Viet Nam Indonesia Brazil	252 576 87 029 79 371
Quinoa	Peru Bolivia Ecuador	78 657 66 792 1 286
Vanilla	Madagaskar Indonesia China	3 227 2 402 662

JSR A
Journal of Scientific Reports

3. PROPAGATION OF PLANTS CONTAINING SECONDARY METABOLITES WITH PLANT TISSUE CULTURE METHODS

It is important to have knowledge the chemistry and biology of the active substances of medicinal and aromatic plant species that have economic value today and to produce these plants. With the increase in the consumption of natural products all over the world, there are difficulties in obtaining sufficient amount of herbal raw materials. Plant metabolites can be isolated from plants grown in nature but some problems are also encountered in obtaining secondary metabolites from plants grown in natural environment. Some of these problems can be listed as climatic factors, the risk of extinction of the plant generation, the inability to obtain sufficient secondary metabolites and inability to provide a drug of high quality and efficiency [28-30,31]. Important medicinal plants can be propagated by plant tissue culture methods. In addition, plant tissue cultures are a promising strategy especially in rare or endangered species or in plants producing secondary metabolites that are difficult to propagate.

In recent years, interest in plant tissue cultures has increased in various countries of the world. Advances in this technique contribute to the solution of problems related to subjects such as physiology, biochemistry, cytology, genetics and molecular biology in plants [17,18,28,30,32-33].

Plant tissue culture methods have great industrial importance in plant propagation, conservation of plant resources and production of secondary metabolites in recent years. This methods offers new and sustainable opportunities in solving numerous problems in the field of medicinal plant breeding and conservation biology [5,23,28,34,35]. Secondary metabolites are compounds that are not a direct metabolism product in plants but appear as by-products, are produced by plants and do not have a direct relationship with the plant's primary metabolism, but are produced to the organism advantage and essentially have very important roles in plants. Secondary metabolites defend plants against microorganisms, insects, herbivores and even other plants. In addition, secondary metabolites have an ecological role in nature. They function as substances that attract animals that assist in pollination or seed distribution [2,32,34,36,37]. Plants, used in pharmacy, agriculture, food additives and as bio pesticide, are main materials constitute an important source of secondary metabolites.

In previous years, secondary metabolites were obtained by isolating from plants. After the 1970s, cell cultures followed by tissue culture methods began to be used to produce secondary metabolites under in vitro conditions. Plant secondary metabolites are used directly or indirectly in many industries, especially in the pharmaceutical and food industry [5,32,36,38,39]. With the rapid increase in the world population, excessive pressure on the existing arable lands has caused disappearance of the natural habitats and it has become increasingly difficult to obtain plant-derived compounds. Plant secondary metabolites can be produced by in vitro callus induction, cell suspension cultures and organ cultures. As an alternative for secondary metabolite production, plant cells and organ cultures have been developed. The advantages of production of secondary metabolites with plant tissue culture is desired production at desired time, uniform quality product in a short time, independent production throughout the year regardless of climatic conditions, conservation of wild species at risk of extinction and production of novel compounds. New plant compounds that are not normally found in natural populations of certain species can also be isolated by plant tissue culture methods. Sustainability of important medicinal plant species for future can be achieved by reducing the dependence on the natural population by producing these compounds by in vitro culture methods. [30,40-43].

JSR A
Journal of Scientific Reports

Commercial production of some secondary metabolite products from plant cell and tissue cultures has successfully been carried out recently. Therefore, the selection of a suitable species and organs is necessary for induction of in vitro callus, cells or organs. Cell and organ cultures are started by selecting a mother plant with a high amount of secondary metabolites. In fact, plant tissue cultures are an alternative and effective technique in the production of bioactive compounds, and the amount of secondary metabolites produced in this technique is higher than the mother plant [5,30,38,41,42,44]. In a study by Kumar et al. [45], it was determined that the amount of secondary metabolites in the plantlets grown *in vitro* of *Swertia chirayita* plant is higher than *in vivo* plantlets. *Fritillaria unibracteata* was rapidly propagated directly from small cuttings of the bulb by organ culture technique. Compared to natural wild growth conditions, the growth rate was about 30-50 times higher and alkaloid and useful microelements content were higher than these found in wild bulbs [46]. Thus, the controlled production of secondary metabolites with plant cell and tissue cultures, are numerous benefits in is highly promising [28].

4. STRESS FACTORS IN PLANT TISSUE CULTURES

Secondary metabolite production from medicinal plants has accelerated in the last decade. In land conditions, both internal factors such as the genotype, plant organ and age of the plant, and external factors such as photoperiod, temperature, soil type, light intensity and wavelength, and amount of water available and climatic conditions affect the concentration and content of compounds obtained from medicinal plants. The reaction of plants to stress factors varies depending on the intensity and duration of stress [30,36,47,48]. The above-mentioned factors may also affect the content of medicinal plants produced *in vitro*. In a study by Kapoor et al. [49], it was revealed that the quality of light in callus cultures of the medicinal plant *Rhodiola imbricata* is an important factor in the growth rate of callus biomass and in the production of industrially important secondary metabolites. Biomass and alkaloid production of *Catharanthus roseus* increased by the inclusion of 200 mg/L tryptophan or phenylalanine as a nitrogen source in the B5 nutrient medium with a pH of 5.82 [50].

The response of plants to abiotic stress factors consists of four stages in general: 1- Initial alarm phase, 2- Acclimation phase, 3- Maintenance phase and 4- Exhaustion phase (Figure 1) [51]. Plant response to stress is a dynamic process that is dependent on stress intensity and stress duration. Plant's response to stress can be distinguished several stage: *An initial alarm phase*, when stress in plant causes a shock effect, stress tolerance level of plant decreases and stress-responsive signalling pathways are stimulated; biosynthesis of various stress-protective proteins takes place and plant stress tolerance level increases during *acclimation phase*; homeostasis is maintained and plant stress tolerance level remains constant during the *maintenance phase*; plant stress tolerance level declines during *exhaustion phase* and if stress application takes too long, the plant maintains stress-induced homeostasis will fail (Figure 1).

JSR A
Journal of Scientific Reports

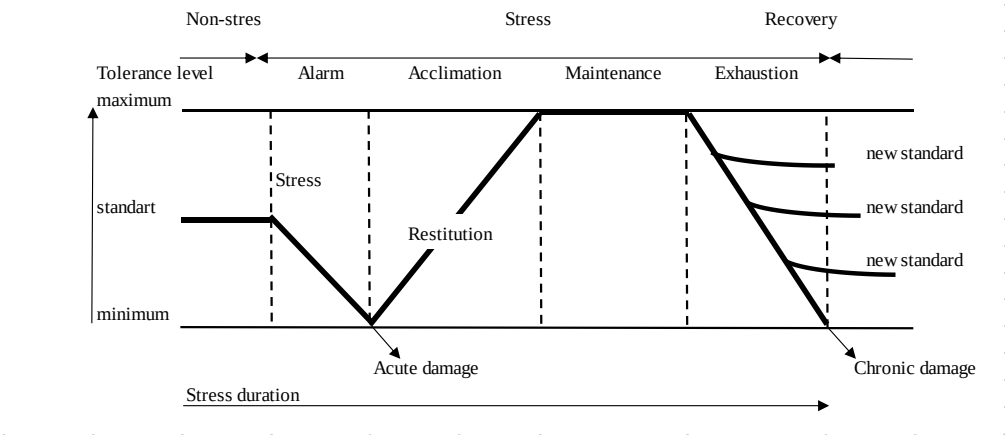

Figure 1. A generalized scheme of plant responses to abiotic stress factors [49].

Secondary metabolites production, role in plant defence and whose synthesis is triggered by stress factors such as climatic factors, drought, light and microbial activities, can be increased in plant tissue and cell cultures by factors defined as stimulants (elicitor). Elicitors can be used for triggering the secondary metabolic pathway in plant cell. Elicitors can be divided into biotic and abiotic. For this purpose, biotic and abiotic stimulants indicated in Figure 2 can be used. Abiotic stimulants consist of substances of non-biological origin and can be grouped as physical, chemical and hormonal factors. Biotic stimulants are substances of biological origin like are polysaccharides, proteins, glycoproteins, bacteria, fungi and yeasts [52-57].

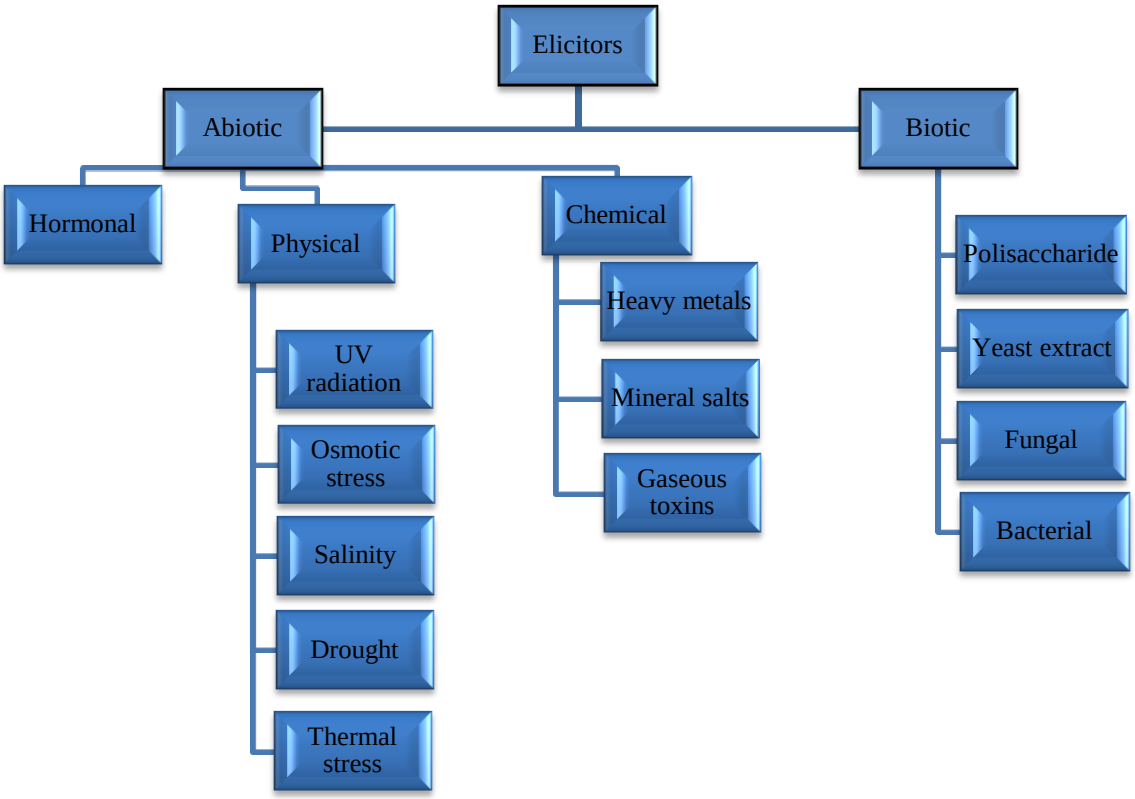

Figure 2. Classification of biotic and abiotic elicitors in plants [50].

Yamaner et al. [58] indicated that mannan and pectin added to the MS nutrient medium stimulate of hypericin biosynthesis in *Hypericum adenotrichum* seedlings. Accordingly, the production of pseudohypericin was increased by 2.8 times and the production of hypericine was increased by 1.7 times with the treatment of varying levels of mannan. Pectin treatment stimulated pseudohypericin production up to 4.8-fold and hypericine production up to 2.7-fold. It was revealed by the study that these elicitors can be used in the secondary metabolites production in *Hypericum adenotrichum* plant. Also, Yu et al. [59] indicated that jasmonic acid is an effective elicitor for secondary metabolite production. Thus in their study 1.0-5.0 mg/L jasmonic acid, strongly promoted total ginsenoside content and ginsenoside productivity. *In vitro* cultures of *Merwilla plumbea*, the nutrient medium containing 100 mg/L yeast extract (YE) stimulated the accumulation of total phenolic substances in the roots, followed by 100 mg/L yeast malt broth (YMB) in shoots [60]. Açıkgöz et al. [61] reported that different concentrations of methyl jasmonate and salicylic acid treatments increased the the camphor and phenolic compounds accumulation. The highest amount of camphor accumulation was seen in cells treated with 100 µM MeJA (0.3449 µg/g) and 50 µM SA (0.3816 µg/g). Sutini et al. [62]

demonstrated that with the addition of cobalt metal ion elicitors to the nutrient medium, the secondary metabolite of cinnamic acid was obtained in the *Camellia sinensis* by 11.9%.

5. CONCLUSION

There are many plant species with medicinal value in the world. Collection and export of some plant species for medicinal purposes destroy the flora and threaten some of the plant species [63]. Demand for herbal products has increased rapidly in past three decades due to the low side effects of herbal medicines [64]. Medicinal and aromatic plants are herbal sources preferred by the majority of the world population for a healthy life and are also used as a preventive and therapeutic treatment [65]. Plant tissue cultures methods play an important role in obtaining secondary metabolites from medicinal and aromatic plants and meeting the growing demands of the pharmaceutical industry in an environmentally friendly way. Plant tissue culture techniques are often used for large-scale production of secondary metabolites in plant species that are often difficult to cultivate or of medicinal importance. However, tissue culture methods also play an important role in conserving biodiversity and propagating rare endangered plant species [66].
In vitro propagation has an important potential for the production of high quality medicinal products. Despite the fact that endangered medicinal plants are protected by *in vitro* propagation, many plant species of medicinal importance are unconsciously exploited by the pharmaceutical industry. In order to reduce the pressure caused by excessive collection of medicinal plants from nature and to produce metabolites effectively, these plant species should be cultured quickly and studies on *in vitro* production should be increased.

REFERENCES

[1] Shimomura, K., Yoshimatsu, K., Jaziri, M. and Ishimaru, K. (1997). In plant biotechnology and plant genetic resources for sustainability and productivity. In K. Watanabe and E. Pehu (Eds.), Traditional medicinal plant genetic resources and biotechnology applications, R.G. Landes Company, Austin, Texas, USA, pp. 209-225.

[2] Mammadov, R. (2014). Tohumlu Bitkilerde Sekonder Metabolitler. Türkiye: Nobel Yayınevi, 428.

[3] Pant, B. (2014). Application of plant cell and tissue culture for the production of phytochemicals in medicinal plants. Advances in Experimental Medicine and Biology, 808, 25-39.

[4] Acıbuca, V. and Budak, D.B. (2018). Dünya'da ve Türkiye'de tıbbi ve aromatik bitkilerin yeri ve önemi. Çukurova Tarım ve Gıda Bilimleri Dergisi, 33(1), 37-44.

[5] Chandana, B.C., Nagaveni, H.C., Kumari, Lakshmana, D., Shashikala, S.K. and Heena, M.S. (2018). Role of plant tissue culture in micropropagation, secondary metabolites production and conservation of some endangered medicinal crops. Journal of Pharmacognosy and Phytochemistry, 7, 246-251.

[6] Inoue, M., Hayashi, S. and Craker, L.E. (2019). Role of medicinal and aromatic plants: past, present, and future. In S. Perveen, and A. Al-Taweel (Eds.), In Pharmacognosy-medicinal plants, IntechOpen, London, UK, pp. 1-13.

[7] Karunamoorthi, K., Jegajeevanram, K., Vijayalakshmi, J., Mengistie, E. (2013). Traditional medicinal plants: a source of phytotherapeutic modality in resource-constrained health care settings. Journal of Evidence- Based Complementary Alternative Medicine, 18(1), 67-74.

[8] Petrovska, B.B. (2012). Historical review of medicinal plants usage. Pharmacognosy Reviews, 6, 1-5.

[9] Pan, S.Y., Litscher, G., Gao, S.H., Zhou, S.F., Yu, Z.L., Chen, H.Q., Zhang, S.F., Tang, M.K., Sun, J.N.,& Ko, K.M. (2014). Historical perspective of traditional indigenous medical practices: the current renaissance and conservation of herbal resources. Evidence-Based Complementary and Alternative Medicine, Article ID 525340, pp. 20.

[10] Baytop, T. (1963). Türkiye'nin tıbbi ve zehirli bitkileri. Türkiye: İstanbul Üniversitesi Yayını, 499.

[11] Temel, M., Tınmaz, A.B, Öztürk, M. and Gündüz, O. (2018). Dünyada ve Türkiye'de tıbbi - aromatik bitkilerin üretimi ve ticareti. Kahramanmaraş Sütçü İmam Üniversitesi Tarım ve Doğa Dergisi, 21, 198-214.

[12] Christaki, E., Bonos, E., Giannenas, I. And Florou-Paneri, P. (2012). Aromatic plants as a source of bioactive compounds. Agriculture, 2, 228-243.

[13] Street, R.A. and Prinsloo, G. (2013). Commercially important medicinal plants of South Africa: a review. Journal of Chemistry, Article ID 205048, pp. 16.

[14] Arslan, N., Baydar, H., Kızıl, S., Karik, Ü., Şekeroğlu, N. and Gümüşçü, A. (2015). Tıbbi ve aromatik bitkiler üretiminde değişimler ve yeni arayişlar. TMMOB Agricultural Engineering VIII. Technical Congress, Ankara, Turkey, 483–505.

[15] Samarth, R.M., Samarth, M. and Matsumoto, Y. (2017). Medicinally important aromatic plants with radioprotective activity. Future Science OA, 3(4), FSO247.

[16] Pandey, A.K. and Patra A.K. (2004). Indigenous knowledge and sustainable development by medicinal plants. In M.K. Rai, N.J. Chikhale, P.A. Wadegaonkar, P.V. Thakare and A.P. Ramteke (Eds.), Recent trends in biotechnology, Scientific Publishers, India, pp. 160-170.

[17] Sidhu, Y. (2010). *In vitro* micropropagation of medicinal plants by tissue culture. The Plymouth Student Scientist, 4, 432-449.

[18] Chen, S.L., Yu, H., Luo, H.M., Wu, Q., Li, C.F. and Steinmetz, A. (2016). Conservation and sustainable use of medicinal plants: problems, progress, and prospects. Chinese Medicine, 11, 37.

[19] Ekor, M. (2014). The growing use of herbal medicines: issues relating to adverse reactions and challenges in monitoring safety. Frontiers in Pharmacology, 4, 1-10.

JSR A
Journal of Scientific Reports

[20] Agra, M.F., Freitas, P.F., Barbosa-Filho, J.M. (2007). Synopsis of the plants known as medicinal and poisonous in Northeast of Brazil. Revista Brasileira Farmacognosia, 17, 114-140.

[21] Öztürk, M., Altundağ, E. and Gücel, S. (2012). Medicinal and aromatic plants (Turkey). Ethnopharmacology, Encycl. Life Support Syst., 6, 181-206 (EOLSS).

[22] Avcı, M. (2005) Çeşitlilik ve endemizm açısından Türkiye'nin bitki örtüsü. Coğrafya Dergisi, 13, 27-55.

[23] Chandran, H., Meena, M., Barupal, T., Sharma, K. (2020). Plant tissue culture as a perpetual source for production of industrially important bioactive compounds. Biotechnology Reports, 26, e00450, 1-10.

[24] Dinçer, D., Bekçi, B. and Bekiryazıcı, F. (2016). Türkiye'deki doğal bitki türlerinin üretiminde doku kültürü tekniklerinin kullanımı. Nevşehir Bilim ve Teknoloji Dergisi, 5, 295-302.

[25] TÜİK (2018). Turkish Statistical Enstitute. http://www.tuik.gov.tr.

[26] Allkin, B. (2017). Useful Plants–Medicines: at least 28,187 plant species are currently recorded as being of medicinal use. In K.J. Willis (Ed.), Royal Botanic Gardens, Kew, London, pp. 22-29.

[27] FAO (2019). Food and Agriculture Organization of the United Nations. http://www.fao.org/faostat/en/#data/QC.

[28] Hussain, M.S., Fareed, S., Ansari, S., Rahman, A., Ahmad, I.Z. and Saeed, M. (2012). Current approaches toward production of secondary plant metabolites. Journal of Pharmacy & Bioallied Sciences, 4, 10-20.

[29] Veeresham, C. and Chitti, P. (2013). Therapeutic agents from tissue cultures of medicinal plants. Natural Products Chemistry & Research, 1, 1-5.

[30] Cardoso, J.C., Oliveira, M.E.B.S. and Cardoso, F.C.I. (2019). Advances and challenges on the *in vitro* production of secondary metabolites from medicinal plants. Horticultura Brasileira, 37, 124-132.

[31] Yue, W., Ming, Q.L., Lin, B., Rahman, K., Zheng, C.J., Han, T., Qin, L.P. (2016). Medicinal plant cell suspension cultures: pharmaceutical applications and high-yielding strategies for the desired secondary metabolites. Critical Reviews in Biotechnology, 36, 215-232.

[32] Kocaçalışkan, İ. (2017). Doku ve Hücre Kültürü Teknikleri (İkinci baskı). Türkiye: Nobel Akademik Yayıncılık, 156.

[33] Dakah, A., Zaid, S., Suleiman, M., Abbas, S. and Wink, M. (2014). *In vitro* propagation of the medicinal plant *Ziziphora tenuior* L. and evaluation of its antioxidant activity. Saudi Journal of Biological Sciences, 21(4), 317-323.

[34] Yoshimatsu, K. (2008). Tissue culture of medicinal plants: micropropagation, transformation and production of useful secondary metabolites. Studies in Natural Products Chemistry, 34, 647-752.

[35] Gonzalez-Rabade, N., Del Carmen Oliver-Salvador, M., Salgado-Manjarrez, E. and Badillo-Corona, J.A. (2012). *In vitro* production of plant peroxidases-a review. Applied Biochemistry and Biotechnology, 166, 1644-1660.

[36] Isah, T. (2019). Stress and defense responses in plant secondary metabolites production. Biological Research, 52, 1-25.

[37] Pagare, S., Bhatia, M., Tripathi, N., Pagare, S. and Bansal, Y.K. (2015). Secondary metabolites of plants and their role: overview. Current Trends in Biotechnology and Pharmacy, 9, 293-304.

[38] Zhou, L.G. and Wu, J.Y. (2006). Development and application of medicinal plant tissue cultures for production of drugs and herbal medicinals in China. Natural Product Reports, 23, 789-810.

[39] Çalışkan, T., Hatipoğlu, R. and Kırıcı, S. (2019). Sekonder bitki metabolitlerinin in vitro koşullarda üretimi. Türk Tarım – Gıda Bilim ve Teknoloji Dergisi, 7(7), 971-980.

[40] Filová, A. (2014). Production of secondary metabolities in plant tissue cultures. Research Journal of Agricultural Science, 46, 236-245.

[41] Nalawade, S.M. and Tsay, H.S. (2004). *In vitro* propagation of some important chinese medicinal plants and their sustainable usage. In Vitro Cellular & Developmental Biology - Plant, 40, 143-154.

[42] Ramachandra Rao, S. and Ravishankar, G.A. (2002). Plant cell cultures: chemical factories of secondary metabolites. Biotechnology Advances, 20, 101-153.

[43] McDonald, K.A., Jackman, A.P., Thorup, J.E. and Dandekar, A.M. (1995). Plant callus as a source of biochemicals. Applied Biochemistry and Biotechnology, 54, 93-108.

[44] Murthy, H.N., Lee, E. and Paek, K. (2014). Production of secondary metabolites from cell and organ cultures: strategies and approaches for biomass improvement and metabolite accumulation. Plant Cell Tissue Organ Culture, 118, 1-16.

[45] Kumar, V., Singh, S.K., Bandopadhyay, R., Sharma, M.M. and Chandra, S. (2014). *In vitro* organogenesis secondary metabolite production and heavy metal analysis in *Swertia chirayita*. Central European Journal of Biology, 9, 686-698.

[46] Gao, S.L., Zhu, D.N., Cai, Z.H., Jiang, Y. and Xu, D.R. (1999). Organ culture of a precious chinese medicinal plant-*Fritillaria unibracteata*. Plant Cell, Tissue and Organ Culture, 59, 197-201.

[47] Rejeb, I., Pastor, V. and Mauch-Mani, B. (2014). Plant responses to simultaneous biotic and abiotic stress: molecular mechanisms. Plants, 3, 458-475.

JSR A
Journal of Scientific Reports

[48] Figueiredo, A.C., Barroso, J.G., Pedro, L.G. and Scheffe, J.J.C. (2008). Factors affecting secondary metabolite production in plants: volatile components and essential oils. Flavour and Fragrance Journal, 23, 213-226.

[49] Kapoor, S, Raghuvanshi, R, Bhardwaj, P, Sood, H, Saxena, S. and Chaurasia, O.P. (2018). Influence of light quality on growth, secondary metabolites production and antioxidant activity ın callus culture of *Rhodiola imbricata* Edgew. Journal of Photochemistry and Photobiology, B: Biology, 183, 258-265.

[50] Mishra, M., Srivastava, R. and Akhtar, N. (2019). Effect of nitrogen, phosphorus and medium pH to enhance alkaloid production from *Catharanthus roseus* cell suspension culture. International Journal of Secondary Metabolite, 6, 137-153.

[51] Kosová, K., Vítámvás, P., Prášil, I. T. and Renaut, J. (2011). Plant proteome changes under abiotic stress - contribution of proteomics studies to understanding plant stress response. Journal of Proteomics, 74, 1301-1322.

[52] Naik, P.M. and Al–Khayri, J.M. (2016). Abiotic and biotic elicitors–role in secondary metabolites production through *in vitro* culture of medicinal plants. In A.K. Shanker and C. Shanker (Eds.), Abiotic and biotic stress in plants - recent advances and future perspectives, IntechOpen, pp. 247-277.

[53] Matkowski, A. (2008). Plant *in vitro* culture for the production of antioxidants-a review. Biotechnology Advances, 26, 548-560.

[54] Radman, R., Saez, T., Bucke, C., Keshavarz, T. (2013). Elicitation of plants and microbial cell systems. Biotechnology and Applied Biochemistry, 37, 91-102.

[55] Roy, S.K., Roy, D.K. (2016). Use of medicinal plant and its vulnerability due to climate change in northern part of Bangladesh. American Journal of Plant Sciences, 7, 1782-1793.

[56] Gorelick, J., Bernstein, N. (2014). Elicitation: An underutilized tool in the development of medicinal plants as a source of therapeutic secondary metabolites. In D.L. Sparks (Ed.), Advances in Agronomy, 124, Elsevier, Amsterdam, The Netherlands, pp. 201-230.

[57] Baenas, N., Garcia-Viguera, C., Moreno, D.A. (2014). Elicitation: a tool for enriching the bioactive composition of foods. Molecules, 19, 13541-13563.

[58] Yamaner, Ö., Erdağ, B. and Gökbulut, C. (2013). Stimulation of the production of hypericins in *ın vitro* seedlings of H*ypericum adenotrichum* by some biotic elicitors. Turkish Journal of Botany, 37, 153-159.

[59] Yu, K.W., Gao, W.Y., Son, S. H. and Paek, K.Y. (2000). Improvement of ginsenoside production by jasmonic acid and some other elicitors in hairy root culture of ginseng (*Panax ginseng* C.A. Meyer). In Vitro Cellular & Developmental Biology, 36, 424-428.

[60] Baskaran, P., Ncube, B. and Staden, J.V. (2012). *In vitro* propagation and secondary product production by *Merwilla plumbea* (Lindl.) Speta. Plant Growth Regulation, 67, 235-245.

[61] Açıkgöz, M.A., Kara, Ş.M., Aygün, A., Özcan, M.M. and Ay, E.B. (2019). Effects of methyl jasmonate and salicylic acid on the production of camphor and phenolic compounds in cell suspension culture of endemic turkish yarrow (*Achillea gypsicola*) species. Turkish Journal of Agriculture and Forestry, 43, 351-359.

[62] Sutini, Widiwurjani, Augustien, N., Purwanto, D.A. and Muslihatin, W. (2019). The production of cinnamic acid secondary metabolites through *in vitro* culture of callus *Camellia sinensis* L. with the elicitor of cobalt metal ions. AIP Conference Proceedings, 2120, 030028. https://aip.scitation.org/doi/10.1063/1.5115632.

[63] Chen, S.L, Yu, H., Luo, H.M., Wu, Q., Li, C.F. and Steinmetz, A. (2016). Conservation and sustainable use of medicinal plants: problems, progress, and prospects. Chinese Medicine (United Kingdom), 11, 1-10.

[64] Ekor, M. (2014). The growing use of herbal medicines: issues relating to adverse reactions and challenges in monitoring safety. Frontiers in Pharmacology, 4,1-10.

[65] Yuan, H., Ma, Q., Ye, L., Piao, G. (2016). The traditional medicine and modern medicine from natural products. Molecules 21, 559, 1-18.

[66] Verpoorte, R., Contin, A., Memelink, J. (2002). Biotechnology for the production of plant secondary metabolites. Phytochemistry Reviews, 1, 13-25.

Kütahya Dumlupınar University
Institute of Graduate Studies

Journal of Scientific
Reports-A
E-ISSN: 2687-6167
Number 45, December 2020

REVIEW ARTICLE

THE ROLE OF TELOMERIC ACTIVITY AND TELOMERASES IN AGING WITH NEOPLASIC CHANGES

Esra BİLİCİ[1*]

[1] Afyon Kocatepe University, Faculty of Veterinary Medicine, Department of Medical Biology and Genetics, Afyon, vet.hekimesrabilici@gmail.com, ORCİD:0000-0001-6636-5975

Recieved Date: 18.04.2020 *Accepted Date:04.11.2020*

ABSTRACT

The effect of telomeres on aging and cancer is very important. Telomere is a necessary structure for the continuous preliferation of human cells and is vital for most cancer cells. Telomeric structures located at the ends of the chromosomes consist of TTAGGG repeat units. Telomere terminal transferase is the enzyme responsible for telomere synthesis. It is also a large enzyme complex. Reverse transcriptase provides activation by strengthening the wearing parts after high telomere loss. In addition, it has been suggested that there are cancer cells that do not have telomerase activity but are able to extend the length of telomeres. In the timeframe of cellular division, telomerase enzyme can repair these errors if telomere sequences are lost. In cases where it is not repaired, the protection of these areas is eliminated. Thus, shortening occurs at the ends of the chromosomes. It has been researched by scientists that this shortening causes cellular aging. Reverse transcriptase enzyme has been reported to cause tumorigenic transformation of human epithelial cells and fibroblasts by cooperating with a number of oncogenes and suppressing several tumor suppressor genes. Studies on telomere shortening prove that this enzyme can have a strong effect in the treatment of cancer and is an important development for many patients who are expecting hope. Studies conducted in recent years are among the ideas that the structures and telomerase activity of telomere regions play an active role in cell aging and cancer formation. In the light of all these data, there is not a complete solution of aging, but studies are still ongoing today and major steps have been taken regarding cancer treatment. In this review, the definition of telomeres, their purpose, measurement methods and current studies are given.

Keywords: *Telomere, Telomerase, Cancer, Aging*

1. INTRODUCTION

Hermann J. Muller described the expression of telomere for the first time by studying the Drosophila melanogaster chromosome in 1938 and examined the structural changes that occur after X radiation and the frequency of these changes. As a result of these examinations, it was observed that deletions and inversions occurring at the ends of the chromosomes were less common. In further studies, it has been observed that the broken-ended chromosomes coalesce easily and the telomere structures of normal chromosomes are stable. As a result, it has been accepted that there are special terminal structures that allow chromosomes to form integrity [1].

JSR A
Journal of Scientific Reports

Telomeres are nucleoprotein structures that prevent the ends of chromosomes from being recognized as DNA breakage and function to maintain genome stability [2,3,4]. Mammalian telomeres are composed of repeats of the TTAGGG DNA sequence linked by a six protein complex called shelterin. Due to the recent replication problem [5] telomeres shorten with each cell division, leading to progressive telomere wear that is considered one of the mechanisms underlying organmal aging [6,7]. When telomeres are critically shortened, they trigger a persistent DNA damage response in cellular aging or apoptosis at chromosome ends [8], ultimately compromising the regenerative capacity of tissues [9].

Telomeres are heterochromatic areas that are located at the ends of chromosomes of eukaryotic organisms and consist of specialized DNA repeat sequences [10,11]. It consists of subtelomeric region and main telomere DNA. The main telomeric region is 10-15 kb in length in humans [12] and is the continuation of the subtelomere. The main telomere region consists of telomere DNA consisting of repetitive sequences and telomere-bound structural proteins. The feature that separates telomeres from the rest of the chromosome; It is the loss and regaining of telomeric DNA due to the cell cycle, which is called 'telomere dynamics'. In human somatic cells, telomere dynamics proceed negatively. The telomeric DNA lost by the cell in each cycle is more than the telomeric DNA to be synthesized again [13].

Thirty years ago, the classic view was that telomeres retain the natural ends of linear chromosomes and that telomerase is a specific telomere-terminal transferase required for the replication of chromosome ends in unicellular organisms. Although this concept is still valid today, many different areas related to telomeres and telomerase have matured significantly. These areas include the discovery of many of the key molecular components of telomerase, the limitations of cellular replication, the identification and characterization of human genetic disorders that cause premature telomere shortening [14].

It is known that telomeres are resistant to exonuclease and ligases, play a role in the stability of chromosomes, but also play a role in nuclear construction and gene expression. In addition, telomeres prevent chromosome ends from sticking to each other by ensuring the completion of replication [15]. Telomeres protect chromosomes from being detected as damaged DNA and from recombination and splicing;ensures full replication, functional organization of chromosomes in meiosis and nucleus; it also acts as a molecular clock to determine a cell's division capacity [16-18].

2.STRUCTURE AND SUB-UNITS OF THE TELOMERASE ENZYME

The structure responsible for telomere synthesis is called telomerase (telomere terminal transferase or reverse transcriptase) enzyme [1]. Telomerase is a reverse-transcriptase synthesized from a single strand of telomeric DNA consisting of a combination of RNA and protein. However, it is also a large enzyme complex [19]. Telomerase is a ribonucleoprotein complex containing a catalytic core, telomerase reverse transcriptase (TERT) and non-coding human telomerase RNA (hTR) that serves as a template for the insertion of telomeric repeats at chromosome ends [20]. The telomerase enzyme has three components. These are: Telomerase RNA subunit (TR), Telomerase protein component (TP1), Telomerase catalytic subunit (TERT) [21].

Telomerase RNA subunit (TR) differs from other terminal transferase enzymes in that it uses its own RNA subunit as a template. This subunit is transcribed by RNA polymerase II and is used as a

JSR A
Journal of Scientific Reports

template for attachment and reverse transcription to telomere DNA on the side close to its 5-end. For this, it is thought to be suitable for anti-telomerase therapy [22]. The telomerase protein component TP1 is the regulatory component of the telomerase enzyme and binds specifically to the RNA subunit of telomerase. It is thought to be ineffective in controlling telomerase enzyme activity. The catalytic subunit of telomerase (TERT) is the portion of telomerase with reverse transcriptase activity. Cancers, through TERT activation or alternative telomere elongation, require telomere maintenance mechanisms for their unlimited potential for division [23]. Complementary bases are added by TERT in accordance with the mold. The mold part of the TR is attached to the telomere, resulting in long telomere length [24]. TERT is generally similar in all living things, but it is known that there are some differences between them. Telomerase has emerged as an important primary target in anticancer therapy. It is a distinctive reverse transcriptase enzyme that elongates telomere length at the 3 'chromosome end and uses domains containing telomerase reverse transcriptase (TERT) and telomerase RNA template. Telomerase is a contributing factor to human health and has a vital role. It mainly affects cell aging and cell proliferation. Because of its unique feature, it provides unlimited cell proliferation in malignancy and plays a major role in cancer [25]. The complex called reverse-transcriptase in humans has two subunits that are important for telomerase activity: human telomerase RNA (hTER),and human telomerase reverse transcriptase (hTERT) [12,26,27].

The gene encoding "h-TERT", which is the catalytic subunit of telomerase, was cloned in 1997 and is known to contain 7 exons. The first exon is specific to telomerase, while others are similar to those of other reverse transcriptase [28]. The strong link between telomerase activity and the expression level of the gene encoding "h-TERT" suggests that "h-TERT" may be responsible for regulation of telomerase activity [29]. Control of telomerase activation in humans has been recognized only at the level of hTERT, as other components are expressed repeatedly [30]. hTERT is the main mechanism in the regulation of telomerase activity. While it negatively regulates the transcription factors p53, IFNα and TGF-β hTERT, it has been reported to positively regulate Human Papilloma Virus 16E6 and estrogen [30-32].

The human telomerase RNA component (hTER) acts as a template for the synthesis of telomeric repeats with 1-6 5'-CUAACCCUAAC-3 'sequences at the 5' end. The hTER gene is the only duplicate gene located in the 3q26.3 region. Recent studies have shown that hTER can act as an oncogene [33,34].

2.1. Working Principle of Telomerase Enzyme

During cell division, an exception occurs at the ends of the linear chromosome in the telomeric region of the chromosome [35]. During cell division, DNA polymerase does not start DNA synthesis directly. Replication occurs from the top 5 to the top 3, but can occur with a pre-RNA fragment of 8-12 bases. This fragment is called "RNA Primer". In order for the DNA polymerase to bind, the RNA primer forms a 3'-OH group. As a result, DNA polymerase; it continues its reading in the batch and continuously synthesized yarn. Since the resulting DNA moves in the 3-way direction, after the RNA is removed, there will be an unfilled portion at the 5-top end of the new double-stranded DNA molecule. This part cannot be cured by DNA polymerase. As a result, the chromosome will theoretically shorten to the length of the RNA primer at the end of each synthesis. Telomerase prevents telomere shortening by attaching to the ends of chromosomes after cell division takes place. Hydrogen bonds are formed between strings curling in the shape of a "hairpin" and mutually lined guanosines. The free 3'-OH end required for DNA polymerase I to fill the gap is formed when the

RNA primer is removed. The hairpin structure is then broken and DNA loss after the cell cycle is prevented [35].

2.2. Telomerase Measurement Methods

It is known that there are more than one method to determine telomerase activity. The first known method is TRAP (Telomeric Repeat Amplification Protocol) method, which is the reproduction of telomeric repeats based on PCR. Kim et al started using this method in 1994. After the TRAP method was started to be used, it turned out that this method was not sensitive enough and after it did not give reliable results, the positive and negative results could not be fully evaluated. Determination of telomerase activity in tissues has enabled the investigation of telomerase expression in more than one cancer type with the development of the method. In order to overcome the difficulties faced, TRAP-eze and TRAP-eze-Elisa kits, which are improved versions of this method, have been used [36].

PicoGreen method is a method developed by Gelmini et al. In 1998. PicoGreen used in naming this method is a fluorescent dye and is based on selectively binding to double stranded DNA. "Stretch-PCR" method is used for the growth of telomerase product [37].

The Transcription-Mediated Amplification and Hybridization Protection Assay (TMA / HPA) method was proposed by Hirose et al. (1998). This method is very simple and can be applied quickly. In addition, it is less affected by TRAP inhibitors that can be obtained from clinical data. There is no drawback in using a water bath in the transcription step, since the redunanz is fast with the transcription of the telomerase product. At the same time, since several billion RNAs can be replicated from a template within an hour, the TMA / HPA method is based on different hydrolysis of probes that hybridize with RNAs or not, and the addition of a promoter to the primer to be extended by the reverse transcriptase enzyme [38].

Aldous and Grabill (1997) used the Fluorescent-TRAP method (F-TRAP) to determine the telomerase activity. This method uses fluorescence-labeled primers and the use of radioisotopes is eliminated [39].

As a result of the studies carried out by Zavlaris et al. In 2009, it is thought that if the TRAP (Telomeric Repeat Amplification Protocol) method is to be used, the application of "stretch-PCR" with the PicoGreen method, and the determination of the gene expression of TERT, even if the Real Time PCR method will be used, may be preferred [40].

3. NEOPLASIC CHANGES AND TELOMER RELATIONSHIP

It was determined that telomerase activity can be detected mostly in cancer cells and rarely in normal somatic cells. After embryogenesis, in contrast to the loss of telomerase activity in most somatic cells, it has been shown that there is little telomerase activity in somatic cells such as hematopoietic stem cells, skin and intestinal epithelium cells, esophageal epithelium, gamete cells, endometrium cells and hair follicles that can regenerate themselves significantly [41]. This suggests that this enzyme is active in cells with high growth rates, whether normal or malignant [42].

Telomerase provides activation after high loss of telomere, by strengthening the worn out ends [43]. It was first suggested by Olovinikov in 1973 that cells lose some DNA from their terminal ends at each replication and this shortening observed in chromosomes leads to cellular aging [44,45]. The shorter

telomere lengths of somatic cells such as fibroblasts and leukocytes in the elderly compared to young ones also supports this hypothesis. In addition, it has been suggested that there are cancer cells that do not have telomerase activity but are able to increase the length of telomeres. It has been reported that this enzyme cooperates with a number of oncogenes and causes the tumorigenic transformation of human epithelial cells and fibroblasts by suppressing several tumor suppressor genes. In the light of this information, it is thought that telomerase may play a role in cancer diagnosis and follow-up, so that telomerase activity may lead new approaches in the fight against cancer [46].

Telomerase, a key enzyme for cell survival, prevents telomere shortening and cellular aging observed after many cells divide. In contrast, telomerase inactivation is observed in most cells of the adult liver. Lack of telomerase activity and shortening of telomeres have played a role in hepatocyte aging and hepatocellular carcinoma (HCC) development. Telomerase reactivation is required to induce uncontrolled cell proliferation leading to HCC development [47].
Telomerase activity yields eukaryotic cells with unlimited proliferation capacity, one of the hallmarks of cancer. More than 90% of human urothelial carcinoma of bladder (UCB) tumors are positive for telomerase activity. Telomerase activation can occur by several mechanisms. While mutations in the core promoter region of the human telomerase reverse transcriptase gene (TERT) cause telomerase reactivation in 60-80% of UCBs, the prevalence of these mutations is lower in urothelial cancers of other mutations. In the future, TERT promoter mutations and telomerase activity may have diagnostic and therapeutic applications in UCB [48].

Prostate cancers protect telomeres predominantly by activating them, but in metastatic disease alternative mechanisms of telomere elongation may occur. Telomerase activity and telomere length assessment may be helpful in prostate cancer diagnosis and prognosis. Disruption of androgen receptor function in prostate cancer cells leads to telomere dysfunction, indicating telomeres and telomerase as potential therapeutic targets in prostate cancer. While telomere shortening in normal stromal cells has been associated with prostate cancer, variable telomere lengths in prostate cancer cells and telomere shortening in cancer-related stromal cells have been associated with lethal disease [49].

Chondrosarcomas are malignant skeletal tumors with chondroid differentiation. The prognosis is largely dependent on histolopathologic grading as double-blinded by two scientists. Telomerase activity and abundant expression of telomerase reverse transcriptase (hTERT) have previously been associated with chondrosarcoma grade and metastasis. Studies have shown that hTERT promoter mutations are common in high-grade conventional chondrosarcomas and strengthen the rationale for telomerase targeted therapy in a chondrosarcoma subset [50].

Alternative telomere extension mechanisms are generally absent in meningiomas. TERT and hTERT promoter changes play an important role in prognosis and potentially treatment during oncogenesis of meningiomas [51].

Recently, the G-quadruplex (G4-DNA) structure found in telomeres has been discovered. These nucleic acid sequences, also called G-tetrad, are rich in guanine. Composed of guanine, G-quadruplex refers to a formation containing four chains. Compounds that stop telomerase activity and provide stable structure of G-4 DNA at the same time prevent telomerase enzyme from reaching telomere and stop telomerase activity have started to attract attention in cancer treatment. These compounds

preserve the G4-quadruplex structure and prevent the reverse transcriptase enzyme from reaching the telomeres [52].

DNA G-quadrupoles have been potential drug targets for cancer therapy [53–56]. G-quadrupoles with various functions have attracted attention as a supramolecular synthesis tool to create nanomaterials [57]. G-four poles are four-stranded structures formed in guanine-rich arrays held together by the guanine-guanine Hoogsteen hydrogen bond. The formation of G-quaternary structures is common in regions of biological significance such as human telomeres and oncogene promoter regions [58–60]. Human telomeric DNA, consisting of 5-8 kb tandem repeat d (TTAGGG) n sequences and terminating with a 100-200 nt 3′ single-stranded overhang, forms caps by nucleoprotein complexes and plays an important role in cell aging and death [4,61-64]. Telomerase has been shown to be active in 80–85% of human cancers to prolong telomere and increase the survival of cancer cells [65,66]. Previous studies in human cancer cells have demonstrated the formation of DNA G-quadrature in telomeres, and G-quadruple stabilization by small molecules has been shown to induce tumor cell aging and apoptosis by suppressing telomerase activity and DNA damage response pathway [67–71]. Therefore, there has been great interest in stabilizing G-quadruplexes as potential drug targets for cancer therapy development and small molecules [72].

JSR A
Journal of Scientific Reports

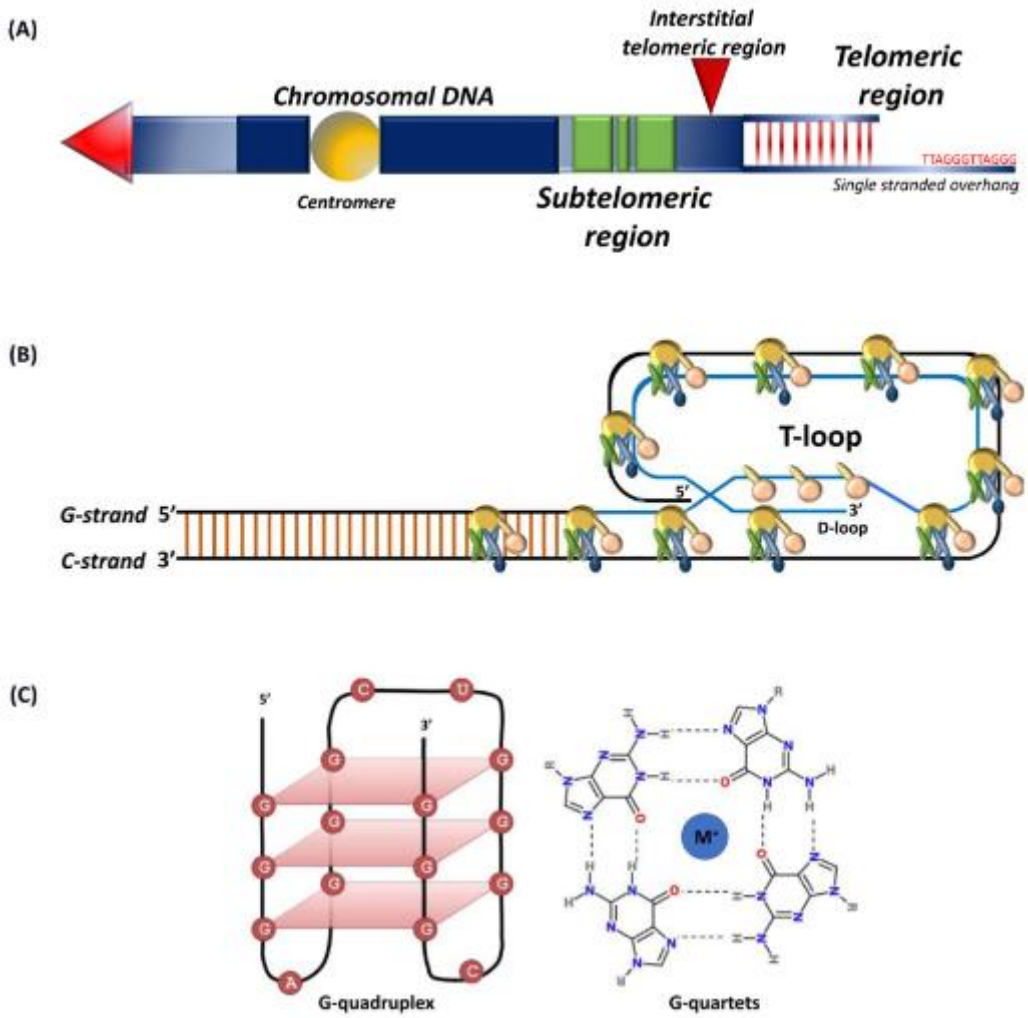

Figure 1. (A) Schematic representation of telomeres and lower telomeric regions. (B) The shelterin complex is folded back into duplex DNA to form the G-tail t-ring; (C) G-quartet formed by the cyclic Hoogsten hydrogen bonding arrangement of four guanines with the G-quadruplex structure [73,74].

4. AGING AND TELOMER RELATIONSHIP

Aging is a biological process that is characterized by a progressive functional decline in tissues and organs and ultimately leads to death [75]. During cell division, an incomplete copy of the DNA of each chromosome is made, causing the telomeres to shorten in successive generations. When a threshold length is reached, replication stops and the cell "ages" [76]. Telomeres play an important role in cellular aging as they are shortened every time the cell divides and trigger a DNA damage response that results in aging [6,8]. Cells with unlimited proliferation potential need to expand their telomeres to avoid cessation of permanent growth. In humans, telomeric DNA is synthesized by the

telomerase enzyme. This RNA protein complex is active in germline and stem cells, but is absent in most somatic cells [77]. In eukaryotes, telomeres determine cell proliferation potential by triggering replicative aging in the absence of telomerase [78].

Telomerase deficiency leads to progressive telomere erosion in human cell division due to the inherent property of DNA polymerase [14]. When telomeres shorten to a critical size and telomeres become dysfunctional, the DNA damage response pathway is activated and cells begin to enter a permanent growth arrest phase called replicative aging. It is believed that aging is a very effective barrier against cancer by blocking proliferation and genetic mutations that result from DNA replication. Since infinite proliferation is the hallmark of malignant cells [79], it is likely to overcome the aging barrier with telomere stabilization in oncogenesis, and in most cases this is achieved by telomerase activation [14,79].

Aging in adult tissues comes into play in response to different types of damage. One of the movements that cause aging is damage to telomeres, highly repetitive DNA structures located at the end of chromosomes. Telomeres are protected by a multiprotein complex known as shelterin. By coating on telomere, shelterin prevents the activation of a DNA damage response, thus preventing end-to-end chromosome assembly that would lead to telomere crisis [80]. The end-of-replication problem is a consequence of the inability of DNA polymerases to synthesize DNA without a template occurring in telomeres. This results in telomeres gradually shortening with each cell cycle division. Embryonic tissues circumvent this erosion by expressing telomerase, which serves to join DNA to the ends of chromosomes and thus provides a template for DNA synthesis [81]. However, in telomerase-deficient adult tissues, repeated cell division results in progressive DNA erosion, decreased shelterin binding, and aging. As an organism ages, cells accumulate more divisions. This results in increased telomere erosion and aging. However, it is not known to what extent telomere erosion affects aging during aging and to what extent the aging process contributes to it [82].

Aging and death occur in human cells in two stages. The first of these is the replicative aging M1 named as "Mortality Stage". At this stage, chromosomes reach a critical size as a result of shortening of telomeres. Hayflick and Moorhead first described the critical point definition [83]. Leonard Hayflick studied replicative aging and the cells of young people showed the most division in culture medium than cells of the elderly. After dividing about 60 - 80 times, Human embryo cells have started to age. He reported that while senescent cells remained metabolically active, no new cell formation (Hayflick Limit) and eventually died [84]. This event stopped the cell cycle and initiated the senile program [18].

It is the M1 point that represents the replicative life span. If a cell passes the mortality stage, its telomeres shorten to the M2 point. M2 point is called "crisis" or "second mortality stage". Major cell death occurs in this second mortality stage. The cause of cell mortality may be due to chromosome death due to weakened telomere function. Telomerase activity is required to prevent these mortalities. As a result, telomere length and structure can be restored and cells formed at the M2 point can divide infinitely (cellular immortalization). Data obtained as a result of research to date revealed that one of the characteristic features of aging cells is telomeres [85].

Age is a strong prognostic indicator of reduced survival in many cancers [86]. Senescence is a potent tumor suppressor mechanism that limits cancer onset through both cell-intrinsic [87] and cell-extrinsic mechanisms [88]. Aging cells may contribute to tumor progression by increasing the proliferative

potential of cancer cells [89] or by contributing epithelial cells to the mesenchymal transition [90]. Therefore, the increasing number of senescent cells found in aged tissues may contribute to the increase in cancer incidence with age. Supporting this, a delayed onset of tumor formation is observed when senescent cells are eliminated [91].

5. CONCLUSION

From the original study of Barbara Mc Clintock [92] in 1941 until today, it is obvious that telomere structures are important in terms of ensuring chromosomal integrity. There are several studies showing that the mechanism that keeps telomere loss in balance in vertebrates is telomerase enzyme. For this reason, reverse transcriptases are of great interest in cancer therapy. Preventing the functionality of telomerase leads to shortening of the extremely important telomeres. As a result, chromosomes that are shorter cause instability and mortality. It is known that telomerase expression is closely related to cellular immortalization and early stages of cellular change. However, it has nothing to do with the growth rate. In other words, we can say that immortal cells regulate telomerase expression. This event demonstrates how important replication is for telomerase activation [93].

The systems responsible for the elongation of telomeres in tissues during division cannot continue their activity. Therefore, telomeres shrink during cell replication. Telomer length determines the replicative survival time of cells. When telomeres reach critical stature, the aging program is activated. Cell replication then stops. But they continue to live and function. Telomeres are actively maintained in reproductive cells because it is imperative that chromosome be passed on to the next generation. This necessity in telomeric division is provided by the activation of the telomerase enzyme [94]. In order to explain the relationship between telomere length and age, studies have been carried out in some cancer cells by cell culture of human fibroblasts in human cells of different age groups, and it has been found that telomere length decreases with increasing cell division rate and age [95].

Telomeres are extended by mechanisms that include telomerase-mediated reverse transcription, subtelomeric DNA amplification, and telomeric DNA homologous recombination. It eliminates the risk of uncontrolled telomere elongation such as end-to-end junction, premature aging and related disorders such as cancer. In addition, the mechanisms that determine different aspects of longevity, early replicative aging, and chronological aging appear to depend on the accuracy of DNA damage response and repair. For example, the investigation of effective and adequate regulation of telomere DNA damage response and repair by examining the molecular interactions between different telomere maintenance pathways in telomere care will shed light on the mechanisms of preventing telomere damage from environmental stresses during aging [96]. The answer to the question of whether we can have a young and alive body by increasing our telomere length has shown itself with the latest studies. It has shown that it can be reversed by increasing the telomerase ratio inside the cell and stopping aging. Researchers who cultured and then cloned telomerase genes in human cells; they reported that the cell continues to divide even after the aging point, with telomeres that stretch up to a thousand base pairs. It should also be known that a procedure performed only in this way carries a serious cancer risk [1,93]. Within all these data, it would not be wrong to say that these formations that form "happy ends" of chromosomes have the potential to sign a happy future for humanity [90].

JSR A
Journal of Scientific Reports

REFERENCES

[1] Atlı, K., Bozcuk, A.N., (2002), Telomerler ve hücresel yaşlanma, Geriatri, 5, 111-4.

[2] Turner, K.J., Vasu, V., Griffin, D.K., (2019), Telomere Biology and Human Phenotype, Cells, doi.org/10.3390/cells8010073.

[3] Blackburn, E.H., (1991), Structure and function of telomeres, Nature, 350, 569–573.

[4] de Lange, T., (2005), Shelterin: the protein complex that shapes and safeguards human telomeres, Genes Dev., 19, 2100–2110.

[5] Watson, J.D., (1972), Origin of concatemeric T7 DNA, Nat. N. Biol., 239, 197–201.

[6] Harley, C.B., Futcher, A.B., Greider, C.W., (1990), Telomeres shorten during ageing of human fibroblasts, Nature, 345, 458–460.

[7] López-Otín, C., Blasco, M.A., Partridge, L., Serrano, M., Kroemer, G., (2013), The hallmarks of aging, Cell, doi.org/10.1016/j.cell.2013.05.039.

[8] d'Adda di Fagagna, F., (2003), A DNA damage checkpoint response ın telomere-ınitiated senescence, Nature, 426, 194–198.

[9] Blasco, M.A., (2007), Telomere length, stem cells and aging, Nat. Chem. Biol., doi.org/10.1038/nchembio.2007.38.

[10] Blackburn, E.H., (1992), Telomerases, Annu. Rev. Biochem, 61,113-129.

[11] Başaran, A., (2000), Telomer-telomeraz ve hücre yaşlanması, Denizli Tıbbi Biyoloji Kongre Özet Kitabı, 40-41.

[12] de Lange, T., Shiue, L., Myers, R.M., Cox, D.R., Naylor, S.L., Killery, A.M., Varmus, H.E., (1990), Structure and variability of human chromosome ends, Mol Cell Biol., 10(2), 518-527.

[13] Slijepcevic, P., (1998), Telomere length regulation-a view from the ındividual chromosome perspective, Experimental Cell Research, 244, 268-74.

[14] Shay, J.W., Wright, W.E., (2019), Telomeres And Telomerase: three decades of progress, Nature Reviews Genetics, 20, 299–309.

[15] Sun, D., Lopez-Guajardo, C.C., Quada, J., (1999), Regulation of catalytic activity and processivity of human telomerase, Biochemistry, 38, 4037-44.

[16] Shay, J.W., Zou, Y., Hiyama, E., Wright, W.E., (2001), Telomerase and cancer, Hum. Mol. Genet., 10, 677-685.

[17] Grander, M.P., Wright, W.E., Shay, J.W., (2002), Telomerase in cancer and aging. Crit. Rev. Oncol. Hematol., 41, 29-40.

[18] Hahn, W.C., (2005), Telomere and telomerase dynamics in human cells. Curr. Mol. Med., 5, 227-31.

[19] Prescott, J.C., Blackburn, E.H., (1999), Telomerase: Dr Jekyll or Mr. Hyde, Curr. Opin, Genetics and Development, 9, 368-373.

[20] Roake, C.M., Artandi, S.E., (2020), Regulation of human telomerase in homeostasis and disease. Nature Reviews Molecular Cell Biology, 551, 6.

[21] Kurt, N., (2014), Köpeklerde telomeraz mRNA (dogtert) ekspresyonunun belirlenmesi, Adnan Menderes Üniversitesi Sağlık Bilimleri Enstitüsü Yüksek Lisans Tezi (Basılmış).

[22] Angelopoulou, K., Zavlaris, M., Papaioannou, N., Vlemmas, I., (2008), canis familiaris telomerase reverse transcriptase undergoes alternative splicing, Mamm Genome, 19(9), 647-53.

[23] Sieverling, L., Hong, C., Koser, S., Ginsbach, P., Kleinheinz, K., Hutter, B., Braun, D., Cortés-Ciriano, I., Xi, R., Kabbe, R., Park, P., Eils, R., Schlesner, M., (2020), Genomic footprints of activated telomere maintenance mechanisms in cancer, Nature Communications volume 11, 733.

[24] Edo, M.D., Andrés, V., (2005), Aging telomeres and atherosclerosis, Cardiovasc Res., 1,66(2), 213-21.

[25] Bajaj, S., Kumar, M.S., Peters, G.J., Mayur, Y.C., (2020), Targeting telomerase for its advent in cancer therapeutics, doi: 10.1002/med.21674.

[26] Nugent, C.I., Lundblad, V., (1998), The telomerase reverse transcriptase. components and regülation, Genes and Developments, 12, 1073-1085.

[27] Qulton, R., Harrington, L., (2000), Telomeres telomerase and cancer life on the edge of genomic stability, Curr. Opin Oncol., 12, 74-81.

[28] Kevser, P.Ö., (2000), Telomeraz. Hacettepe Tıp Dergisi, 31(2), 158-68.

[29] Zakian, V.A., (1995), Telomeres beginning to understand the end. Science, 270, 1601-6.

[30] Liu, D., O'connor, M.S., Quin, J., Songyang, Z., (2004), Telosome: mammalian telomere-associated complex formed by multiple telomeric proteins, J. Biol. Chem., 279, 51338-51342.

[31] Cong, Y.S., Woodring, E., Shay, J.W., (2002), Human telomerase and its regulation, Microbiol. Mol. Biol. Rev., 66, 407-425.

[32] Horikawa, I., Barrette, J.C., (2003), Transcriptional regulation of the telomerase hTERT gene as a target for cellular and viral oncogenic mechanisms, Carcinogenesis, 24(7), 1167-76.

[33] Kim, N.W., Piatyszek, M.A., Prowse, K.R., (1994), Specific association of human telomerase activity with immortal cells and cancer, Science, 266, 2011-15.

[34] Chan, S.R.W.L., Blackburn, E.H., (2004), Telomeres and telomerase, Phil.Trans. R. Soc. Lond, 359, 109-121.

[35] Geyikli, İ., Bayıl, S., Çiçek, H., (2007), Yaşlanma ve telomeraz, Türk Klin Biyok Der., 5(3), 111- 115.

[36] McKevitt, T.P., Nasir, L., Devlin, P., Argyle, D.J., (2002), Telomere lengths in dogs decrease with increasing donor age, J Nutr. Jun, 132(6 Suppl 2), 1604S-6S.

[37] Gelmini, S., Caldini, A., Becherini, L, Capaccioli, S., Pazzagli, M., Orlando, C., (1998), Rapid quantitative nonisotopic assay for telomerase activity in human tumors, Clin Chem., 44(10), 2133 8.

[38] Hirose, M., Hashımoto, J.A., Tahara, H., Ide, T., Yoshimura, T., (1998), New method to measure telomerase activity by transcription-mediated amplification and hybridization protection assay, Clinical Chemeistry, 44(12), 2446-2452.

[39] Aldous, W.K., Grabill, N.R., (1997), A fluorescent method for detection of telomerase activity, Diagnostic Molecular Pathology, 6(2), 102-110.

[40] Zavlaris, M., Angelopoulou, K., Vlemmas, I., Papaioannou, N., (2009), Telomerase reverse transcriptase (TERT) expression in canine mammary tissues: a specific marker for malignancy, AnticancerRes., 29(1), 319-25.

[41] Liu, D.Y., Peng, Z.H., Qiu, G.Q., Zhou, C.Z., (2003), Expression of telomerase activity and oxidative stres in human hepatocellular carcinoma with cirrhosis, World J Gastroentero, 9(8), 1859-1862.

[42] Dikmen, G., Doğan, P., (2003), Telomeraz ve kanser, Turk Klin Tip Bilim, 23, 334-341.

[43] Greenberg, R.A., (2005), Telomeres crisis and cancer, Curr. Mol. Med., 5, 213-218.

[44] Kavaler, E., Landman, J., Chang, Y., (1998), Detecting human bladder carcinoma cells in voided urine samples by assaying for the presence of telomerase activity, Cancer, 82,708-14 11.

[45] Brian, C.S., Liu, K., Loughlin, R., (2000), Telomerase in human bladder cancer, Urologic Clinics of North America, 27(1), 115-23.

[46] Shay, J.W., (1998), Telomerase in cancer: diacnostic, prognostic and therapeutic implications, Cancer J Sci Am, 4, 26-34.

[47] Nault, J.C., Ningarhari, M., Rebouissou, S., Zucman, R.J., (2019), The role of telomeres and telomerase in cirrhosis and liver cancer, Nature Reviews Gastroenterology & Hepatology, 16, 544–558.

[48] Güneş, Ç., Wezel, F., Southgate, J., Bolenz, C., (2018), Implications of TERT promoter mutations and telomerase activity in urothelial carcinogenesis, Nature Reviews Urology, 15, 386–393.

[49] Graham, M.K., Meeker, A., (2017), Telomeres and telomerase in prostate cancer development and therapy, Nature Reviews Urology, 14, 607–619.

[50] Lin, Y., Seger, N., Chen, Y., Hesla, A.C., Wejde, J., Ghaderi, M., Tsagkozis, P., Larsson, O., Haglund, F., (2018), hTERT promoter mutations in chondrosarcomas associate with progression and disease-related mortality, Modern Pathology, 31, 1834–1841.

[51] Stögbauer, L., Stummer, W., Senner, V., Brokinkel, B., (2020), Telomerase activity, TERT expression, hTERT promoter alterations, and alternative lengthening of the telomeres (ALT) in meningiomas - a systematic review, Neurosurg Rev., doi: 10.1007/s10143-019-01087-3.

[52] Smith, J.S., Johnson, F.B., (2010), Isolation of G-Quadruplex DNA using nmm-sepharose affinity chromatography ın baumann p. (eds), G-Quadruplex DNA: methods and protocols, Methods in Molecular Biology, 608 DOI 10. 1007/978-1-59745-363-9_13.

[53] Neidle, S., (2017), Quadruplex nucleic acids as targets for anticancer therapeutics, Nat. Rev. Chem., 1, 0041.

[54] Hansel-Hertsch, R., Di Antonio, M., Balasubramanian, S., (2017), DNA G-quadruplexes in the human genome: detection, functions and therapeutic potential. Nat. Rev. Mol. Cell Biol., 18, 279–284.

[55] Wu, Y.L., (2017), G-quadruplex organic frameworks, Nat. Chem., 9, 466–472.

[56] Yatsunyk, L.A., Mendoza, O., Mergny, J.L., (2014), "Nano-oddities": unusual nucleic acid assemblies for DNA-based nanostructures and nanodevices, Acc. Chem. Res., 2014, 47, 6, 1836-1844.

[57] Davis, J.T., (2004), G-quartets 40 years later: from 5'-GMP to molecular biology and supramolecular chemistry, Angew. Chem. Int. Ed., 43, 668–698.

[58] Neidle, S., Parkinson, G., (2002), Telomere maintenance as a target for anticancer drug discovery, Nat Rev Drug Discov., 1(5),383-93.

[59] Qin, Y., Hurley, L.H., (2008), Structures, folding patterns, and functions of intramolecular DNA G-quadruplexes found in eukaryotic promoter regions, Biochimie, 90, 1149–1171.

[60] Balasubramanian, S., Hurley, L.H., Neidle, S., (2011), Targeting G-quadruplexes in gene promoters: a novel anticancer strategy, Nat. Rev. Drug. Discov., 10, 261–275.

[61] Moyzis, R.K., (1988), A highly conserved repetitive DNA sequence, (TTAGGG)n, present at the telomeres of human chromosomes, Proc. Natl Acad. Sci., 85, 6622–6626.

[62] Wright, W.E., Tesmer, V.M., Huffman, K.E., Levene, S.D., Shay, J.W., (1997), Normal human chromosomes have long G-rich telomeric overhangs at one end. Genes Dev., 11, 2801–2809.

[63] Bodnar, A.G., (1998), Extension of life-span by introduction of telomerase into normal human cells, Science, 279, 349–352.

[64] Hurley, L.H., (2002), DNA and its associated processes as targets for cancer therapy, Nat. Rev. Cancer, 2, 188–200.

[65] Greider, C.W., Blackburn, E.H., (1985), Identification of a specific telomere terminal transferase activity in Tetrahymena extracts, Cell, 43, 405–413.

[66] Kim, N.W., Piatyszek, M.A., Prowse, K.R., Harley, C.B., West, M.D., Ho, P.L., Coviello, G.M., Wright, W.E., Weinrich, S.L., Shay, J.W., (1994), Specific association of human telomerase activity with immortal cells and cancer, Science, 266(5193),2011-5.

[67] Phan, A.T., (2010), Human telomeric G-quadruplex: structures of DNA and RNA sequences, Febs. J., 277, 1107–1117.

[68] Lin, C., Yang, D., (2017), İn telomeres and telomerase: methods and protocols (ed. Songyang, Z.) 171–196.

[69] Zahler, A.M., Williamson, J.R., Cech, T.R., Prescott, D.M, (1991), Inhibition of telomerase by G-quartet DNA structures, Nature, 350, 718–720.

[70] Sfeir, A., de Lange, T.. (2012), Removal of shelterin reveals the telomere end-protection problem, Science, 336, 593–597.

[71] Rizzo, A., (2009), Stabilization of quadruplex DNA perturbs telomere replication leading to the activation of an ATR-dependent ATM signaling pathway, Nucleic Acids Res., 37, 5353–5364.

[72] Liu, W., Zhong, Y.F., Liu, L.Y., Shen, C.T., Zeng, W., Wang, F., Yang, D., Mao, Z.W., (2018), Solution structures of multiple g-quadruplex complexes induced by a platinum(ıı)-based tripod reveal dynamic binding, Nature Communications, 9, 3496.

[73] Martinez, P., Blasco, M.A., (2018), Heart-breaking telomeres. Circ. Res., 123, 787–802.

[74] Frees, S., Menendez, C., Crum, M., Bagga, P.S., (2014), Qgrs-conserve: A computational method for discovering evolutionarily conserved g-quadruplex motifs, Hum. Genom, 8, 8.

[75] Zhu, Y., Liu, X., Ding, X., Wang, F., Geng, X., (2019), Telomere and its role in the aging pathways: telomere shortening, cell senescence and mitochondria dysfunction, Biogerontology, doi: 10.1007/s10522-018-9769-1.

[76] Wattis, J.A.D., Qi, Q., Byrne, H.M., (2020), Mathematical modelling of telomere length dynamics, J Math Biol., doi: 10.1007/s00285-019-01448-y.

[77] Wright, W.E., Piatyszek, M.A., Rainey, W.E., Byrd, W., Shay, J.W., (1996), Telomerase activity in human germline and embryonic tissues and cells, Dev. Genet., 18, 173–179.

[78] Jolivet, P., Serhal, K., Graf, M., Eberhard, S., Xu, Z., Luke, B., Teixeia, M.T., (2019), A Subtelomeric region affects telomerase-negative replicative senescence ın saccharomyces cerevisiae, Scientific Reports, 9, 1845.

[79] Hanahan, D., Weinberg, R.A., (2011), Hallmarks of cancer: the next generation, Cell, 144, 646–74.

[80] Palm, W., de Lange, T., (2008), How shelterin protects mammalian telomeres, Annu Rev Genet., 42, 301-34.

[81] Nandakumar, J., Cech, T.R., (2013), Finding the end: recruitment of telomerase to telomeres, Nat Rev Mol Cell Biol., 14(2),69-82.

[82] McHugh, D., Gil, J., (2018), Senescence and aging: causes, consequences, and therapeutic avenues, doi: 10.1083/jcb.201708092.

[83] Hayflick, L., Moorhead, P.S., (1961), The serial cultivation of human telomerase activity diploid cell strains, Exp. Cell Res., 25, 585-621.

[84] Hayflict L, 1991. Aging Under Glass. Mutation Research. 256: 69-80.

[85] Klug, W.S., (2000), Cummings M. R, Concept of Genetics, Chapter 12, 340-341.

[86] de Magalhães, J.P., (2013), How ageing processes influence cancer, Nat Rev Cancer, 13(5), 357-65.

[87] Collado, M., Serrano, M., (2010), Senescence in tumours: evidence from mice and humans, Nat Rev Cancer, 10(1),51-7.

[88] Kang, T.W., Yevsa, T., Woller, N., Hoenicke, L., Wuestefeld, T., Dauch, D., Hohmeyer, A., Gereke, M., Rudalska, R., Potapova, A., Iken, M., Vucur, M., Weiss, S., Heikenwalder, M., Khan, S., Gil, J., Bruder, D., Manns, M., Schirmacher, P., Tacke, F., Ott, M., Luedde, T., Longerich, T., Kubicka, S., Zender, L., (2011), Senescence surveillance of pre-malignant hepatocytes limits liver cancer development, Nature, 479(7374), 547-51.

[89] Krtolica, A., Parrinello, S., Lockett, S., Desprez, P.Y., Campisi, J., (2001), Senescent fibroblasts promote epithelial cell growth and tumorigenesis: a link between cancer and aging, Proc Natl Acad Sci U S A, 98(21),12072-7.

[90] Coppé, J.P., Desprez, P.Y., Krtolica, A., Campisi, J., (2010), The senescence-associated secretory phenotype: the dark side of tumor suppression, Annu Rev Pathol., 5, 99-118.

[91] Baker, D.J., Childs, B.G., Durik, M., Wijers, M.E., Sieben, C.J., Zhong, J., Saltness, R.A., Jeganathan, K.B., Verzosa, G.C., Pezeshki, A., Khazaie, K., Miller, J.D., van Deursen, J.M.,

(2016), Naturally occurring p16(Ink4a)-positive cells shorten healthy lifespan, Nature, 530(7589), 184-9.

[92] Mc Clintock, B., (1941), The stability of broken ends of chromosomes in zea mays, Genetics, 41, 234-82.

[93] Blasco, M.A., (2005), Telomeres and human disease: aging, cancer and beyond, Nature Reviews Genetics, 6, 611-22.

[94] Güzelgül, F., Aksoy, K., (2010), Telomeraz enziminin tanı ve tedavide kullanım alanı, Arşiv 16, 69.

[95] Yıldız, M., Aras, S., Duman, D., (2009), Telomerlerin yaşlanma ve kanser ilişkisindeki rolü, Türk Hijyen ve Deneysel Biyoloji Dergisi, 66 (4), 187-195.

[96] Liu, J., Wang, L., Wang, Z., Liu, J.P., (2019), Roles of telomere biology in cell senescence, Replicative and Chronological Ageing Cells, 8(1), 54.